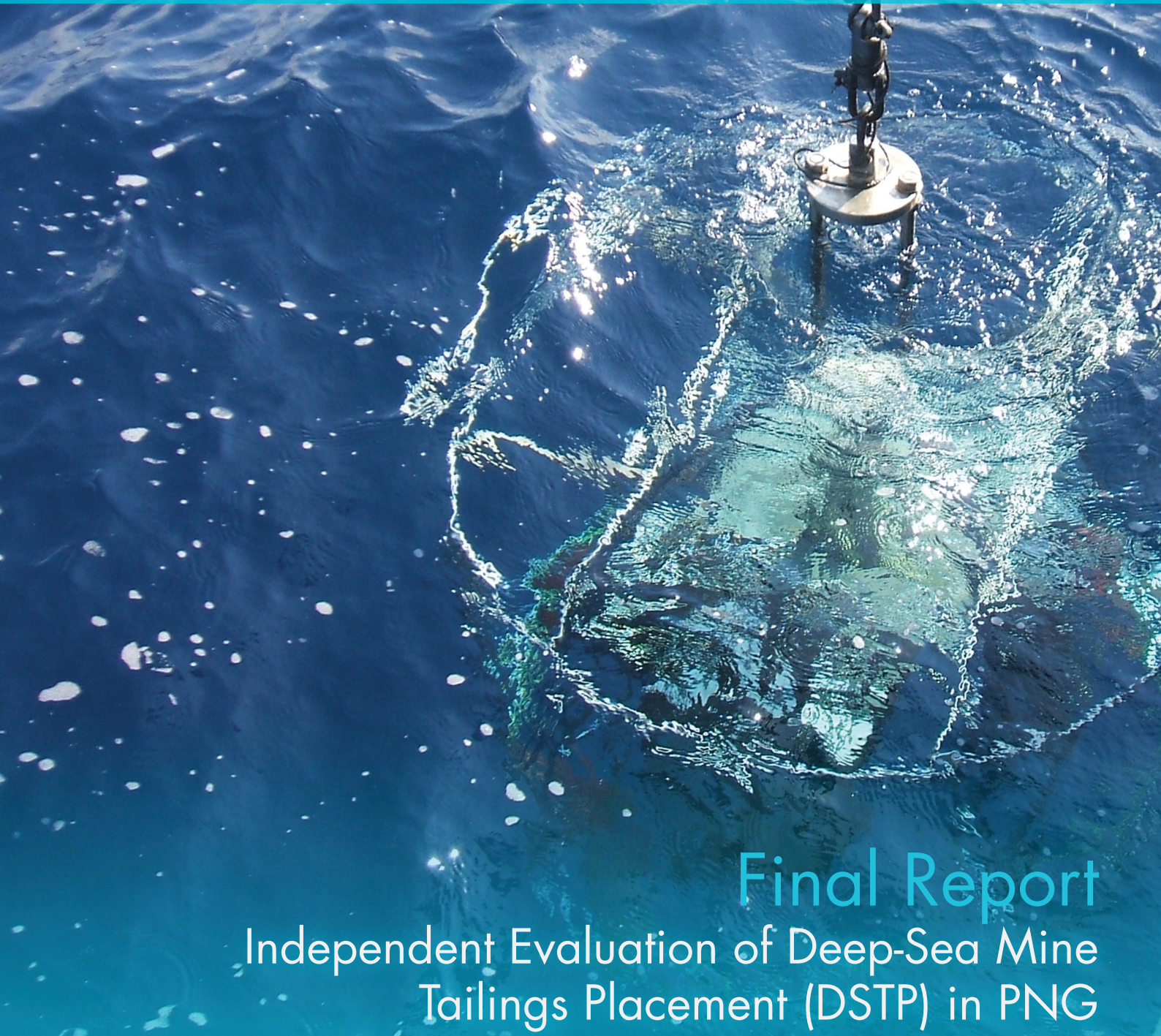SAMS RESEARCH
SERVICES LIMITED

Final Report

Independent Evaluation of Deep-Sea Mine Tailings Placement (DSTP) in PNG

Project Number: 8.ACP.PNG.18-B/15

Authors:
Tracy M Shimmield
Kenneth D Black
John A Howe
David J Hughes
Toby Sherwin

Deep Sea Tailings Placement in Papua New Guinea

Marine Environmental Impacts – case studies at proposed, operational and closed DSTP outfalls;

Basamuk, Lihir and Misima

Acknowledgements

Cite this report as: Final Report: Independent Evaluation of Deep-Sea Mine Tailings Placement (DSTP) in PNG, SAMS, 2010

Contents

0. Non-technical summary

The Scottish Association for Marine Science (SAMS) was contracted through its trading company SAMS Research Services Limited (SRSL) by the Papua New Guinea (PNG) Government to provide research services as a component of the EU funded Mining Sector Support Programme (MSSP). Our brief was to improve understanding of the ecological and geochemical processes in deep water that accompany Deep Sea Mine Tailings Placement (DSTP) in Papua New Guinea (PNG). The focus on deep-water processes was appropriate because much less is known about these than processes in shallow water which are focussed in the vicinity of the mines and processing plants. This is because monitoring programmes in the near-shore environment are logistically much easier to conduct on a routine basis. In contrast, studies of the deep water environment, which is the intended final disposal storage site of the mine tailings, require specialist equipment and expertise and, therefore, research is a much more complex and expensive operation where sampling opportunities are much more limited. The deep water environment around PNG has received very little attention from the international research community and there is very little information in the scientific literature. SAMS has a long history of research in deep water ecological and geochemical processes and has indeed pioneered many of the sampling methods now regarded as best practice in terms of scientific research.

Initially SRSL were contracted to consider the operational DSTP at Lihir and that at Misima which had ceased discharge 3 years before our sampling trip in 2007. Subsequent to our investigations at Misima and Lihir, the project was extended to include a baseline survey of the intended DSTP site at Basamuk. The present report outlines the mining context for each DSTP, the background environmental information gathered by the mining companies during their monitoring programmes and some additional information from the scientific literature, the methods used in the present research, the results and a discussion of these results. The data collected are included in full in appendices. Additionally, guidelines on best practice for DSTP have been developed in consultation with a large group of stakeholders and are included in an appendix.

Basamuk

The DSTP outfall planned at Basamuk will discharge tailings from the Ramu Nickel-cobalt mine. Our objective was to conduct a high quality, replicated baseline study of the seabed and water column ecology and geochemistry using the same methods as for the Misima and Lihir surveys. The purpose of a baseline study is to have a precise record of environmental conditions prior to any industrial impact so that future monitoring can much better define the levels of impact in the

context of natural changes that may occur at reference stations. This will also give a very sound base to determine the accuracy of the predictions made by the operators on the likely extent of the tailings.

The study characterised the benthos and sediment geochemistry of the Rai coast that has hitherto received little scientific study. In addition, further information of the wider scale hydrodynamic processes was obtained using water column profiles for temperature, salinity and suspended particulate material and also by interpreting data publically available from an Argo drifter that fortuitously entered this area during the project.

The Rai coast is typified by a steep seabed incised with canyons with a large amount of land derived material moving down the slope. This is in contrast to Misima and Lihir which are small islands and therefore discharge much less terrestrial material into the deep sea. This may have some future bearing on the recycling of elements of the future tailings fuelled by the degradation of terrestrial organic matter.

Lihir

The Lihir Gold mine DSTP has been discharging mine tailings from 1996 to the present. In contrast to the Misima site, a very large body of data has been collected in a regular monitoring programme and so a great deal is known about the location and extent of the mine tailings on the seafloor, estimated in 2005 to extend to approximately 60 km^2. SAMS survey was not designed to better map the spatial extent of seabed tailings, rather the survey aimed to add detail to the understanding of benthic and geochemical processes at an active DSTP site through use of state-of-the-art sampling techniques and sample replication. The seabed stations closest to the mine had thick, laminated, mine-derived sediments patchily distributed amongst natural and mine derived coarser material regularly re-disturbed by movements down the steeply sloping seabed. The tailings were orange in colour from the iron added during gold extraction so rather easy to distinguish from natural sediments. Further from the mine, the tailings layer became thinner being draped several centimetres deep over natural sediments. Numbers of the smallest class of sediment-dwelling animals (meiofauna) were much lower at 800 m depth to the east of the island (tailings-affected) than in natural sediments at comparable depth to the west of Lihir. The contrast in meiofaunal abundance between natural and tailings-affected stations diminished with increasing water depth, implying an improvement in conditions as the tailings input rate decreased with distance from the mine and the steepness of the slope reduced. However, the composition of the meiofaunal community showed an influence of tailings at all depths sampled.

The larger sediment-dwelling animals (macrofauna) were very sparse at all of the impacted sites but much more abundant and diverse at the reference stations. These results show clearly that ongoing DSTP at Lihir has a major impact on the abundance and diversity of animals in deep-sea sediments.

Zooplankton can display vertical migrations in the water column that can couple processes at depth with those at the surface. However, we did not detect any such migration at the impacted or reference stations and also did not detect any significant difference between the populations at the two stations.

As tailings travel down the slope, it is well known that plumes of fine particulate material can be shed into the water column, typically where there are rapid changes in seawater density (pycnoclines). Samples of water were taken to examine the chemistry of the particulate material at various depths in the water column.

The maximum concentration of suspended particulate material was found closest to the discharge pipe with the concentration of suspended material decreasing with increasing distance from the mine. Similarly the metal concentrations of the suspended material were highest at the stations closest to the mine with concentrations decreasing with increasing distance from the mine. At the closest station to the mine, elevated concentrations of metals within the suspended material were found in the water column above the depth of the tailings pipe outfall. It is most likely that this is coming from surface run off from the mine.

The mine tailings have a very different geochemical signature to that of the natural sediment surrounding Lihir enabling sediment impacted by mine tailings to be identified. The mine tailings were restricted to the top part of the sediment core allowing underlying natural sediment to be obtained at all sampling sites.

The sediment accumulation rates at the impacted sites are higher than would be expected for typical deep sea sediments at these water depths and are highly mixed although there is a low abundance of fauna. The amount of heavy metals at the impacted sites is far greater than that found in natural sediments - in some cases fifty times higher.

The dissolved metal concentrations in sediment pore-waters are considerably higher at the impacted sites than the reference stations, however these are mostly being retained in the upper sediment and are not being released to the over lying water column.

Misima

The Misima silver and gold mine was the first DSTP system commissioned in PNG and operated between 1989 and 2004 discharging approximately 90 Mt to the marine environment. Virtually no monitoring of the fate of the tailings was carried out at the Misima mine during its operation. Our results show that the Bwagaoia basin to the south-east of the pipeline, which was the intended target for the tailings, is largely filled with tailings. We do not have enough information to determine how deep the tailings deposit is as our sediment corer is designed to precisely sample the surface layer (ca. 1 m) and the pre-mine bathymetry of the area is not well known. However, it is very likely that the tailings within the basin are several tens of metres deep. In addition to the main tailings deposit we found evidence of tailings in the surface sediments west of the Bwagaoia basin either derived directly from the mine or advected there from the adjacent basin through resuspension/deposition processes - we have insufficient information to rule out either option.

The steep slope leading down to the basin is likely to be still active in terms of slumps of sediments being dislodged, for example through seismic activity, and accumulating further down the slope and so sediments near to the slope are likely to be in a cyclic state of re-colonisation followed by smothering. This is a natural process typical of steeply sloping margins but made more dramatic by the addition of a large amount of mine derived material.

At Misima the geochemical fingerprint of the mine tailings is significantly different from that of the natural sediments of the area, having a higher concentration of heavy metals, allowing sediments derived from mine tailings to be distinguished from natural sediments on the seabed.

At stations in the Bwagaoia Basin the sediment is composed entirely of tailings but a site west of these impacted stations also shows signs of tailings deposition in the surface layer. When correlated to the sediment accumulation rate this indicates that the onset of impact of the mine tailings at this station occurred in 1990. This is in excellent agreement with the start of mining in 1989.

Studies of the sediments and pore-waters indicate that geochemical processes occurring at the impacted sites bring about a release of metals to the porewater with a possible release of some metals to the overlying water column.

Three years after the tailings discharge finished, the benthic community (living organisms on/in the seabed) in the Bwagaoia Basin was very different from that at local reference locations: the number of animals and the numbers of types of animal (i.e. biodiversity) was much lower at the

three stations showing clear chemical signals of tailings in the bottom sediments. Polychaetes (bristle worms) were the largest contributor to the macrofauna at each of the sampling stations but there was a significant difference in the structure of the assemblage at impacted compared with references stations. These results suggest that seabed animal communities in the Bwagaoia Basin are still significantly affected by tailings three years after the cessation of DSTP at Misima.

DSTP Guidlines

During reviews of previous works on DSTP, and bearing in mind various failures that have taken place in PNG and elsewhere, a set of draft guidelines have been produced which will reduce the risk of DSTP to the environment and the human population. The most important aspect of deep sea tailings is that the tailings are deposited at great depth where exchanges between the seabed and the surface layers are small. The four processes that are most likely to compromise this are 1) the tailings pipe out fall is too shallow, 2) the slope is not steep enough, 3) the tailings pipe breaks and discharges tailings into the coastal area and 4) the tailings slurry is insufficiently dense to travel rapidly to depth as a coherent gravity current. The first two factors directly relate to the design of the outfall and the second two relate both to design and subsequent management of the outfall.

DSTP

Our results indicate that DSTP has major impacts on deep-sea sediments and their biological communities, and that the effects persist for at least three years after tailings discharge has ended. Where it is incorrectly designed or badly managed DSTP can also cause serious damage to coastal resources and, potentially, communities. In PNG the deep sea bed has very weak interactions with the surface and coastal zones and so might be thought to be a safer long term repository than a terrestrial impoundment – especially given the high rainfall and frequency of earthquakes in PNG. There are several examples of disastrous failures of tailings impoundments. Tailings impoundments may need to be maintained for decades or even centuries after the mine has closed and the company dissolved.

Ultimately, the decision to allow DSTP must be a political decision and the logical outcome of that may be that some areas cannot be mined even though they may have valuable resources. Alternatively, society may value the provision of income that can improve public services and amenities more highly than the deep ocean floor. These are not scientific questions and in different countries there may be different answers - not least because they are geographically different. What science can provide are measures to reduce environmental risk once a decision to

utilise DSTP is taken. If these measures are accepted then it is then a political decision to ensure that monitoring, policing and adaptive management is sufficient to reduce environmental and societal risks to the absolute minimum.

1. Introduction

1.1 Deep Sea Mine Tailings Placement (DSTP)

1.1.1 Mining

Mining in the widest sense means the acquisition of non-renewable resources from the environment. Metals have been mined as ores since pre-history but metal production has increased dramatically in modern times driven by expanding Global GDP[1]. Metal ore mining produces large amounts of waste rock and mine tailings. Mine tailings are the wastes produced after extracting the desired metal from the ore. A typical copper ore, for example, is less than 1% copper and, therefore, 99% is produced as tailings. Waste rock is non-processed rock, for example: overlying rock (over-burden) that is removed to uncover an underlying ore body.There are several ways of dealing with this waste, and Ritcey (2005) identifies the following possibilities:

- Land-based storage

- Backfill to the mine

- Deep lake disposal

- Marine disposal

- Reprocessing for secondary metal recovery

In a sense, the fifth of these cannot really be considered a disposal option, since reprocessing does not, itself, address the issue.

In Papua New Guinea (PNG), both the Misima and Lihir Mines adopted the marine disposal option, releasing tailings through a submerged pipe onto the sea floor. This special case is referred to as Submarine Tailings Disposal (STD) or Deep Sea Tailings Placement (DSTP). DSTP is a special case of STD, in which the tailings deposition is sufficiently deep as to be below the euphotic zone. The Misima Mine pioneered DSTP (Jones and Ellis, 1995; Ellis and Ellis, 1994) with an outflow depth of 112m.

---

[1] http://www.google.com/publicdata?ds=wb-wdi&met=ny_gdp_mktp_cd&tdim=true&dl=en&hl=en&q=trends+in+global+gdp

Land based storage in terrestrial impoundments or tailings dams are the norm for the constraint of mine tailings. However, Martin and Davies (2000)[2] estimate that of the ~3500 active tailings impoundments worldwide,

> "major failures occur at a frequency of less than 2 to 5 per year (i.e. about 0.1%), and minor failures at a frequency of about 35 per year (i.e. 1%). While low, these figures are still unacceptably high."

Major failures can have extremely large and long-lived environmental and social consequencies (Section 1.2.3).

1.1.2 Environmental aspects of mine waste disposal.

There are three general concerns associated with mine waste disposal: cyanide toxicity (if cyanide is used in the process), heavy-metal contamination (especially from arsenic-bearing ores) and acid mine drainage.

Cyanide toxicity

The toxicity of cyanide is a result of the dissociation of metal cyanides to form hydrocyanic acid, HCN. In the case of gold plants, the metal cyanide in question is sodium cyanide, NaCN. The toxicity of cyanide for trout, given as a 96-h LC_{50}, may be as low as 0.05mg L^{-1} CN^{-}. There are a variety of methods for recovering or destroying cyanide in mine tailings, including natural degradation, ozonation, bacterial oxidation, the SO_2 process, acidification and ion exchange. Ritcey (2005) discusses each of these in some detail. In the case of the Lihir plant, detoxification is achieved by mixing the tailings with iron (Lihir Gold Ltd). This leads to the formation of the highly stable hexacyanoferrates $Fe[CN]_6^{4-}$ and $Fe[CN]_6^{3-}$; dissociation constants for these compounds are 10^{-35} and 10^{-42} respectively, compared with ~10^{-5} for sodium and potassium cyanides (CHEMINFO Database). The great stability of these iron complexes renders them much less likely to liberate free cyanide ions, and consequently far less toxic in the environment than the corresponding alkali metal species.

Heavy metal contamination

Heavy metals present in the tailings from the Lihir Mine include zinc, copper, cadmium, lead and mercury (Lihir Gold Ltd). However, one of the main impurities, as stated above, is arsenic, of which the Lihir ore contains between 0.05 and 0.2%, mainly in the form of arsenopyrite (Ketcham

---

[2] http://www.infomine.com/publications/docs/Martin2000.pdf

et al., 1993). The pressure-leach reaction for the oxidation of arsenopyrite is as follows (Fleming, 1992):

$$2FeAsS + 7O_2 + H_2SO_4 + 2H_2O \rightarrow Fe_2(SO_4)_3 + 2H_3AsO_4$$
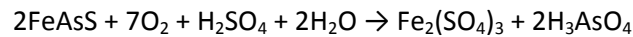
The sulphuric acid in this reaction is a by product of the pyrite oxidation reaction:

$$2FeS_2 + 7\tfrac{1}{2}O_2 + H_2O \rightarrow Fe_2(SO_4)_3 + H_2SO_4$$
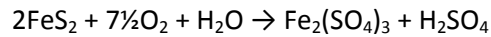
Arsenic acid, H_3AsO_4, liberated in the first of the above reactions is subsequently reprecipitated in the autoclave as ferric arsenate, $FeAsO_4$, which is very stable. Ritcey (2005) even refers to the deliberate precipitation of ferric arsenate as a way of removing arsenic from tailings before disposal. However, despite this stability, arsenic may still be liberated from the land-based tailings by the atmospheric weathering of ferric arsenate to form an iron carbonate, liberating the arsenic. Possible fates of tailings-derived ferric arsenate in the marine environment are unclear.

Acid mine drainage

Acid mine drainage is very much an issue associated with land-based tailings storage rather than submarine disposal. It occurs when waste sulphides – for example, various iron sulphides, sphalerite (ZnS), galena (PbS), and chalcopyrite ($CuFeS_2$) – are weathered in the terrestrial environment (Blowes *et al.*, 2007). In a pressure oxidation circuit the objective is usually to oxidize the vast majority (>98%) of the sulphide anyway. Accordingly, where whole-ore pressure oxidation is used, sulphides will be more associated with waste rock than with tailings *per se*. The reactions are similar to those exploited in the oxidative pre-treatment of refractory ores, although the oxidation is not always complete, resulting in ferrous rather than ferric sulphates:

$$FeS_2 + 3\tfrac{1}{2}O_2 + H_2O \rightarrow FeSO_4 + H_2SO_4$$
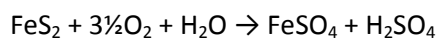
This liberation of sulphuric acid causes a significant drop in the pH of the tailings pile, which may give rise to a variety of environmental problems including the acidification of ground and surface waters, the liberation of heavy metals, and the release of cyanide from weak acid dissociable (WAD) cyanide species such as those of copper, zinc and nickel (Donato *et al.*, 2007). In this way, the third environmental concern discussed here, acid mine drainage, may actually be a causal factor in the first two.

1.1.3 Definition of DSTP

Mine wastes have been discharged to the sea at varying depths worldwide for many years, however, the concept of 'very deep' disposal of mine tailings in the marine environment was first proposed as an attractive option for disposal of mine waste in the scientific literature by Ellis and Ellis (1994). The concept of deep submarine tailings placement (DSTP) is based on discharge at the edge of an extended drop-off, to 1000 m or more, and at a depth below the euphotic zone (Ellis and Ellis, 1994). Discharge must be at a location where the tailings slurry from the pipeline will form a turbidity current flowing coherently with minimum discharge until it reaches the base of the drop-off. In principle, channels beyond fringing reefs are suitable sites (Figure 1.1.3.1). There must be very little or no risk at the site of hazardous amounts of tailings upwelling back into shallow water where toxic components may enter the food chain.

The general concepts of DSTP include:

- Discharge on the edge of an extended drop-off (to 1000 m or more)

- Discharge below the euphotic zone

- Discharge in the form of a coherent turbidity current which flows with minimum dispersal until it reaches the base of the drop-off.

- Minimal chance of tailings upwelling back into shallow water

The fundamental premise of DSTP is that tailings discharged at a depth below the euphotic zone form a stable plume which descends to the ocean floor. The tailings solids eventually deposit on the ocean floor as a footprint.

DSTP methodology involves removal of air bubbles from the tailings to reduce their buoyancy and prevent them from becoming entrained in the surface waters. If air is not removed from the tailings prior to discharge, as was the case at the Atlas Copper Mine in the Philippines, the tailings may form noticeable surface plumes. The tailings can either be de-aerated at a concentration plant, or at a de-aeration tank on the coast. Prior to de-aeration, the tailings are usually thickened to recycle water and process chemicals. The tailings may also be treated to remove process chemicals.
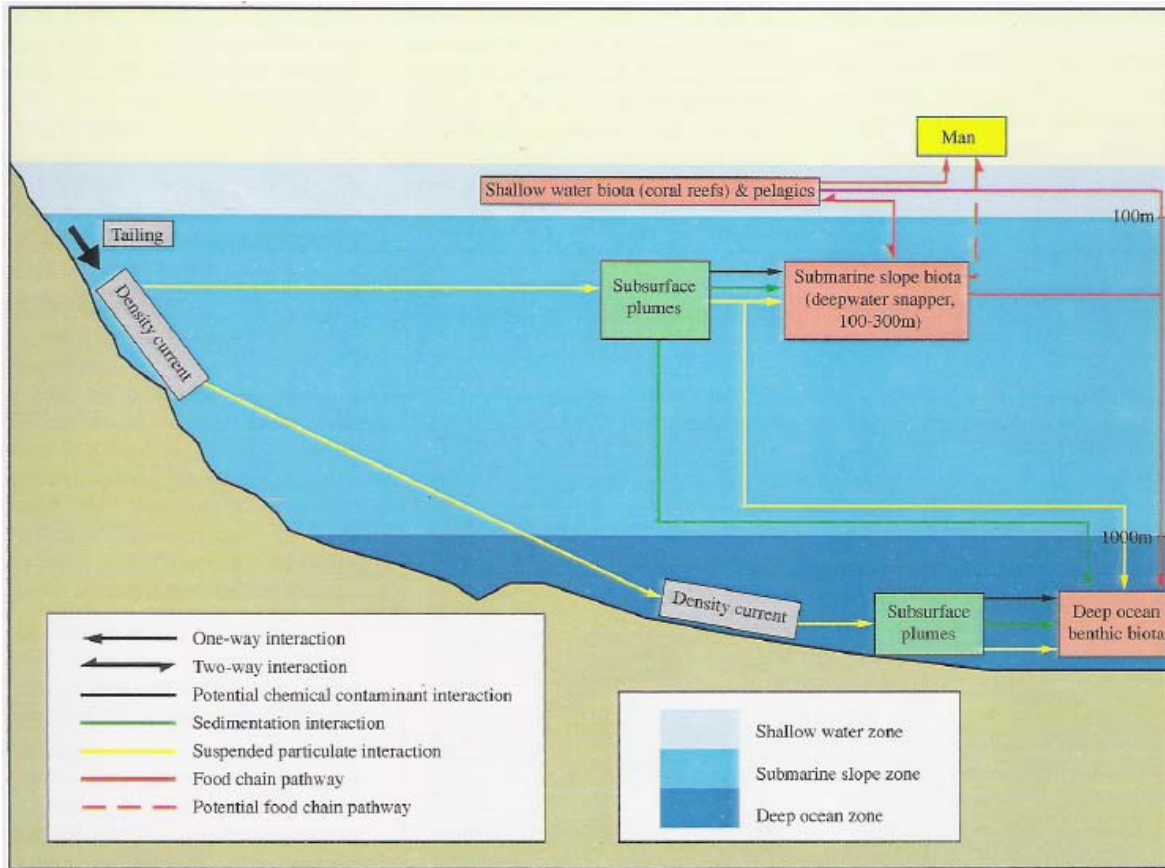
Figure 1.1.3.1 Simplified conceptual model of the major physical, chemical and biological interactions relevant to DSTP (source: NSR, 1997).

The tailings are then mixed with seawater pumped from an appropriate depth, so it is a suitable density and temperature, into a mixing tank. Mixing with seawater also has a coagulating action on the tailings slurry, and flocculants are broken up during the mixing process. However, because mixing tanks involve higher capital investment and maintenance costs, they are not always used, as was the case at Minahasa Raya in Indonesia.

The tailings pipeline should be located on a slope greater than 12 degrees to maintain a density current flow down the slope (IIED, 2002), allowing the tailings to flow to deeper areas, rather than accumulating at the outfall site. Discharge onto slopes less than this is likely to result in blockage of the pipeline, as occurred at Minahasa Raya, where the pipe discharged onto a 2 degree slope (Apte and Kwong, 2004).

The tailings are released from the pipe terminus as a high-velocity jet, which becomes diluted with seawater and dissipates with increasing distance from the pipeline due to entrainment of seawater and frictional losses (IIED, 2002). The mixture continues to descend along the seafloor

as long as it remains denser than the surrounding water, and the gradient is greater than 12 degrees.

As the tailings current becomes neutrally buoyant (attains the same density as the surrounding water), portions of the liquid phase separate from the solid phase, forming subsurface plumes. This can occur at any depth as the tailings current flows down the seafloor slope towards its final deposition area (IIED, 2002). The subsurface tailings plumes consist of fine suspended sediment particles, residual process chemicals, and trace metals. They are diluted relative to the initial tailings discharge, but have a higher turbidity compared to the surrounding water. Because of water stratification, the detached plumes remain within the depth zone where they separate from the main density current until they flocculate and settle out.

1.1.4 Global distribution of DSTP operations

Submarine tailings disposal has been utilised at a number of coastal mining sites around the world (Table 1.1.4.1). Mines that have, or are still, utilising 'deep' STP include Island Copper and Kitsault Mines in Canada, Black Angel in Greenland, Minahasa Raya in the Philippines, Cayeli Bakir in Turkey, Batu Hijau in Indonesia, and Misima and Lihir in PNG. Of these, the most detailed and accessible documentation detailing the STP system and environmental monitoring programmes are available for the decommissioned Canadian mines Island Copper and Kitsault.

Island Copper, British Columbia, Canada

The STP system at Island Copper Mine discharged a mean volume of 50,000 t tailings per day at a depth of 50 m into Rupert Inlet. The STP system was permitted following a public enquiry into the proposed system of disposal (Anon 1970; cited in Ellis, 2006). Submarine tailings discharge began in October 1971, and the mine closed in 1995. The mine company suggested that the tailings would flow down-slope and down-inlet from the discharge point in Rupert Inlet, into the deep basin (maximum depth of 165 m), with a final deposition zone below 100 m depth, where it would not be affected by strong tidal currents. The final deposition area was considerably greater than expected due to the strong tidal currents and a well-mixed water column. It was accepted that tailings deposition in the deep basin would adversely affect fauna below 100 m in the Inlet (see Burd, 2002 and papers cited therein).

Kitsault, British Columbia, Canada

For a period of 18 months from 6 April 1981 to 2 November 1982, approximately 4 M t of tailings from the Kitsault open-pit mine were discharged through a submarine disposal pipe at a depth of

50 m into Alice Arm, a steep-sided fjord with a maximum depth of 410 m. At the end of the discharge period, tailings accumulations of 120 cm were observed near the outfall, tapering to about 30 cm deep, 5 km down-inlet (McDonald and O'Brien, 1996). The distribution of metals in surface sediments shortly after mine closure implied that about half the area of Alice Arm (about 14 km^2 of the inlet floor) had been measurably affected by tailings, and that 7 km^2 were highly impacted (Odhiambo et al., 1996). In 1983, a large tailings slump transported about 50 cm depth of tailings near the outfall to the deep basin (Burd et al., 2000). It is likely that a second resuspension of the tailings also occurred between 1988 and 1990. Sediment accumulation rates and metal concentrations suggest that most of the deposited tailings remained within Alice Arm (Odhiambo et al., 1996).

Cayeli Bakir, Turkey

The DSTP system at Cayeli Bakir Mine is currently the world's longest and deepest submarine tailings outfall, discharging a combined effluent of tailings, mine water and sewage along a 3.5 km pipe to a depth of 350 m in the Black Sea. There is currently consideration to reduce the depth of the outfall from 350 m to 250 m (Berkun, 2005). The tailings are de-aerated and diluted with seawater taken from a depth of 15 m prior to discharge at a rate of 0.075 to 0.092 m^3 s^{-1} (Berkun 2005). The final tailings deposition zone is in anoxic water at a depth of > 2000 m. The Black Sea is a highly stratified inland sea with a large anoxic zone (90% of the water column), and a permanent pycnocline at depths of 35 to 150 m (Ivanov et al., 2001), which limits exchanges between surface and deep water. Concentrations of H$_2$S are greater than 3 mg L^{-1} in the anoxic layer, which helps to precipitate dissolved heavy metals (Ellis et al., 1994). Predictions of tailings flow and deposition by Rescan (1992a-c, cited in Berkun, 2005) indicated that there could be some separation of buoyant plumes comprising very fine tailings particles, which would be trapped within the deep anoxic zone and thus would not surface. Further calculations and tank experiments by Berkun (2005) confirmed that buoyant plumes could potentially separate from the main tailings plume prior to deposition, and that they could rise to about 89 m above the discharge depth.

Black Angel, Marmorilik, West Greenland

Black Angel was the first modern mine in the Western hemisphere to be located within the Arctic (Ellis et al., 1994). More than 8 M t of mine tailings were discharged into Affarlikassaa Fjord at a depth of 33 m. Affarlikassaa fjord is a small fjord (2 km^2) located in the inner part of the Uummannaq fjord system, which is separated from the larger Qaamarujuk fjord by a shallow sill 23 m deep. The fjord has an average water depth of 40 m and maximum depth of 65 m. The fjord

stratifies strongly in summer, but sea ice growth and density currents of heavy salt water over the sill from Qaamarujuk fjord, homogenise the water column during winter. Consequently, during winter, sediment contaminants (lead and zinc) were re-suspended and dispersed throughout Affarlikassaa fjord and over the sill into Qaamarujuk fjord.

Atlas Copper, Cebu Island, The Philippines

The submarine tailings discharge at Atlas Copper was located at a depth of 30 m. The targeted deposit area was at a depth of 350 m in the Tanon Channel, 1.5 km from the shore. A strong south easterly shoreline current was expected to disperse suspended slimes. Surveys indicated some shoreline deposition of tailings, which stabilised at 12 m below sea level in the area immediately below the discharge point (Salazar and Gonzales, 1973; Salazar and Dira, 1977; Dira and Canete, 1980). There was some evidence of deposition back to the discharge point, but no evidence of tailings surfacing on the beaches (Salazar and Gonzales, 1973).

Minahasa Raya, North Sulawesi, Indonesia

There is little information available of the STP system at Minahasa Raya Mine. During its seven years of operation, more than 4 M t of mine tailings were disposed of in Buyat Bay. The tailings were piped 5 miles into the bay to an outfall located at a depth of 82 m on a slope of 2 degrees. A pre-mine environmental impact assessment (Newmont, 1994) stated that the presence of a thermocline at a depth of 50 to 70 m would reduce mixing and spread of tailings. However, a number of later studies have failed to confirm the presence of a thermocline[3]. The depth of Buyat bay has reduced by 10 to 12 m at the pipe outfall, and upwelling currents and pipe breakages have dispersed tailings throughout most of the bay to a depth of 13 m, covering sea grass and coral reefs.

Batu Hijau, Sumbawa Island, Indonesia

The DSTP system at Batu Hijau involves the gravity flow of tailings via a pipeline from the process plant to a location 3.2 km offshore at a depth of 108 m. The tailings density current flows down a steep offshore canyon towards the Java Trench, with the final deposition zone located at a depth of 3000 to 4000 m. Quarterly monitoring of the tailings deposition area in 2002 confirmed that the tailings were travelling down the submarine slope and were not being deposited on the upper shelf area (Newmont, 2002).

---

[3] http://dte.gn.apc.org/63MIN1.HTM

Table 1.1.4.1 Mining systems using deep submarine tailings disposal (compiled from Apte and Kwong, 2004; Ellis, 2006)

Mine	Country	Years of Operation	Discharge depth (m)	Setting and deposition depth (m)
Island Copper Cu/Mo/Au	British Columbia Canada	1971 - 1995	30-50	Silled fjord > 100
Atlas Copper Cu	Cebu Island Philippines	1971 - 1988	10-30	Island strait 350 - >500
Wesfrob Fe/Cu	British Columbia, Canada	1967 - 1983	Not known	Tasu Sound
Black Angel Pb/Zn	Greenland	1973 - 1991	30	Shallow fjord ~80
Kitsault Mo	British Columbia Canada	1981 - 1982	50	Silled fjord >350
Misima Au/Ag	Misima Island Papua New Guinea	1988 - 2004	112	Deep basin ~1500
Sydvaranger Fe	Bokfjorden Norway	1975 - 1996	22	Fjord 220
Titania Ilmenite	Jossingfjord Norway	1960 - 1980	100	Fjord > 100
Cayeli Bakir Cu/Zn/Pb	Turkey	1994 -	385 then 275	Black Sea > 2000
Lihir Au	Lihir Island Papua New Guinea	1996 -	128	Submarine slope > 1000
Minahasa Raya Au	North Sulawesi Indonesia	1996 - 2004	82	Buyat Bay > 160
Batu Hijau Cu/Au	Sumbawa Island Indonesia	2000 -	108	Open ocean > 2000
Rana Gruber Fe	Norway	1964 -	15 then 50	Ranafjorden 700

(compiled from Apte and Kwong, 2004; Ellis, 2006)

1.1.5 Environmental studies on non-PNG DSTP operations

Island Copper, Canada

The environmental monitoring programme at Island Copper Mine, Rupert Inlet, represents the most extensive and long-term study of the extent and geographic range of effects and recovery from submarine tailings deposition. The monitoring programme involved baseline surveys prior to the mine opening, environmental impact studies to determine whether the conditions of the discharge permit were being met during the operation phase, and continued sampling following closure of the mine to monitor recovery (Burd, 2002; Ellis, 2006).

Parameters monitored included the following (Apte and Kwong 2004):

- Phytoplankton sampling at 7 stations (4 depths 3 times a year)

- Quarterly periphyton sampling at 16 stations

- Semi-annual zooplankton sampling at 4 stations

- Triplicate samples of benthic organisms from 24 stations every year

- Annual trapping of crabs and clams at 6 stations in June

- Annual collection of mussels at 5 stations in June

- Annual survey of tailings distribution by (a) marine sediment coring and analysis at 24 stations in March; and, (b) echo sounding survey at 18 stations in March

- Quarterly survey of suspended sediment distribution at 4 stations by (a) water sampling at 10 depths and (b) suspended sediment settling traps at 2 depths

- Quarterly water column profiling at 5 stations at 4 depths

The resulting data set is unique not only in the duration of the study, but also in the consistency of sampling (Burd, 2002). The sediment chemistry and benthic infaunal monitoring programme in Rupert Inlet was conducted annually or quarterly for 29 years, starting in January 1970 and finishing in September 1998. A government review of the monitoring data in 1978 confirmed that although impacts were apparent, they were acceptable, and no changes to the system were required (Waldichuk and Buchanan, 1978). In the 1970s, localised tailings plumes, driven by tidal

jets, deposited tailings on algal forests and in depressions in the rocky reefs in some of the shallow bays. At this time, it was considered that the muddy bottom benthos would be eliminated under the tailings deposits and that the plankton was at risk due to contamination and/or reduced photosynthesis caused by the higher turbidity (Ellis, 2006). However, throughout the 1980s and 1990s it became increasingly apparent that the marine ecosystem had some tolerance to the tailings discharge. Marine primary productivity (Kessler, 1986; cited in Ellis, 2006) and the plankton remained unaffected, and a crab fishery in the fjord maintained its yield throughout the mine operations (Island Copper Mine, 1970-1993; cited in Ellis, 2006). Changes in the tailings thickness and copper concentrations before, during, and after mining showed three distinct zones of impact below the discharge depth: near-field (< 5 km from outfall); mid-field (5-16 km); and far-field (20+ km; Burd, 2002). During mining operations, faunal declines occurred at sediment particulate copper concentrations > 300 µg g^{-1} and sediment tailings thickness > 15 to 20 cm (Burd 2002). Biomass and total taxa numbers showed a distinct decline in the near-field during mining operations, but within three years following closure, were returning to far-field conditions. Benthic species richness and composition, biomass, and indicator taxa were identified as useful for differentiating between affected and non-affected stations by Burd (2002).

Kitsault, British Columbia, Canada

Environmental monitoring in Alice Arm involved sediment organic and metal chemistry, benthic infauna, and tissue contamination surveys over 19 years, prior to and following 18 months of submarine tailings disposal from Kitsault Mine (Burd *et al.*, 2000). Changes in the benthic fauna and habitat after the tailings disposal were predictable in terms of the sediment chemistry and faunal recolonisation, however, recovery was not continuous due to instability of the tailings deposit and failure of the submarine slope. A large tailings slump on the submarine slope transported tailings to the deep basin, impeding recovery in the slump region and the deep basin. Three years after mine closure, declining metals concentrations in surface sediments were accompanied by considerable recovery of the fauna, although stations defaunated during mine operations could still be distinguished from all other stations (Burd *et al.*, 2000). Further resuspension of tailings between 1988 and 1990 coincided with a moderate decline in all macrofauna taxa. Dominant species patterns and biomass values indicate that the larger fauna take considerably longer than the smaller taxa to recover. The bivalve *Yoldia* spp. accumulated metals in a pattern similar to the sediment chemistry, indicating metals had entered the benthic food chain. Burd *et al.* (2000) concluded that it was not possible to differentiate between the affects of metal toxicity and physical disruption from the tailings on the benthic biota.

Cayeli Bakir, Turkey

Sampling at seven stations around the discharge point in the Black Sea began prior to, and continues during mine operations. The following parameters and elements are measured in the water column at discrete depths to 400 m: temperature, density, conductivity, light transmission, DO, H_2S, alkalinity, pH, Cu, Pb, Zn, Hg, Cd, Fe, Mn, As, TOC, DOC (Berkun, 2005).

Black Angel, Marmorilik, West Greenland

Environmental monitoring at Black Angel involved analysis of total metal concentrations in sediments and biota over time in both Affarlikassaa and Qaamarujuk fjord. Elevated concentrations of lead and zinc were detected in seaweed, blue mussels, and wolf fish liver and kidneys soon after mine operations began (Asmund *et al*., 1975; Bollingberg and Johansen, 1979; Ellis *et al*., 1994). Since the mines closure, metal contaminated biota (*Mytilus edulis*) have been documented up to 35 km from the inner part of Qaamarujuk fjord (Asmund *et al*., 1994). Foraminiferal stratigraphy in sediments cores taken in 1999, indicate that benthic foraminifera completely disappeared during mining operations and that re-colonisation began immediately after tailings disposal was stopped (Elberling *et al*., 2003). However, 10 years later, foraminifera species composition still did not indicate recovery of environmental conditions in the area.

Atlas Copper, Cebu Island, The Philippines

There is limited documentation of environmental monitoring at Atlas Mine. Salazar and Dira (1973), and Dira and Canete (1980), cited in Ellis *et al*. (1994), refer to government reports stating that benthos was absent in an area extending 3.5 km from the shoreline and 6 km either side of the pipe discharge parallel to the shoreline. The sampling equipment used for the benthic survey is not known. The government documents also reported no significant effect on plankton, and tested physical and chemical conditions were within ambient levels (cited in Ellis *et al*., 1994). In 1981, Alino (1983; cited in Ellis *et al*., 1994) found evidence of elevated sedimentation, metal contamination, reduced coral cover, and surfacing tailings.

Minahasa Raya, North Sulawesi, Indonesia

There is little information available on environmental monitoring of the STP system at Minahasa Raya, although independent studies have reported considerable contamination of Buyat Bay by mine tailings[4]. In particular, sediment concentrations of arsenic and mercury exceeded water

---

[4] http://dte.gn.apc.org/63MIN1.HTM

quality criteria. Arsenic and mercury concentrations were also high in benthic species, and concentrations in fish were suggested to pose an unacceptable risk to humans.

Batu Hijau, Sumbawa Island, Indonesia

Monitoring of the DSTP system at Batu Hijau comprises fourteen parameters, including tailings chemistry, water and sediment chemistry, tailings footprint and plume tracking that are monitored at frequencies ranging from daily to twice yearly (Newmont, 2002). In 2002, seawater copper concentrations at all sample locations were within background concentrations and below the limits established in the Indonesia Sea Garden Conservation for Marine Biota Standards (Newmont, 2002). Marine ecology programmes include coral reef, intertidal, deep water fish, benthic, and plankton studies. According to Newmont (2002) the results of these studies are consistent with predictions made during the environmental impact analysis.

1.2 Generic understanding of the environmental consequences of DSTP

1.2.1 Principal Environmental issues related to DSTP

The over-riding impact of deep-sea tailings discharges involves alteration of the physical environment due to the volume of waste material that is discharged, which smothers benthic organisms residing within the trajectory of the tailings density plume and inhabiting the final deposition area. This is particularly significant for sessile benthic organisms and organisms that move too slowly to escape being smothered. The extent of this impact can be difficult to predict given the lack of knowledge on specific marine benthic organisms. Secondary effects relate to the toxicity of both particulate metals and metals released from the tailings solids, and the effects of residual process chemicals in the tailing waste, which may result in acute or chronic effects on the organisms exposed.

Depending on the nature of the deposited tailings waste, the deposition footprint is likely to represent a very different habitat compared to the adjacent un-impacted seabed. Changes in grain size may affect both burrow dwellers and deposit feeders. A reduction in the particulate organic matter content will also reduce the general nutritional value of the solids material.

Overall, the following benthic impacts are likely:

- Alteration of the physical environment (smothering of the benthos).

- Changes in species composition/abundance and biodiversity.

- Increased metal bioaccumulation.

Following the cessation of mining, the tailings footprint environment becomes less dynamic, leading to changes in community structure and organism abundance but, as illustrated at Kitsault, following the cessation of mining operations, submarine slumps and re-suspension of unstable tailings deposits can impede recovery (Burd *et al*., 2000). Average natural sediment deposition rates are very low in the deep ocean. Thus, depending on the location of the tailings depository, it may take many thousands of years before the footprint zone is capped by an appreciable layer of natural sediments. There is a potential advantage in selecting ocean floor sites for DSTP that are subject to relatively high natural sediment deposition rates, as this would result in much quicker burial of tailing deposits following the cessation of mining activity (Apte and Kwong, 2004).

Studies conducted at the decommissioned Canadian mines Island Copper and Kitsault, indicate that recolonisation of the tailings surface will occur, but not necessarily with the same species that were originally present at the sites (Burd *et al*., 2000; Burd, 2002). Recovery of the larger infaunal species may be protracted.

Within the water column, increased turbidity and dissolved and particulate metal concentrations, will directly impact organisms in the vicinity of the mixing zone and the tailings density current. Surface tailings plumes resulting from pipeline failures and upwelling, and the formation of subsurface tailings plumes will also increase turbidity and metal concentrations in localized areas, potentially impacting shallow-reef and sea grass communities, pelagic communities and coastal fisheries.

The risk of potential biological impacts will depend on levels of turbidity and toxicity, the depth at which plumes form, and the sensitivity of marine organisms to these disturbances. The more mobile animals may be able to migrate from affected areas. Direct effects can include the flocculation of fine particulate material entrapping small organisms such as phytoplankton and larva at early stages of development. The trapped organisms will ultimately sink, transporting the particulate material to deeper depths. Fine particles will also clog fish gills and filtering mechanisms in other organisms. Given that primary productivity in the euphotic zone is a major source of organic carbon for the ocean floor, pelagic impacts may also indirectly affect benthic organisms.

Bio-accumulation of metals is likely to occur depending on the levels of metals or other potentially toxic elements in the tailings discharge, and trophic transfer of contaminants is possible. Larger

zooplankton that ingest tailings particles will increase their specific gravity and have to expend more energy to maintain buoyancy, and species that undergo daily vertical migrations may increase the speed and efficiency of contaminant transport from the surface waters to epipelagic and mesopelagic environments, and the benthos.

The potential impacts on shallow water organisims after accident or upwelling are (Apte and Kwong 2004):

- Local decreases in primary productivity as a result of increased turbidity

- Local acute toxicity of dissolved metals, particulate metals, process chemicals

- Chronic/sublethal effects of metals on organisms

- Metal bioaccumulation leading to increased trophic transfer of metals

- Habitat alteration (e.g. increased turbidity, smothering of coral reefs)

- Changes in species composition/abundance

- Changes in biodiversity

- Reduction in food availability

- Effect of fine particles on organisms: e.g. clogging of gills and feeding mechanisms

- Local effects of increased turbidity on organisms that utilise bioluminescence

- Increased productivity due to iron or other nutrient availability.

While the recovery of pelagic environments following cessation of mining is likely to be rapid, more long lasting impacts are expected for benthic organisms.

Risk assessments need to include predictions of where and under what conditions surface and subsurface plumes are likely to develop, their turbidity, toxicity and toxicant leaching potential, as well as potential mixing zone impacts. Unforeseen natural events, such as typhoons and storms, submarine slumps, and operational failures also have the potential to impact shallow coastal waters, reefs and fisheries. Operational failures can arise due to blockage of seawater intakes by

marine organisms, air entering the tailings pipe, and submarine landslides damaging the tailings pipe (Misima Mines Ltd, 2001, IIED, 2002).

1.2.2 Environments where DSTP is a feasible disposal option

None of the tailings disposal options currently available to the mining industry come without some risk of environmental impact. The case for DSTP as a feasible disposal option should only be justified following extensive analysis of the various disposal options available, including terrestrial tailings disposal. Risk-based assessments of DSTP versus terrestrial tailings disposal should include the environmental, social, and economic issues involved.

Some environmental criteria for potential DSTP sites that have been suggested include:

1.   Accessibility to the coast: tailings can be piped overland providing the topography is suitable (at Batu Hijau the tailings are piped 16 km overland to the coast; the Ramu Nickel project involves a 134 km pipeline between mine and coastal processing plant).

2.   Suitable bathymetry and physical oceanography: steep submarine slopes, submarine canyons, or naturally-excised channels beyond fringing coral reefs near-shore, which allow generation of a density current flowing to a deep deposition site. The slope angle should be greater than 12 degrees to prevent build-up of tailings at the pipe outfall.

3.   Silled fjord or other embayment enclosing a deep basin with side formation allowing development of a tailings density current, and of sufficient volume to ensure tailings are contained below the euphotic zone.

4.   The pipeline discharge depth should be at depths greater than the maximum depth of the surface mixed layer, euphotic zone, and the upwelling zone. Placing tailings below these zones maximises their stable deposition on the seafloor. Due to seasonal changes of the depths of these zones, it is the maximum depth of the euphotic zone that has to be estimated accordingly and used.

5.   Absence of upwelling or seasonal overturning: to reduce tailings resuspension into the euphotic zone.

6.   Siting in a low energy environment to reduce the likelihood of pipe breaks, allow the tailings discharge to form a density current, reduce the formation of sub-surface tailings plumes

and re-suspension of deposited tailings. Ocean currents and waves have to be considered, including the possibility of typhoons and other storm events. The entry point of the pipe into the sea and its location are important to maintain pipeline integrity and avoid breakage problems. Sheltered sites are preferable and adequate pipe material must be used.

7.   The receiving deep water environment should be a soft bottom depositional area.

8.   Anoxic sediment conditions: low oxygen results in reducing conditions within the tailings by sulphate reducing bacteria, hence minimising trace toxin leaching (at Cayeli Bakir tailings are disposed of in the anoxic zone in the Black sea).

9.   Low productivity environments: to reduce the potential impact on resources, such as fisheries, utilised by the locals. If other resources are present they must either not be impacted, or there must be potential for their recovery in ways that are socially acceptable to local people, or the locals must be compensated for the loss of the resource (Ellis *et al*., 1994).

Given the above, suitable sites for very deep STP are restricted to some oceanic islands and archipelagos where very deep water occurs close to shore. These criteria occur at many potential mine sites in Indonesia, the Philippines and Papua New Guinea.

1.2.3 Alternatives to DSTP

Alternative tailings disposal systems include:

1.   Terrestrial disposal: placement of tailings on land in dams

2.   Riverine disposal

3.   Near-shore marine disposal

The following examples detail some of the potential problems and environmental impacts that can arise at mines utilising alternative tailings disposal systems to DSTP.

1.2.3.1 Terrestrial disposal

Marcopper Mine, Marinduque, The Philippines (1969 -1996)

Terrestrial storage of tailings waste in dams involves continuous monitoring and post-mine remediation to ensure the integrity of the dam structure and prevent catastrophic failure and tailings spills into local waterways, as occurred in 1996 at Marcopper mine (Plumlee *et al*., 2000).

Marcopper utilised a number of tailings disposal options including tailings impoundment on land, near-shore disposal, and backfilling of an old open mining pit (the Tapian open pit). Backfilling of the old pit required plugging a de-watering tunnel that had drained the pit into the Makulapnit River. In 1996, the plug in the drainage adit failed, releasing 1.5 to 3 Mm^3 of sulphidic tailings slurry into the Makulapnit River, Boac River, and eventually the ocean to the west coast of the island. Tailings were deposited along the rivers, on the floodplain, and in the ocean at and near the Boac River mouth. Following the tailings spill the drainage adit was re-plugged to prevent further discharge of tailings in to the river. Consequently, the water level in the pit (and a second mine pit) began to rise, presenting the possibility of a potential over-flow into the river system, or another failure of the drainage adit due to increasing pressure from the pit waters (Plumlee *et al*., 2000). The acidic, metal contaminated pit waters may also migrate into the groundwater, affecting the water quality in domestic wells and local springs.

1.2.3.2 Riverine disposal

Bouganville Copper Mine, PNG (1972 - 1989)

Bouganville copper mine was a large and very profitable open pit mine that utilised riverine disposal of its mine tailings waste. The mine was located 20 km from the nearest coast in mountainous terrain and discharged 130,000 t per day of tailings waste into the Kawerong River, which then flowed into the Jaba River and across a coastal plain before reaching the shallow Empress Augusta Bay. The tailings partially silted out two major basins and were deposited on the coastal plain during flooding, destroying fisheries and agricultural land. In the shallow Empress Augusta Bay, the tailings formed an extensive delta. Communities downstream of the mine had to be compensated and many were relocated. The deposited tailings have caused substantial and long-lasting environmental problems. In 1990, the mine was abandoned due to civil unrest.

Ok Tedi Mine, PNG (1984 -)[5]

Ok Tedi gold and copper mine is too far inland in mountainous terrain to utilise appropriate near-shore bathymetry for submarine disposal of its mine tailings. Consequently, since 1984, the mine has disposed of 80 Mt of mine tailings into the Fly River system each year. The discharge has caused widespread and diverse harm, both environmentally and socially, to the 50,000 people who live in the 120 villages downstream of the mine. Chemicals from the tailings have killed and contaminated fish, which subsequently caused harm to all animal species that live in the area as well as the indigenous people. The dumping has changed the riverbed, causing a relatively deep

---

[5] www.wri.org/wr2002 World Resources 2002–2004: Decisions for the Earth:Balance, Voice, and Power

and slow river to become shallower and develop rapids, thereby disrupting indigenous transportation routes. Flooding caused by the raised riverbed has left a thick layer of contaminated mud on the flood plain plantations of taro, bananas and sago palm that are the staples of the local diet. About 1300 km^2 of land have been damaged due to the disposal and accumulation of disposed tailings in the river system.

The reasons for the environmental disaster at Ok Tedi are complex. The original plans included an Environmental Impact Statement that called for a tailings dam to be built near the mine. This would allow heavy metals and solid particles to settle, before releasing the clean 'high-water' into the river system where remaining contaminants would be diluted. But the plan was seriously flawed, and in 1984 an earthquake caused the half-built dam to collapse. The company continued mining operations without completing the dam, initially because of the expense involved to rebuild it. Subsequently, the PNG government decided a dam was not necessary.

The system of land ownership in PNG complicates matters further. Most of the land in PNG is held under a complex system of native title, with ownership divided amongst a huge number of small clans, while the central government retains control over how resources that lie under the ground are used. The 2000 members of the clan that held ownership of the land on which Ok Tedi is located were included in the formal negotiations and were compensated with cash, jobs, and infrastructure (schools, health care, etc.), but the indigenous communities living downstream from the mine were not consulted, and received none of the benefits.

1.2.3.3 Near-shore disposal

Jordan River Copper Mine, British Columbia, Canada (1972 - 1974)

Jordon River disposed of its mine tailings waste through a pipeline that discharged at a depth of 12 m onto a wave-exposed, high-energy, gently sloping near-shore shelf. The pipeline was laid over the beach and sub-tidal shelf, and anchored by concrete blocks, rather than being buried in a trench, as was originally planned. The pipeline broke several times, and for most of the mine's operational period, tailings were discharged at low tide level from the broken end of the pipe. During very low spring tides the outfall and surrounding tailings were exposed. Longshore drift and wave action formed a near-shore deposit of metal contaminated mine tailings, and there was extensive smothering of algal beds and rocky shore organisms (Ellis *et al*., 1994).

1.3 Background and rationale for the present work

1.3.1 Mining Sector Support programme

The Mining Sector Support Programme's (MSSP) overall objectives are to sustain the country's economic performance through mineral production and exports and to alleviate poverty, increase employment opportunities and mitigate mine-induced environmental impacts.

Its specific purpose is to enhance institutional capacities to effectively promote and regulate the mineral resource sector in order to reverse the current trend of reduced private-sector mineral exploration. It aims at improving geo-scientific data acquisition, conservation, processing and dissemination, enhancing small-scale miners' capacity and improving mining environment monitoring and protection.

Project B: Independent evaluation of Deep Sea Tailings Placement in PNG

The purpose of Project B is an evaluation of existing deep-sea tailings placement (DSTP) practice in order to establish a consensual, clear, environmentally defensible, enforceable policy on the disposal of Deep Sea Tailings in PNG, thus decreasing uncertainties for prospective investors in PNG, and creating greater legitimacy for the mining industry.

In addition, this project will improve the capacity of PNG's authorities to manage the environmental impact of deep sea tailings placement and select the best mine waste disposal technology and sites. Iniitially focussed at the operating DSTP at Lihir and the closed DSTP at Misima, the project was extended to consider baseline conditions at a newly proposed DSTP (Basamuk)

The project brief involved:

- Compilation of all existing information on the operational and closed mining operations using DSTP in PNG (Lihir, Misima), from Mining Companies, Department of Environment and Conservation (DEC), Research Institutes and scientific publications.

- Collation of all the work done on monitoring and research of the DSTP activity, together with data on the methods employed and models used.

- Analysis of data and an evaluation of the work done to date, and of the reliability and completeness of the results.

- Identification of existing monitoring paramteres and those that require to be monitored.

- Formulation of a programme of further fieldwork (at Misima and Lihir) and analysis to rectify any shortcomings or gaps.

- Implimentation of new fieldwork, which will involve a research cruise to Lihir and Misima Islands and subsequently to the Rai coast at Basamuk.

- Drafting of guidelines; the conclusions from the cumulative database will be drafted as: (a) preliminary guidelines for the improvements of the Lihir environmental studies including the technical assessment of, the impact, techniques used; (b) general guidelines and criteria for future mining and post mining operations in PNG involving DSTP. The drafted guidelines will be submitted to the stakeholders to comment on.

- Holding of an international workshop/conference on DSTP practices and environmental monitoring.

- Finalising guidelines. Preparation of a report including the following apects: 1) the technical assessment of the impact, which DSTP techniques can be improved or are not acceptable; 2) recommendations on improvement of environmental performances and reduction of impact; 3) general guidelines and criteria for future mining operations in PNG involving DSTP.

1.3.2 Aims and Objectives of Mining Sector Support Programme (MSSP)

1.3.2.1 Overall Objective of MSSP

The overall objective of the MSSP is to increase foreign investment in PNG's mineral sector, with special emphasis on mineral exploration expenditures. This in turn will lead to the development of the country's infrastructure and the exploitation of the mineral resources of the country.

1.3.2.2 Specific Objectives of DSTP Project

The expected results of Project B are;

- To critically evaluate the present environmental monitoring results of DSTP in PNG focussing on Lihir and Misima investigations,

- To identify shortcomings and to identify tasks for a better understanding of the marine environmental impact of DSTP resulting in advanced strategies and guidelines for present environmental studies involving DSTP,

- To execute oceanographic investigations with a vessel in two areas of PNG (Lihir, Misima),

- To provide a data base, protocols and models (numerical, qualitative) to DoM and DEC for future DSTP related investigations,

- To provide guidelines for future DSTP practice in PNG,

- To suggest future strategies considering indicators for environmental monitoring in the post-closure monitoring phase,

- To provide a comprehensive report and archived data sets on completion of the project, including an analysis and interpretation of the results,

- To hold an international workshop in PNG at the end of the project,

- To provide on the job training for DEC and DoM/MRA officers.

2. An environmental baseline: the Basamuk Study

2.1 Ramu and the Basamuk DSTP plans

Ramu NiCo Management (MCC) Limited is developing the Ramu Nickel Project, which is located approximately 75 km west-south-west of Madang, in Madang Province, Papua New Guinea (PNG). The project will mine lateritic ores, which will be processed to produce a mixed nickel and cobalt sulfide for market (ENESAR, 2007, Environmental Baseline Report).

The project will comprise:

• A series of shallow open-cut mine pits and a beneficiation plant to produce ore slurry feedstock at Kurumbukari.

• A slurry pipeline approximately 134 km long to transport the ore slurry from the Kurumbukari mine site eastwards to the process plant at Basamuk on the Rai Coast.

• At Basamuk, a process plant to produce a mixed nickel-cobalt sulfide as an intermediate product. Components of this process plant include: acid plant, hydrogen sulfide plant, lime plant, power station, wharf, limestone quarry and accommodation area.

Tailings will be disposed by deep sea tailing placement (DSTP) on the ocean floor of the Vitiaz Basin immediately north of the refinery site discharging into the head of an offshore canyon, the Basamuk Canyon, in water depths of 150 m.

2.2 Environmental Background

2.2.1 Geomorphology

The Basamuk site occurs on the Rai coast of the Vitiaz Straits. This region of Papua New Guinea is notable as one of the most geologically active regions in the world. The raised beaches of Huon Peninsula are a world-renowned example of the rapid tectonic uplift the region has experienced. High rainfall combined with the proximity of the Finnisterre mountain range provides large volumes of sediment (estimated at 80 Mt p.a. (NSR, 1999)) carried by rivers to the coast. The Rai coast itself is bisected by rivers such as the Yaganon and Gowar. The sediments from these rivers are carried into the sea and have deeply eroded canyons in water depths from 100-800 m on the steep continental slope. In deeper water beyond 800 m the erosional v-profile canyons broaden into more depositional flat-floored turbidity channels suppling sediments into the Vitiaz Basin. It has been estimated that the Vitiaz Basin contains deep-water sediments approximately 2 km thick

(Milliman, 1995), mostly the product of down-slope sedimentation of terrestrial origin. Most significant sedimentation occurs at the base of slope between 1000-1600m water depths (NSR, 1999).

2.2.2 Physical Oceanography

Location

The northern and eastern sides of the PNG archipelago are mainly tectonic and consequently the bathymetry is typically very steep so that very deep waters can be found very close to the coast.

Tides

Tidal elevation stations in the region are sparse, although the variation in tidal range over the region is fairly small, and the OTIS (Oregon Tidal Inversion Software) web site (see also Egbert and Erofeeva, 2002) suggests that maximum range anywhere in the region is likely to be less than 1.2 m. This is of similar magnitude to the interannual variability in sea level due to ENSO events (see below).

For a number of reasons, mainly related to the effects of bathymetry, the amplitudes of tidal currents in shallow waters are much more difficult to estimate than elevation. Thus although one can be confident that deepwater currents in the region are small of order 1 cm s^{-1}, around islands, in narrow channels and over reefs they can reach speeds as high as 2.5 m s^{-1} (Admiralty, 1988).

Climate and Meteorology

In general the mean monthly wind stress throughout the region is weak, generally < 0.05 Pascal (Pa), which is equivalent to a wind speed of about 5 m s^{-1} (Hellerman and Rosenstein, 1983). According to Admiralty (1988) the SE Monsoon, with wind speeds of up to 5 m s^{-1}, predominates in equatorial regions between June and October. From November onwards the NW monsoon (wind speeds again $\sim 5 \text{ m s}^{-1}$) migrates progressively southward from the equator to about 10° S. Between these two regions lies the Intertropical Convergence Zone (ITCZ) an equatorial band of very light winds with high precipitation. Throughout the PNG archipelago, lying as it does just south of the equator, cyclones (with wind speeds up to gale force) are rare.

The region is one of high evaporation and high precipitation, with the heaviest rainfalls being experienced very locally over the higher land of the larger islands.

Ocean circulation

Papua New Guinea lies at the western end of the 14,000 km stretch of the Equatorial Pacific. Thus the forces that drive the circulation of water in the region are to be found at (or integrated over) very large distances.

The seasonal variation in the surface currents in the Equatorial Pacific just east of the region is given from the syntheses of the tracks of surface drifters (with drogues set at 15 m) available from the Global Drifter Center[6]. They suggest that mean surface transport is ~10 cm s^{-1} towards the west both to the north, and to the south, of Papua New Guinea. Along the north coast of PNG there is a north-westward current (the New Guinea Coastal Current, NGCC) with speeds of between 0.4 and 0.7 m s^{-1} at a depth of 200 m and transports of up to 8 Sv in the Vitiaz Strait. In the surface waters this current can be reversed during the NW monsoon (Tsuchiya *et al.*, 1989) (Figures 2.2.2.1; 2.2.2.2).
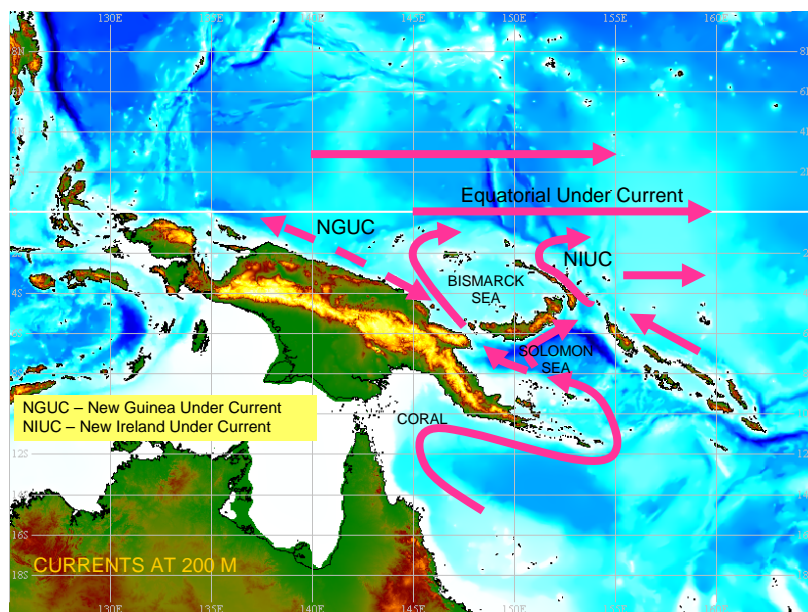
Figure 2.2.2.1 Mean circulation at 200 m in the Western Equatorial Pacific. (Based on Tsuchiya *et al.*, 1989)

---

[6] www.aoml.noaa.gov/phod/dac/gdp.html
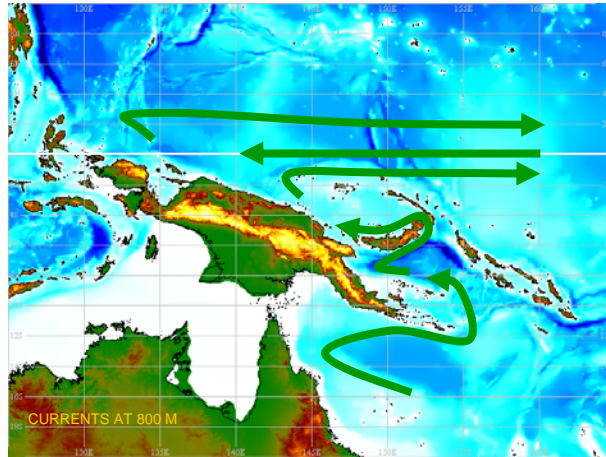
Figure 2.2.2.2. Mean circulation at 800 m in the Western Equatorial Pacific. (Based on Zenk, 2005)

Ocean Stratification

Given the relatively weak winds one would expect the surface waters of the Equatorial Pacific to be fairly uniformly stratified, at least when averaged over a period of order one month. Density anomaly (σ_θ, where σ_θ = ρ-1000 kg m^{-3}, and ρ is the density of a parcel of water that has been brought from depth to the surface) sections across the Equator between 6° S and 8° N at 156° E from the Tropical Atmosphere Ocean project (TAO) (www.pmel.noaa.gov/tao/) reveal that this is roughly the case. At and south of the Equator to 5° S, σ_θ increases with depth from about 21 kg m^{-3} at the surface to 25 kg m^{-3} at about 175 m in the boreal winter (January to March) and to about 150 m in the boreal summer (July to September). This uniformity in the surface density gradient is not repeated in the gradients of temperature and salinity. The upper 100 m are nearly isothermal, ranging from 30.5° C at the surface to 29° C at 100 m in winter, to 29° C at the surface to 28° C at about 90 m in the summer. By contrast, surface salinities south of the Equator increase almost uniformly from about 34.8 at the surface to > 35.8 at 200 m in winter, and from 34.5 at the surface to > 35.8 at 150 m in summer. Below these maxima, salinity decreases rapidly with depth to 300 m where the salinity is 35.0 (winter) to 34.8 (summer).

El Niño Southern Oscillation

It has long been recognised that the surface waters of the Equatorial Pacific go through periodic changes in structure that have wide ranging climate implications for the countries that border the Pacific. Known originally as 'El Niño', a more comprehensive title that includes atmospheric effects is the El Niño Southern Oscillation (ENSO). In normal years, trade winds blow westward so that warm surface water piles up downwind making the sea surface about 0.5 m higher at

Indonesia than at Peru. During El Niño years the trade winds relax and the thermocline in the western Pacific is depressed, whilst that in the east is raised. Droughts accompany the fall in sea level in the western Pacific. The most recent El Niños occurred during 1986-7, 1991-4 and 1997-8.

The effect of latitude

In most parts of the world large scale ocean processes are strongly influenced by the Earth's rotation, which results in an acceleration given by $f=2\Pi\sin\phi/(12*3600)$ s^{-1} where ϕ is latitude. This acceleration allows large horizontal pressure gradients (through sloping density surfaces) to exist because they can be balanced by ocean currents. An important parameter is the internal Rossby radius, *a*, which is used as measure of the distance over which a topographic feature affects water movement around it. Its definition is $a = c/f$ where $c = g\Delta\rho/(\rho D\pi^2)$; *g* is gravitational acceleration; $\Delta\rho$ and ρ are the top to bottom inherent density difference and mean inherent density respectively; and *D* is the total depth of water. For typical values of *g* and ρ and assuming $\Delta\rho = 10$ kg m^{-3} and $D = 1000$ m gives $c \sim 3$ m s^{-1}. At the latitude of PNG *f* is small and *a* can be up to 400 km (at 3° S), so that estimates of geostrophic currents from CTD density sections (a normal oceanographic practice elsewhere) are likely to be unreliable. Thus, for example, the geostrophic calculations of Butt and Lindstrom (1994) bear little semblance to their direct current observations made off Lihir.

2.2.3 Sediments

Preliminary sediment sampling and analyses were conducted by Enesar Consulting Ltd (2006) and Coffey Natural Systems (2007). During these projects, on behalf of Ramu Nickel Ltd, the area offshore from Basamuk, Saidor and the adjacent Vitiaz basin were sampled using a box corer. The sediments were found to be soft brown and grey-black silts. Horizons of black sands and clays were also encountered with plant debris common throughout. These were interpreted as being indicative of sediment supply from the coast becoming remobilised down-slope as density currents on the steep margin.

2.2.4 Benthos

Deep-sea benthic biological research in the Bismarck Sea is limited to studies of the rich hydrothermal vent faunas of the Manus Basin, west of New Ireland (Galkin, 1992; Bruns *et al.*, 1997; Erickson *et al.*, 2009). These communities occupy a very different environment to that likely to occur along the Rai coast and are not discussed further here. The continental margin along the Rai coast is steep, with numerous deeply-incised canyons channeling large volumes of terrigenous

sediment into the Vitiaz Basin. Studies of deep-water canyons in other parts of the world show that canyon sediments are often enriched in organic matter as a result of the accumulation and "funneling" of detritus from the coastal zone (Vetter and Dayton, 1999; Garcia *et al*., 2007). Off the coast of California, organic enrichment by kelp and seagrass debris in the Scripps and La Jolla Canyons was reflected in higher macrofaunal density and biomass than on the adjacent continental slope (Vetter and Dayton, 1998). In contrast, meiofaunal abundance in the Nazaré Canyon off Portugal was depressed in canyon sediments, possibly as a result of frequent disturbance by sediment slides and turbidity flows (Garcia *et al*., 2007). Sediment stability and the frequency of severe disturbance events probably dictate whether canyons are more or less biologically productive than adjacent continental slopes. The Rai coast is located in a tectonically-active region, which may mean that such events occur at high frequency. In addition, the organic matter entering the canyons is likely to consist largely of woody terrestrial detritus, which is highly refractory and of limited nutritional value to most benthic animals. In combination, these factors would lead to the prediction of relatively low benthic standing stock in the canyons around Basamuk, with communities dominated by a small number of opportunistic taxa capable of rapid recolonization after disturbance events.

2.2.5 Pelagic ecosystem

The main ecological concerns regarding disposal of mine waste into the marine environment are: (1) the potential uptake of bioavailable trace metals into the tissues of marine organisms, (2) bio-accumulation of these metals through food webs and into humans, (3) potential reduction in biodiversity and abundance of marine communities (Brewer *et al*., 2007). Most studies of these effects have focused on benthic communities and relatively little information is available on the impacts of DSTP on pelagic communities, even though components of these communities (especially fish) are likely to be eaten by humans (Brewer *et al*., 2007).

Marine pelagic communities comprise the following functional groups of organisms: the phytoplankton (plants), bacterioplankton (bacteria), protozooplantkon (herbivores and bacterivores), metazoan zooplankton (herbivores and carnivores), fish (herbivores and carnivores) and other higher predators including molluscs (squid), reptiles (turtles) and mammals (whales and dophins). Little information is available on the effects of DSTP on most of these groups except fish; however, a range of impacts can be anticipated. Impacts on phytoplankton may derive from enhanced heavy metals concentrations or from altered levels of photosynthetically available radiation and inorganic nutrient concentrations; however to our knowledge only one study, undertaken in temperate waters, has investigated effects of DSTP on phytoplankton primary

production (Kessler, 1986). Impacts on heterotrophic pelagic organisms are likely to derive from altered system productivity and bio-accumulation of heavy metals. The latter have been investigated in fish from tropical environments including studies from coastal waters of Papua New Guinea offshore from Lihir Island Group (Brewer *et al.*, 2007) and Bougainville Island (Powell and Powell, 2001) which observed little DSTP derived bio-accumulaton of heavy metals. It should be noted that the effects of DSTP on pelagic organisms may be relatively more difficult to discern in low productivity (i.e. oligotrophic) tropical environments due to potentially slower organism/community/ecosystem response.

2.3 Methods

2.3.1 Cruise Summary

The purpose of the field work was to collect physical oceanographic, sedimentological, geochemical, plankton/nekton and benthic biological samples and data with the specific objective of providing a baseline study of the environment before the Basamuk pipeline is established.

The cruise took place in the Vitiaz Basin and Rai Coast from 31st August to 2nd October 2008 using the MV Miss Rankin equipped with a winch and crane supplied by Lihir Gold Limited. The sampling programme included the collection of 198 sediment cores for chemical and biological analysis from 13 stations. At 9 stations, sediment cores were processed to extract pore-water which was collected to provide samples for nutrient and dissolved metal analysis. Water column sampling included 72 CTD casts, collection of 84 suspended particulate material samples (SPM) from 10 stations and completion of 36 zooplankton (day and night) casts at 2 stations. In addition, the water column was sampled to provide nutrient, chlorophyll and salinity samples for calibration of the CTD sensors.

2.3.2 Bathymetry and Acoustic Character

In addition to the above sediment and water column sampling, seabed surveys were conducted using the Mk III Echotrack 12 kHz echo-sounder. All stations were subject to a brief echo-sounder survey to enable the corer to be safely deployed in a known water depth. Also obtained were longer echo-sounder profiles used to develop a working model of the seabed morphology. Typically these profiles were up to 10 km long and run either perpendicular or parallel to the slope.

Seabed photographs were taken at 5 stations, 2 from the proposed pipeline transect and three from the eastern control transect.

2.3.3 Physical Oceanography

CTD data were collected using a Seabird instrument equipped with a carousel of twelve 5-litre bottles and with sensors for light transmission, oxygen, fluorescence, depth, conductivity and temperature (Figure 2.3.3.1, Table 2.3.3.1). Typically the instrument was deployed to a depth of 5 m and then switched to the pump for the sensors. Once the pump was activated the instrument was raised to just below the water surface and the data acquisition commenced. The rate of descent was kept to 0.5 ms^{-1} for the first 100 m and then approximately 0.75 ms^{-1} until close to the bottom. In general the descent was halted about 20 m from the sea bed. Bottles were fired on the up-cast at depths determined by the display of sensor data indicating water-column features of interest.

Figure 2.3.3.1 CTD water bottles rosette and sensor carousel

Oxygen calibration

The CTD oxygen sensor was calibrated at stations J8, BP2 and BC3 using quintuplet analyses of standard followed by quintuplet analysis of water from 3 water depths of apparently significantly different oxygen concentration. Samples were drawn from the CTD bottles (one bottle per depth) directly into oxygen sample bottles of known volume using a silicon tube after excluding all bubbles. They were then immediately fixed by the addition of manganese sulphate and alkaline iodide and then stored under water in an air conditioned room prior to analysis. Analysis was carried out using the standard Winkler method using an auto-titrator with potentiometric

endpoint detection. The thiosulphate secondary standard was titrated against an iodate primary standard.

Table 2.3.3.1 The CTD sensors

Sensor	Manufacturer	units
Pressure	Digiquartz	db
Temperature	Seabird SBE	ITS-90, ° C
Conductivity	Seabird SBE	mS cm^{-1}
Oxygen	Seabird SBE 43	mg L^{-1}
Beam attenuation	Chelsea/Seatech/Wetlab CStar	m^{-1}
Beam attenuation	Chelsea/Seatech/Wetlab CStar	%
Fluorescence	Wetlab ECO-AFL/FL	volts

Salinity calibration sample collection

Salinity samples were taken from the CTD at different depths within a cast. The depths were chosen to reflect different salinity values as indicated by the salinity sensor. The water samples were placed into calibrated, numbered glass bottles. Each bottle was rinsed 5 times with water from the CTD bottle before finally filling to the top with water. The bottles were then sealed and stored for return to the laboratory for analysis.

The method of salinity calibration is described in the attached appendix 2A. When outliers were removed a credible calibration was achieved from the remaining 99 samples with (see Figure 2.3.3.2)

$$S(cor) = S(raw) \times 0.9981 + 0.0721 \ (R^2 = 0.9997)$$
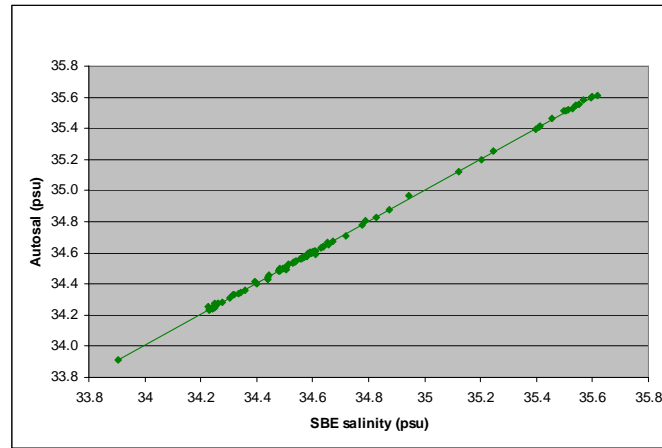
Figure 2.3.2.2 Salinity calibration for the Basamuk survey

2.3.4 Stations selected

Three sampling transects in the Vitiaz Basin were occupied: Astrolabe Bay (AB Stations), Basamuk Pipeline (BP Stations) and an Eastern Control (BC stations) and a single control station, (BC12) was occupied off Helmholtz Point (Figure 2.3.4.1). In addition, a near-coast CTD transect was also obtained (J stations, shown unlabled in Figure 2.3.4.1).
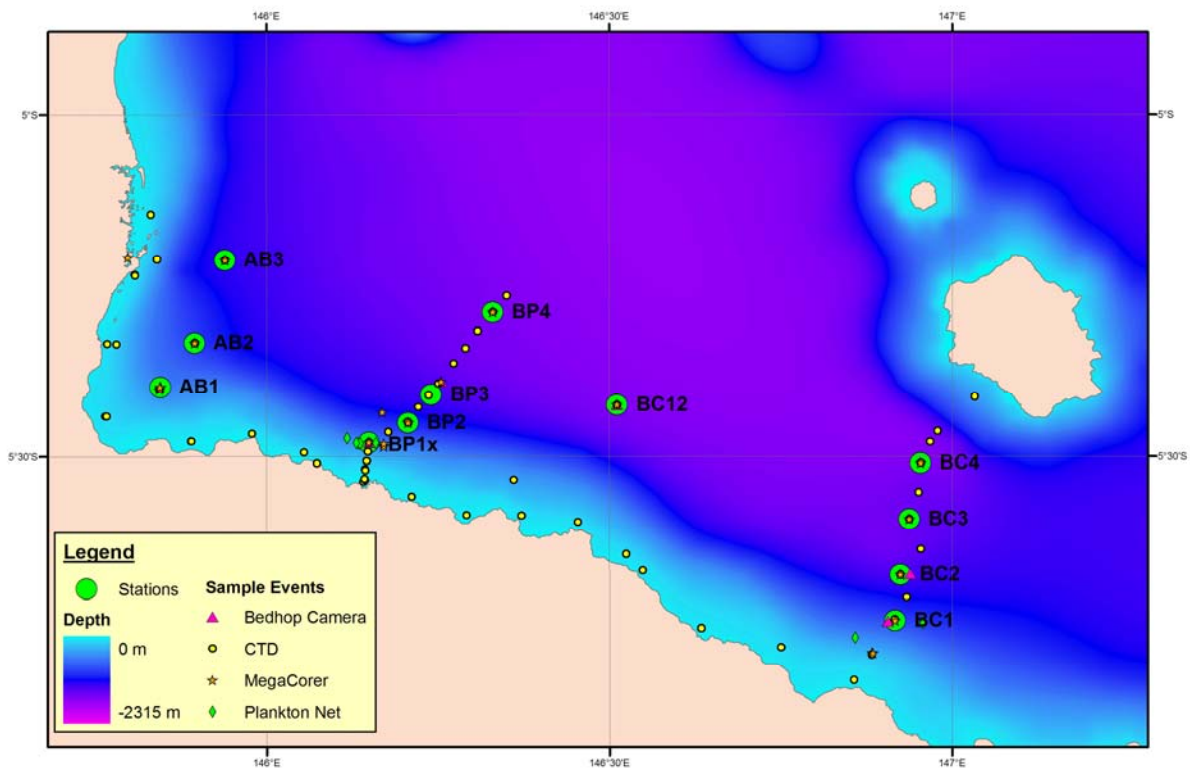
Figure 2.3.4.1. Vitiaz Basin sampling stations

2.3.5 Sediment sampling and sedimentology

All coring was carried out using the SAMS megacorer. This instrument is capable of carrying eight 10 cm diameter core tubes and is designed to take sediment cores without bow-wave disturbance. It accomplishes this by being hydraulically damped such that once the corer frame reaches the bed the weighted core head carrying the core tubes descends slowly into the sediment on a piston.

In practice the corer velocity was moderated about 10 m above the bed and lowered at about 0.5 ms^{-1} until touchdown. Thereafter about 5 m of slack wire was spooled out to ensure that movements of the ship did not disturb the corer as it was penetrating the seabed.

The onboard LGL crane had insufficient power to slew with the corer suspended and so an alternative method of deployment was devised by Ian Helmond, before the Lihir survey in December 2007. This involved attaching a wire strop to the corer shackle and a second strop to the block. This second strop was fitted with a hook and when this was hooked through the strop attached to the corer it allowed the crane to lift and slew the corer over the side with the main wire slack. Once in position over the stern the main wire was tensioned and the strops unhooked allowing the deployment of the instrument. This process was reversed on recovery. Although this may appear complex it had the advantage that either the crane driver or the winch driver had control of the corer at any one time. This is in contrast to when the lighter CTD was deployed without the use of strops as during that operation both winch and crane drivers must work together to control the height of the instrument from the deck and its distance from the block. With practice this operation became routine and rapid. The corer was stabilised while above the deck by the use of ropes and as many pairs of hands as required by the motion of the ship. Cores were assessed for length and any obvious layering on retrieval. Turbidity in the overlying water resulted in the rejection of the core as did any cracking or bubbling.

On board the cores were visually described including Munsell (1994) colour and subsequently extruded and sliced into bags at 0.5 cm intervals to 5 cm, 1 cm to 20 cm and at 2 cm intervals below 20 cm. Once ashore, the sediment samples were freeze-dried and a sub-sample taken for subsequent particle size analysis (PSA). PSA was conducted at SAMS using a Coulter LS230 laser-sizer. Approximately 5 g of dry sediment was resuspended in a solution of 10ml de-ionised water and 5ml sodium hexametaphosphate to inhibit flocculation of the fine (<10 μm) fraction. The sediment suspension was insonified for 15 minutes and spun using a vortex mixer. After analysis the data were plotted using Excel and the GRADISTAT software developed by Blott and Pye (2001).

The data were plotted against the core log and sediment description as down-core grain size histograms, percentage clay silt sand (down-core and ternary) and down-core mean grain size (See Appendix 1).

2.3.6 Sediment Geochemistry

At all three study sites (Basamuk, Lihir and Misima) sediment cores for chemical analysis were obtained from each of the stations. Only sediments with clear overlying water and no other physical disturbance, such as bubbles or slumping of the core within the core tube, were taken to be processed for sediment chemistry.

At the main stations of all sites, sediment cores for solid phase analysis and pore-water analysis were sampled in triplicate, each core was obtained from a separate deployment of the megacorer.

A further three cores were taken at each site, one for particle size analysis and carbon analysis, a second for radionuclide analysis and a third as a spare core. Each core was sliced at 0.5 cm interval to a depth of 5 cm, 1 cm interval to a depth of 20 cm and then 2 cm thereafter to the bottom of the core. The samples were sectioned and each slice placed in a labelled zip locked bag. All samples pertaining to a single core were placed in a large plastic labelled bag and placed in a freezer for storage.

Pore-water was extracted from retrieved sediments and collected to ascertain the nutrient and dissolved metal concentrations. The sediment pore-water was obtained from cores by the slicing and extraction of sediment in a nitrogen filled glove bag to prevent oxidation of any elements in the dissolved and solid phases of the sediment. An aliquot of sediment was placed in a zip lock bag to provide a sample for water content and total metal analysis. Pore-water was collected from the top 15 cm of the sediment core where available. There after the sediment core was sectioned as described above, placed in zip lock bags and frozen.

To separate the pore-water from the sediment, the extracted sediment was placed in a gas tight centrifuge tube (within a nitrogen atmosphere) and centrifuged at 4000 rpm to extract the pore-water. The extracted pore-water was filtered under nitrogen through a combination of 5 μm and 0.20 μm filters to collect samples for metal analysis and through a 0.20 μm filter to collect samples for nutrient analysis. The filtered samples for metal analysis were placed in small polycarbonate bottles, acidified with nitric acid and stored in a fridge at 4^oC. A separate sample was filtered for pore-water nutrient analysis and was placed in a micro centrifuge tube and immediately fozen at -20^oC.

In the laboratory, the solid phase samples were dissolved using a microwave digestion technique that achieved total dissolution of the sediment. The resultant solutions were analysed for major, minor and trace elements using Inductively Coupled Plasma Optical Emission Spectrometry (ICP-OES) and Inductively Coupled Plasma Mass Spectrometry (ICP-MS).

The pore-water samples were diluted with 5% HNO_3 acid and analysed for trace elements using ICP-MS. Pore-water nutrient concentrations were determined using a Lachate 'QuikChem 8000' instrument.

2.3.7 Suspended Particulate Material Geochemistry

Suspended Particulate Material (SPM) samples were obtained to determine the chemical constituents of the SPM. Samples at different depths in the water column were collected using the CTD. Where possible, 10 litres of water were collected at each of 10 depths by firing 2 bottles at each chosen depth. The samples were then filtered through pre weighed cellulose nitrate 0.45 µm filters using a SPM filter rig. The rig comprises of 6 x 10 litre Nalgene bottles and uses filtered compressed air to push the water through the filter. The filtered water was run to waste and any water left in the bottles was measured to obtain an accurate volume of filtered water. The amount of water filtered depended on the amount of particulates in the water column. After filtration the filter was placed back in its pre-weighed numbered housing for analysis. In the laboratory the filter was re weighed, dissolved and analysed for major, minor and trace elements using ICP-MS analysis.

Figure 2.3.7.1: SPM filter rig   **Figure 2.3.7.2: Filtered tailings**
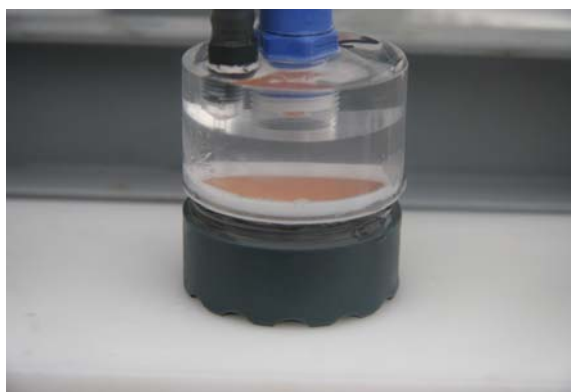
Water column nutrient sample collection

Nutrient samples were obtained by collecting the water that had been filtered during the collection of the SPM samples. This water was collected in 150ml polyethylene bottles which were

stoppered and sealed and then immediately frozen and stored for return to the laboratory for analysis.

Water column chlorophyll sample collection

Chlorophyll samples were collected by filtering about 200 ml of water through a GFF filter. The volume of filtered water was measured and the filters were removed from the filter housing, folded and placed in a ziplock bag, and immediately frozen and stored for return to the laboratory for analysis.

2.3.8 Benthos

For all three studies (Basamuk, Lihir and Misima) sediment infauna were classified as meio- or macrofauna according to taxonomic identity rather than the sieve mesh size use to retain them. This is in accord with common practice in modern deep-sea benthic studies. All members of the Foraminifera, Nematoda, Copepoda, Ostracoda and a few minor groups (e.g. Kinorhyncha) were classed as meiofauna. Other metazoan groups were classed as macrofauna.

Cores intended for macrofaunal analysis were mounted on a wooden core stand and gently lowered to remove all but approximately 1 cm depth of the overlying water. Photographs were taken if the core surface showed any interesting features (visible surface fauna, burrows or other traces of biological activity). The remaining overlying water was carefully transferred to a sample container using a plastic pipette. This was done to ensure collection of any small organisms present in the superficial sediment or surface floc. The sediment core was then sliced at the 5 cm and 10 cm depth horizons, and the 0-5 and 5-10 cm sections placed in separate containers. Fixative solution (4% buffered formaldehyde with Rose Bengal stain) was then added to each container. After addition of fixative the sediment in each container was broken up and thoroughly stirred with a knife blade to ensure penetration of the solution throughout the sample. Labelled sample containers were then sealed and placed into storage on deck. Sediment below 10 cm depth was not preserved, as in our experience of deep-sea sampling the scarcity of animals below this level means that it is not cost-effective to process this material. However, the deeper sediment of each core was carefully broken open and examined visually before being discarded to ensure that rare, larger animals (which are occasionally found below 10 cm) were retained.

Sediment samples were left in fixative for at least 48 hours before any further treatment. Each sample was then washed through stacked sieves (500 μm and 250 μm) using gently flowing, filtered seawater. The residues on each sieve were then carefully washed into separate sample

containers (glass vials, ziplock polythene bags or polypropylene pots, according to volume of material), and topped-up with a small volume of fixative (4% buffered formaldehyde). All samples were labelled both internally and externally to ensure correct identification on return to the laboratory.

Cores intended for meiofaunal analysis by sediment depth horizon were mounted on the core stand and gently lowered to leave only 1 cm depth of overlying water, which was then removed by pipette as described above. The sediment column was then sliced at 1 cm intervals to a depth of 5 cm, and each section washed into a separate labelled ziplock polythene bag. Fixative solution was then added to each bag. The 5-10 cm depth horizon was also retained and fixed in order to allow use of these cores as additional replicates for quantification of macrofauna. The 1 cm-thick slices from the 0-5 cm depth horizon were not processed further on the ship, but were sieved on return to the laboratory. The 5-10 cm layer of each core was left in fixative for at least 48 hours, washed through 500 μm and 250 μm sieves and the residues preserved as described above. Three cores per station were analysed in this way, each from a separate corer drop.

In the laboratory, core samples were washed in fresh water through the same sieve mesh (500 or 250 μm) orignally used to retain them. Meiofaunal 1 cm core slices were in addition washed through 125 and 63 μm sieve meshes. Available time did not allow analysis of these finer fractions but they were retained and stored in 70% ethanol.

After sieving, small subsamples were then decanted into a glass Petri dish and examined carefully under a binocular dissecting microscope. Organisms were picked out with fine forceps and put to one side for later identification. When the entire sample had been processed in this way, the recovered macrofauna were sorted, counted and indentified to major taxon (Phylum or Class), or to Family level in the case of polychaete worms. Living (stained) calcified and organic-walled Foraminifera were counted in the 500 μm and 250 μm fractions. Agglutinated forams were excluded from analysis as these taxa tended to be highly fragmented and difficult to enumerate accurately. No biomass measurements were made, as in most samples the animals recovered were too small to be weighed individually, and in many cases even the collected biomass per core would have been difficult to weigh accurately when wet. Dry-weighing was not considered as this would have resulted in the destruction of specimens which may be required for more detailed taxonomic identification in the future. After counting and identification all recovered organisms were stored in 70% ethanol in sealed, labelled glass vials.

2.3.9 Seabed photography

Seabed photographs were taken using a "bed-hop" camera system consisting of a 35 mm film camera and strobe light in separate pressure housings, mounted on a steel frame. Camera and strobe were connected via a bottom-switch linked to a lead weight suspended on a wire cable below the frame. The camera and strobe are triggered (and a photograph taken) by the bottom-switch when the suspended weight touches the seabed and releases the tension on the wire cable. The camera gives an oblique view of the seabed and records an image of approximately 1 m (horizontal extent) x 2.5 m (depth of field). The camera is usually loaded with 36-exposure colour transparency film, but to allow easy unloading of film only 25 exposures are made per deployment. For use off Miss Rankin, the camera frame was fitted with a BENTHOS altimeter which recorded the elevation above the seabed. It was found that the system could be deployed successfully with two operators in the cabin monitoring the readout from the altimeter and communicating with the winch driver by two-way radio. After each recorded contact with the seabed the system was raised 5 m on the winch for approximately 1 min to allow time for the strobe to recharge and the ship's movement to carry the system some distance from the spot previously photographed. The system was then lowered slowly on the winch until the next seabed contact. In calm conditions the ship was allowed to drift freely during the deployment but in a swell it was necessary for the ship to steam slowly (approximately 0.5 knot) into the wind. The ship's position was recorded at the start, mid-point and end of each sequence of images.

Facilities were not available for on-board processing of films, so a deployment was judged successful if, on recovery, the film was found to have passed through the camera, indicating that exposures had been made at the seabed. Deployments were made at stations BP1x, BP3, BC1, BC2 and BC12. Calm conditions were experienced at BP1x, BP3 and BC12, but at the other two stations a 1.5 knot current resulted in the wire trailing behind the ship at a steep angle and necessitated paying out a length of wire much greater than the water depth to achieve contact with the seabed. Films from all camera deployments were processed after return to the UK.

2.3.10 Zooplankton

Plankton sampling and analysis followed standard methods as detailed in Harris *et al.,*(2000). Plankton was collected using a KC opening and closing ring-net (KC Research Equipment Denmark). The net had an opening of 0.25 m^2 and 200 µm mesh. The net was lowered vertically to the deepest point of the haul and pulled up at a steady rate (Figure 2.3.10.1). Once the length of wire out indicated the net had reached the upper level of the haul a messenger was dispatched down the cable. The messenger triggers a release mechanism which frees a throttle closing the

net opening (Figure 2.3.10.2). The water volume filtered was estimated as the mouth opening area multiplied by the depth range towed through. The net was then recovered to the ship and, after rinsing the outside of the net, the sample removed from the end bucket. Samples were fixed in 4% formalin and returned to Scotland for analysis. Three samples were collected at each of three depth-bands; 500-300 m; 300-100 m and 100-0 m at 2 stations (BC1 and BP1x; at Lihir the same methods were employed at stations L1 and L8). Sampling was repeated once during daylight and once at night.

Figure 2.3.10.1 Plankton net deployment   **Figure 2.3.10.2 Plankton net recovery**

In the laboratory each sample was transferred to a 250 ml whirling flask and thoroughly mixed. A sub-sample of known volume was withdrawn using a Stempel pipette and placed in a gridded analysis tray. The sample was examined using an Olympus SZX16 binocular microscope attached to an interactive image analysis system (Biometrix ToolBox (BTB), Pilkington Scientific Imaging, Haywards Heath, UK). The BTB system allows the user to classify organisms to pre-defined taxa and to record biometric measurements such as length and width. All organisms in the sub-sample were identified. If less than 200 organisms were present in the sub-sample, a further sub-sample was analysed. Adult calanoid copepods were identified to family level; harpacticoids and cyclopoids were recorded at order level. Tropical copepodite and nauplii stages cannot normally be identified to low taxa and so were recorded as major groups. Other planktonic organisms were

also only identified to major group level. Copepod identification was largely based on Rose (1933) and Boxshall and Halsey (2004) and cross-referenced with the mid-Pacific lists at Marine Planktonic Copepods website of CNRS (http://copepodes.obs-banyuls.fr/en/index.php). Identification of other plankton was based on Todd *et al*.(2000), Newell and Newell (1967), Smith and Johnson (1996) and Boltovskoy (2005).

The electronic files from the BTB system were converted to .csv format and imported into an ACCESS database. The ACCESS database consists of a table of zooplankton data linked to a table containing station details. Queries to check the number of data records and convert data extracts to numbers of organisms per cubic metre are included.

2.3.11 Microplankton

Microplankton samples were collected from only 2 depths (10 and 69 m) at one station (BP14). Water samples were collected during daylight hours by Niskin bottle, and 400 ml preserved with 1% final concentration formaldehyde. On return to the UK, 50 ml sub-samples were concentrated by settling for 24 hours and observed by inverted microscopy at x200 to x400 magnification. All microplankton (20 to 200 μm size) present in the sub-sampled were identified, where possible to species, and enumerated. The analysis does not include small nano- (2-20 μm) or pico- (<2 μm) sized plankton with the exception of choanoflagellates.

2.4 Results

2.4.1 Bathymetry and Acoustic Character

The seabed morphology at Basamuk is characterised by a steep continental slope dominated by v-profile erosional down-slope channels, typically terminating at 1300 m water depth. Beyond this to the northeast, the seabed is smoother and dominated by soft fine-grained sediments. In addition, the northernmost station of the Basamuk Control transect, (BC4) displayed thinner sediment cover, possibly relating to the proximity to Long Island and a notable rockfall and associated debris flow was visible on the echo-sounder profile. The acoustic character of the margin is typically highly reflective, with little or no sub-bottom penetration (Figure 2.4.1.1). The rough, irregular seabed produced hyperbolic reflectors, the softer depositional regions producing strong reflectors.
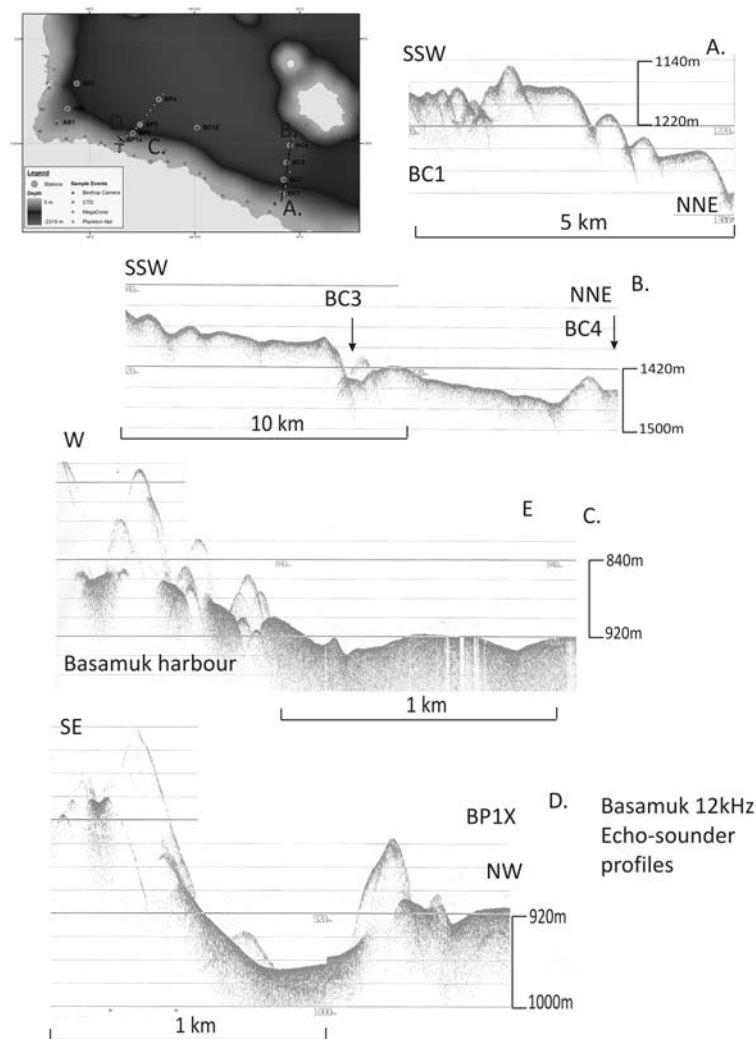
Figure 2.4.1.1. Examples of echo-sounder profiles, Rai coast.

2.4.2 Physical Oceanography

At the time of the investigations the Australian Bureau of Meteorology Southern Oscillation Index was strongly positive at 14.1. This indicates that the Equatorial Pacific was in a La Nina cycle and can be expected to exhibit strong easterly trades forcing warm surface water westwards along the Equator towards the Bismarck Archipelago. However, conditions at the nearest functioning TAO/TRITTON buoy (2S156E) located at 156° E, 2° S (Figure 3.2.2.1, 2.4.2.1)) indicate that the background wind forcing was from the west. Although this buoy was over 1000 km to the east of the survey region, nevertheless it provides some indication of the oceanographic conditions that form the backdrop to the Basamuk survey. Wind speeds reduced from typically 5 m s^{-1} at the start of the cruise to close to 0 m s^{-1} by the end of September.

During the period of the cruise, sea surface temperature at the buoy rose from 29 to 30.5 °C, with the air temperature slightly cooler (between 28 and 29 °C).
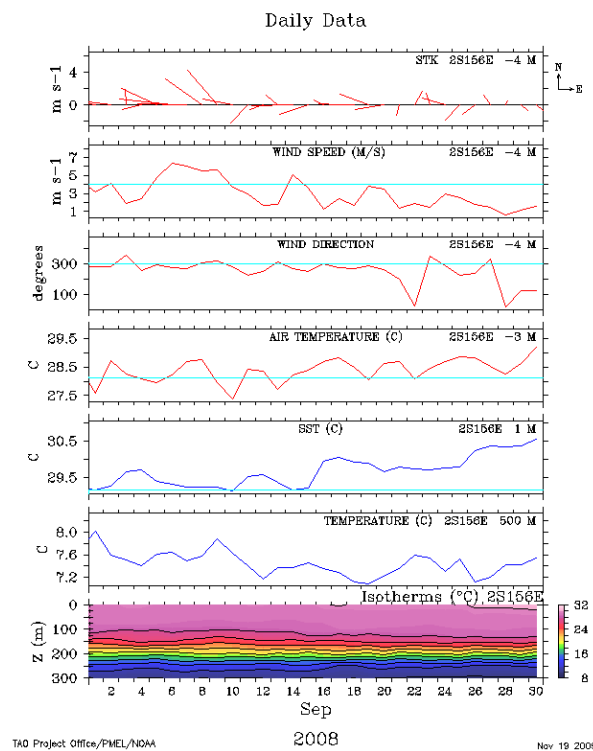
Figure 2.4.2.1.   Meteorological and surface oceanographic conditions at TAO buoy 2S156E (for position see Figure 3.2.2.1). Source:http://www.pmel.noaa.gov/tao/jsdisplay/

The physical oceanography of the Western Equatorial Pacific (WEP) is subject to daily, seasonal and, particularly inter-annual variability. This section is limited to describing the conditions that

prevailed during the cruise in September 2008 during a La Nina phase of ENSO, and thus it may not reflect conditions at other times.

Deep offshore waters

Most of the DSTP material will end up in the deep water of the Vitiaz Basin. It is therefore important to investigate the circulation and stratification of the deep waters of the basin.
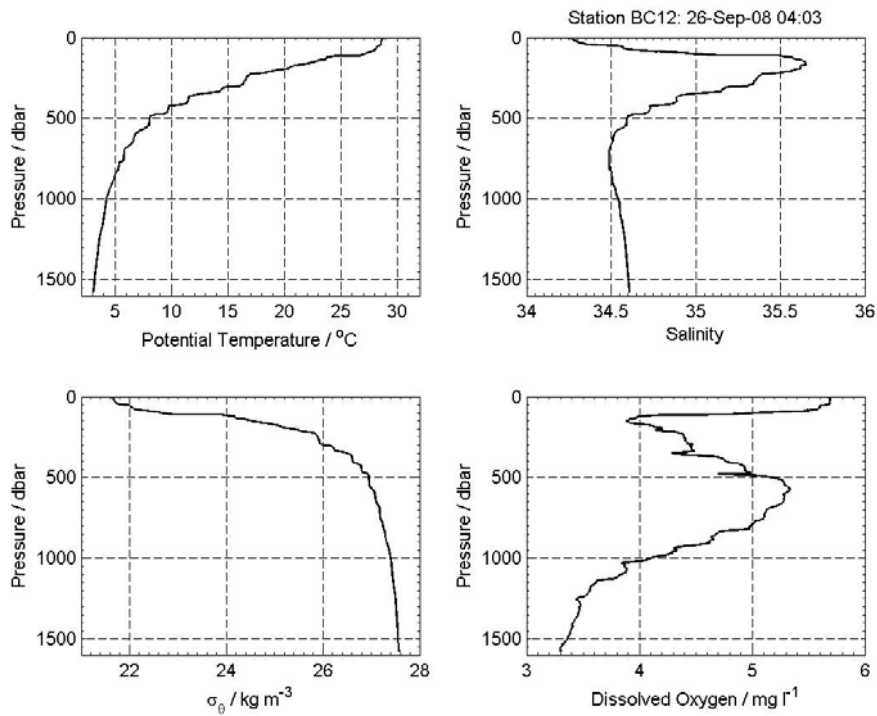
Figure 2.4.2.2. Potential temperature, salinity σ_t and dissolved oxygen profiles for a typical station in the centre of the Vitiaz Basin (BC12).
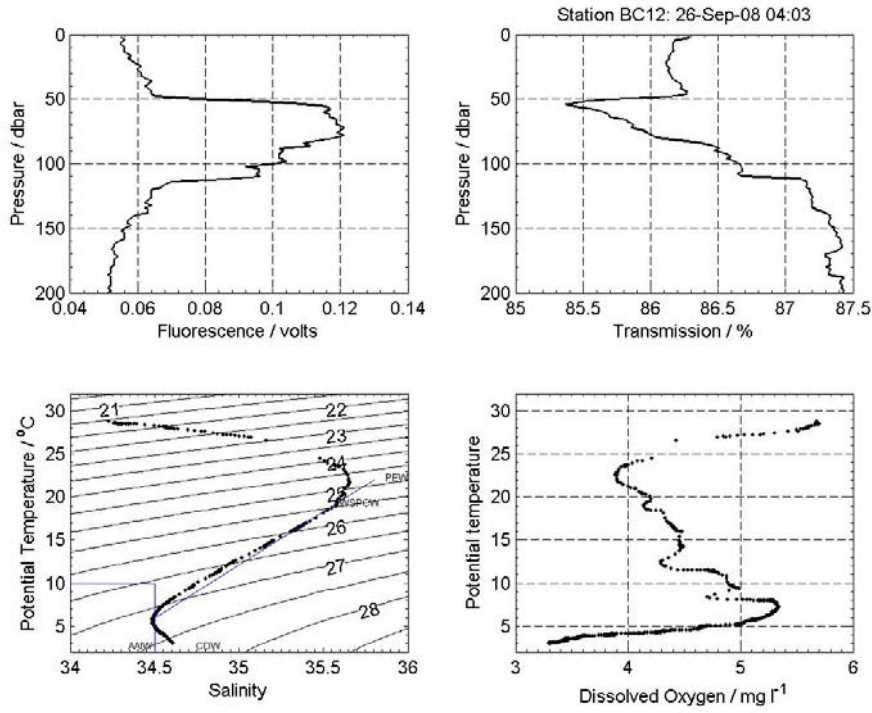
Figure 2.4.2.3. Fluorescence and transmission in the top 200 m, and full water column potential temperature against salinity and dissolved oxygen at Sta. BC12.
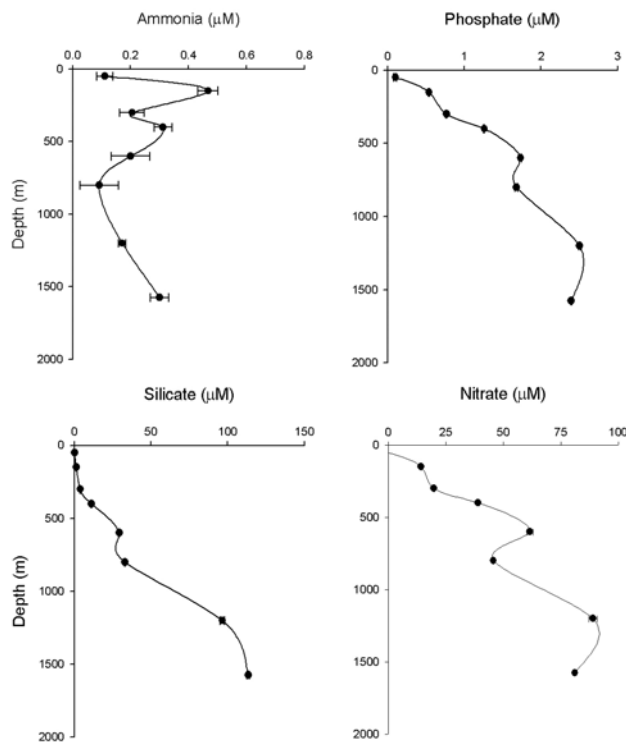
Figure 2.4.2.4. Water column nutrients at Sta. BC12.

The physical characteristics of the water in the deep parts of the Vitiaz Basin (Figure 2.4.2.2) were typical of the Western Equatorial Pacific, with water lying between ~ 500 m and the salinity minimum at ~ 700 m (σ_t = 26.5 to 28.8 kg m^{-3}) falling close to or on the West South Pacific Central Water (WSPCW, Figure 2.4.2.3) mixing line. This line connects Pacific Equatorial Water (PEW) with Antarctic Intermediate Water (AAIW). Below ~700 m water trends towards Circumpolar Deep Water (CDW). Thus most of the water column was originally derived from the Southern Ocean. Bottom temperatures, at 1600 m, were ~ 3° C.

Above 500 m (σ_t < 27.5) salinity increased to a maximum of about 35.6 at about 160 m depth. This is recognised as the depth of the high salinity New Guinea Coastal UnderCurrent (NGCUC) which contains Pacific Equatorial Water (PEW) that originates to the east of PNG (Zenk *et al.*, 2005). Above the PEW there was a very sharp pycnocline at about 110 m where σ_t drops from 24 to 23 kg m^{-3} as we approach the surface, and in the upper 80 m potential temperature, θ, was relatively mixed but salinity, *S*, was stratified so that the lowest salinities were found at the surface.

Two things stand out in the θ, *S* and density profiles. The first is the intensity of the surface pycnocline in which σ_t dropped from 26.0 to 21.6 kg m^{-3} in just 250 m, and the second is the step like nature of the θ, *S* and σ_t profiles between 160 and 250 m where the upper WSPCW meets PEW. Both these phenomena imply very weak vertical mixing in the upper layers: the step-like profiles suggest interleaving between the two water masses with suppressed isopycnal mixing; and the intense pycnocline is likely to have dampened the scales of vertical diffusion. A further indication of the water mass identity may be seen in the dissolved oxygen (and silicate, see below) concentrations. Below the well-oxygenated surface layer at about 150 m there was a minimum of 4.1 mg L^{-1} at the level that PEW mixes into the upper layers of WSPCW.

Descending along the WSPCW mixing line, oxygen levels increased to peak of 5.4 mg L^{-1} at 600 m at the top of the AAIW. Thereafter there was a monotonic decrease in oxygen to 3.3 mg L^{-1} in the deoxygenated CDW at 1500 m.

The nutrient profiles in the Vitiaz Basin (Figure 2.4.2.4) appear to be consistent with similar observations made in this part of the Pacific Ocean. The surface waters are nutrient depleted which, considering the relatively high ammonia and low silicate levels, may be due to a combination of phytoplankton growth (increasing ammonia and depleting phosphate and nitrate) and dilution due to surface rainfall (diluting silicate).
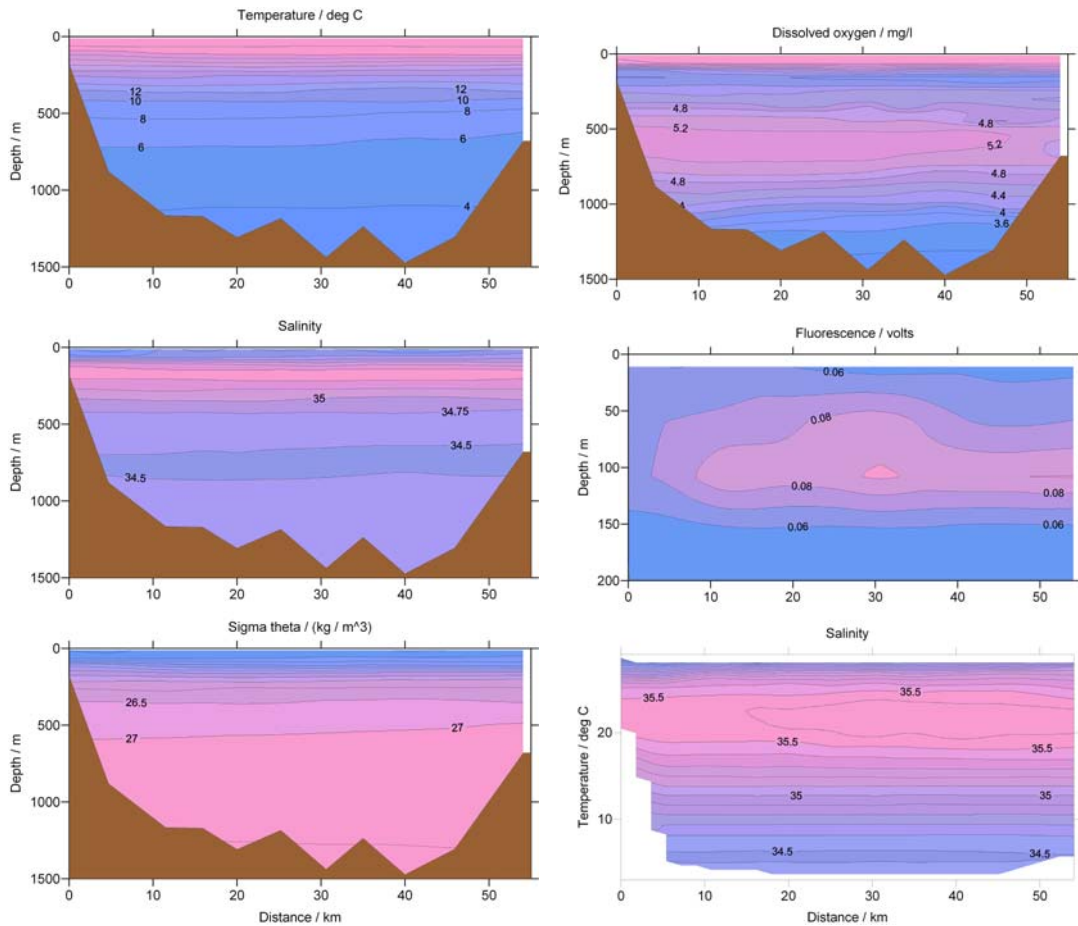
Figure 2.4.2.5. The BC section between the PNG mainland (LHS) and Long Island (RHS). Left panel (from top to bottom) potential temperature (° C), salinity and σ_θ (kg m^{-3}). Right panel (from top to bottom) dissolved oxygen (mg L^{-1}), fluorescence (volts) and salinity (against potential temperature). Krigging has been used to contour all except the temperature / salinity section.

Section BC (Figures 2.4.2.5 and 2.3.4.1) shows that offshore there was a reasonably uniform distribution of the main parameters. However, close inspection reveals that the σ_θ = 27 kg m^{-3} surface sloped upward towards the right. Simple geostrophic considerations suggest that this slope is indicative of a westward surface flow (see below). The dissolved oxygen (DO) section shows better oxygenated waters at 500 m on the PNG side, and the increase in salinity (with respect to temperature) is indicative of a higher proportion of PEW towards the north of PNG.

The coastal zone

Any port or coastal operations relating to the mine will inevitably disturb the sediments, and movement and quality of water in the coastal zone. With this in mind, and taking into

consideration the possible local impact of rivers discharging along the coast a survey was made just offshore along the 200 m contour (Section J, Figure 2.3.4.1).
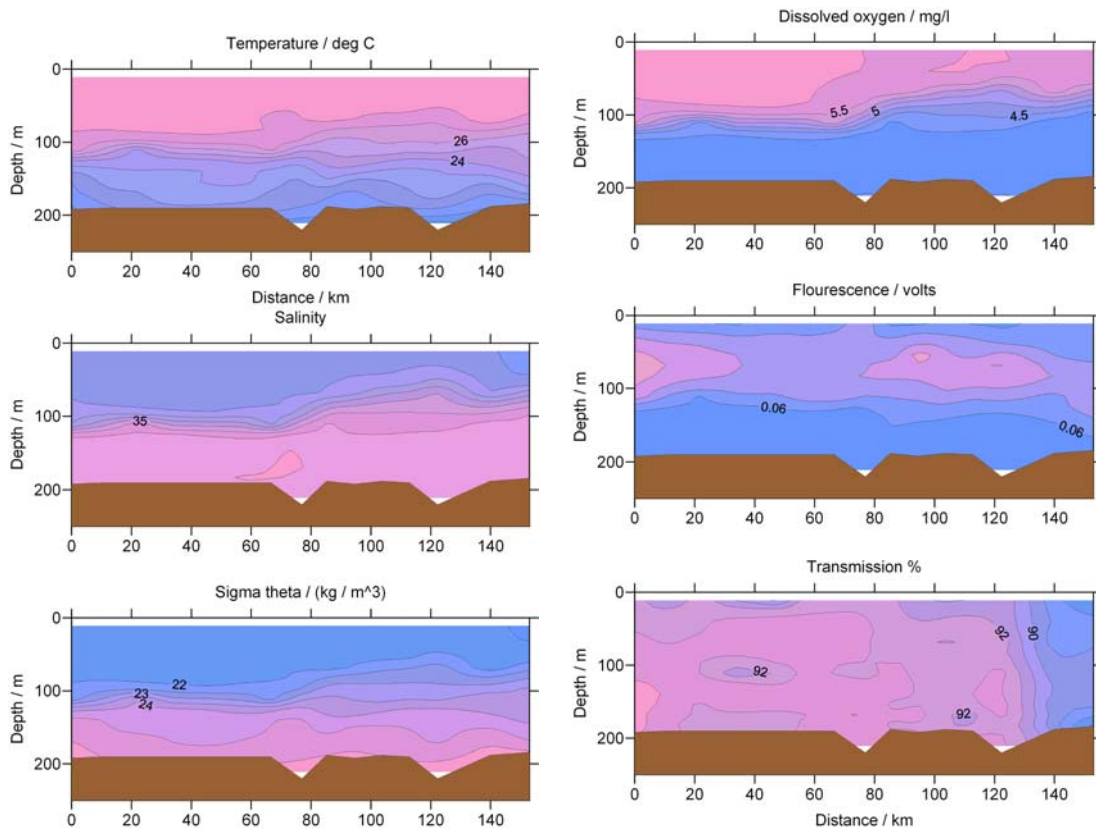
Figure 2.4.2.6. The J section from west (LHS) to east (RHS) along the northern coast of PNG. Left panel (from top to bottom) potential temperature (° C), salinity and σ_t (kg m^{-3}). Right panel (from top to bottom) dissolved oxygen (mg L^{-1}), fluorescence (mg m^{-3}) and transmittance (%). Krigging has been used to contour all plots.

This section (Figure 2.4.2.6) revealed that there was little alongshore variation in the main physical parameters, although there was a tendency for the pycnocline to be more diffuse towards the east. There were no obvious variations in salinity from the rivers that flow into the sea from the mountains bordering the Vitiaz Basin, although clearly their signal must have been present. Marginally lower transmittance values (to 88 %) were found at the eastern end of the line, the reasons for which are not fully understood.

The offshore current field

The sloping isopycnal surfaces observed in Figure 2.4.2.5 imply that a geostrophic current flows through the Vitiaz Strait. A section of the mean geostrophic velocity profile was derived from the (almost) extreme CTD stations along Section BC with the velocity at the bottom set to the speed

observed by an Argo float that drifted north-westwards through the strait in early July at 0.135 m s^{-1}. The profile revealed a high velocity surface current centred on ~ 80 m, with a maximum velocity of ~ 0.65 m s^{-1} (Figure 2.4.2.7). Although this current is assumed to have been part of the NGCUC it appears to have been somewhat shallower than the core observed in the salinity profile. The reason for this discrepancy is unclear but, as will be shown below, the currents in the Vitiaz basin were highly variable during the cruise.
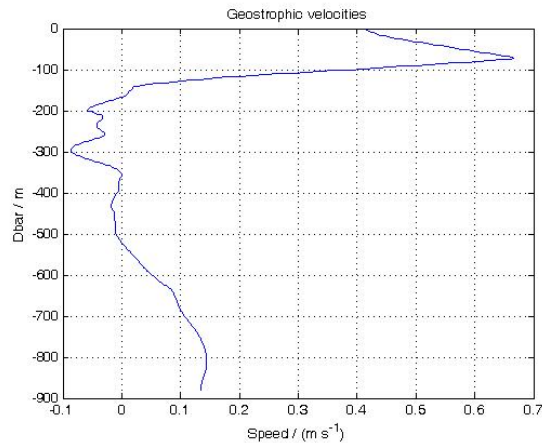
Figure 2.4.2.7. The geostrophic velocity profile across the Vitiaz Strait between the PNG mainland and Long Island.

Below this peak (between 200 and 500 m) there was a region of very weak current reversal. Further down these velocities picked up again to ~ 0.14 at 800 m in a current that seems to be carrying low salinity, high oxygen Antarctic Intermediate Water (*c.f.* Figure 2.4.2.2, and also Zenk *et al.*, 2005).

It was fortunate that before, during and after the cruise the Vitiaz Basin was occupied by Argo float 5901161, released by CSIRO in the Coral Sea in August 2006. The drifter has a parking depth of 1000 m and comes to the surface every ~10 days for ~8 h to relay data back to base via satellite. It entered the Vitiaz Basin through the Vitiaz Strait in July 2008 and remained there throughout the cruise and beyond until March 2009[7]. Using track data available from the web it has been possible to map the surface and 1000 m current fields.

---

[7] http://www.cmar.csiro.au/argo/dmqc/html/DMQCnotes_5901161.html

a)

b)
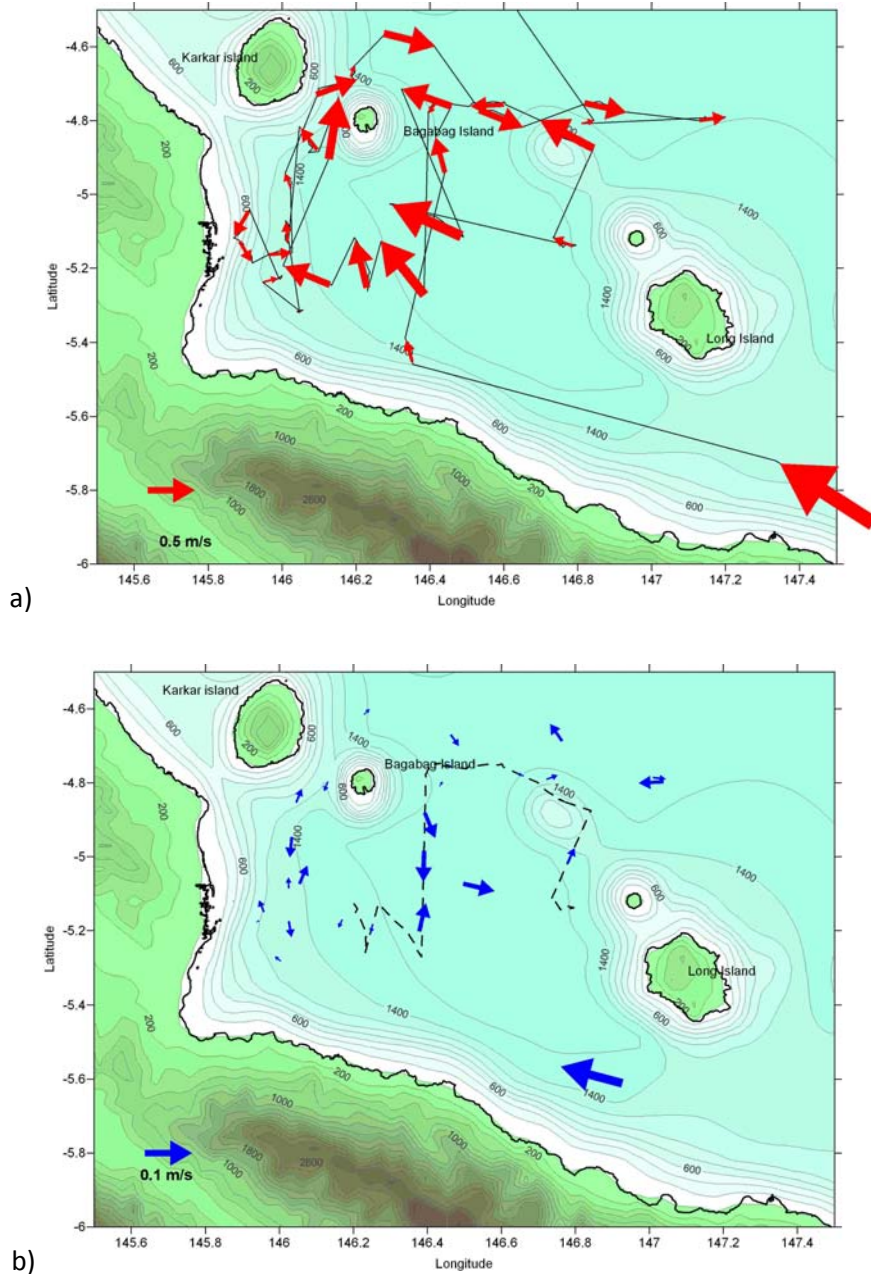
Figure 2.4.2.8. Velocity vectors at a) the surface and b) 1000 m from Argo float 5901161 between July 2008 and March 2009. Note the difference in velocity scale. The continuous line in a) shows the full track, whilst the dotted line in b) shows the track for September 2008.

Figure 2.4.2.8 shows quite clearly that although the currents in the upper and lower layers are quite strong (0.8 m s^{-1} at the surface, 0.135 m s^{-1} at 1000 m) and coherent as they enter the basin, the pathway of water through the basin and out of it to the north is quite diffuse. Shortly after it entered the basin, drifter 5901161 became trapped in a large anticyclonic eddy that was located between Karkar and Long islands. Even after it was released from this eddy the drifter took a long time to escape the basin, and spent a considerable period of time off Madang.

We take the duration of the drifter within the basin (8 months) to be indicative of the flushing time for the deep waters. Part of the reason that the drifter remained trapped for so long may be because it was unable to pass between Karkar Island and the mainland due to the relatively shallow sill (~600 m) that exists there. It is possible (but by no means certain, see Figure 2.4.2.8a) that some of the shallower NGCUC flowed through that gap.

2.4.3 Seabed stations

Of the 12 stations occupied in the Vitiaz Basin three were within Astrolabe Bay (AB 1-3), four at Basamuk (BP 1-4), one station off Helmholtz point (BC12), and 4 eastern control stations (BC1-4), Figure 2.3.4.1.

2.4.4 Sediment sampling and sedimentology

Astrolabe Bay transect (AB1-AB3).

The Astrolabe Bay transect revealed a variety of sediment types. The inshore station AB1 in 763m depth produced poorly to moderately well sorted olive silty clays with sub-surface layers of coarse sands and gravels. Mean grain sizes are between <50->200 μm (coarse silt to medium sand) with sand content varying from 10-88% across the sand layers. In contrast station AB2 in 902m water depth contained homogenous poorly sorted olive silty mud. Mean grain sizes varied from 14-26 μm (fine to medium silt) sand contents are <12%. The most distal station on the transect AB3, in 1155m depth contained homogenous poorly sorted olive silty mud. Mean grain sizes are between 12-49 μm (fine-medium silt). Sand content is low at <20% (see Appendix 1).

Basamuk Pipeline transect (BP1x-BP4).

Sediments offshore from the proposed pipeline at Basamuk are predominantly homogenous and fine-grained mud. The station closest to the proposed tailings pipeline, BP1x, in 917m depth, contained poorly-sorted olive mud, becoming sandier with lithic clasts below 27 cm. Mean grain sizes are between 29-53 μm (medium silt). Sand content is low throughout between 10-24%. Station BP2, in 1164m depth, contained poorly sorted greenish-grey silty mud with a thin sand layer occurring between 36-37 cm. Mean grain sizes are between 31-49 μm (medium silt). Sand content is low at <23%. Station BP3 in 1420m water depth produced two main sediment units, an upper unit of moderately well sorted sands from 0-12 cm below which were poorly sorted homogenous greenish-gray silty mud. A discrete sand horizon occurs at 20 cm. Mean grain sizes ranged between 26 to 176 μm (medium silt to medium sands). Sand content is high being up to 92%. In contrast the most distal station in the transect station BP4, from 1598m depth produced

homogenous very poorly sorted olive silty mud. Mean grain sizes are between 22-56 µm (medium-coarse silt). Sand content is very low at <23% (see Appendix 1).

Control transects. (BC1-BC4 and BC12).

North of Weber Point the sediments of the Vitiaz Straits are predominantly homogenous mud with occasional sand layers. Station BC1 in 1190m depth contained poorly-sorted olive grey mud; becoming sandier below 40 cm. Mean grain sizes are between 16-43 µm (fine to coarse silt) two layers in the core produced grain sizes exceeding 100 µm (medium sand) at 4 and 19 cm. With the exception of the sandier layers overall sand content is low throughout below 20%. Station BC2 in 1340 m of water produced poorly sorted greenish-gray sandy mud with a thin sand horizon at 30 cm. Mean grain sizes are 17 to 78 µm (medium silt to fine sand). Sand contents vary from 4-30%. Station BC3 in 1430m of water contained olive gray mud with a sharp contact at 35 cm overlying dark gray mud. No grain sizes analyses were undertaken at this station. Station BC4 from 1470m water depth contained poorly sorted olive-gray and dark gray mud with a sharp contact at 9 cm. Mean grain sizes typically range from 43 to 91 µm (medium silt to fine sand). Sand content is variable between 16-45%. BC12 located off Helmholtz Point in 1597m produced poorly sorted grrenish gray sandy mud, becoming sandier below 20 cm. A diffuse thin sand layer occurs at 5 cm. The mean grain sizes are between 40 to 118 µm (medium silt to medium sand). Sand content is highly variable between 18-74% (see Appendix 1).

2.4.5 Sediment geochemistry

The sediments and pore-waters from Vitiaz Basin were analysed for major, minor and trace elements and the combined data were used to evaluate sediment composition and provenance, identify biogeochemical controls and assess any post depositional mobility of elements within the marine environment of the Vitiaz basin which encompasses Astrolabe Bay and Pommern Bay (Basamuk) in Papua New Guinea.

The geochemical analysis carried out on the sediments, pore-water and suspended particulate material obtained at the twelve stations are summarised in Table 2.4.5.1. The depth profiles of elemental concentrations for 33 elements within the solid phase and 24 elements in the pore-water of sediments collected from the Basamuk study are presented in Appendix 4B. Depth plots of elemental concentrations for each core are presented in Appendix 4A.

Table 2.4.5.1 Summary of the number of geochemical analysis, Basamuk Study

Station	Depth	Sediment metals	Sediment C:N	Sediment radionuclide	Pore-water metals	Pore-water Nutrients	SPM analysis
AB1	765	1 core	1 core	1 core	3 cores	3 cores	1 station
AB2	902	1 core	1 core	1 core			1 station
AB3	1155	1 core	1 core	1 core	2 cores	3 cores	1 station
BP1x	917	1 core	1 core	1 core	3 cores	3 cores	1 station
BP2	1165	1 core	1 core	1 core	3 cores	3 cores	1 station
BP3	1364	1 core	1 core	1 core			
BP4	1598	1 core	1 core	1 core	3 cores	3 cores	1 station
BC1	1190	1 core	1 core	1 core	3 cores	3 cores	1 station
BC2	1340	1 core	1 core	1 core	3 cores	3 cores	1 station
BC3	1340	1 core	1 core	1 core			
BC4	1470	1 core	1 core	1 core			1 station
BC12	1597	1 core	1 core	1 core	3 cores	3 cores	1 station

The primary objective of the study was to provide a sound environmental baseline on which any future impact of mine tailings could be assessed. This required a multi-element geochemical data set that could be used to determine the natural sediment signature, assess sediment accumulation and mixing rates within the area and identify and assess biogeochemical processes occurring within the marine environment surrounding Basamuk Bay.

There are no published scientific papers on the geochemical composition of sediments surrounding Basamuk Bay and the only data available are from previous studies carried out by NSR Ltd (1998), Enesar Ltd (2007) and Coffey Natural Systems (2007). The data are limited to metal

concentrations in surface samples obtained from box coring and does not consider either the down-core variations within the sediment or the effects of biogeochemical processes on the redistribution of trace elements within the sediment and overlying water column.

Marine sediments can be broadly described as being a mixture of lithogenic material, biogenic carbonate and silicate and organic matter. Element/Aluminium (Al) ratios can be used to indicate changes in sediment composition that are not caused by lithogenic dilution. For example, Silicon (Si)/Al, Titanium (Ti)/Al, Magnesium (Mg)/Al can all be used as a proxy for aeolian inputs, Zirconium (Zr)/Al for sediment texture and reworking. The major elemental/Al ratios for the surface sediments are given in Table 2.4.5.2 and shown in Figure 2.4.5.1.

Table 2.4.5.2 Elemental/Al ratios in surface sediments for all sampling stations

Stn	Ba/Al	Ca/Al	Fe/Al	K/Al	Mg/Al	Mn/Al	Sr/Al	Ti/Al
AB1	0.0020	0.399	0.906	0.176	0.393	0.013	0.003	0.090
AB2	0.0022	0.712	0.893	0.195	0.459	0.025	0.005	0.067
AB3	0.0022	0.569	0.964	0.209	0.431	0.026	0.005	0.072
BP1x	0.0028	1.437	0.865	0.212	0.544	0.025	0.009	0.058
BP2	0.0028	1.347	0.949	0.212	0.516	0.045	0.008	0.064
BP3	0.0032	1.656	1.044	0.243	0.542	0.045	0.010	0.072
BP4	0.0027	1.325	1.003	0.201	0.478	0.051	0.008	0.077
BC12	0.0029	1.645	1.232	0.223	0.890	0.053	0.008	0.066
BC1	0.0033	2.448	1.373	0.247	1.280	0.026	0.012	0.064
BC2	0.0033	2.774	1.267	0.240	1.121	0.027	0.014	0.061
BC3	0.0028	2.588	1.220	0.224	1.033	0.037	0.013	0.058
BC4	0.0041	2.258	1.017	0.196	0.578	0.058	0.013	0.053

The Ba/Al, Ca/Al and Sr/Al ratios in surface sediments are lowest at Astrolabe Bay (AB) with all ratios increasing south eastwards towards the control stations (BC). Conversely, Ti/Al ratios

decrease eastwards with the highest ratios occurring at the AB stations and the lowest at station BC4 indicating possible higher aeolian inputs or enhanced delivery of riverine inputs at the AB stations. Mg/Al and Fe/Al show similar trends with stations BC12, BC1-BC3 having higher ratios than the other stations which could indicate a higher input of altered volcanic ash. Mn/Al generally increases eastwards with the highest ratios being found at the Basamuk stations (BP) and BC4.
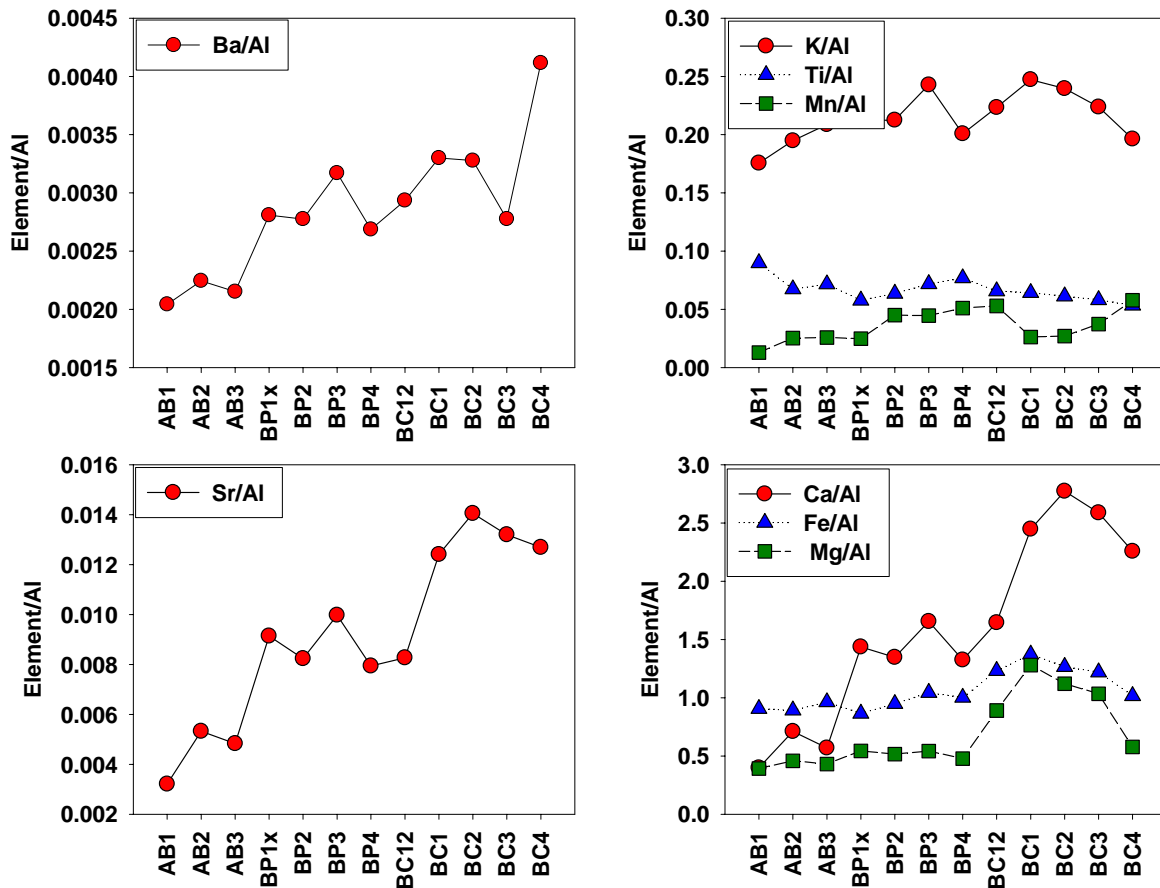
Figure 2.4.5.1. Elemental/Al ratios for surface sediments at all stations

In order to assess the rate of accumulation of the sediments at each of the stations, the activity of the naturally occurring radionuclide ^{210}Pb was measured using gamma spectroscopy. The decay of ^{210}Pb, which has a half life ($t_{1/2}$) of 22.3 years, can be used to assess the sediment accumulation rate. There are a number of assumptions made in the use of this method. There must be a constant rate of supply of ^{210}Pb to the sediment and there must be no post-depositional movement of the [210]Pb. As typical deep-sea sediments accumulate very slowly, in the order of centimetres per thousand years, profiles of ^{210}Pb activity in deep sea sediments are typically a

result of mixing by the benthic biota and often do not represent true sediment accumulation rates. Therefore any sediment accumulation rates must be considered in this light.

The sediment accumulation rates (g cm^{-2} yr^{-1}) and the average linear sedimentation rates (mm yr^{-1}) are given in Table 2.4.5.3 along with the organic carbon content (% wt) and excess ^{210}Pb inventories (Bq cm^{-2}). Figure 2.4.5.2 illustrates the ^{210}Pb activity profiles down-core.
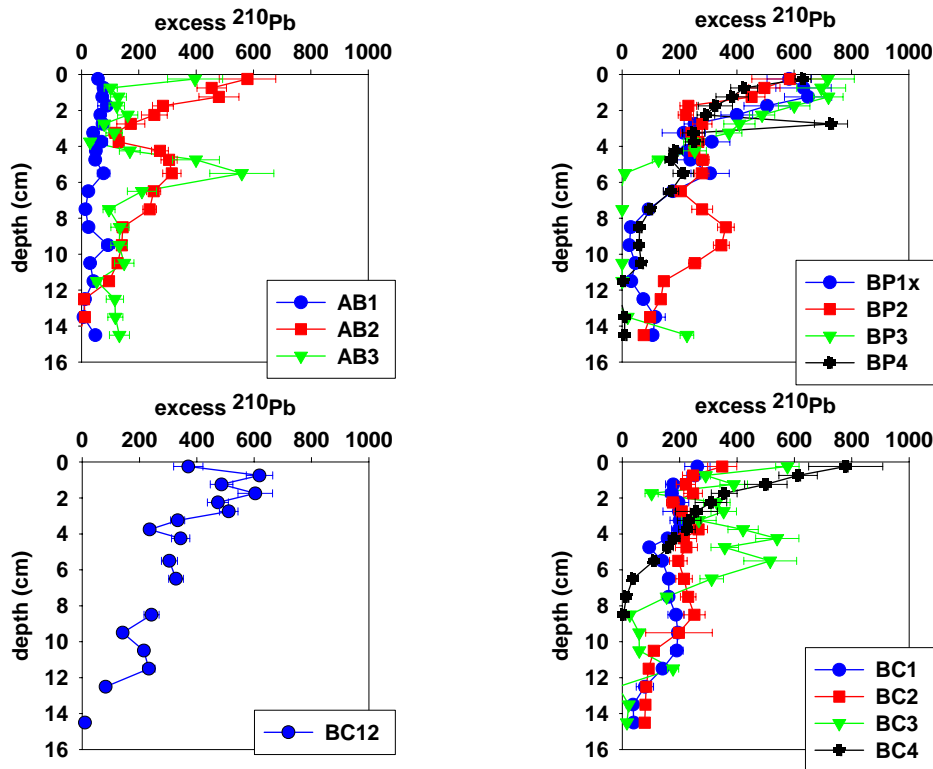
Figure 2.4.5.2 excess ^{210}Pb activities (Bq kg^{-1}) for all stations

BP2 and BP4 had higher sediment accumulation rates of 0.056 and 0.107 g cm^{-2} yr^{-1} respectively. Station BC3 had the lowest sedimentation rate of 0.019 g cm^{-2} yr^{-1}. The ^{210}Pb profile for BC4 indicated that there had been an increase in the rate of sediment accumulation at 5.5 cm depth. This may indicate a true increase in sedimentation rates over the last 60 years, however, mixing may have influenced this result.

Table 2.4.5.3 Organic carbon content, extent of mixing, accumulation rate and excess ^{210}Pb inventories for all stations

Station	Depth	Organic C	Degree of mixing	mass accum. rate	linear sed rate	Surface xs Pb210	xsPb-210 inventory
	m	%		g cm^{-2} yr^{-1}	mm yr^{-1}	Bq kg^{-1}	Bq cm^{-2}
AB1	765	0.06 - 0.72	Intensely mixed/ high sed rate	NA	NA	58	5.66
AB2	902	0.57 - 1.66	mixed below 3.5 cm	0.031	0.47	579	9.07
AB3	1155	0.70 - 1.17	mixed	NA	NA	396	12.33
BP1x	917	0.68 - 1.26	mixed, two areas showing exp. decay	1) 0.038 2) 0.032	1) 0.56 2) 0.48	583	10.35
BP2	1165	0.33 - 1.19	mixed, tentative sed rate from surface to 2 cm	0.056	0.87	585	17.03
BP3	1364	0.27 - 1.02		0.033	0.3	719	4.46
BP4	1598	0.63 - 1.40		0.107	1.3	631	8.43
BC12	1597	0.26 - 0.69	moderately mixed	NA	NA	370	17.18
BC1	1190	0.30 - 0.80	heavily mixed	NA	NA	263	10.86
BC2	1340	0.24 - 1.63	intensely mixed	NA	NA	348	11.05
BC3	1340	0.36 - 0.95	mixed zone to 5.5 cm	0.019	0.3	576	9.98
BC4	1470	0.14 - 0.71	no mixing but change in sed rate at 5.5 cm	1) 0.065 2) 0.029	1) 1.17 2) 0.53	755	5.30

The organic content of the sediment ranges from 0.06 to 1.66 %. Stations AB1 and BC12 have the lowest organic carbon content with the BP stations having generally higher organic content than the other stations (Figure 2.4.5.3). The organic carbon content varies down-core.

Marine and terrigenous organic materials have different carbon: nitrogen (C:N) ratios with marine algae having a C:N ratio of approximately 4 and terrestrial plant material having C:N ratios above 20. By plotting the C:N molar ratio it is possible to ascertain the lability (i.e. how susceptible to

biodegradation) of the carbon, the lower the ratio the more labile the carbon. Figure 2.4.5.4 illustrates the C:N ratios for all stations. The majority of the data lie between the C:N ratios of 10 and 20 indicating that there is a mix of both marine derived (labile) and terrestrial carbon (more refractory). The C:N ratio for stations BP3, BC2 and BC4 have data that lie between the C:N ratios for 4 and 10 indicating a larger input of marine derived carbon at these stations. All three stations have depths greater than 1300m. In contrast, at BC12 the majority of the data lie above the C:N ratio of 20 indicating that the organic carbon content of this core is more refractory than that of the other stations. This may indicate older, more-degraded carbon or a higher input of terrestrial carbon at this station.

The C:N ratios of the surface samples from the stations indicate that the C:N ratio is lowest at BC4, (BC4<AB3<BP2< BP4<BC3) with the deeper stations having a larger component of marine derived carbon. The eastern transect (BC) has the highest C:N ratio, the trend in C:N ratio is BC1>BC2>B3>BC4, again indicating that the supply of marine carbon is depth related, with shallower stations showing higher values of refractory organic material.
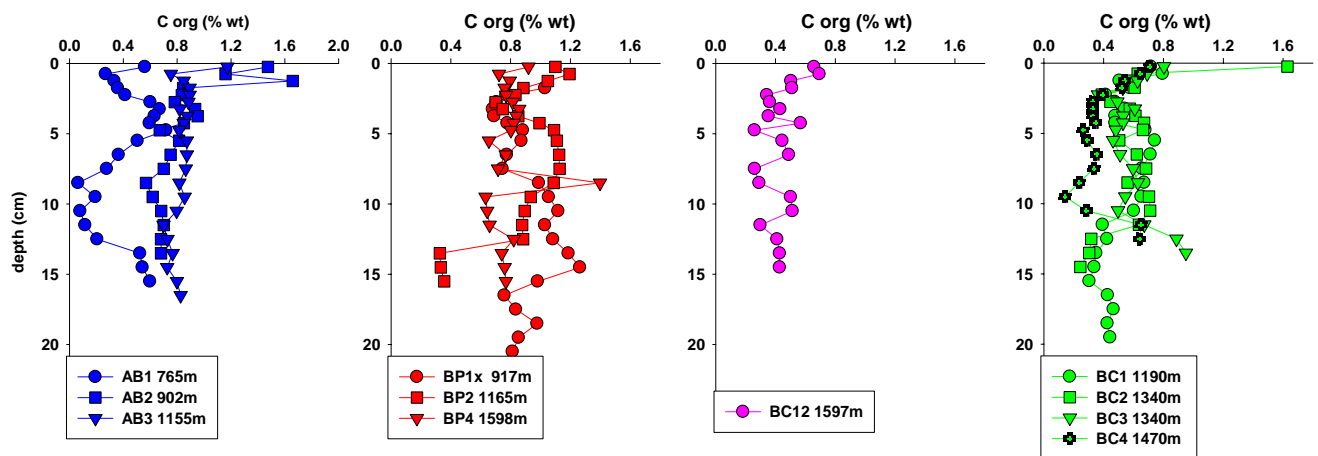
Figure 2.4.5.3 Organic carbon content (% weight) depth profiles at all stations
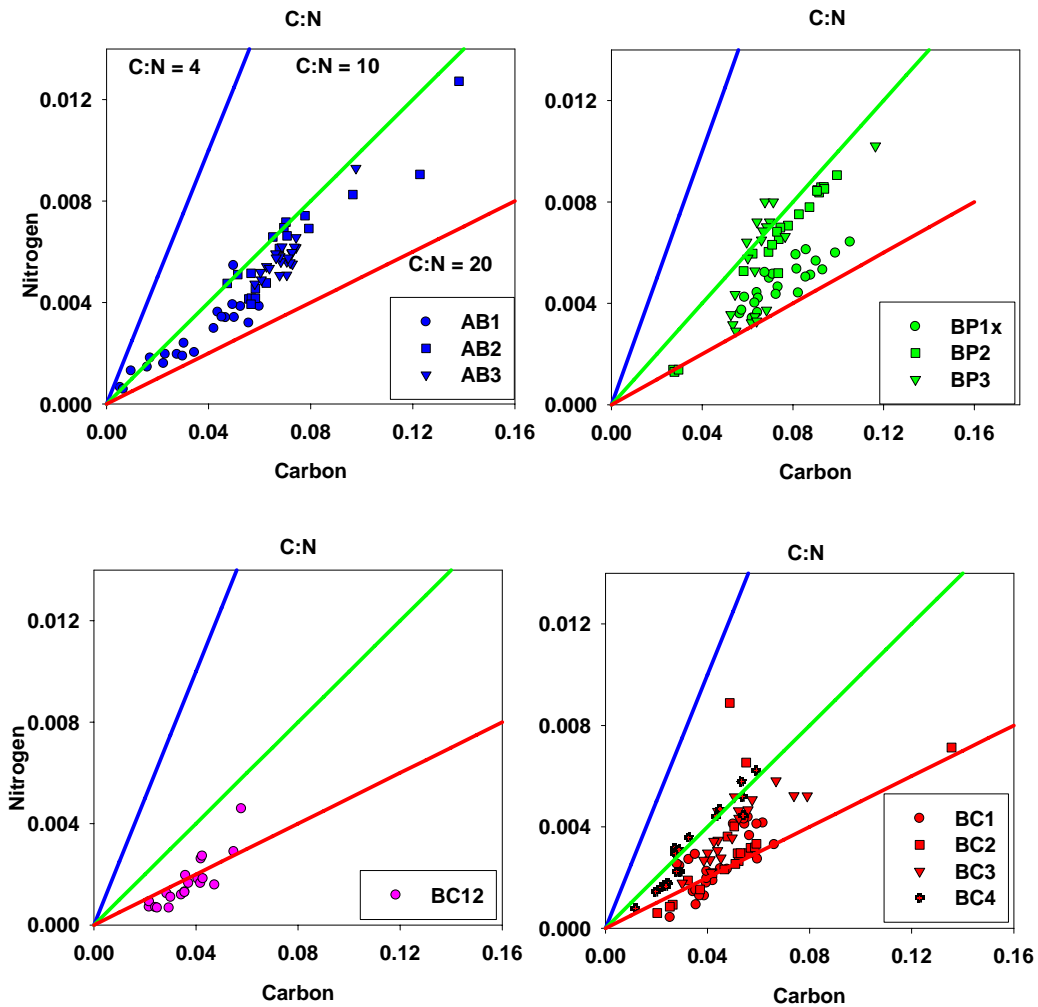
Figure 2.4.5.4 C:N molar ratios for all stations, blue line C:N = 4, green line C:N = 10, red line C:N = 20.

All elemental concentration versus depth plots are given in Appendix 4A. A number of major, minor and trace elemental concentration depth profiles within the sediments are shown below. The major element composition is shown in Figure 2.4.5.5-9 with minor and trace elements in Figures 2.4.5.10-13.

Aluminium (Al) concentrations for Astrolabe Bay (AB) stations range from 5.4% to 7.9%, with a pronounced decrease at 8.5 cm depth at AB1, Basamuk (BP) stations from 4.6 to 7.8%, BC12 station from 4.9 to 5.7% and the eastern transect (BC) stations from 3.8 to 7.3%, (Figure 2.4.5.5). Astrolabe Bay has generally higher concentrations of Al with Basamuk having similar concentrations. Stations BC1-3 have far lower concentrations, around 4%, with the deeper station BC4 having higher Al concentrations at depth.

Calcium (Ca) concentrations are lowest for the AB stations, 1.9 to 4.9%, with the BP and BC12 stations having similar concentrations ranging from 6.9 to 10.6%. The eastern control (BC) stations have the highest concentration of Ca ranging from 7.7 to 14.5%, (Figure 2.4.5.6).

Iron (Fe) concentrations are similar with concentrations for all stations ranging from 4.0 to 7.9%. The sharp decrease in Al concentration at 8.5 cm depth in AB1 is also reflected in the Fe profile with the minimum concentration of Fe (4.6%) occurring at 9.5 cm. A maximum concentration of Fe (8.4%) occurs at BP3 at 10.5 cm depth, (Figure 2.4.5.7).
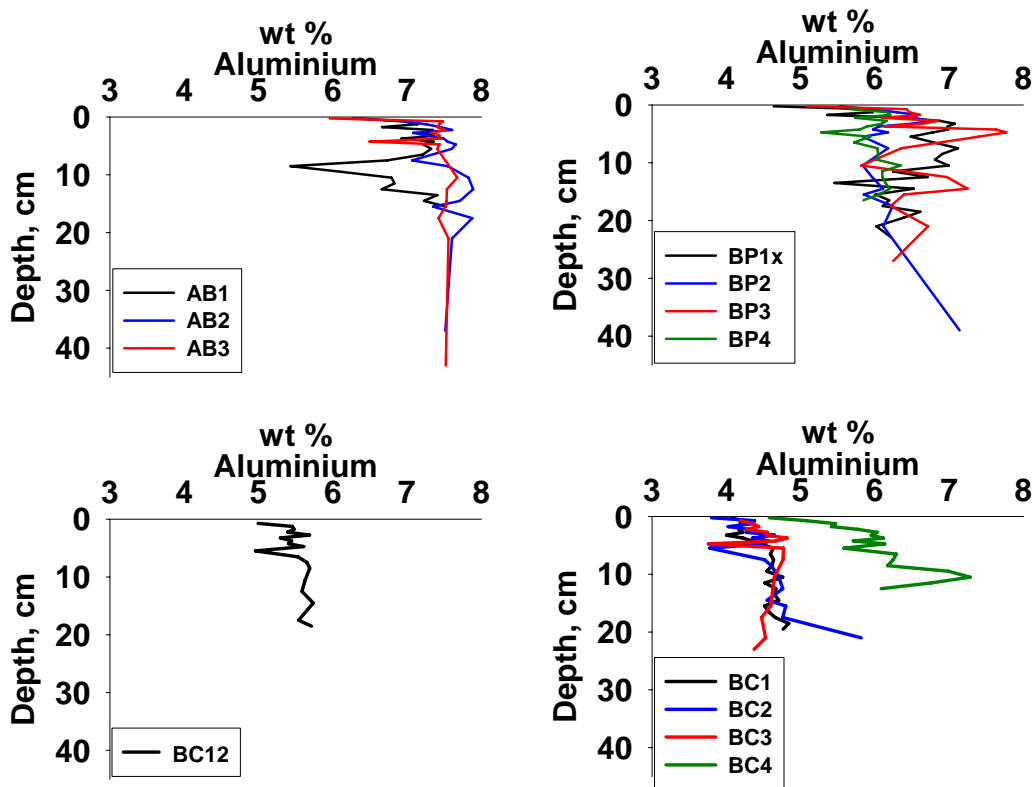
Figure 2.4.5.5 Aluminium (Al) sediment concentrations at all Basamuk stations
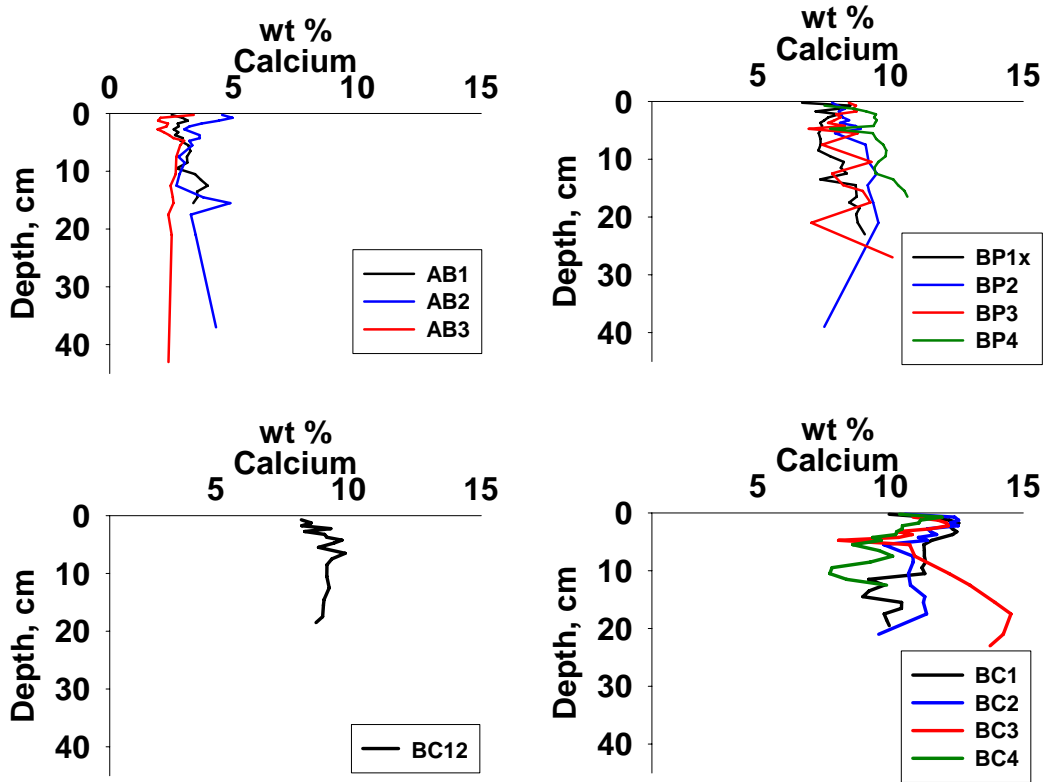
Figure 2.4.5.6 Calcium (Ca) sediment concentrations at all Basamuk stations
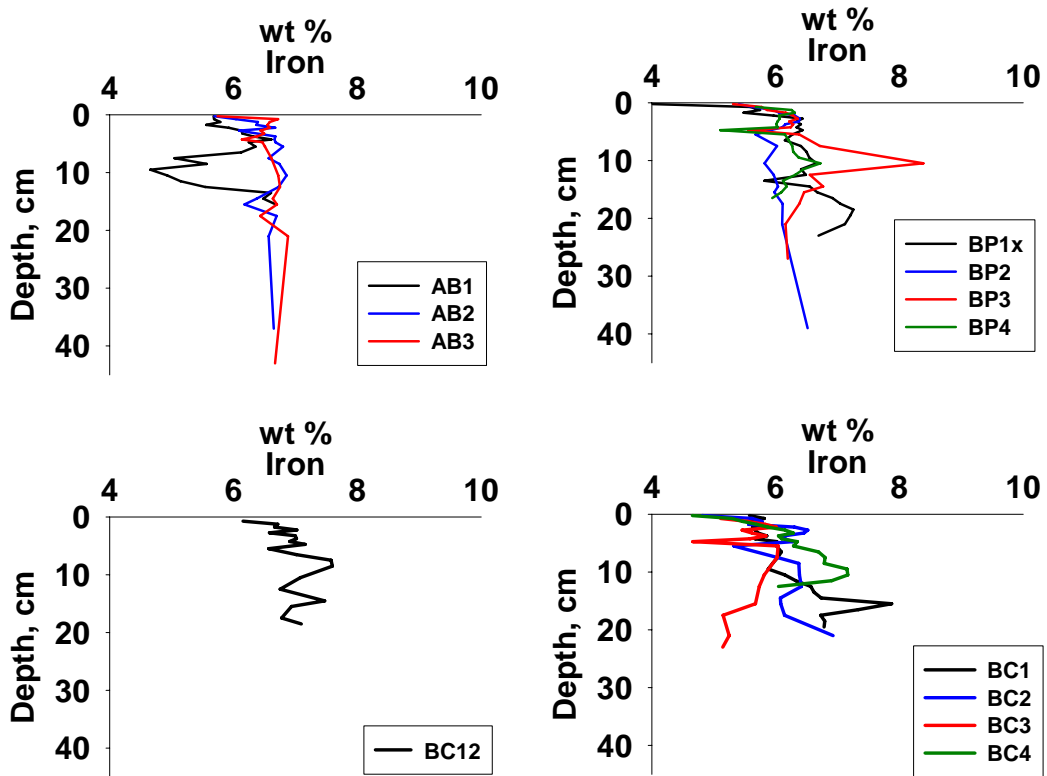
Figure 2.4.5.7 Iron (Fe) sediment concentrations at all Basamuk stations
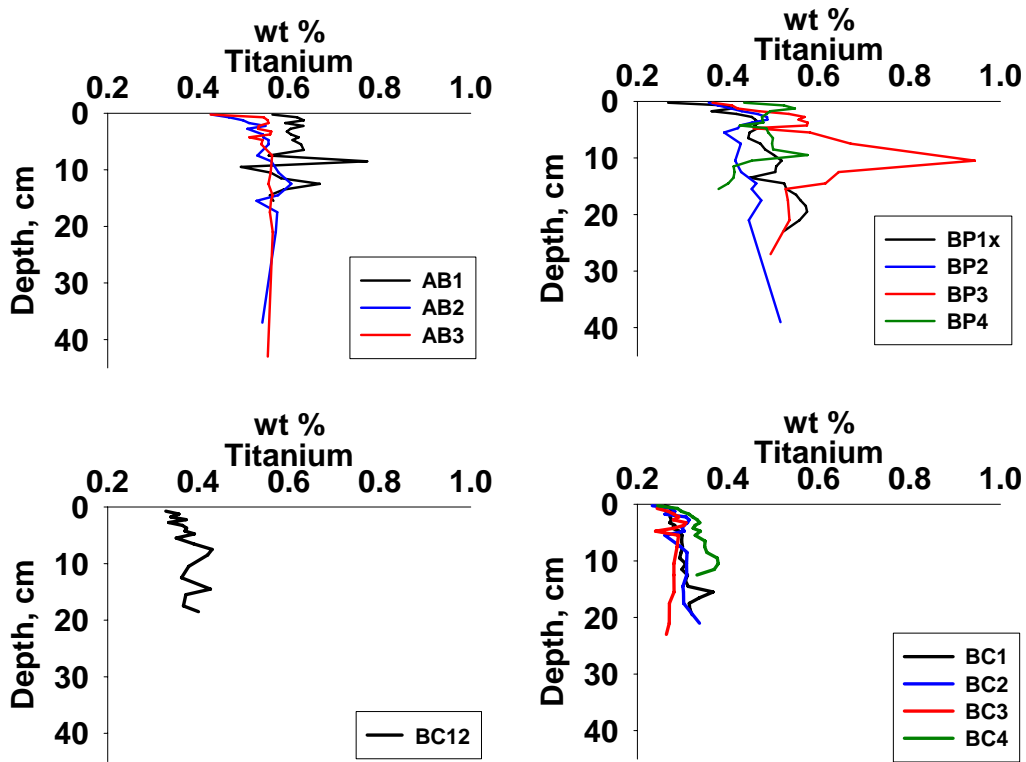
Figure 2.4.5.8 Titanium (Ti) sediment concentrations at all Basamuk stations
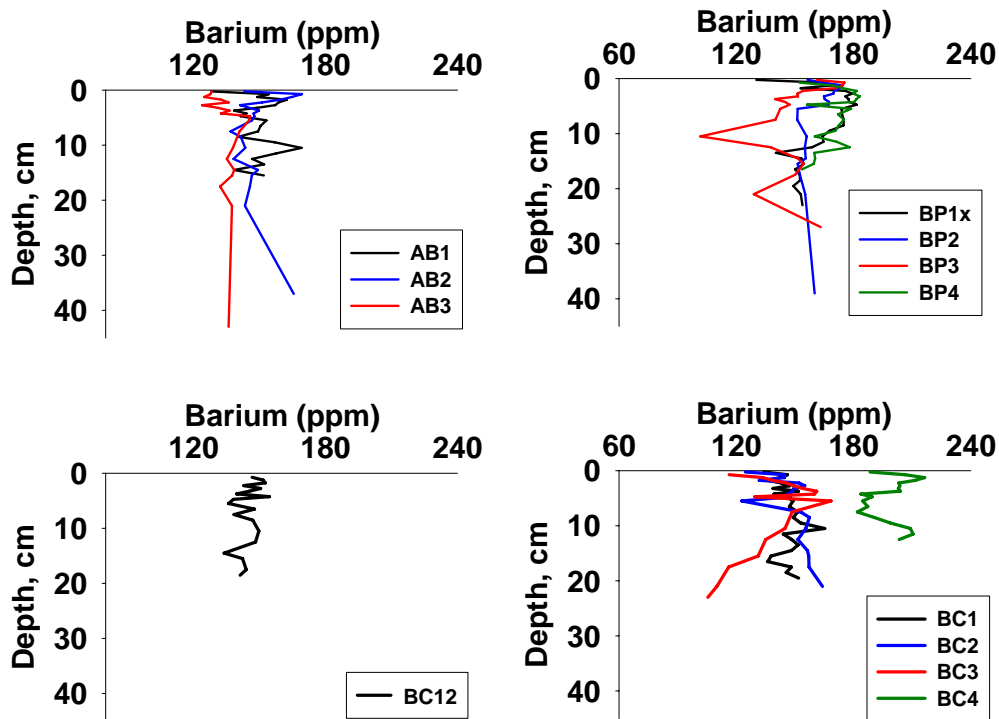
Figure 2.4.5.9 Barium (Ba) sediment concentrations at all Basamuk stations

Titanium (Ti) concentrations are lowest at the eastern transect stations (BC) and range from 0.23% to 0.38 %, BC12, 0.33 to 0.43 %. AB and BP stations have similar concentrations (0.30 to 0.77%) with the shallowest station AB1 having the highest concentration of Ti indicating higher riverine input to this station. BP3 has a maximum concentration of 0.94% at a depth of 10.5 cm, (Figure 2.4.5.8).

Barium (Ba) concentration for AB range from 124 to 169 ppm, BP from 101 to 183 ppm, BC12 from 134 to 155 ppm and eastern control transect (BC1-3) 105 to 168 ppm. BC4, the deepest station of the eastern control transect, has significantly higher Ba concentrations ranging from 182 to 216 ppm.

The concentrations of these key major and minor elements indicate that there are significant differences in the elemental signature of the sediments at the 4 main areas AB(1-3), BP(1-4), BC12 and BC(1-4) suggesting that the source of sediment supply is different to the stations. The shallowest station located in Astrolabe Bay (AB1) is receiving significant inputs of riverine and/ or aeolian inputs.

All elemental plots are given in Appendix 4A; however Figures 2.4.5.10-14 illustrates selected minor and trace elemental concentrations in sediments from all stations.
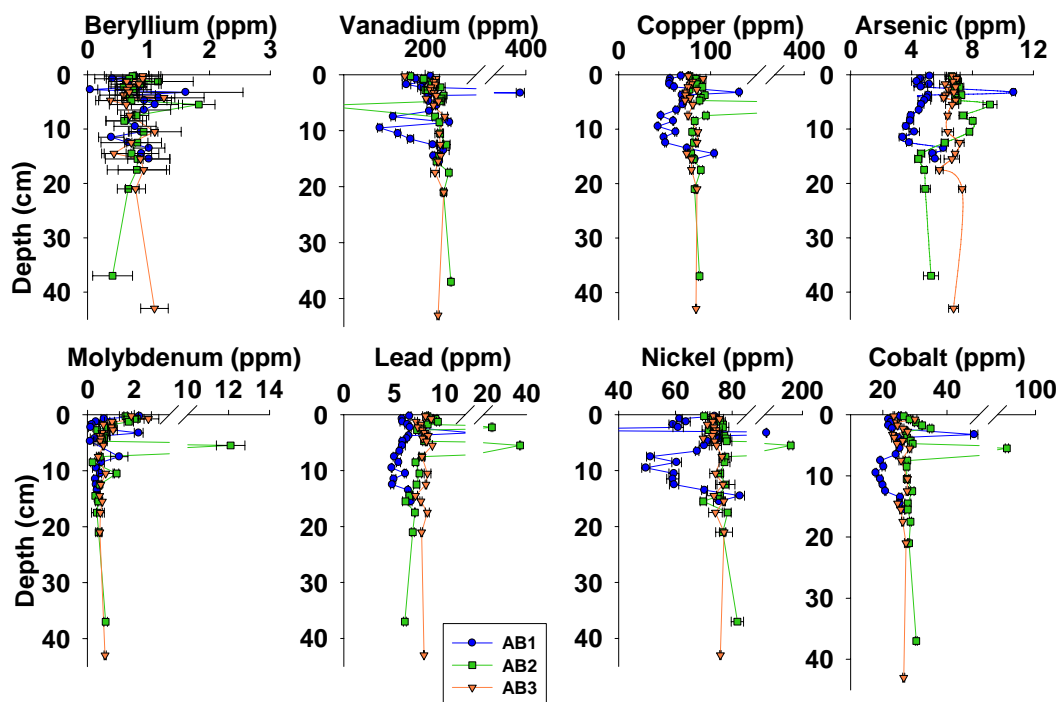
Figure 2.4.5.10 Minor and trace elemental sediment concentrations, Astrolabe Bay (AB1-3)
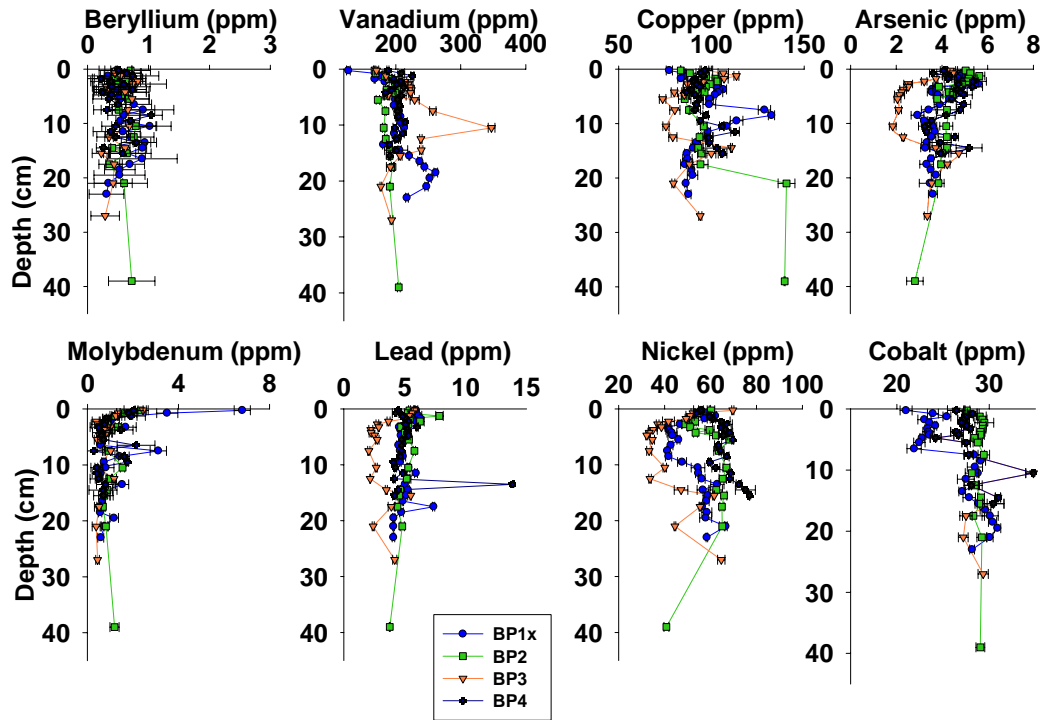
Figure 2.4.5.11 Minor and trace elemental sediment concentrations, Basamuk Bay (BP1x-4)
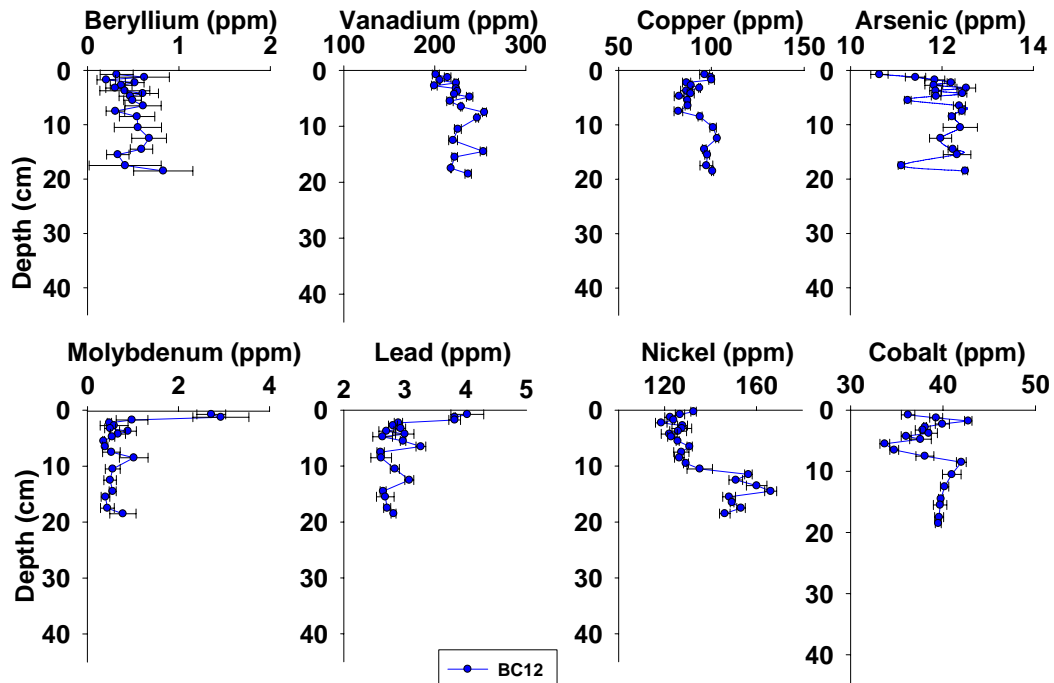
Figure 2.4.5.12 Minor and trace elemental sediment concentrations, BC12
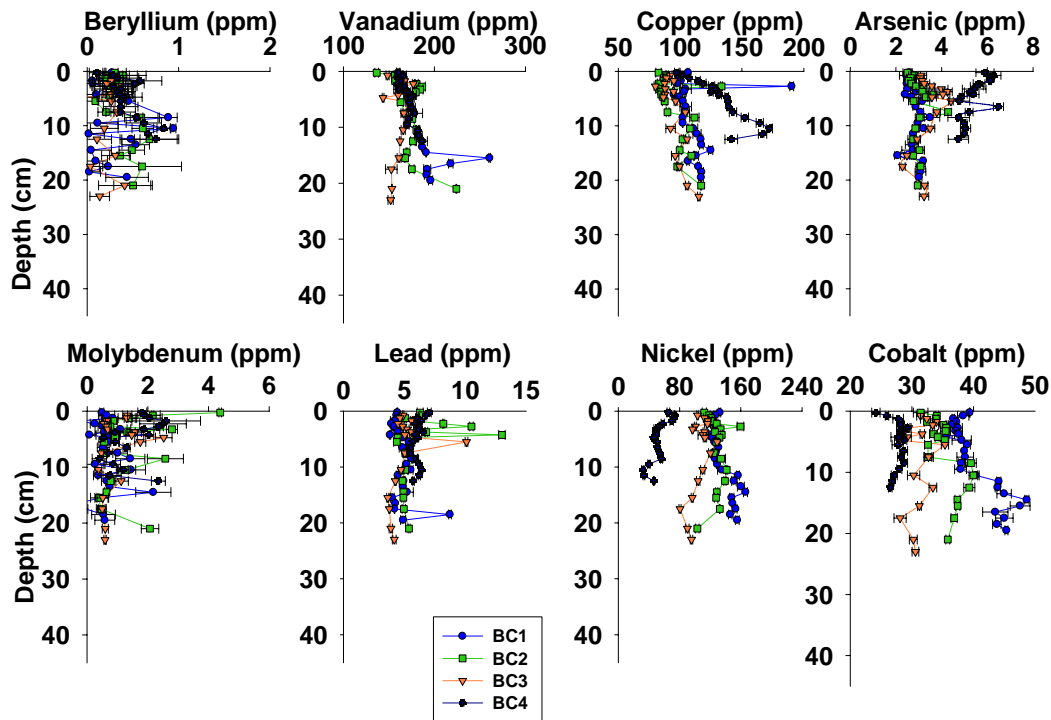
Figure 2.4.5.13 Minor and trace elemental sediment concentrations, eastern control transect, (BC1-4)

Beryllium (Be) concentrations are similar at all stations and range from 0.02 to 1.8 ppm with Astrolabe Bay having the highest concentration.

Vanadium (V) concentration ranges are, AB 155 – 397 ppm with AB1 having the highest concentration, BP, 127 – 347ppm, BP3 having the highest concentration, BC12, 200 -255 ppm and BC, 137 – 261ppm with BC1 having the highest concentration. The eastern control transect has the lowest concentrations of V compared to all other stations.

Copper (Cu) concentrations for AB, BP, BC12 and BC1-3 are all within a similar range (43- 140 ppm), however BC4 has increasing Cu concentrations with depth reaching a maximum concentration at 10.5 cm depth.

Arsenic (As) concentrations for AB, BP and BC4 stations are all similar and range from 1.8 to 10.7 with AB1 having the highest concentrations. Station BC12 has higher concentrations of As (10.6 - 12.5 ppm) and BC1-3 have lower concentrations (2.1 -4.4 ppm).

Molybdenum (Mo) concentration depth profiles are similar for AB, BP and BC12, with concentrations ranging from 0.1 to 11.9 ppm. Stations BC have lower Mo concentrations (0.3 -4.4 ppm).

Lead concentrations (Pb) at stations AB, BP and BC are all similar and range from 3.6 to 36.7ppm with AB2 having the highest concentration of Pb. BC12 has lower concentrations of Pb ranging from 2.6 to 4.0 ppm.

Nickel concentrations are generally higher at stations BC12, BC1-3 (80.6 – 166.2 ppm). AB stations have concentrations of Ni ranging from 69.8 to 178.6 ppm with AB2 having the highest concentration. BC4 has Ni concentrations similar to that of AB stations.

Cobalt (Co) concentration depth profiles are similar to the trends in Ni concentration with AB concentrations ranging from 17.8 to 54.7 ppm, BP, 21.0 to 30.9 ppm, BC12, 33.7 to 42.7 ppm and BC, 24.2 to 48.6 ppm.

The minor and trace element data indicate differences between stations. Cu, Ni and Co have the same structure within the concentration vs depth profiles for all stations, however the concentration of elements at BC stations differ with BC4 having higher Cu and lower Ni and Co concentrations from BC1-3 indicating that there is a different sediment supply possibly being influenced by Long Island and the tectonic activity prevalent in this area.

Table 2.4.5.4 gives the average concentrations of minor and trace elements found in sediments from Basamuk, Lihir and Misima stations and compares these with concentrations found in the upper crust, shale and pelagic clay sediments. Table 2.4.5.5 gives the abundance of these elements relative to upper crust, shale and pelagic clay concentrations. These trends are also illustrated for Basamuk, Figure 2.4.5.14, and compared with Lihir and Misima sediment, Figure 2.4.5.15.

When comparing the concentrations of Be and Pb found in the sediments from the Basamuk study it can be seen that concentrations within the sediments at all stations are far lower than average values of Be for upper crust, shale or pelagic clay sediments. However, although Mo concentrations at all stations are lower than both shale and pelagic clay, the sediments have similar values of Mo to the upper crust with the eastern control stations BC12 and BC2-BC4 having twice as much Mo.

Arsenic concentrations at all stations are greater than As concentrations in the upper crust, ranging from 2 to 7 times greater, with BC12 having the greatest enrichment which has similar concentrations of As to shale. All other stations have lower concentrations of As than shale. All stations have lower As than the average pelagic clay concentrations. V concentrations at all stations are greater than upper crust, shale or pelagic clay average values with the concentration

of V with in the sediments being approximately 1.5 times greater than the average value for upper crust and shale and approximately 1.8 times higher than pelagic clay.

Table 2.4.5.4 Average minor metal concentrations within Basamuk, Lihir, Misima compared to average crustal concentration, shale, pelagic clays, seawater and hydrothermal vent fluid.

Station	Be ppm	V ppm	Cu ppm	As ppm	Mo ppm	Pb ppm	Ni ppm	Co ppm
Basamuk								
AB1	0.80	208.2	67.1	4.9	0.7	6.2	65.8	24.2
AB2	0.80	205.7	99.8	6.6	1.4	9.9	81.4	31.6
AB3	0.78	209.4	79.5	6.6	0.8	7.9	74.3	26.0
BP1x	0.59	205.4	96.6	3.9	1.3	5.2	52.7	26.4
BP2	0.59	188.7	98.4	4.4	1.0	5.2	58.9	28.8
BP3	0.52	216.3	91.3	3.1	0.8	3.5	45.0	28.0
BP4	0.51	202.2	95.9	4.4	1.0	5.2	65.5	29.3
BC12	0.48	225.0	93.1	12.0	0.8	3.0	111.7	38.6
BC1	0.30	180.3	110.5	2.8	0.6	4.8	136.5	40.5
BC2	0.38	172.8	95.8	3.0	1.3	6.2	128.8	35.4
BC3	0.24	161.1	94.9	3.4	1.0	5.1	106.5	31.2
BC4	0.45	170.7	133.6	5.4	1.5	6.1	52.8	27.7
Lihir								
L1	1.16	320.0	178.9	527.7	64.43	89.9	17.2	14.4
L2	1.02	250.3	182.1	221.4	42.44	68.7	21.8	15.5
L3	0.67	158.8	100.9	87.3	15.26	31.6	19.7	15.2
L4	0.59	188.5	67.6	11.7	0.95	4.9	22.1	17.5
L5	0.46	86.2	46.9	11.7	1.43	6.0	21.6	10.7
L6	0.56	82.7	55.2	7.9	1.89	6.3	25.4	10.6
Misima								
M1	0.89	135.7	171.9	12.3	1.84	562.6	31.0	18.0
M2	1.05	139.9	191.3	12.9	1.84	690.9	34.2	18.4
M3	1.05	133.0	208.0	13.9	2.19	777.8	36.8	19.3
M4	0.32	43.3	48.8	4.4	0.88	105.4	29.8	6.6
M5	0.17	23.1	19.3	2.3	0.52	17.4	15.3	3.2
M6	0.13	11.4	13.0	1.5	0.53	2.8	16.8	1.6
Crustal abundance*	3.2	140	39	1.6	1.6	17	55	17
Shale*	3	130	45	13	2.6	20	50	19
Pelagic Clay*	2.6	120	250	20	27	80	230	74
	ng l^{-1}	ng l^{-1}	ng l^{-1}	ng l^{-1}	ng l^{-1}	ng l^{-1}	ng l^{-1}	ng l^{-1}
Seawater*	0.21	2150	210	1700	10300	2.7	530	1.2
vent solution*	120		2800000	35000		75000		13000

*Li Y-H and Schoonmaker J.E. (2003) Chemical composition and mineralogy of marine sediments, pp 1-35. In *Sediments, Diagenesis, and Sedimentary Rocks* (ed F.T. MacKenzie) Vol. 7 *Treatise on Geochemistry* (eds H.D. Holland and K.K. Turekian), Elsevier-Pergamon, Oxford.

Cu concentrations found in the Basamuk study sediments are all higher than the upper crust and shale but lower than the average Cu concentration in pelagic clay.

Ni concentrations at all stations are lower than the average value found in pelagic clay. Ni concentrations at stations AB1-3 are higher than crustal abundance and shale, BP1x and BP4 have similar concentration of Ni as the upper crust but lower than shale. BP3 has lower values than both the upper crust and shale and BP4 has twice as much Ni as both the crust and shale. Stations BC12 and BC1 - 3 have twice as much Ni as the crust and shale with BP4 having a similar value to the crust but a small enrichment in Ni when compared to average values of Ni concentration in shale.

Finally, Co concentrations for the Basamuk study sediments are all greater than the average concentrations in the crust and shale with stations BC12, BC1- 2 having the greatest enrichment.

Table 2.4.5.5 Average minor metal abundances within Basamuk, Lihir and Misima when compared to shale and pelagic clays.

| Station	Be			V			Cu			As			Mo			Pb			Ni			Co		
	crust	shale	clay	crust	shale	clay	crust	shale	clay	crust	shale	clay	crust	shale	clay	crust	shale	clay	crust	shale	clay	crust	shale	clay
Basamuk																								
AB1	0.25	0.27	0.31	1.49	1.60	1.73	1.72	1.49	0.27	3.08	0.38	0.25	1.20	0.25	0.02	0.36	0.31	0.08	1.20	1.32	0.29	1.42	1.27	0.33
AB2	0.25	0.27	0.31	1.47	1.58	1.71	2.56	2.22	0.40	4.11	0.51	0.33	1.48	0.55	0.05	0.58	0.49	0.12	1.48	1.63	0.35	1.86	1.66	0.43
AB3	0.24	0.26	0.30	1.50	1.61	1.75	2.04	1.77	0.32	4.14	0.51	0.33	1.35	0.32	0.03	0.47	0.40	0.10	1.35	1.49	0.32	1.53	1.37	0.35
BP1x	0.19	0.20	0.23	1.47	1.58	1.71	2.48	2.15	0.39	2.42	0.30	0.19	0.96	0.49	0.05	0.30	0.26	0.06	0.96	1.05	0.23	1.55	1.39	0.36
BP2	0.18	0.20	0.23	1.35	1.45	1.57	2.52	2.19	0.39	2.75	0.34	0.22	1.07	0.40	0.04	0.31	0.26	0.07	1.07	1.18	0.26	1.70	1.52	0.39
BP3	0.16	0.17	0.20	1.55	1.66	1.80	2.34	2.03	0.37	1.96	0.24	0.16	0.82	0.32	0.03	0.21	0.18	0.04	0.82	0.90	0.20	1.65	1.48	0.38
BP4	0.16	0.17	0.20	1.44	1.56	1.69	2.46	2.13	0.38	2.74	0.34	0.22	1.19	0.39	0.04	0.31	0.26	0.07	1.19	1.31	0.28	1.72	1.54	0.40
BC12	0.15	0.16	0.19	1.61	1.73	1.87	2.39	2.07	0.37	7.48	0.92	0.60	2.03	0.32	0.03	0.18	0.15	0.04	2.03	2.23	0.49	2.27	2.03	0.52
BC1	0.09	0.10	0.12	1.29	1.39	1.50	2.83	2.46	0.44	1.76	0.22	0.14	2.48	0.24	0.02	0.28	0.24	0.06	2.48	2.73	0.59	2.38	2.13	0.55
BC2	0.12	0.13	0.15	1.23	1.33	1.44	2.46	2.13	0.38	1.87	0.23	0.15	2.34	0.52	0.05	0.37	0.31	0.08	2.34	2.58	0.56	2.08	1.86	0.48
BC3	0.08	0.08	0.09	1.15	1.24	1.34	2.43	2.11	0.38	2.13	0.26	0.17	1.94	0.38	0.04	0.30	0.25	0.06	1.94	2.13	0.46	1.83	1.64	0.42
BC4	0.14	0.15	0.17	1.22	1.31	1.42	3.43	2.97	0.53	3.38	0.42	0.27	0.96	0.58	0.06	0.36	0.31	0.08	0.96	1.06	0.23	1.63	1.46	0.37
Station	Be			V			Cu			As			Mo			Pb			Ni			Co		
	crust	shale	clay	crust	shale	clay	crust	shale	clay	crust	shale	clay	crust	shale	clay	crust	shale	clay	crust	shale	clay	crust	shale	clay
Lihir																								
L1	0.36	0.39	0.45	2.29	2.46	2.67	4.59	3.97	0.72	329.83	40.60	26.39	0.31	24.78	2.39	5.29	4.50	1.12	0.31	0.34	0.07	0.85	0.76	0.19
L2	0.32	0.34	0.39	1.79	1.93	2.09	4.67	4.05	0.73	138.36	17.03	11.07	0.40	16.32	1.57	4.04	3.43	0.86	0.40	0.44	0.09	0.91	0.81	0.21
L3	0.21	0.22	0.26	1.13	1.22	1.32	2.59	2.24	0.40	54.56	6.71	4.36	0.36	5.87	0.57	1.86	1.58	0.39	0.36	0.39	0.09	0.89	0.80	0.21
L4	0.19	0.20	0.23	1.35	1.45	1.57	1.73	1.50	0.27	7.31	0.90	0.58	0.40	0.36	0.04	0.29	0.24	0.06	0.40	0.44	0.10	1.03	0.92	0.24
L5	0.15	0.15	0.18	0.62	0.66	0.72	1.20	1.04	0.19	7.33	0.90	0.59	0.39	0.55	0.05	0.35	0.30	0.08	0.39	0.43	0.09	0.63	0.56	0.14
L6	0.18	0.19	0.22	0.59	0.64	0.69	1.42	1.23	0.22	4.93	0.61	0.39	0.46	0.73	0.07	0.37	0.31	0.08	0.46	0.51	0.11	0.62	0.56	0.14
Misima																								
M1	0.28	0.30	0.34	0.97	1.04	1.13	4.41	3.82	0.69	7.70	0.95	0.62	0.56	0.71	0.07	33.09	28.13	7.03	0.56	0.62	0.13	1.06	0.95	0.24
M2	0.33	0.35	0.40	1.00	1.08	1.17	4.91	4.25	0.77	8.06	0.99	0.64	0.62	0.71	0.07	40.64	34.55	8.64	0.62	0.68	0.15	1.08	0.97	0.25
M3	0.33	0.35	0.40	0.95	1.02	1.11	5.33	4.62	0.83	8.71	1.07	0.70	0.67	0.84	0.08	45.75	38.89	9.72	0.67	0.74	0.16	1.13	1.01	0.26
M4	0.10	0.11	0.12	0.31	0.33	0.36	1.25	1.08	0.20	2.72	0.34	0.22	0.54	0.34	0.03	6.20	5.27	1.32	0.54	0.60	0.13	0.39	0.35	0.09
M5	0.05	0.06	0.07	0.17	0.18	0.19	0.49	0.43	0.08	1.44	0.18	0.12	0.28	0.20	0.02	1.02	0.87	0.22	0.28	0.31	0.07	0.19	0.17	0.04
M6	0.04	0.04	0.05	0.08	0.09	0.09	0.33	0.29	0.05	0.95	0.12	0.08	0.31	0.20	0.02	0.17	0.14	0.04	0.31	0.34	0.07	0.09	0.08	0.02
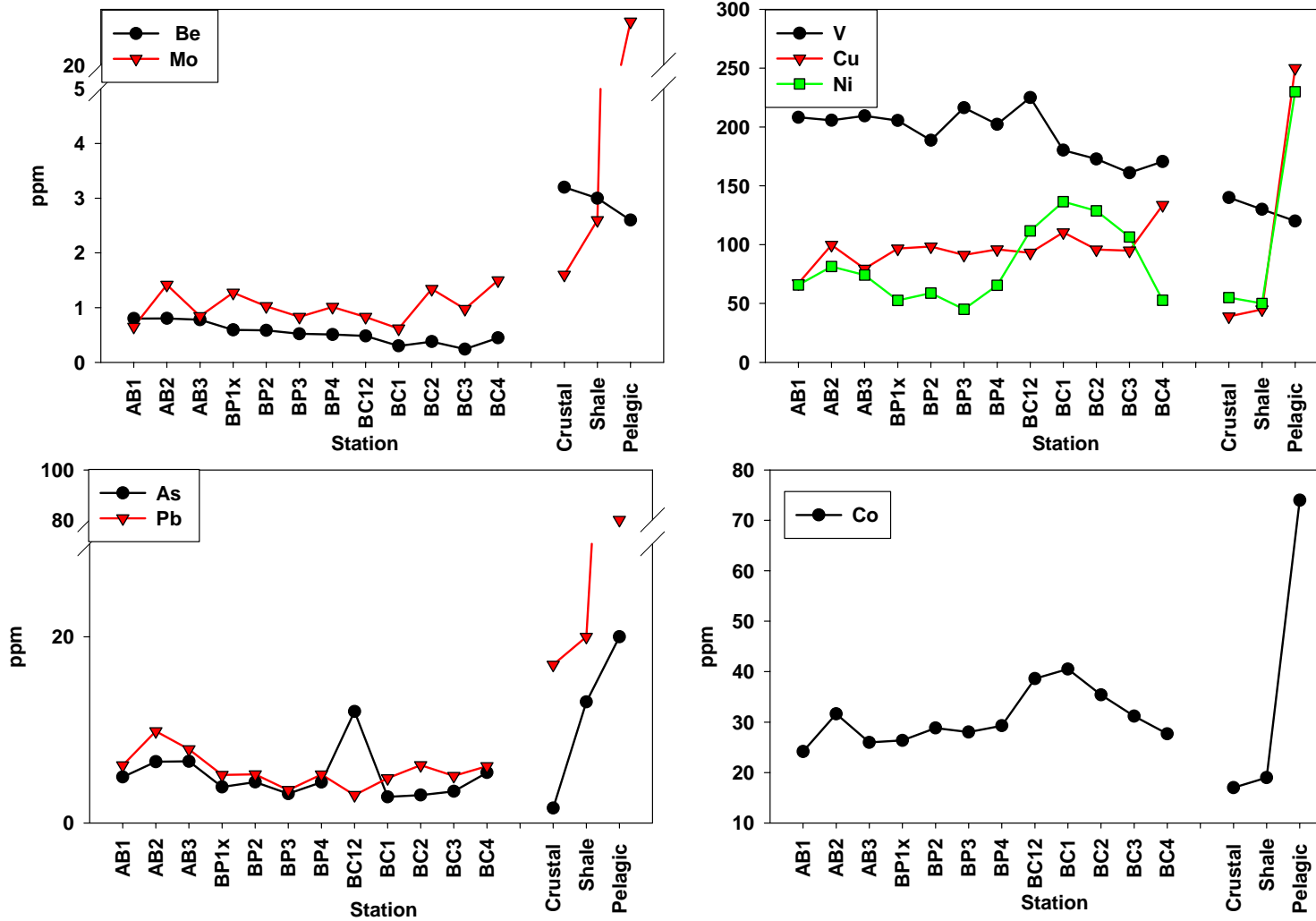
Figure 2.4.5.14 Average minor metal concentrations within sediments from Basamuk Study compared to average crustal abundance, shale and pelagic clays.
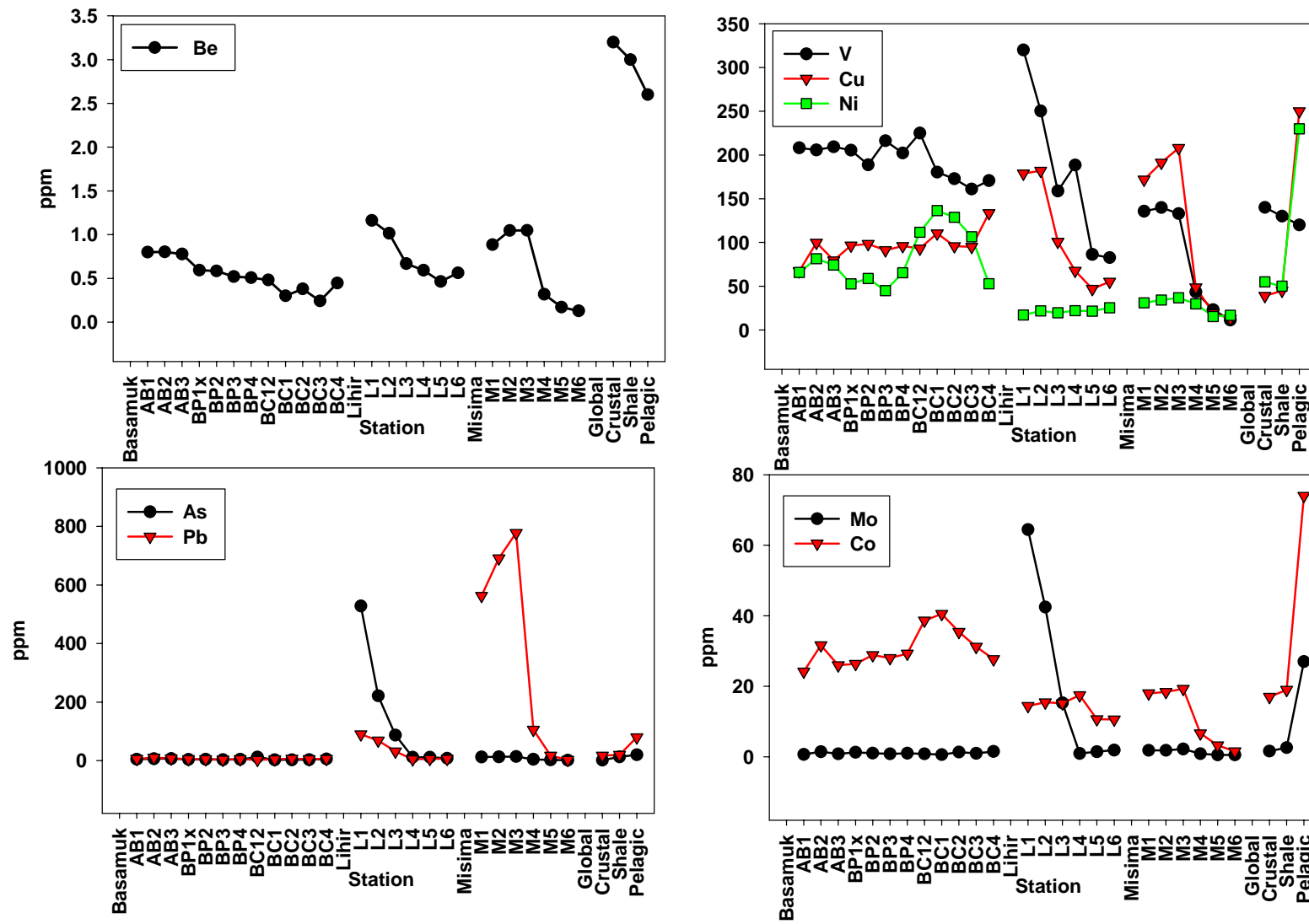
Figure 2.4.5.15 Average minor metal concentrations within Basamuk, Lihir, Misima compared to average crustal abundance, shale and pelagic clays.

To investigate any statistical relationships between elements, Pearson Product Moment Correlation coefficients were calculated for sediment cores at each of the twelve stations. The pairs of elements that showed positive correlation coefficients with a P value below 0.05 were considered to increase together. For the pairs with negative correlation coefficients and P values below 0.05, one element tends to decrease while the other increases.The correlation coefficients were calculated on the complete data set for each core.The results of the Pearson Product Moment Correlation tests are given in Appendix 4B, tables 4B:162-173.

The correlation coefficients are useful in indicating which mineral assemblages are dictating the distribution of heavy metals within the system. The sediments will comprise of a combination of lithogenic, biogenic and authigenic material. However for this area where there are massive amounts of land runoff, tectonic activity, hydrothermal vents and volcanic input, it is a complicated picture.

The Pearson Product Moment Correlations for stations AB 1-3 show that AB1 has the least number of negative correlations. Station AB1 has the strongest correlations between Co, Cr, Cu, Ni and V of the three AB stations. The main negative correlations occurring at station AB2 are with Cr and V and a large number of minor and trace elements. Ca, Sr and Ba have strong correlations at AB2 and AB3 with AB1 having no strong correlation with Ba and Sr and Ca but a correlation between Sr and Ca. AB1 has the largest number of positive correlations of organic C with other elements suggesting that this coastal station is influenced by land runoff.

The correlations for the Basamuk stations (BP1x- 4) suggest that V, Cr and Ni are being controlled by Ca, Fe, Mg, Li and Ti. In addition V has a strong correlation with Al. This relationship is not apparent in the other stations although there are some positive correlations between the elements. The organic carbon has most correlations (both positive and negative) at station BP1x.

For station BC12 the main correlations are between Fe, K, Mg, Ba, Ca and Ti. V and Cr have strongest correlations with Fe and Ti. Pb and Cd have a large number of negative correlations with Al, Ba, Ca, Fe, Mg, Ti, V and Cr. Co and Ni have correlations with K and Mg and there are no correlations between Ba, Ca and Sr.

The eastern control transect shows similar tends in that the most positive correlations are found at the shallower station BC1 with BC3 having the least number of correlations. BC4, the deepest station of the transect, has the largest number of negative correlations. The correlation

coefficients for elements differ within transect and indicate the effects of land and marine derived inputs.

It is also important for a baseline survey to assess the amounts of elements within the sediment regime so that any future impact of metals can be assessed. Inventories of all elements for all twelve cores were calculated and expressed as $g\ m^{-2}$. In order to compare the excess inventories of elements at all stations the depth range that the excess was calculated for was determined to a similar depth in each core. In this case this was a depth of 16 cm with the exception of BC4 which has been calculated to 13 cm, the entire length of the core. The total elemental inventories for cores at all stations are given in Appendix 4B, tables 4B:140-161.

The total elemental inventories ($g\ m^{-2}$) for all stations are shown in Figure 2.4.5.14 and 2.4.5.15. The range of inventories calculated for each element expressed as $g\ cm^{-2}$ is given in Table 2.4.5.6.

Firstly considering the major element inventories, Al inventories range from 4695 to 12577 $g\ m^{-2}$ and are highest at stations AB1, BP3 and BC12 with lowest inventories found at the eastern control transect (BC1-3).

The highest Ca inventories, (15094, 14913 $g\ m^{-2}$), occur at BP3 and BC12 stations with the lowest occurring at stations AB1-3 (2846 – 5905 $g\ m^{-2}$).

Fe inventories range from 5850 to 12455 $g\ m^{-2}$ and are highest at stations BP3, BC12 and AB1, similar to Al. The lowest Fe inventory occurs at station BC3.

K inventories are similar at all stations and range from 1042 to 2244 $g\ m^{-2}$, with Station BP3 having the highest inventory and station BC3 having the lowest.

Ti inventories range from 287 to 1205 $g\ m^{-2}$ with highest inventories occurring at BP3 and AB1 and the lowest at BC3.

In contrast to Al, Ca, Fe, K and Ti where BC3 has the lowest inventories, the highest inventory of Mg occurs at BC3. Mg inventories range from 3000 to 8288 $g\ m^{-2}$ with the lowest occurring at AB3.

Minor element inventories are as follows. Ba inventories range from 15 to 28 $g\ m^{-2}$ with highest inventories occurring at BP3, BC12 and BC4, the deeper stations and the lowest at AB1, the shallowest station.

Table 2.4.5.6 Elemental inventory ranges occurring at Basamuk study stations.

Element	Min. inventory g m^{-2}	Max. inventory g m^{-2}
Aluminium (Al)	4695	12577
Barium (Ba)	15	28
Calcium (Ca)	2846	15094
Iron (Fe)	5860	12455
Potassium (K)	1042	2244
Magnesium (Mg)	3000	8288
Manganese (Mn)	98	231
Sodium (Na)	2514	5267
Strontium (Sr)	26	84
Titanium (Ti)	287	1205
Lithium (Li)	1.4	4.6
Beryllium (Be)	0.04	0.15
Boron (B)	2	73
Vanadium (V)	17	46
Chromium Cr)	9	66
Cobalt (Co)	3	6
Nickel (Ni)	6	18
Zinc (Zn)	10	59
Copper (Cu)	9	16
Gallium (Ga)	0.9	2.8
Arsenic (As)	0.3	2.0
Rubidium (Rb)	1.9	5.0
Molybdenum (Mo)	0.08	0.18
Silver (Ag)	0.0	1.8
Cadmium (Cd)	0.00	0.04
Caesium (Cs)	0.06	0.26
Cerium (Ce)	1.2	3.6
Lead (Pb)	0.5	1.1
Thorium (Th)	0.07	0.37
Uranium (U)	0.05	0.12
Corg	428	1138

Sr inventories range from 26 to 84 g m^{-2}, station BP3 has the highest inventory with the lowest inventories of Sr occurring at the AB stations.

Li and Rb inventories range from 1.4 to 4.6 g m^{-2} and 1.9 to 5 g m^{-2} respectively with the highest inventories occurring at the AB stations and the lowest at the BC stations.

Similar trends are apparent for Ce and Ga with the highest two inventories occurring at AB1 and BP3.

Co inventories range from 3 to 6 g m^{-2}, the highest inventories occurring at BC12, BP3 and BC1. The lowest inventory of Co occurs at AB3.

Ni inventories range from 6 to 18 g m^{-2}, station BC12 having the highest inventory and BC4 the lowest. The trend of inventories for the stations is BC12>BC1-3>AB>BP>BC4.

Conversely, Cu inventories range from 9 to 16 g m^{-2} with the highest inventory occurring at BC4 and the lowest at AB3.

V inventories range from 17 to 46 g m^{-2} with the highest values occurring at BP3, BC12 and AB1 and the lowest inventory occurring at BC3.

Cr inventories range from 9 to 66 g m^{-2} with the highest inventory occurring at BC12 which is twice that of the next highest inventories occurring at the BC1-3 stations. The lowest inventory occurs at BC4.

Zn inventories range from 10 to 59 g m^{-2} with the highest inventories occurring at AB1 and BC2, the lowest at BC4.

Mn inventories range form 98 to 231 g m^{-2}; the highest inventories occur at BP3, BC12 and BC4 with the lowest inventory occurring at AB2.

Trace element inventories for all stations are briefly described in the following text. Be inventories range from 0.04 to 0.15 g m^{-2} with the highest inventory occurring at AB1 and the lowest at BC2.

Mo inventories range from 0.08 to 0.18 g m^{-2} with AB2 having the highest inventory and AB3 the lowest.

Cs inventories range from 0.06 to 0.26 g m^{-2} with the highest inventories occurring at the AB stations and the lowest at the eastern control transect BC stations.

Th inventories range from 007 to 0.37 g m^{-2} and follow a similar trend to Cs in that the AB stations have the highest inventories and BC stations the lowest.

U inventories range from 0.05 to 0.12 g m^{-2} with the highest inventories occurring at the AB and BP stations and the lowest at BC12 and BC stations.

Cd inventories range from 0 to 0.04 g m^{-2} with the highest inventory occurring at BP4 and the lowest at AB2.

As inventories range from 0.3 to 2.0 g m^{-2} with station BC12 having the highest inventory, 2.5 times higher than the next highest inventory at station AB1. The As inventories follow the trend BC12>AB>BP>BC.

Ag inventories were only calculated for 5 stations (BP4, BC12, and BC2-BC4). The inventories range from 0.01 to 0.18 g m^{-2} with station BC4 having the highest inventory and BC3 the lowest. The trend in Ag inventories is BC4>BC2>BP4>BC12>BC3.

Cd inventories for all stations were low ranging from 0 to 0.02 g m^{-2}.

Pb inventories ranged from 0.5 to 1.1 g m^{-2} with the AB stations having the highest inventories and BC12 the lowest.

Finally the organic carbon inventory ranges from 428 to 1138 g m^{-2} with the highest inventories occurring at the BP stations and the lowest at the BC stations, with BC4 having the lowest inventory of organic carbon.

The dissolved nutrient and elemental concentrations within the pore-water samples of cores taken at each of the eight stations (Table 2.4.5.1) are reported in Appendix 4B, tables 4B.1-25 and 4B.53-57). No pore-water samples were obtained from station AB2, BP2, BC3 and BC4. Figures of the elemental depth profiles for each station are given in Appendix 4A, Figures 4.A.19-45.

Pore-water nutrient concentrations were measured at 8 stations around the coastal margin of Basamuk region. Seven of these stations were measured using triplicate sediment core deployments in order to better determine the degree of spatial heterogeneity of the pore-water profiles.

In general all the nutrient concentration profiles show good agreement within the triplicate sets suggesting low spatial heterogeneity within each coring location and further suggesting good technique in core recovery and sample processing.

The breakdown of organic material within the sediment leads to the formation of dissolved ammonia and phosphate within the pore-water and, if the organic material contained algal silica frustules, dissolved silica. If the sediment remains oxic with depth the ammonia is oxidised to nitrate, but if the organic loading is sufficient and the pore-water oxygen is depleted to suboxic or anoxic conditions the ammonia remains.

Ammonia profiles generally show an increase in depth and this is associated with the nitrate profiles which tend to decrease just below the sediment surface and then remain constant at around 10µM suggesting that the whole region experiences low oxygen pore-water conditions. Highest ammonia conditions are found to the west of the region along the AB transect and station AB3 also shows highest surficial nitrate concentration suggesting that this station receives the greatest nitrogen loading of the region. Phosphate concentration increase towards the east of the region with station AB1 showing the lowest concentrations (~0.5-1 µM) and stations along the BC transect showing the highest, (4-15 µM). This variation in increasing ammonia and phosphate concentrations has a bearing on the pore-water N:P ratio, which becomes progressively smaller towards the east. A decrease in the N:P ratio suggests an increase in the labile fraction of the organic material reaching the sediment which may further suggest that there is change towards a decreasing influence of a more refractory terrestrially-derived carbon with a lower phosphorus content moving from west to the east of the region.
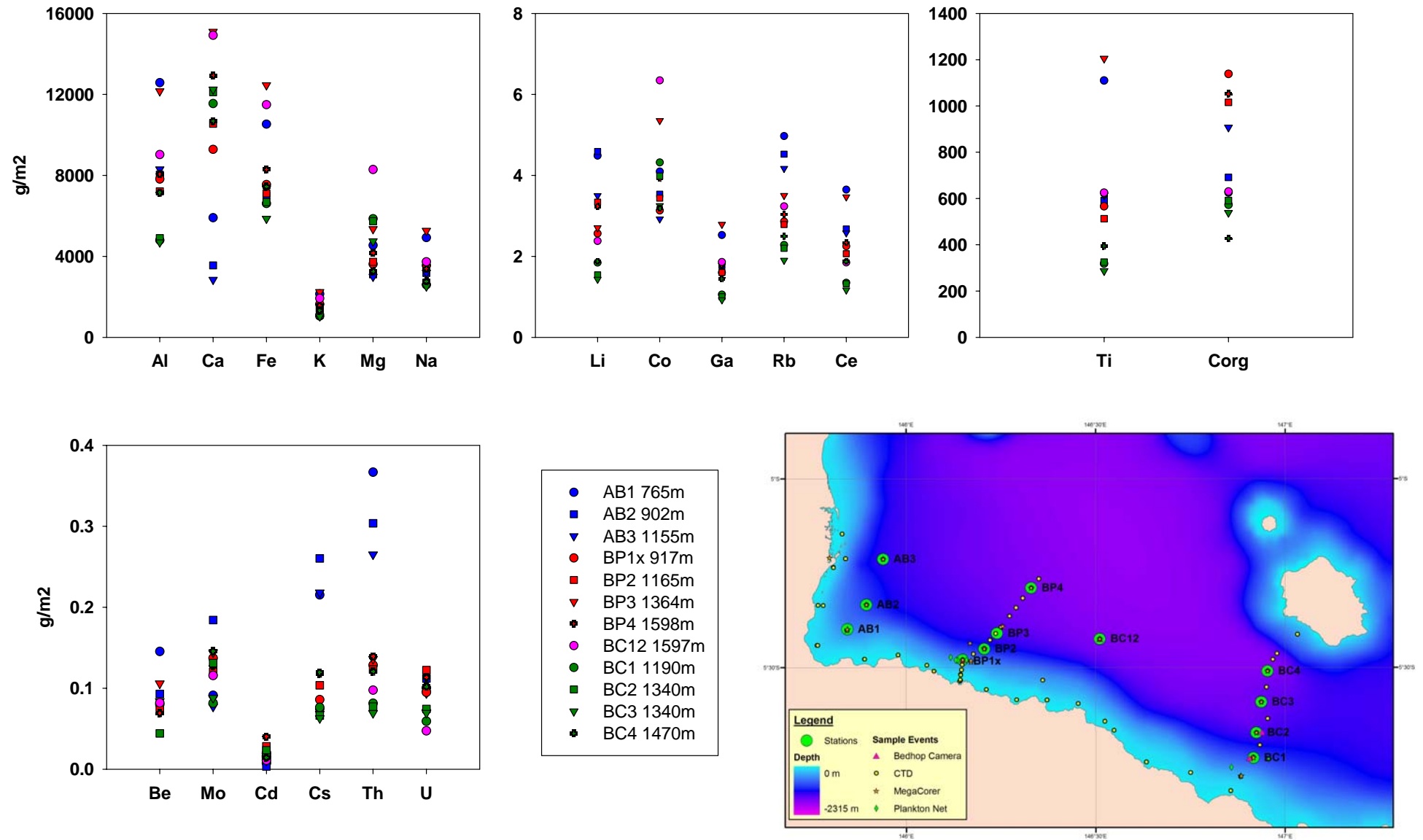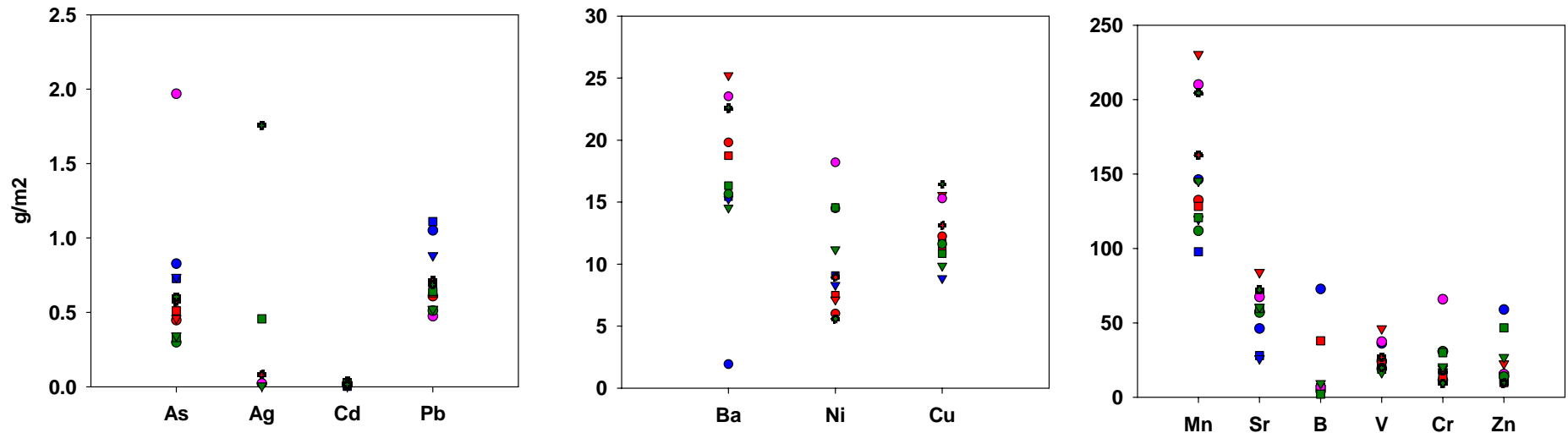
Figure 2.4.5.14 Total inventory of elements within the top 16 cm of Basamuk study sediments (a)
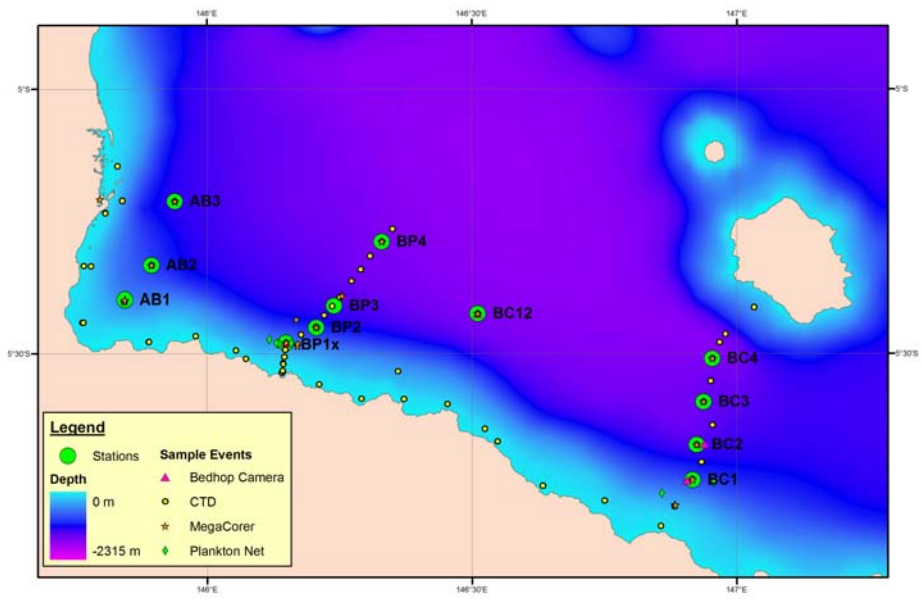
Figure 2.4.5.14 Total inventory of elements within the top 16 cm of Basamuk study sediments (b)

The solid phase and dissolved concentrations of Mn, Fe, Mo and U can be used to determine the redox state of sediment. The redox state of the sediment, either oxidising or reducing, will determine which biogeochemical processes will occur within the sediment environment and hence will give an indication of which elements may move within the sediment core through diffusion in the pore-water to be concentrated in oxidising surface sediments or alternatively released into the overlying water column. An example of this is Mn which is removed to the solid phase under oxidising conditions and is in the dissolved phase under reducing conditions. In comparison, U is soluble in oxidising conditions and removed to the solid phase in reducing conditions.

Manganese, Fe, Mo and U solid phase and aqueous phase for stations within each of the four transects, Astrolabe Bay, Basamuk, eastern control transect and Helmholtz point are illustrated in Figures 2.4.5.15-18.

Figure 2.4.5.15 Mn, Fe, Mo and U solid phase (ppm or %) and pore-water (ppb) concentrations of Astrolabe Bay stations, AB1 and AB3

2.4.5.16 Mn, Fe, Mo and U solid phase and pore-water concentrations of Basamuk stations, BP1x and BP4.
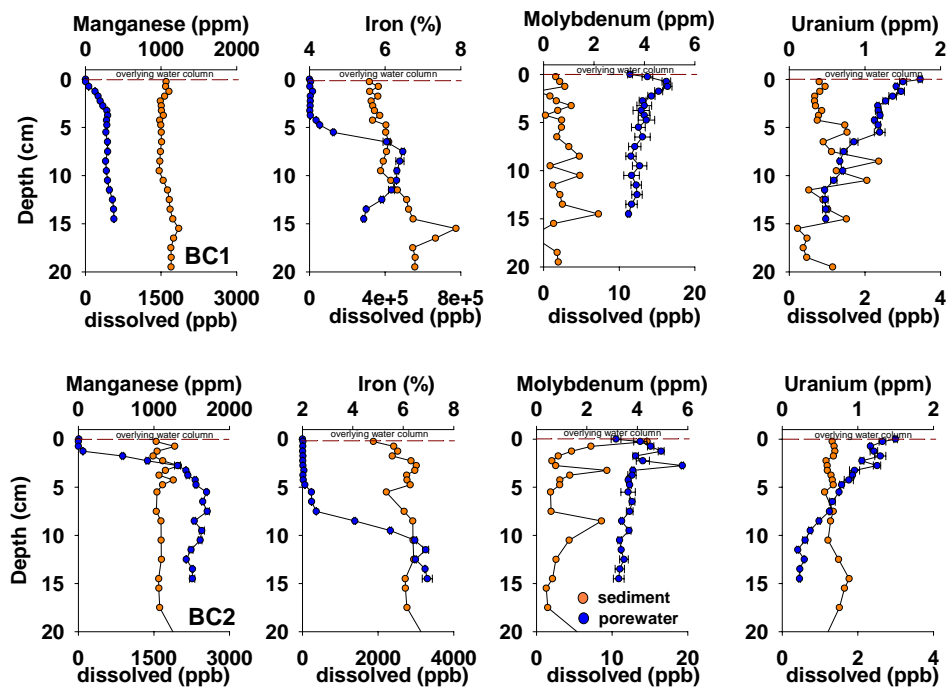
Figure 2.4.5.17 Mn, Fe, Mo and U solid phase (ppm or %) and pore-water (ppb) concentrations of Eastern control transect stations, BC1 and BC2.
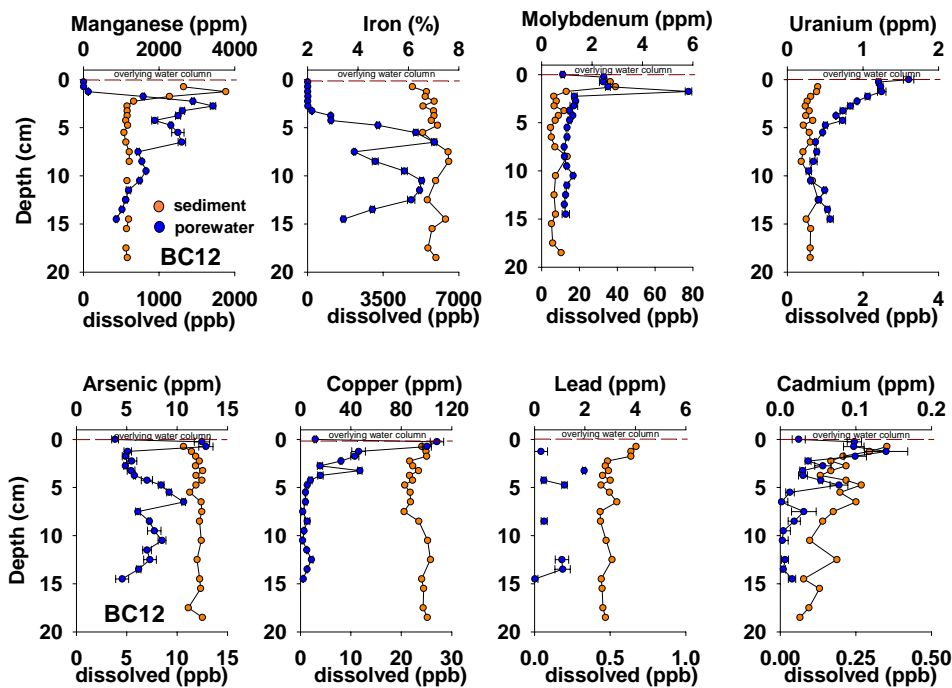
Figure 2.4.5.18 Mn, Fe, Mo,U, As, Cu, Pb and Cd solid phase (ppm or %) and pore-water (ppb) concentrations of Eastern control transect stations, BC12.
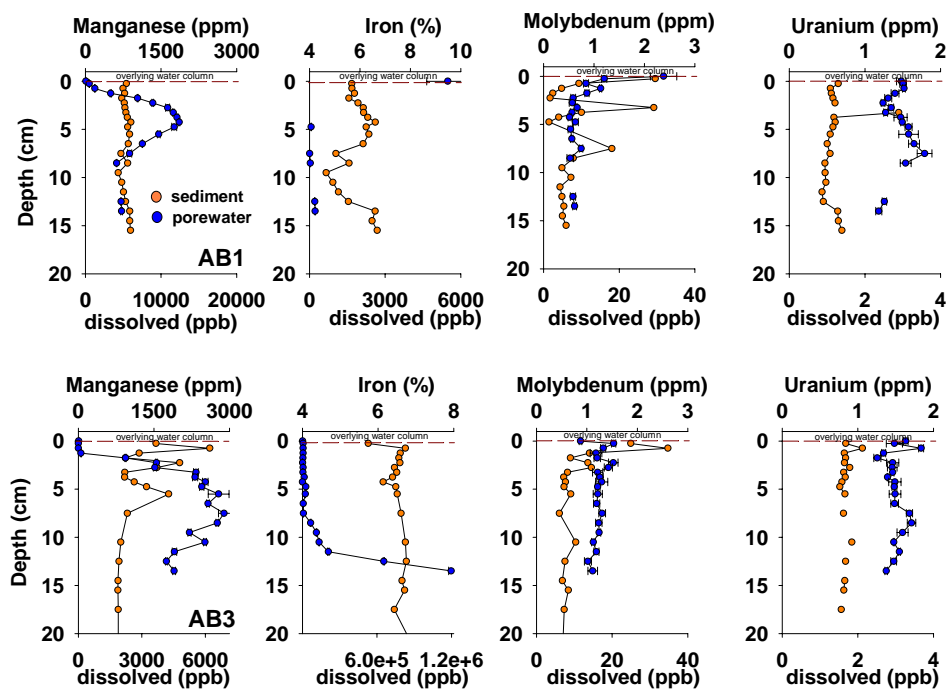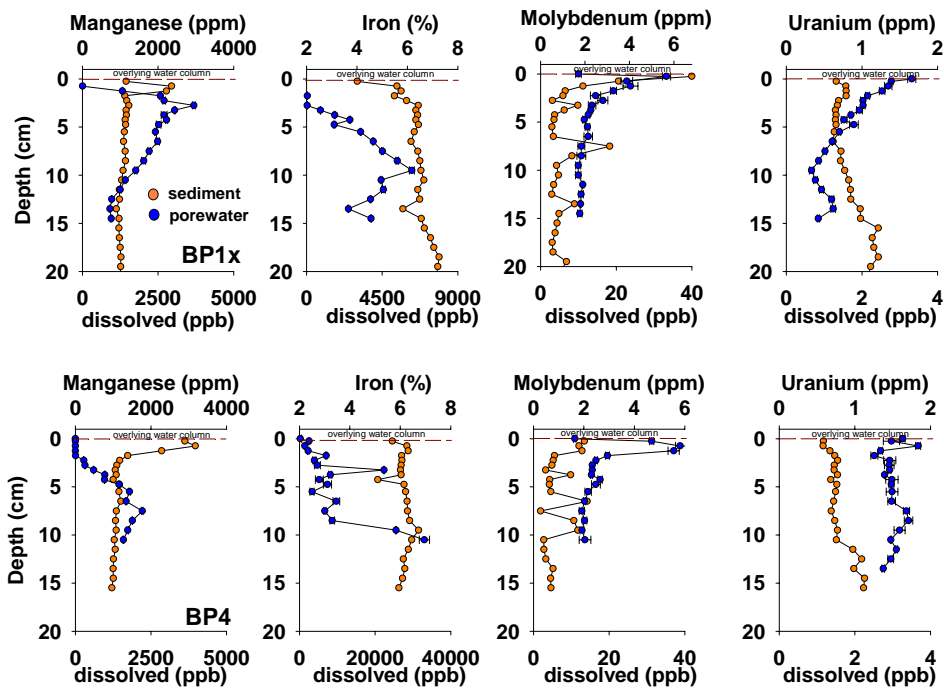
The solid phase concentrations of Mn within sediments from AB1 and AB3 differ in that the concentration of AB1 is lower than that of AB3 (Figure 2.4.5.15). In contrast, the dissolved concentration within the pore-waters at AB1 is double the concentration found within AB3. Solid phase concentrations of Fe are also lower at station AB1 compared to AB3. The dissolved concentration of Fe is very different with a high value at the surface of AB1 and low values at depth. In contrast, AB3 has very low values at the surface of AB3 and the dissolved concentration of Fe increases at depth to very high values below the corresponding depth of dissolution of Mn in this core. Solid phase Mo depth profiles are similar but the solid phase concentration of Mo is higher at the surface of AB1 compared to AB3. A similar trend in observed in the dissolved Mo. Solid phase concentrations of U are generally higher at AB3 with dissolved concentrations similar.

The profiles indicate that early diagenesis is taking place with both Mn and Fe being released to the pore-water system. Mn is being removed from the pore-water at the surface of the sediment due to oxidation. Fe within AB3 is being reduced at a greater depth within the sediment core as would be expected by the differences in redox potential, once again Fe is being removed from the pore-water as it moves towards the oxidising surface sediment. Molybdenum behaviour is being

determined by the Mn biogeochemical cycling. The combined profiles would suggest that both sediment cores are oxidising at the surface with the suboxic boundary closer to the surface at AB1.

The solid phase concentrations for BP1x and BP4 (Figure 2.4.5.16) are similar with BP4 having higher Mn concentrations at the surface. However, dissolved Mn concentrations are different with BP1x having twice the dissolved concentration of Mn than BP4. In addition the dissolved Mn is removed from solution at a greater depth in BP4. Solid phase Fe concentrations are similar but once again the dissolved Fe concentrations are far greater at the deeper station, BP4, which has dissolved concentrations 5 times greater than BP1x. Solid phase Mo concentrations are higher at the surface of BP1x by a factor of three with dissolved Mo concentrations being similar. Solid phase U concentrations are similar with dissolvesd concentrations of U being removed at depth at BP1x compared to BP4. The solid phase and dissolved profiles for the Basamuk stations indicate that BP1x is more reducing than BP4.

The solid phase Mn profiles for BC1 and BC2 are similar (Figure 2.4.5.17), however once again the dissolved Mn concentrations at the stations are different. Dissolved Mn concentrations at station BC1 are 5 times lower than those of BC2. The dissolved Mn concentration decreases from a depth of 3.25 cm towards the surface at BC1 and from 5.5 cm at BC2. The Fe solid phase concentrations are similar with BC1 having lower solid phase Fe concentration at the surface. In this case the dissolved Fe concentrations of BC1 are 2 orders of magnitude higher than that of BC2. The decrease in dissolved Fe concentration towards the surface occurs at 7.5 cm at BC1 and 11.5 cm at BC2.The solid phase concentration of Mo at BC1 is lower than BC2. The dissolved Mo concentrations are similar. U solid phase concentrations are similar with dissolved concentrations at both stations decreasing with depth. The solid phase and dissolved profiles suggest that both stations are experiencing anoxia at depth.

The solid and dissolved phase concentration profiles for BC12 indicate that Mn dissolution is occurring at a depth of 2.75 cm and that the dissolved Mn is being removed to the solid phase towards the surface of the sediment. Fe solid and dissolved phase concentrations show similar profiles with the dissolution of Fe occurring at 7.25 cm and the removal to solid phase occurring at 3 cm depth in the core. The Mo solid phase and dissolved Mo profiles indicate that the Mo distribution is being controlled by the Mn biogeochemical cycling. The dissolved and solid phase U profiles indicate that U is being removed from the dissolved phase to the solid phase under anoxic conditions. The profiles (Figure 2.4.4.18) indicate that the sediment is oxidising towards the surface but anoxic at depth.

Minor and trace element solid phase and pore-water concentrations at stations BC12, AB1 and AB3, BP1x and BP4 and BC1 and BC2 respectively are illustrated in Figures 2.4.5.18-21

Figure 2.4.5.19 As, Cu, Pb and Cd solid phase (ppm) and pore-water (ppb) concentrations Astrolabe Bay stations, AB1 and AB3.

The solid phase and dissolved As, Cu, Pb and Cd concentrations for AB1 and AB3 are given in Figure 2.4.5.19. Down-core solid phase concentration profiles of As, Cu, Pb and Cd are lower in AB1, the shallower station, compared to AB3 the deepest station of the transect. The dissolved phase concentrations are similar with the exception of AB3 having higher dissolved As concentrations near the surface of the sediment. Dissolved Cu concentrations are higher at the surface of the core than at depth. Dissolved Pb was only detected in a few samples indicated that dissolved Pb was below detection limit in most samples. The few analysis of dissolved Pb obtained indicate that dissolved Pb is higher at AB3. Cd dissolved concentrations are low at both AB1 and AB3. The profile of dissolved Cd at AB1 indicates that Cd is released at 5.5 cm depth and may be being influenced by the organic matter cycling within the sediment.

Figure 2.4.5.20 As, Cu, Pb and Cd solid phase (ppm) and pore-water (ppb) concentrations Astrolabe Bay stations, BP1x and BP4.

Arsenic solid phase profiles indicate that both BP1x and PB4 have similar concentrations (Figure 2.4.5.20). Dissolved As concentrations are higher at BP1x and the profile suggests a release of dissolved As at depth, possibly being influenced by the biogeochemical cycling of Fe. The profile for PB1x suggests As is being released into the pore-water at depth and being removed to the surface of the sediment. Cu solid phase concentrations are higher at BP1x than BP4; however the pore-water concentrations of Cu are lower at BP1x than BP4. The dissolved phase Cu profile for BP4 indicates that dissolved Cu concentration is decreasing with depth suggesting that Cu is being removed from the pore-water to the sediment. Solid phase concentrations of Pb are higher at PB1x than BP4. No dissolved Pb was detected at either of the BP stations. Solid phase and dissolved Cd concentrations are similar at both stations with higher dissolved Cd concentrations occurring at the surface of the sediment core from BP1x. The elemental profiles indicate that biogeochemical cycling is occurring and that As, Cu and Cd are being redistributed within the sediment and overlying water column.
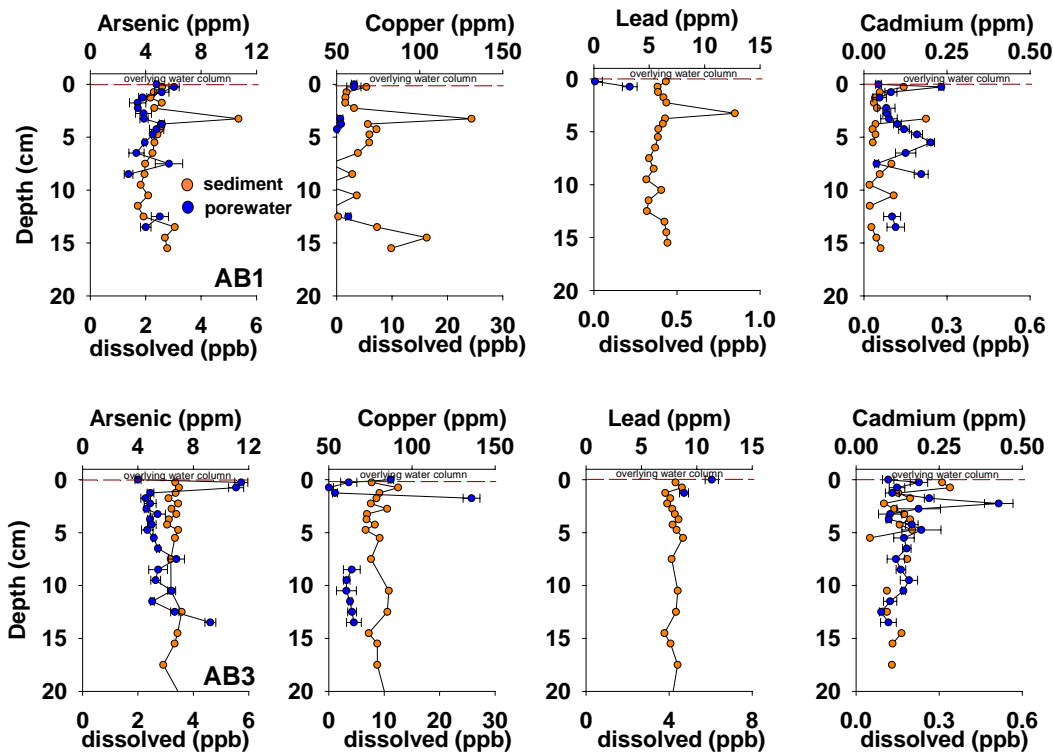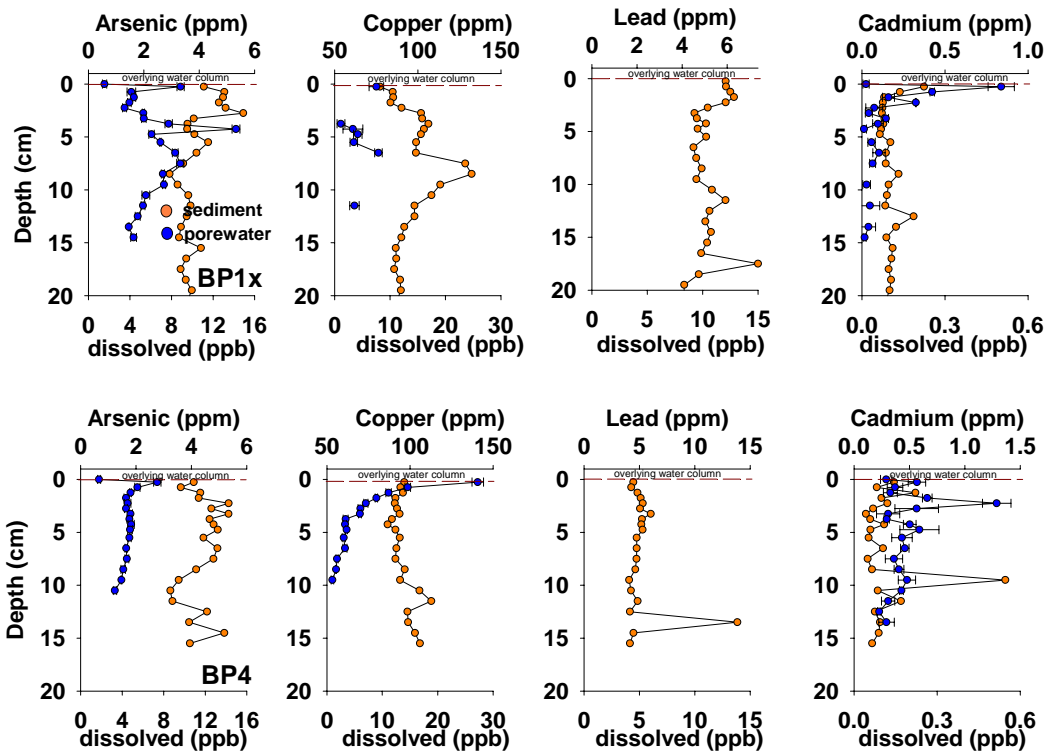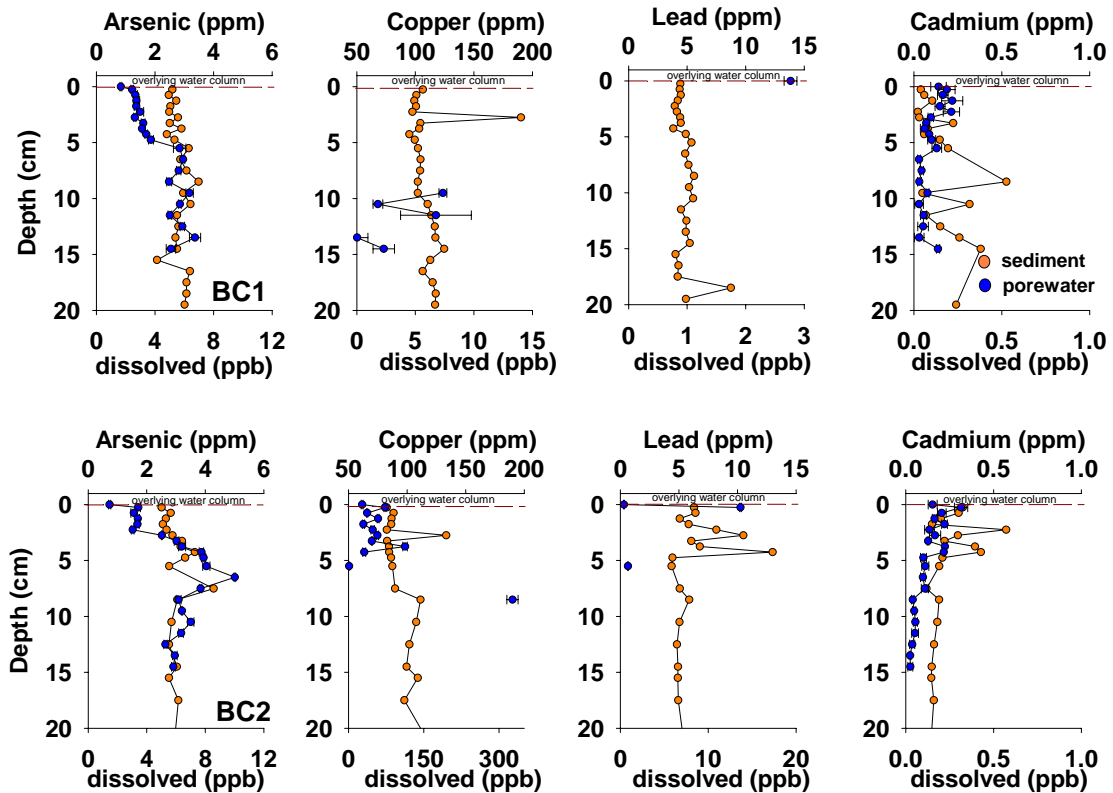
Figure 2.4.5.21 As, Cu, Pb and Cd solid phase (ppm) and pore-water (ppb) concentrations Astrolabe Bay stations, BC1 and BC2.

Solid phase and dissolved As concentrations at station BC2 are higher than those at BC1. Dissolved As concentrations within core BC1 decrease towards the surface and are being controlled by the biogeochemical cycling of Fe (Figure 2.4.5.17). The dissolved As concentrations of BC2 are approximately 3 times higher than that of BC1 and are also being controlled by the cycling of Fe within the sediment. Solid phase Cu concentrations are similar and dissolved Cu was only detectable in a small number of samples at each station. solid phase Pb concentrations are higher at station BC2 with higher concentrations of Pb in the top 5 cm of the core. Dissolved Pb was only detected in a very few samples of pore-waters collected from either station. Solid phase Cd concentrations are similar at both stations with dissolved Cd concentrations at BC2 increasing towards the surface of the sediment.

Solid and dissolved phase concentration profiles for BC12 are shown in Figure 2.4.5.18. Solid phase As concentrations are highest at BC12. Dissolved As concentrations indicate As is being released from the sediment and this process is linked to the biogeochemical cycling of Fe. Solid phase Cu concentrations are similar to the other stations and the dissolved Cu profile suggests

that Cu is being removed from the pore-water to the sediment and the dissolved Cu concentration decreases with depth from the sediment. The Cu may be removed as Mn oxyhroxides are formed towards the surface of the sediment core. Solid phase Pb concentrations are lower at BC12 than the other stations. Dissolved Pb concentrations were only detectable in a small number of pore-water samples at this station. As with the other stations the solid phase pore-water profiles indicate that biogeochemical cycling is taking place at this station and it is affecting the distribution of elements between the sediment, pore-water and overlying water column.

2.4.6 Benthos

Metazoan abundance

Figure 2.4.6.1 shows mean (± SD) densities of metazoan meiofauna and macrofauna (> 250 µm) from stations along the Astrolabe Bay (Figure 2.4.6.1a), Basamuk Pipeline (Figure 2.4.6.1b), and Basamuk Control (Figure 2.4.6.1c) depth transects. In Astrolabe Bay, meio- and macrofaunal densities were much lower at the shallowest station (AB1, 762 m) than at the two deeper stations along this transect. Numbers at the two latter stations were virtually identical, as would be expected given the very small depth increment separating them.

Along the Basamuk Pipeline transect, highest meio- and macrofaunal densities were recorded at the shallowest station (BP1x, 920 m). A progressive decline in meiofaunal abundance was seen across all four stations. Numbers were inversely correlated with water depth. Macrofaunal densities at stations BP2, BP3 and BP4 were all lower than at BP1x but showed no further depth-related decline.

Along the Basamuk Control transect meiofaunal density peaked at station BC2 (1350 m), with the other three stations showing very similar values. There were no major differences between stations in macrofaunal density and no depth-related trend.
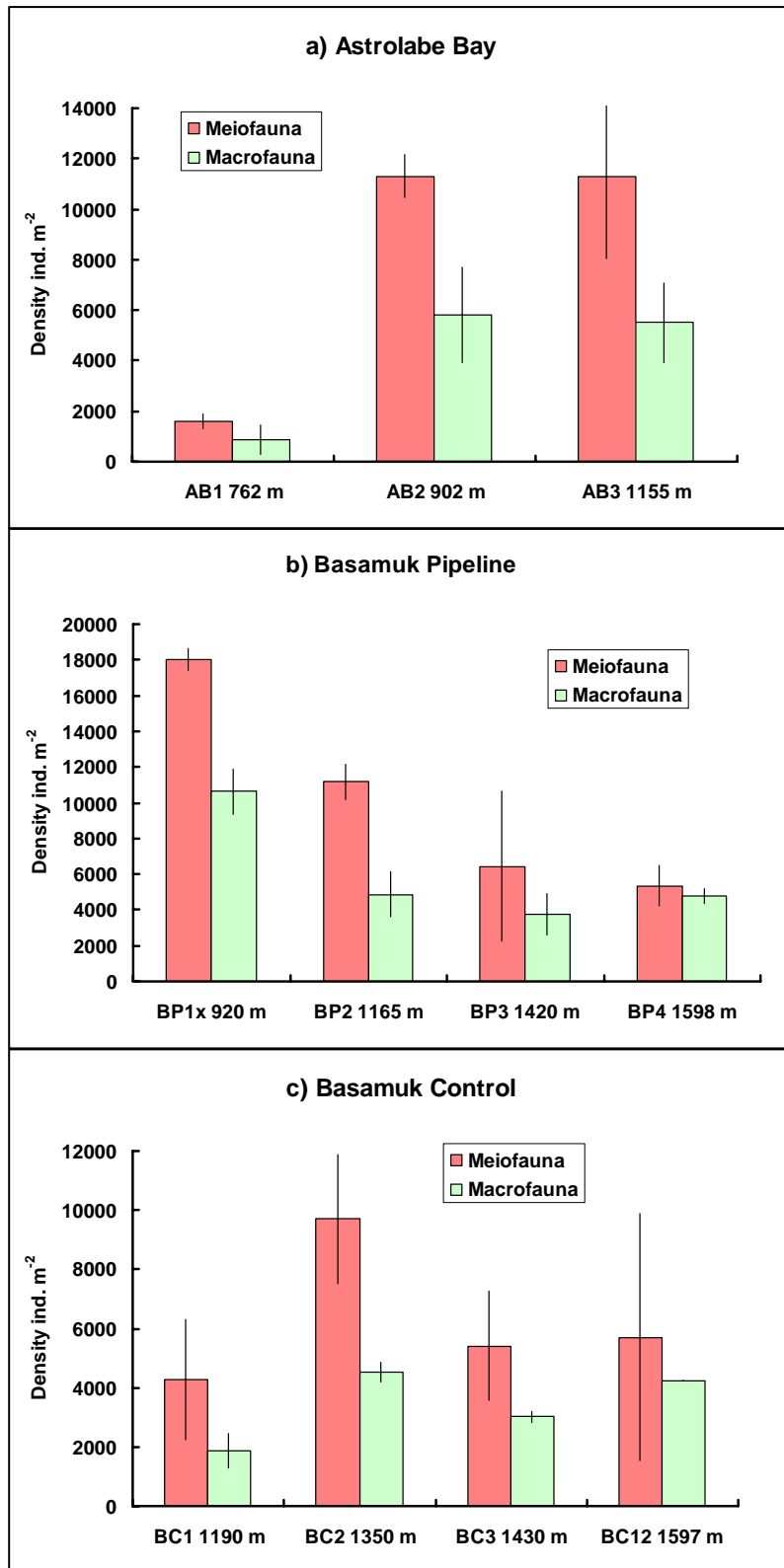
Figure 2.4.6.1. Histograms showing mean densities of metazoan meiofauna and macrofauna (> 250 µm) at stations along three transects on the Rai Coast. Stations are arrayed in order of increasing water depth. Bars represent mean values (± SD) for each station with individual corer drops as replicates. Numbers refer to the upper 10 cm of the sediment column.

Meiofaunal community composition

The metazoan meiofauna at most stations comprised nematodes and harpacticoid copepods in approximately equal numbers, or with a small percentage excess of nematodes. Exceptions to this pattern were seen at station AB1, where copepods accounted for >80% of the metazoan meiofauna (Figure 2.4.6.2a) and at BP2 (Figure 2.4.6.2b) and BC2 (Figure 2.4.6.2c), where the communities were dominated by nematodes. Ostracods and minor metazoan groups were uncommon at all stations.

Macrofaunal community composition

With respect to higher-taxon composition, stations showed little variation with depth or between transects (Figure 2.4.6.3). At all stations Polychaeta was the largest single contributor, usually accounting for > 50% of the total macrofauna. Crustaceans and molluscs each accounted for approximately 20% or less of the total, with the exception of station BP3 (Figure 2.4.6.3b) where crustaceans reached approximately 40% and were almost as abundant as the polychaetes. The relatively large contribution of crustaceans at all Basamuk Pipeline stations was caused by a high abundance of small tanaids.

The polychaete communities at all stations were numerically dominated by a small number of families (Figure 2.4.6.4). The most distinctive feature was the high abundance of small Ampharetidae at several stations, notably AB2, AB3, BP1x, BP2 and BC1. At these five stations, all located in the depth range 902 – 1190 m, this family accounted for 25.2 – 61.8% of the total polychaete abundance. Ampharetids were not recorded in the sparse polychaete fauna from the shallowest station sampled (AB1, 762 m), and did not exceed 11.4% of the total at any station deeper than 1190 m.

Among the other polychaete families, Paraonidae and Cirratulidae were consistently important at all stations. Spionidae were major contributors to polychaete numbers at all stations except AB1 and AB3.
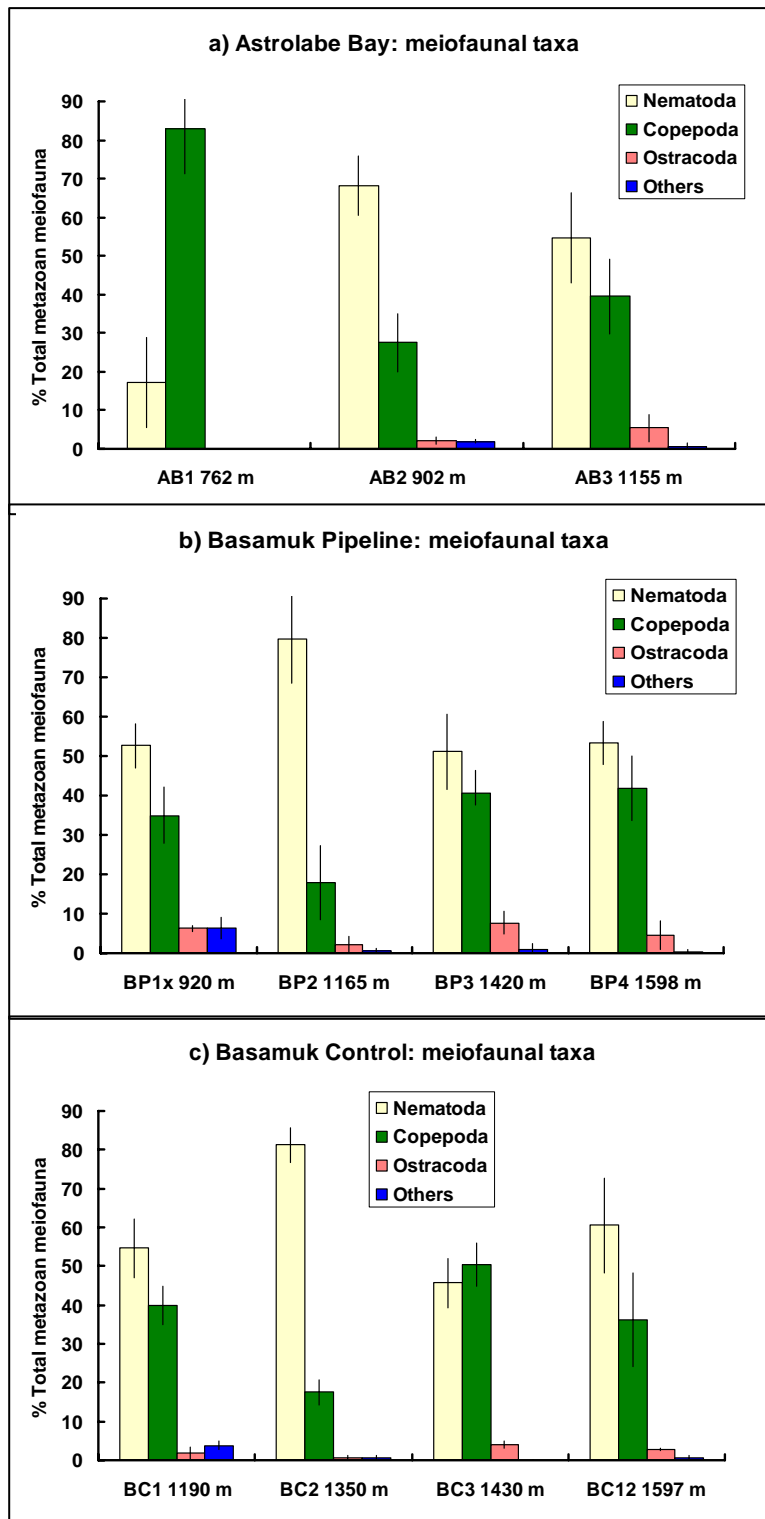
Figure 2.4.6.2. Histograms showing percentage contribution of major taxa to the metazoan meiofaunal community (> 250 μm) at at stations along three transects on the Rai Coast. Bars represent mean values (± SD) for each station with individual corer drops as replicates.
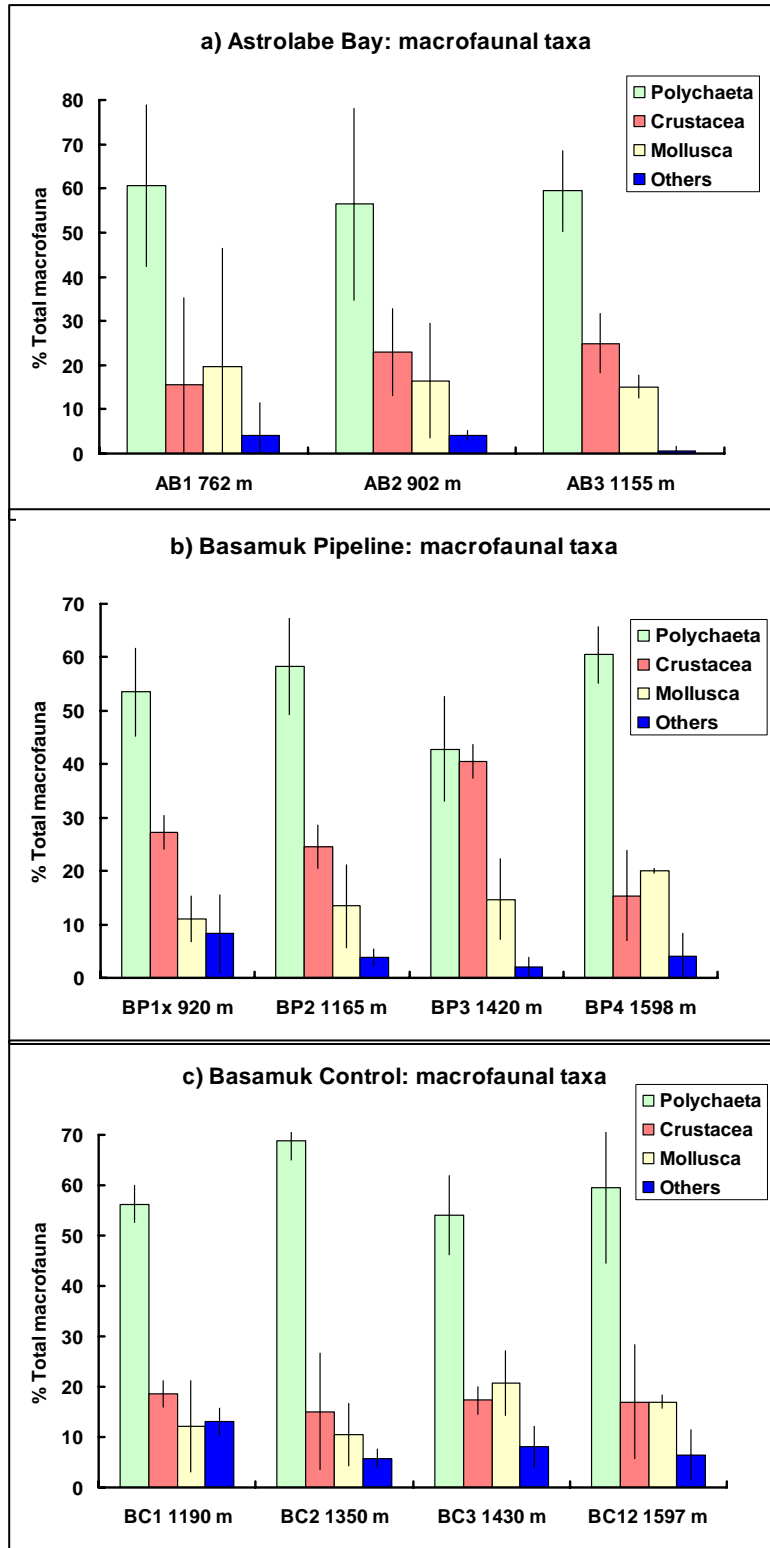
Figure 2.4.6.3. Histograms showing percentage contribution of major taxa to the macrofaunal community (> 250 μm) at at stations along three transects on the Rai Coast. Bars represent mean values (± SD) for each station with individual corer drops as replicates.
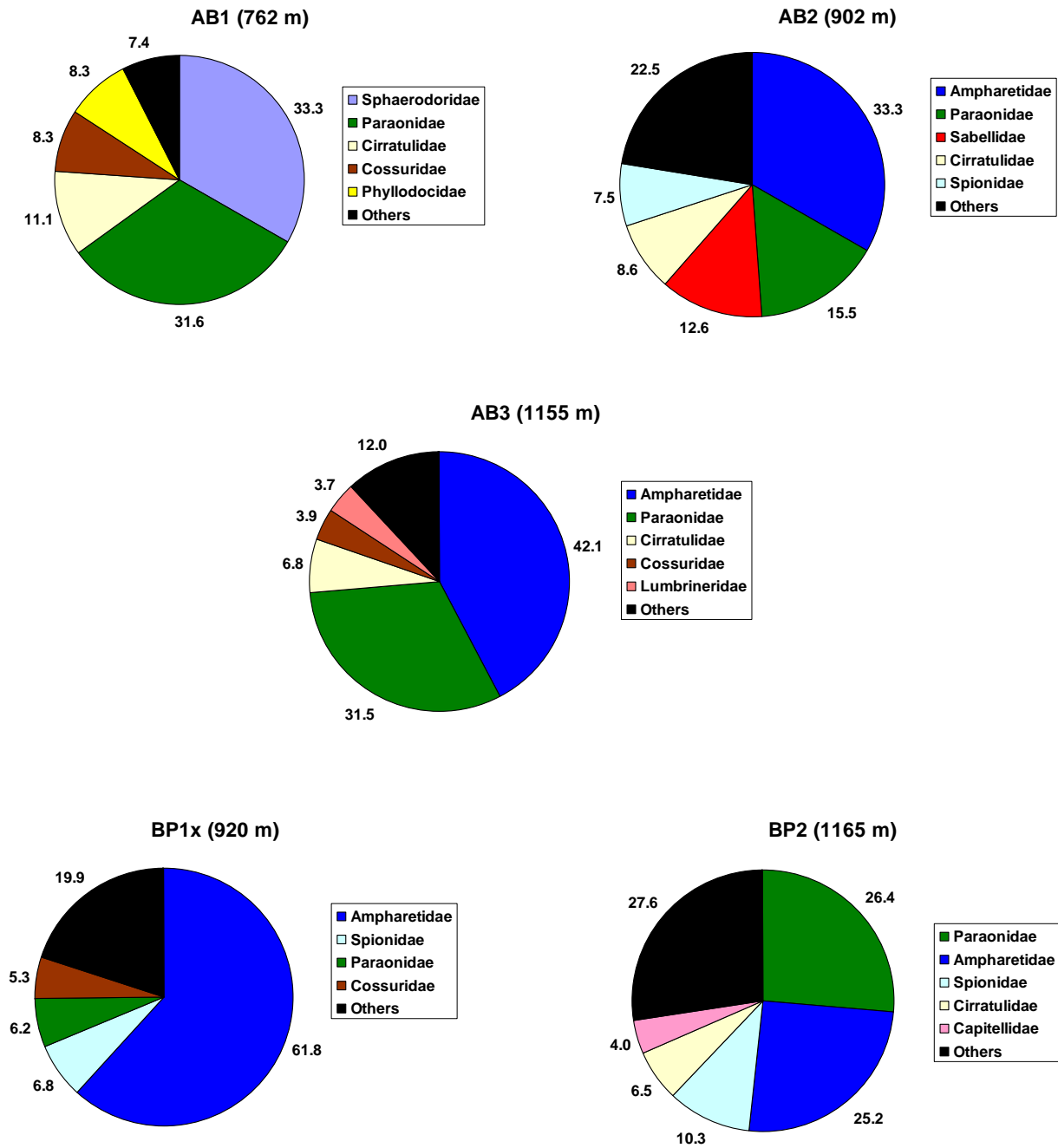
Figure 2.4.6.4. Polychaete community structure at individual stations along the Astrolabe Bay (AB), Basamuk Pipeline (BP) and Basamuk Control (BC) transects. Charts show the mean contributions of the most abundant families at each station as a percentage of total polychaete abundance. Juvenile polychaetes not firmly identified to Family level are excluded from the analysis.
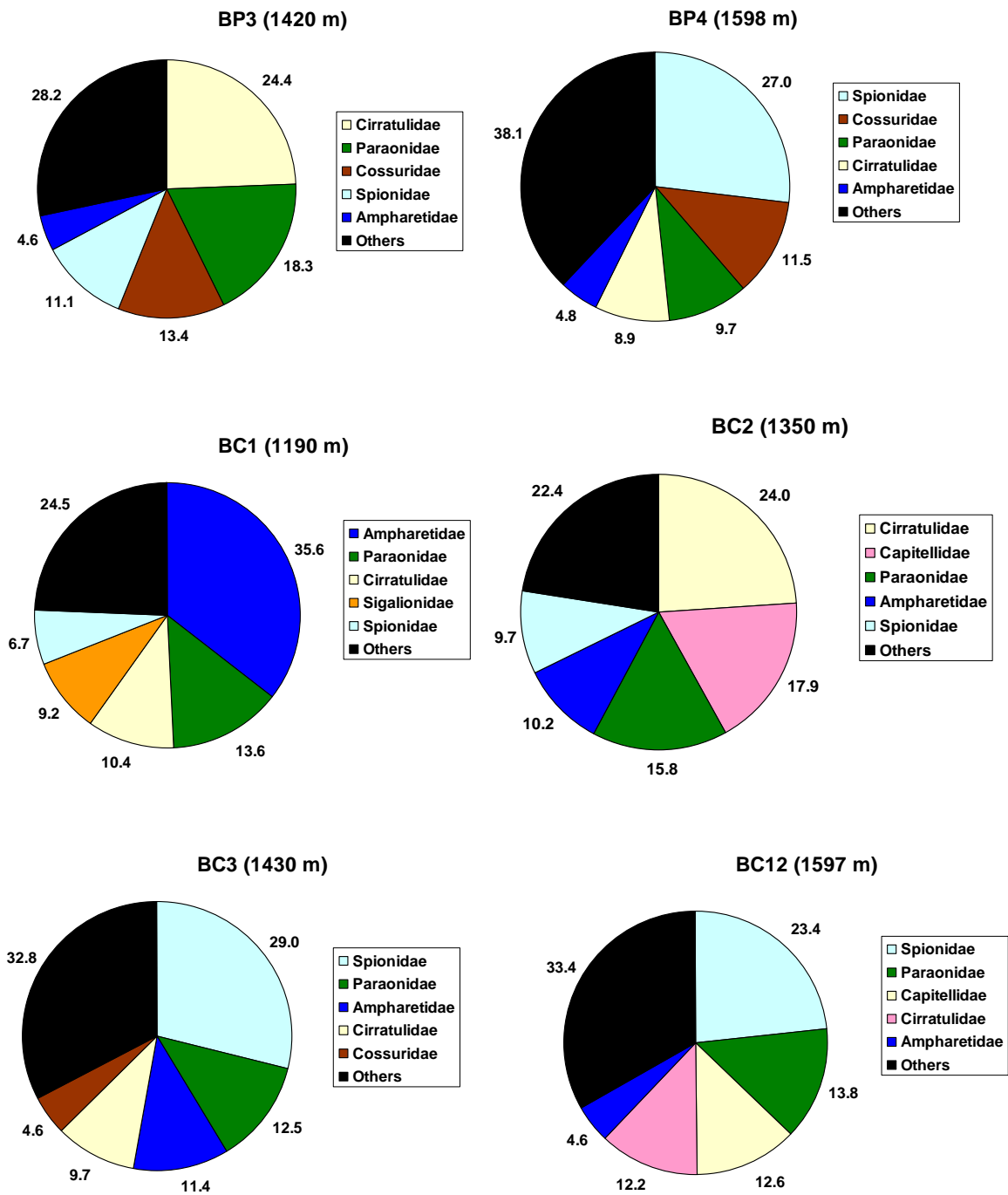
Figure 2.4.6.4. (continued) Polychaete community structure at individual stations along the Astrolabe Bay (AB), Basamuk Pipeline (BP) and Basamuk Control (BC) transects. Charts show the mean contributions of the most abundant families at each station as a percentage of total polychaete abundance. Juvenile polychaetes not firmly identified to Family level are excluded from the analysis.

2.4.7 Seabed photography

The Basamuk stations differed in success rate of seabed photography. At stations BP3 and BC1 only one usable image was obtained, all other frames were completely blank, suggesting failure of the strobe light. Deployments at the other three stations were more successful, with 18, 14 and 23 images obtained at BP1x, BC2 and BC12 respectively. Blank images may have been caused by failure of the strobe light.

Station BP1x

The seabed at station BP1x was relatively flat with small-scale biogenic relief resulting from the activity of burrowing animals. Debris, including land-derived twigs and leaves, is visible on the sediment surface in some photos (e.g. 002, 015). Photo 010 shows what appears to be a coconut husk on the seabed. In addition to small mounds and burrow openings (Figure 2.4.7.1.), biogenic traces include faecal strings (016) and linear trails (004) made by animals moving across the sediment surface. A variety of benthic animals are also recorded. Photo 014 shows a white elasipodid holothurian with long dorsal papillae, possibly *Deima validum,* (Figure 2.4.7.2), while photos 011 and 017 show dark reddish animals swimming just above the sediment surface. These may be benthopelagic holothurians, possibly *Enypniastes* sp. The faecal strings visible on some photos are likely to be produced by holothurians of these or other species. A large red shrimp is faintly visible swimming above the seabed in photo 011. Two photos (001, 004) show whitish worm-like animals with a broad, flattened anterior region, partly buried in the superficial sediments, both associated with a looping faecal cast. These are all characters typical of epifaunal enteropneusts ("acorn worms").

Figure 2.4.7.1. "Bed-hop" camera image taken at Basamuk station BP1x, showing burrow openings and small mounds. Near the lower edge, just to the right of the guide mark, is a sinuous faecal string, probably left by a holothurian. Width of image at lower edge approximately 1m, depth of field approximately 2.5 m.

Figure 2.4.7.2. "Bed-hop" camera image taken at Basamuk station BP1x, showing a relatively flat seabed with small-scale biogenic relief. A white elasipodid holothurian is just visible in shadow in the upper left of the image. Near the lower edge, just to the right of the guide mark, is a sinuous, whitish organism, probably an enteropneust worm. Width of image at lower edge approximately 1m, depth of field approximately 2.5 m.

Station BP3

The single image obtained here (Figure 2.4.7.3) shows an irregular, lumpy seabed with a finely granular surface texture. What may be a fine twig or cane is is visible on the seabed. There are some fine projecting features which may be worm tubes, and faint linear trails are also visible on the sediment surface.

Figure 2.4.7.3. "Bed-hop" camera image taken at Basamuk station BP3, showing an irregular, lumpy seabed with some fine traces suggestive of biological activity. A rod-like object, possibly a twig or cane, is visible near the centre of the image. Width of image at lower edge approximately 1m, depth of field approximately 2.5 m.

Station BC1

The single image obtained here (Figure 2.4.7.4) was taken at an irregular angle to the seabed and is difficult to interpret, but appears to show a smooth substratum with very little surface detail and no clear sign of biological activity.

Station BC2

The seabed at BC2 appears to consist of flat sediment, relatively smooth in places, or with a variable density of fine pinpoint depressions in others. There are no large mounds but a variety of biogenic traces can be seen including burrow openings (e.g. photos 002, 003), fine linear trails (002, 011) (Figure 2.4.7.5), larger pits or depressions (010) and faecal casts (004, 013). The resting

trace of a seastar or brittlestar is visible in photo 001. A distinctive discontinuous linear trail consisting of short crenulated depressions can be seen in photo 006 (Figure 2.4.7.6). Apart from a few possible upright worm tubes there are no animals visible on any image. The leaf of a terrestrial plant is visible on the seabed in photo 007.

Figure 2.4.7.4. "Bed-hop" camera image taken at Basamuk station BC1, showing a smooth seabed with very little surface detail. Width of image at lower edge approximately 1m.

Figure 2.4.7.5. "Bed-hop" camera image taken at Basamuk station BC2, showing a smooth, flat seabed with fine linear trails (far left), burrow openings and other biogenic features. Width of image at lower edge approximately 1m, depth of field approximately 2.5 m.

Figure 2.4.7.6. "Bed-hop" camera image taken at Basamuk station BC2, showing a discontinuous linear trail crossing the field from lower right to upper left. Width of image at lower edge approximately 1m, depth of field approximately 2.5 m.

Station BC12

The 23 photos from BC12 show an irregular, lumpy seabed very similar in general appearance to the single image from BP3. All seabed views are quite uniform with little variation between photos. No animals are visible but there is evidence of biological activity in the form of faecal casts (e.g. photos 005, 007, Figs. 2.4.7.7 and 2.4.7.8), linear trails (011, 016) and possible "spoke traces" (015).
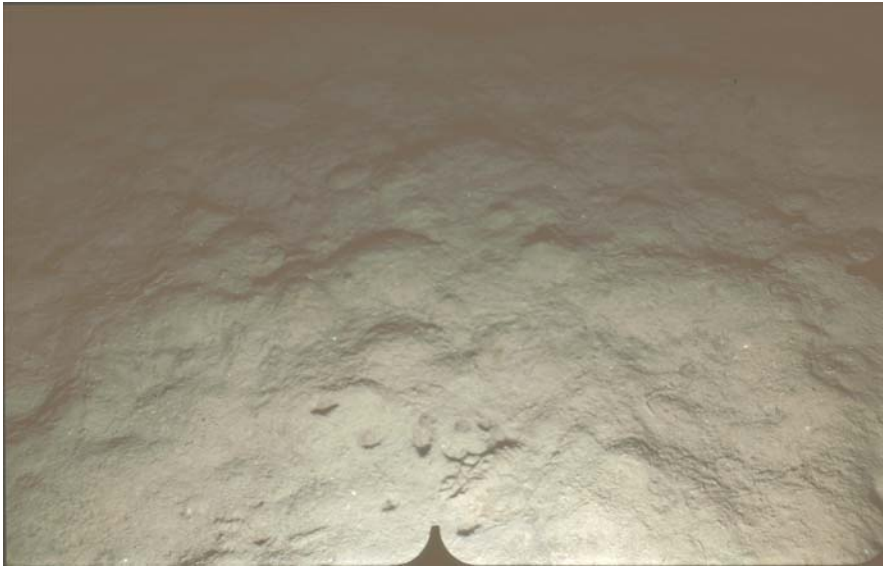
Figure 2.4.7.7. "Bed-hop" camera image taken at Basamuk station BC12, showing an irregular, lumpy seabed. A partly-fragmented faecal coil is visible just above the guide mark along the lower edge. This area also shows a number of pits or holes which may be burrow openings. Width of image at lower edge approximately 1m, depth of field approximately 2.5 m.
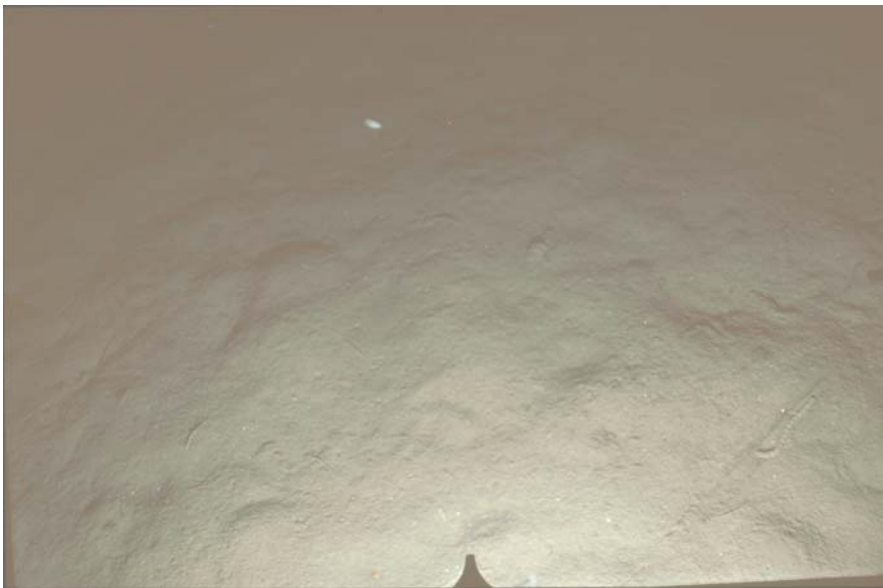
Figure 2.4.7.8. "Bed-hop" camera image taken at Basamuk station BC12, showing a faecal string associated with a linear trail towards the lower right corner of the image. Width of image at lower edge approximately 1m, depth of field approximately 2.5 m.

2.4.8 Water column geochemistry

Water column nutrient concentrations are reported in Appendix 3B, tables 3B.1-10. Figures 2.4.8.1-3 illustrate the water column nutrient concentrations for the Basamuk study water column nutrient transects

The nutrient profiles in the Vitiaz Basin are consistent with similar observations made in this part of the Pacific Ocean and also characteristic of coastal zones with high rainfall. The strong pycnocline caused by the surface runoff inhibits mixing of the nutrient rich waters giving rise to nutrient depleted surface waters as shown along the three transects. Phosphate and nitrate concentrations are generally around the detection limit (~0.1μM) in the surface waters while silicate is somewhat higher and increases towards the coast probably suggesting a small riverine source of the nutrient. Neither phosphate nor nitrate shows any indication of a terrestrial runoff source in this region. The highest nutrient concentrations are seen at depth and reflecting the southern ocean derived bottom waters of this region. Ammonia is in measurable concentrations in the region probably suggesting productivity is reliant on this as a source of nitrogen however Davies (2004) working in the Gulf of Papua found that dissolved organic nitrogen derived from fluvial sources accounted for the majority of the nitrogen pool and that may also be the case here.
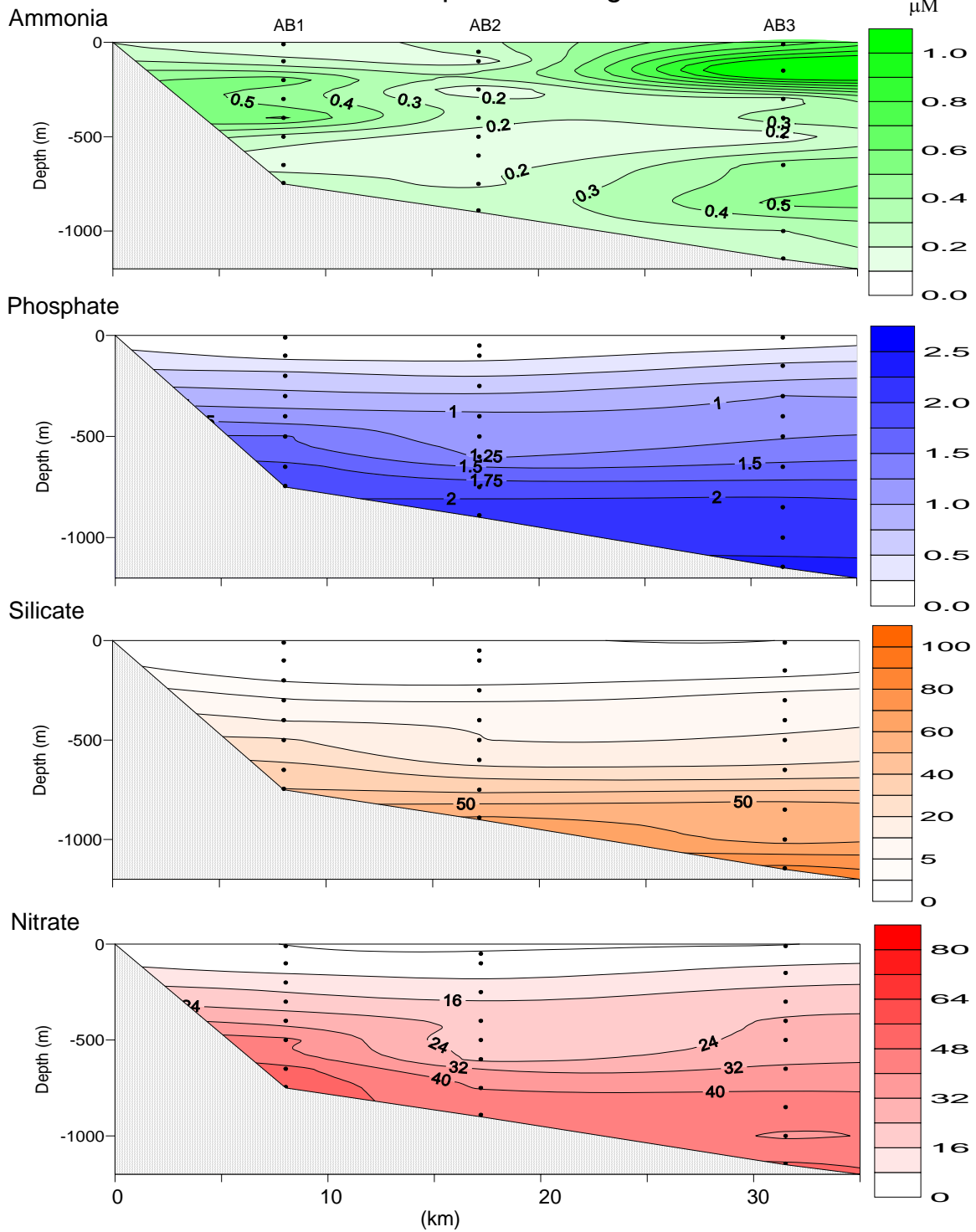
Figure 2.4.8.1 water column nutrient concentrations for the Astrolabe Bay (AB) water column nutrient transects
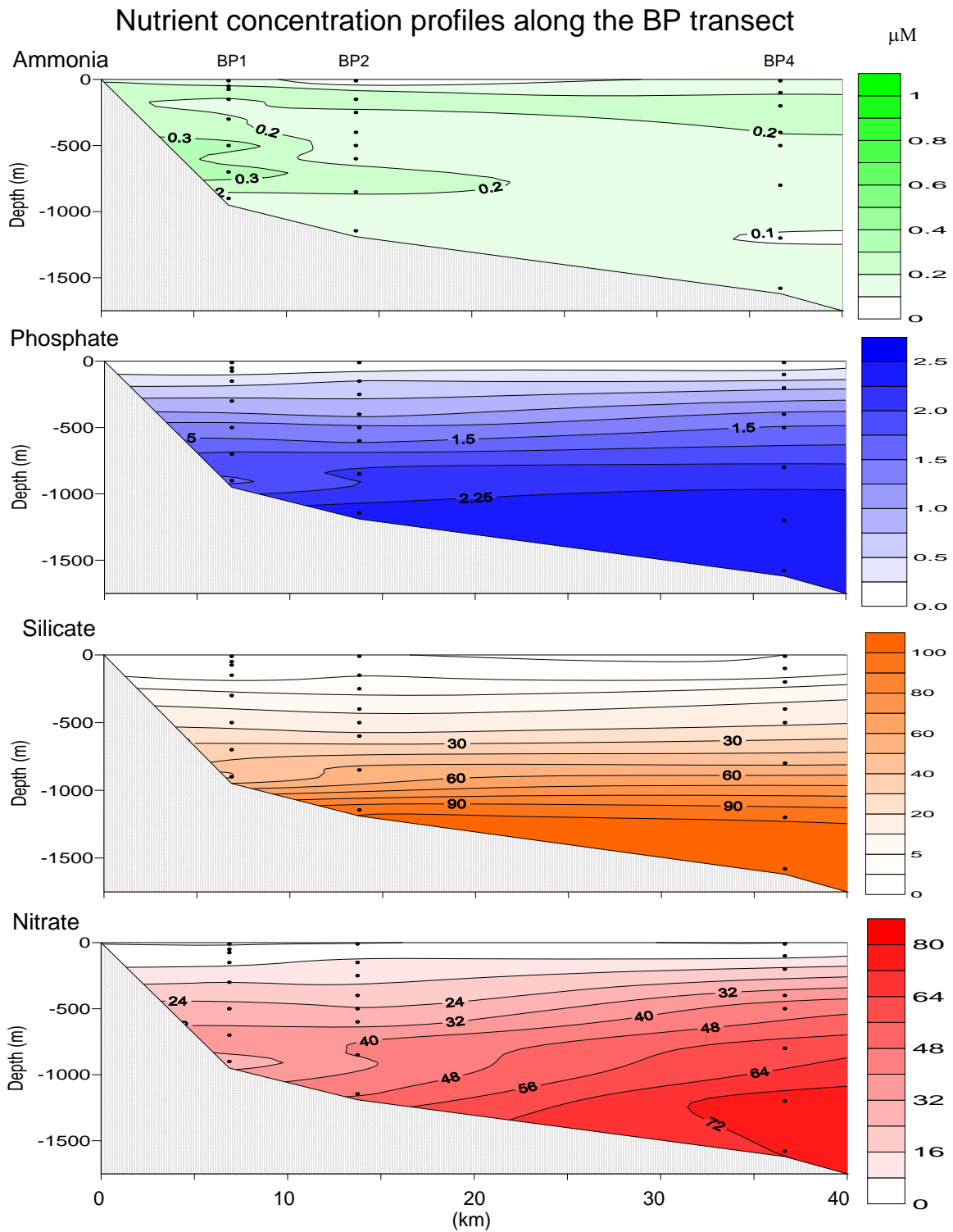
Figure 2.4.8.2 Water column nutrient concentrations for the Basamuk (BP) water column nutrient transects
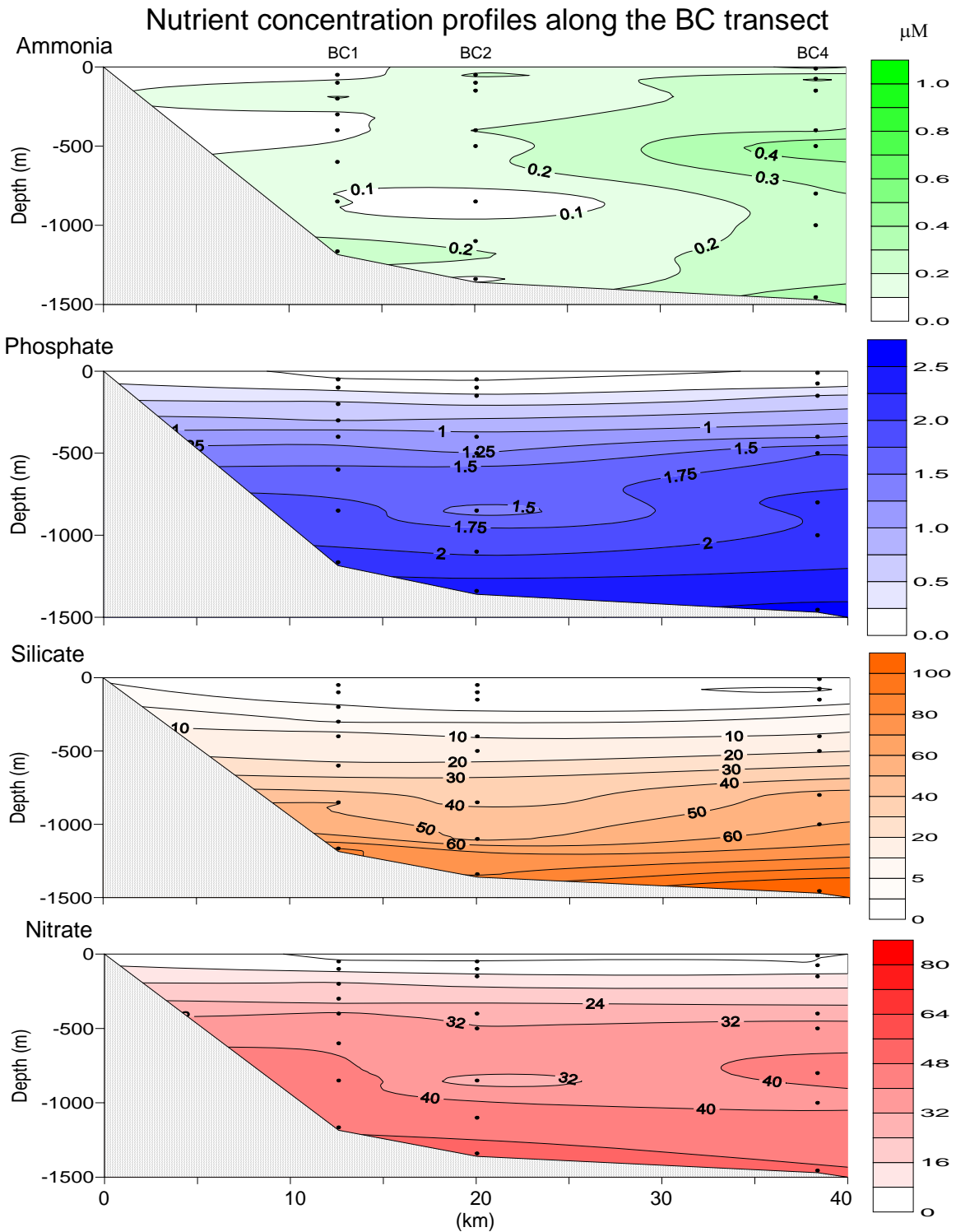
Figure: 2.4.8.3 Water column nutrient concentrations for the Eastern control transect (BC) water column nutrient transects

Suspended particulate material (SPM) was collected at 10 stations AB1-3, BP1x, 2 and 4, BC12 and BC1, 2 and 4. The elemental concentration data for each station are given in Appendix 3B, tables

3B.20-49. The Figures of the depth profiles of elemental concentrations are given in Appendix 3A.19-48.
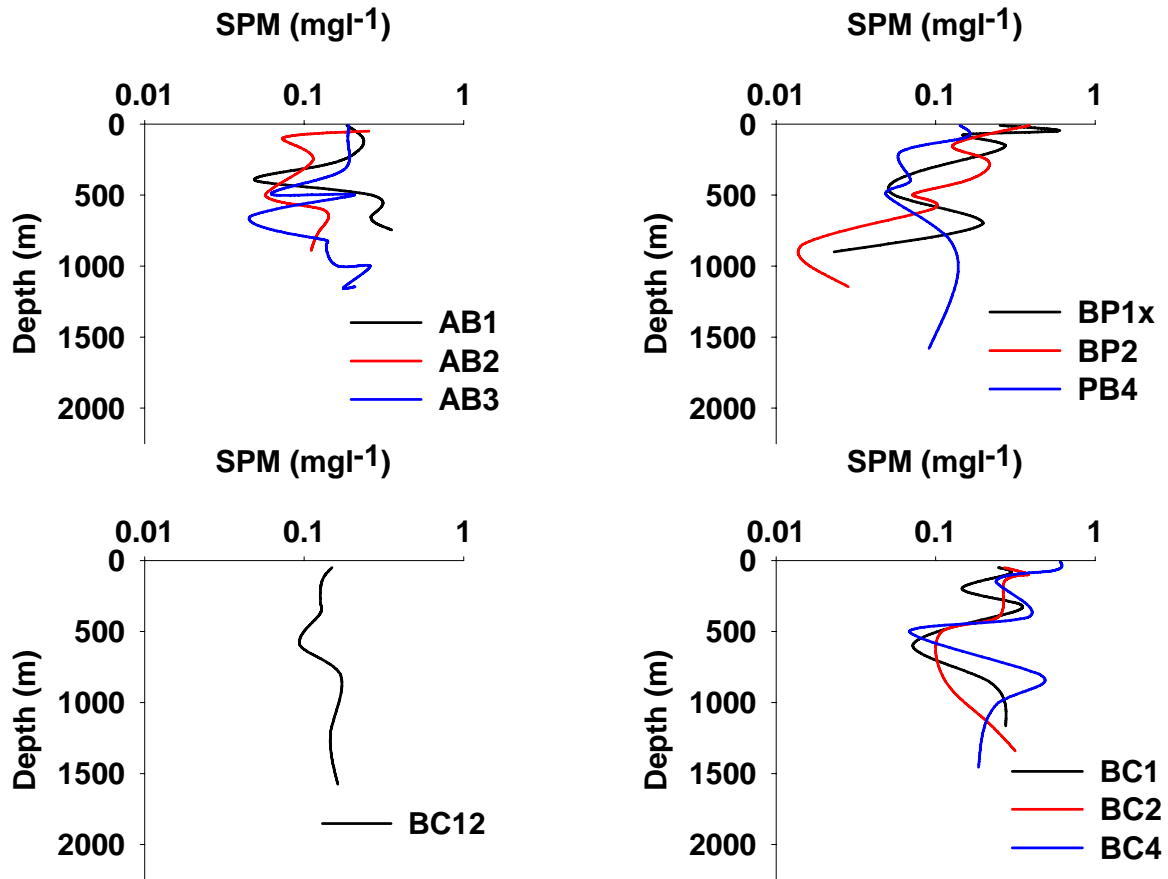
Figure 2.4.8.4 Concentration of suspended particulate material (SPM) at Basamuk stations

Table 2.4.8.1 Depth of maximum SPM concentration at Basamuk stations

Station	AB1	AB2	AB3	BP1x	BP2	BP4	BC12	BC1	BC2	BC4
Maximum concentration (mg L^{-1})	0.26	0.25	0.26	0.57	0.39	0.15	0.17	0.28	0.38	0.61
Depth of maximum (m)	500	50	1000	50	10	100	800	100	100	10
Depth of water column (m)	765	902	1155	917	1165	1598	1597	1190	1340	1470

Table 2.4.8.1 gives the maximum concentration of SPM and the depth at which it occurs at each station. Figure 2.4.8.4 illustrates the depth profiles for the mass of SPM in the water column at each station. All profiles show structure with depth except at BC12 which has low variability with depth. This variability is likely to reflect variability in the physical properties of water column. The concentration of SPM within the Astrolabe Bay transect are all similar but the maximum SPM occur at different depths ranging from 50 to 1000m. The mass of SPM at the Basamuk transect ranges from 0.15 to 0.57 mg L^{-1} with the highest concentration occurring at BP1x and the lowest at BP4. Station BC12 has SPM at 0.17 mg L^{-1} similar to the mass of SPM at BP4. The mass of SPM at the eastern control transect increases from the shallowest to the deepest station, ranging from 0.28 to 0.61 mg L^{-1}.

Figures 2.4.8.5 to 8 illustrate the differences in concentrations of major, minor and trace elements within the water-column SPM. Figures for all elements in ppm in the SPM and mg L^{-1} in the water column are given in Appendix 3A.19-48.
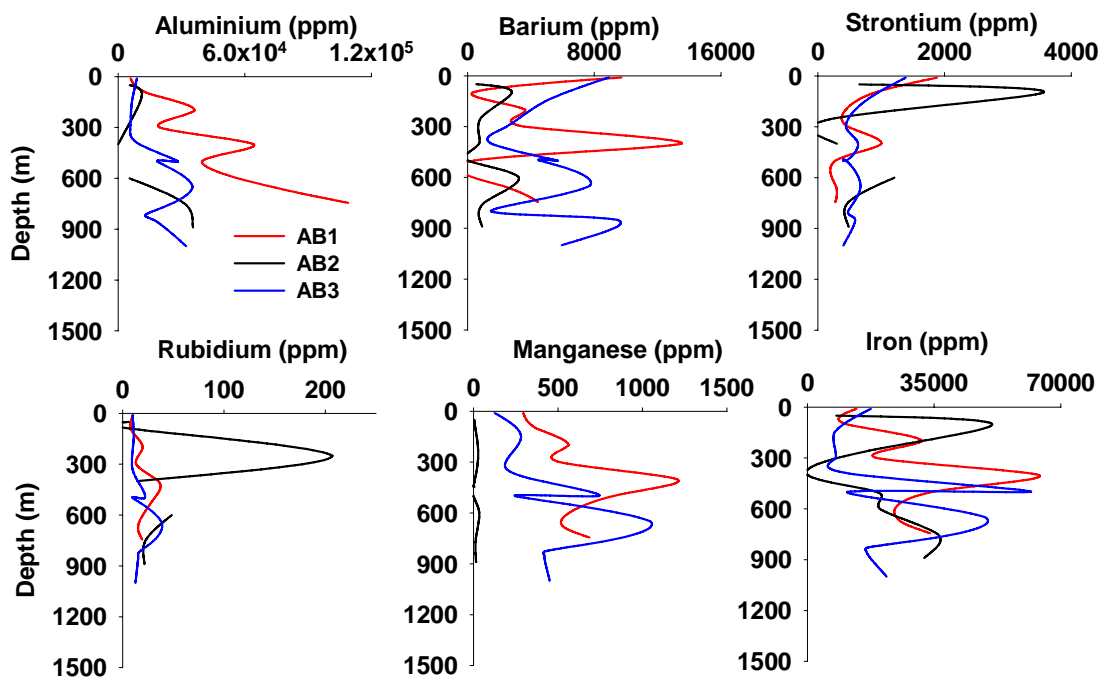
Figure 2.4.8.5 Al, Ba, Sr, Rb, Mn and Fe concentrations of suspended particulate matter (SPM) of Astrolabe Bay stations
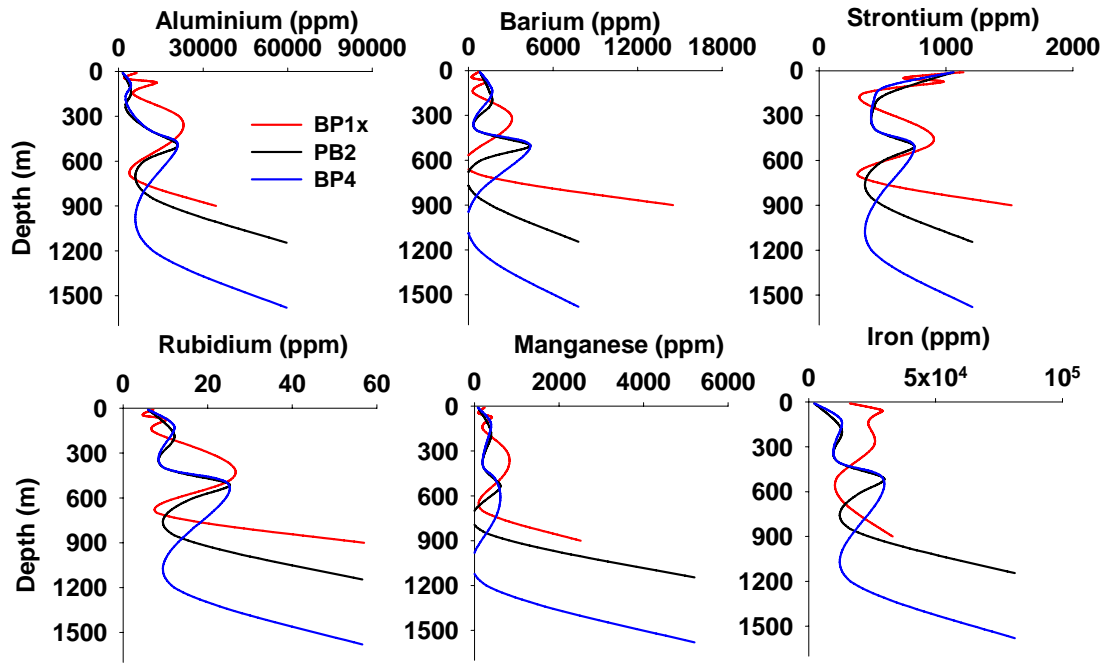
Figure 2.4.8.6 Al, Ba, Sr, Rb, Mn and Fe concentrations of suspended particulate matter (SPM) of Basamuk stations

Figure 2.4.8.7 Al, Ba, Sr, Rb, Mn and Fe concentrations of suspended particulate matter (SPM) of BC12

Figure 2.4.8.8 Al, Ba, Sr, Rb, Mn and Fe concentrations of suspended particulate matter (SPM) of eastern transect stations (BC)

All the concentration profiles indicate structure within the water columns which is influenced by the different water masses and currents existing within the water column (section 2.4.2 Physical Oceanography).

Aluminium concentrations within the SPM are highest at AB1 (103,083 ppm) with AB2 and AB3 having 3 times less Al. At the BP stations, Al concentration of the SPM is lowest at BP1x the station closest to the shore with Al concentration increasing at BP2 and BP4 to a maximum of 59620 ppm. BC12 has similar Al concentration to AB3, BP2 and BP4 ranging from 3333 to 48300 ppm. Al concentrations of the eastern control transect, BC1-3 have the lowest concentrations of Al ranging from 1318 to 15630 ppm.

Sr concentrations within the SPM at the AB stations indicate that the SPM at AB2 has the highest concentration of Sr (3289 ppm) occurring at a depth of 100m, AB1 and AB3 have similar concentrations and depth profiles. Sr concentrations at the BP stations are lower at the shallower depths than those of Astrolabe Bay however all profile increase with depth at these sites. Sr concentrations at BC12 are similar to those of the AB and BP transects but there is less defined structure to the depth profile. The BC stations have a similar Sr profile at all stations and a decrease in Sr with depth.

Rb concentrations are generally higher at BP stations (5-57 ppm) and lowest at BC12 and BC stations (4.8-19.8 ppm) with concentration of Rb at AB stations ranging from 6.2 – 207.1 ppm, the maximum concentration occurring at a depth of 250 m.

Mn concentrations are highest at depth at the BP stations (83.2-6764 ppm), with the BC stations having generally lower Mn concentrations (24.0-1361 ppm). The lowest Mn SPM concetrations occur at AB2 which range from 0.1-34.2 ppm. Mn concentrations are highest at mid depths at the AB stations, in contrast SPM are highest at depth at all other stations, BP, BC12 and BC stations.

Fe concentrations of the SPM are highest at the BP and AB (27-81230 ppm) stations with both BC12 and the BC stations having lower Fe (1957-39340 ppm) concentrations. The most striking feature of the SPM profiles is the sharp increase in concentration at depth within the BP and BC12 stations. The increase in elemental concentrations may be due to resuspension of a flocculent benthic nepheloid layer at this station.
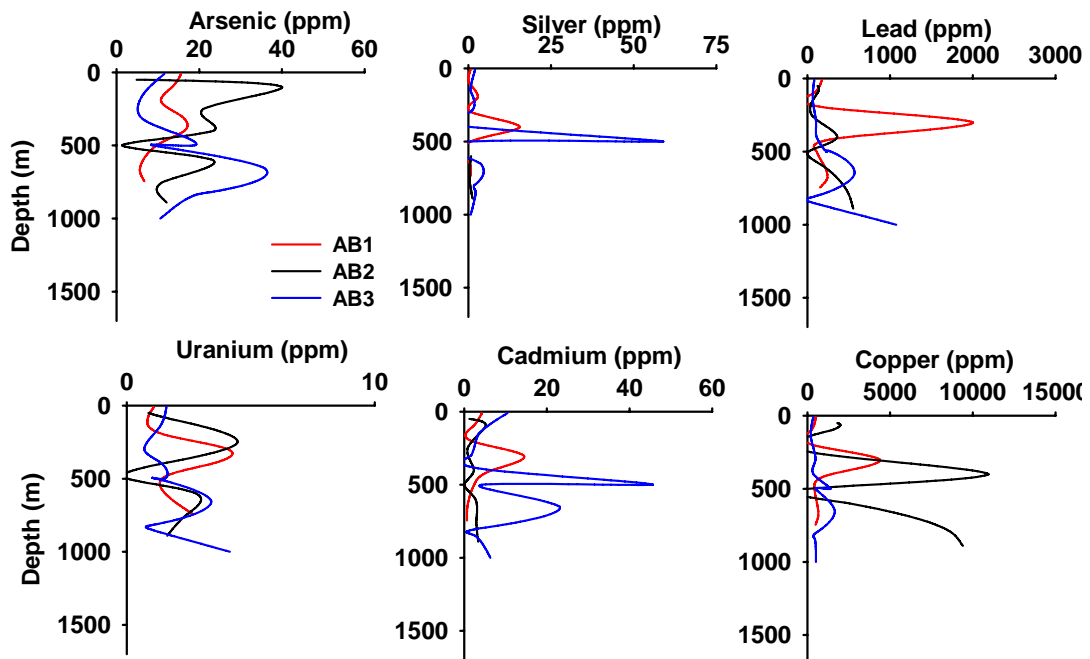
Figure 2.4.8.9 As, Ag, Pb, U, Cd and Cu concentrations of suspended particulate matter (SPM) of Astrolabe Bay stations (AB)
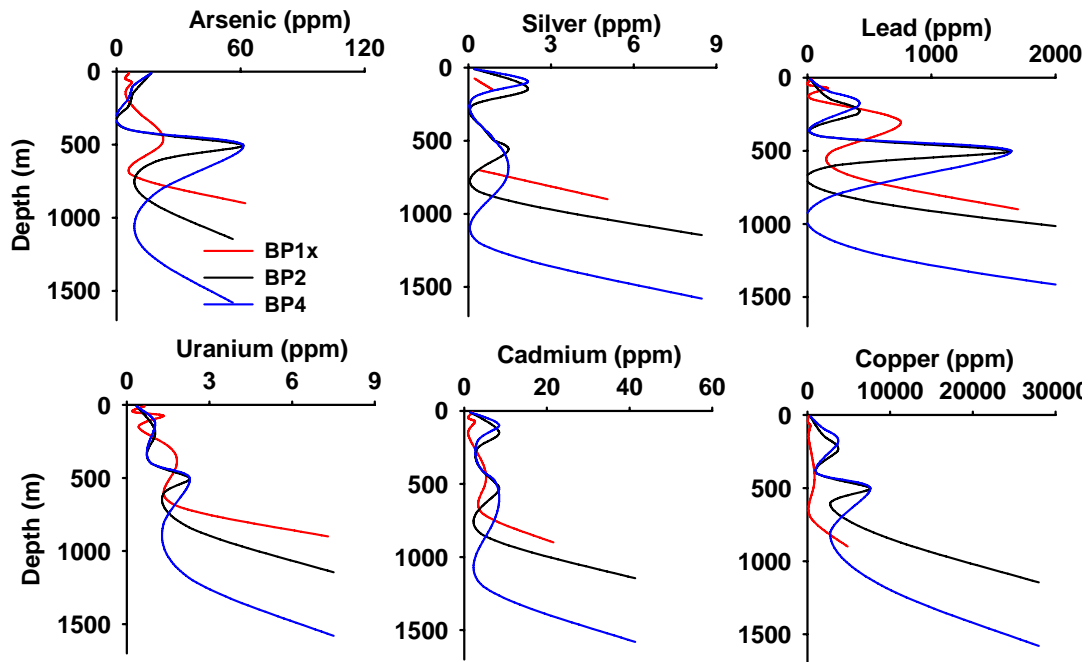
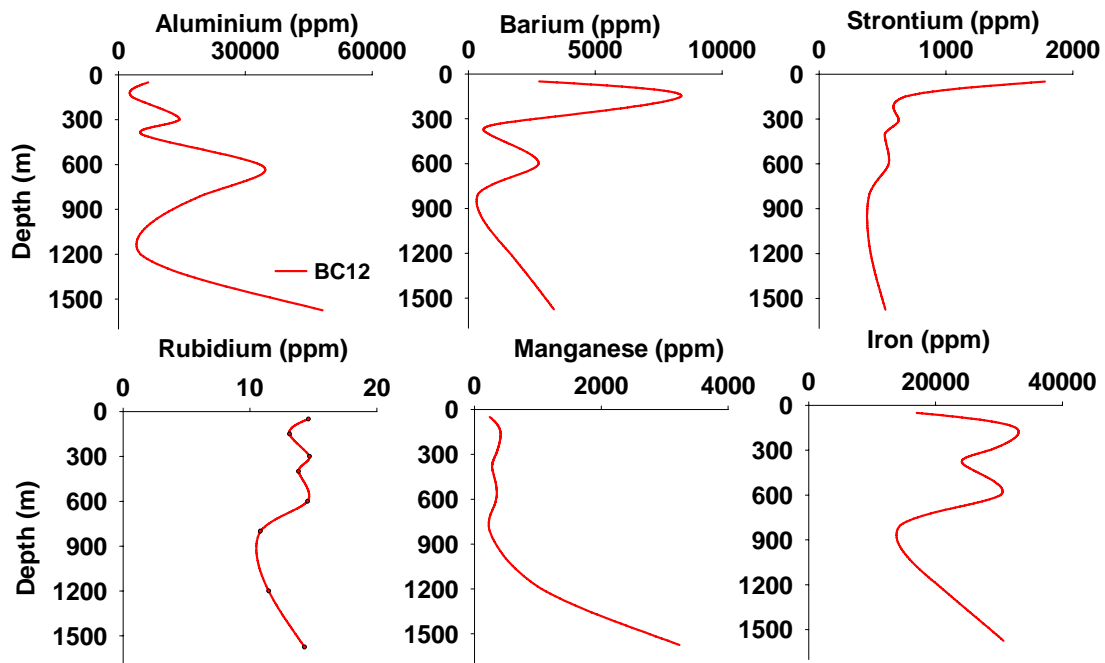**Figure 2.4.8.10 As, Ag, Pb, U, Cd and Cu concentrations of suspended particulate matter (SPM) of Basamuk stations (BP)**

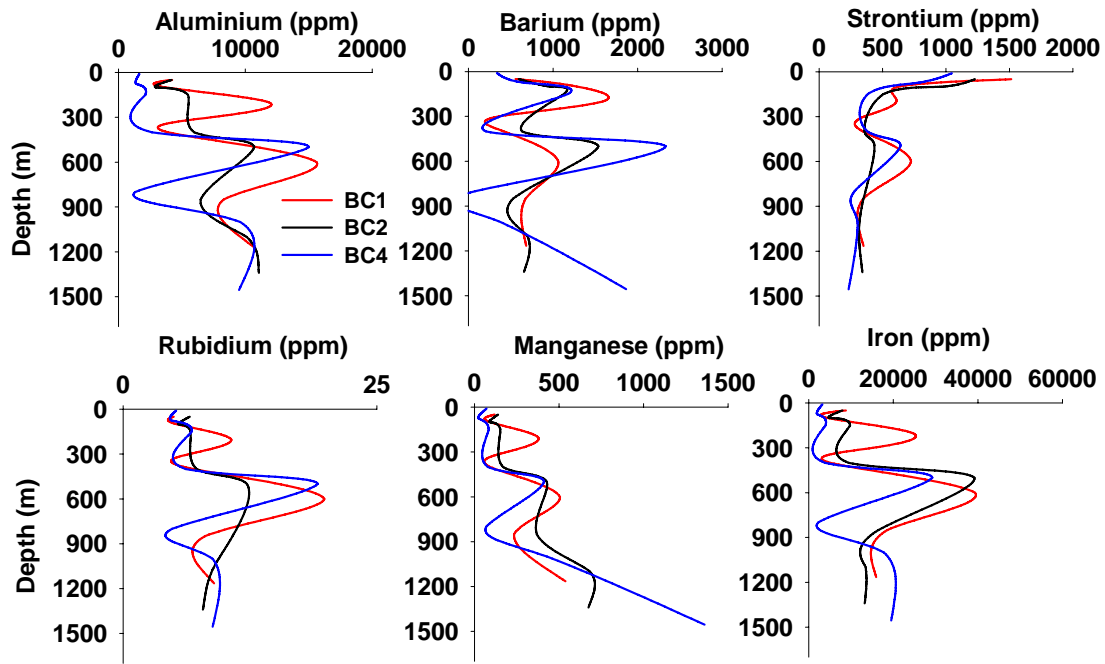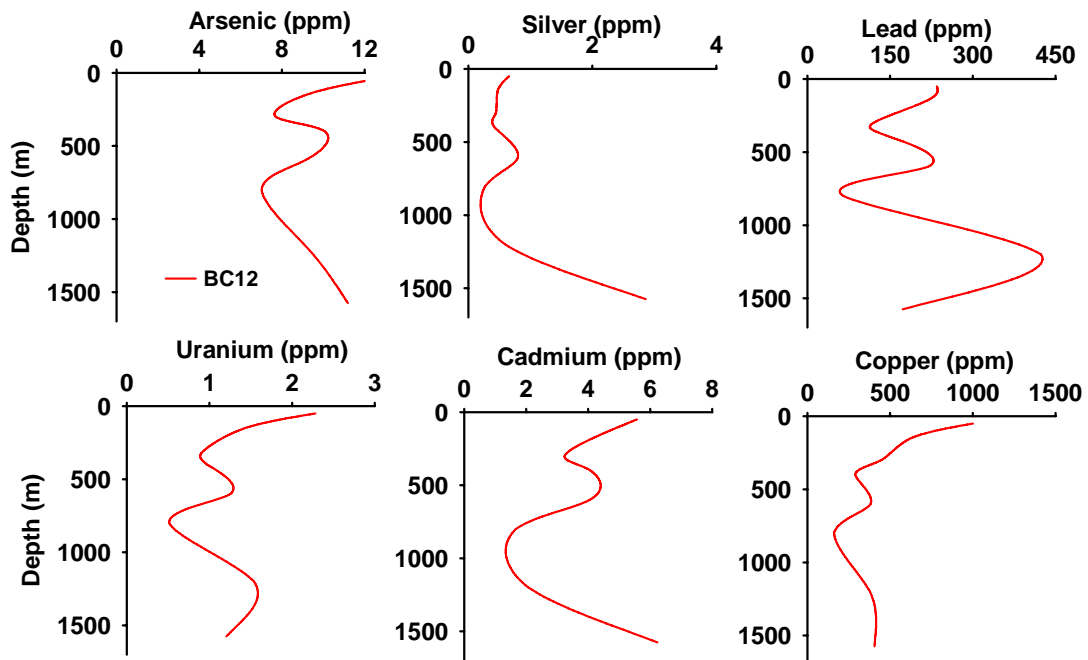**Figure 2.4.8.11 As, Ag, Pb, U, Cd and Cu concentrations of suspended particulate matter (SPM) of BC12 station**
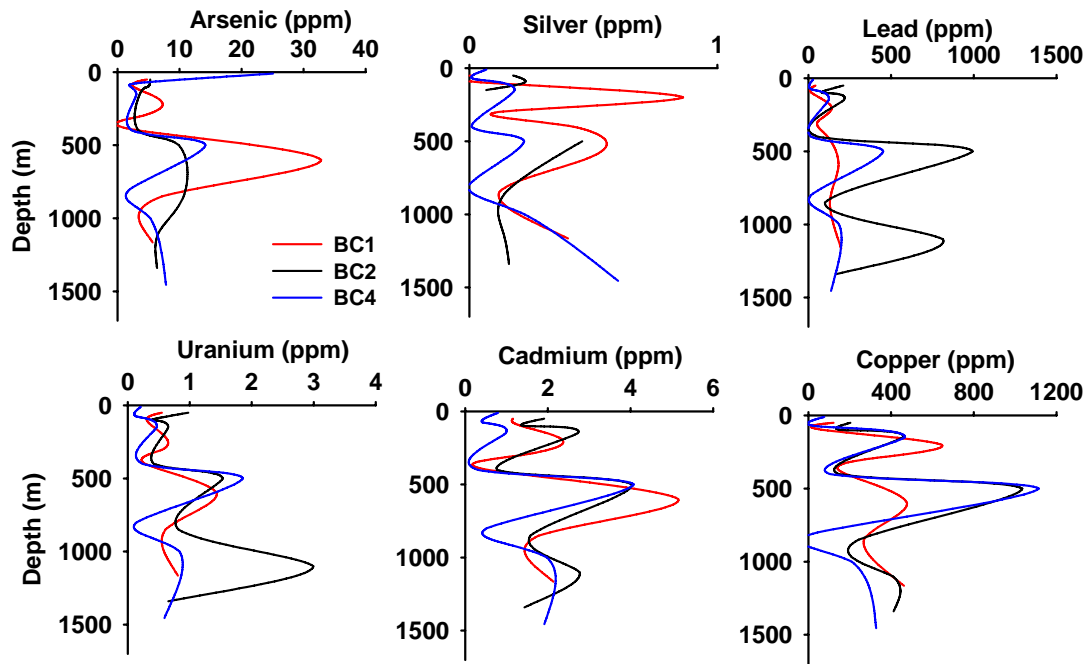
Figure 2.4.8.12 As, Ag, Pb, U, Cd and Cu concentrations of suspended particulate matter (SPM) of eastern control transect (BC)

Figures 2.3.8.5-12 illustrate the differences in concentration of a number of elements within the SPM with depth. Three of these elements will be discussed in more detail, As, Pb and Cu which are all considered to be detrimental to biota when present at large concentrations.

The As concentrations of the SPM are highest at depth at the BP stations (4.4-62.2 ppm) which shows similar concentration trends to Al, Sr, Rb, Mn and Fe at these stations. The As concentrations of the AB transect range from 1.3 to 40.1 ppm with BC12 and the BC stations having generally lower As concentrations ranging from 2.0-32.8 ppm. Arsenic depth profiles show a similar structure to that of Fe suggesting, as with the sediment, that Fe is in some measure controlling the distribution of As within the SPM.

Lead concentrations are highest at the AB and BP transects with concentrations ranging from 12.7 to 3408 ppm Pb within the SPM. The highest concentrations of Pb occur at the deepest stations of the transect AB3 (2683 ppm) and BP4 (3408 ppm). In comparison the deepest station of the BC transect has a lower maximum concentration of 453 ppm Pb.The concentrations of Pb at BC12 and BC transect is lower ranging from 15.4 to 993 ppm.

Finally Cu concentrations within the SPM are highest at the AB and BP transects reaching 5000 ppm in the upper water column and over 10000 ppm in the deeper waters of the BP transect. The Cu concentrations of BC12 and BC transect are lower (44 – 1115 ppm). The concentration depth

profile of Cu in the SPM follow Sr at the BP transect and the BC12 station, best illustrated by the Sr and Cu profiles of BC12. However, this apparent relationship is not present at the AB or BC stations.

The most striking observation is the large increase in the concentration of all elements within the SPM of all of the Basamuk stations, conversely the mass of actually suspended material decreases or remains constant. This may be due to resuspension of a benthic nepheloid layer.

The correlation coefficients for each transect (Appendix 4B, tables 4B.40-49) indicate strong correlations between a large numbers of the elements. For the AB and BP transects the correlation tables for the coastal and deepest stations are similar, however the middle station on each transect (AB2 and BP2) there are considerably less positive elemental correlations at these sites. BC12 has the least number of correlations with BC stations having similar correlations to that of the BP transect.

2.4.9 Zooplankton

The number of organisms identified from each station ranged from 232-968 (cf. 114-648 at Lihir 3.4.9). Across both Lihir and Basamuk a total of 65 taxa were identified (Table 2.4.9.1). At Basamuk, the list of most abundant taxa at both stations BC1 and BP1x was similar to that observed in Lihir (3.4.9) except that thaliaceans were more abundant and tintinnids less abundant. At both stations the concentrations of organisms were highest in the surface sampled depth-band with little obvious day-night differences. Organism concentrations for individual taxa were noticeably higher at station BC1 reaching up to 2000 organisms m^{-3} for radiolarians. The abundance of other taxa was however more in line with the levels previously observed being less than 600 m^{-3}. At station BP1x there was a slightly different depth distribution to that observed at other locations with some taxa including adult and copepodite stages of copepods being more abundant in the deepest depth-band (500-300 m) than the mid-depth-band (300-100 m). This was slightly more pronounced in the night time samples compared with the daytime and may reflect some degree of vertical migration at this location.

Table 2.4.9.1 Scientific and common names of zooplankton taxa identified

Scientific name	Common name	Scientific name	Common name
1. Acartiidae	Calanoid copepod (Family)	33. Isopoda	Isopods
2. Aetideidae	Calanoid copepod (Family)	34. Euphausiidae	Eucaridan order
3. Amphipoda	Amphipod shrimps	35. Lucicutiidae	Calanoid copepod (Family)
4. Appendicularia	Larvaceans	36. Mecynoceridae	Calanoid copepod (Family)
5. Arietellidae	Calanoid copepod (Family)	37. Metrinidae	Calanoid copepod (Family)
6. Augaptilidae	Calanoid copepod (Family)	38. Mysidacea	Opposum shrimps (Order)
7. Bathypontiidae	Calanoid copepod (Family)	39. Mollusca	Molluscs
8. Polychaeta	Bristle worms (Class)	40. Mormonilloida	Copepoda (Order)
9. Candaciidae	Calanoid copepod (Family)	41. Monstrilloida	Copepoda (Order)
10. Calanidae	Calanoid copepod (Family)	42. Nemertea	Ribbon worms (Phylum)
11. Caridea	Shrimp	43. Oithonidae	Cyclopoid copepod (Family)
12. Brachyura	Crabs	44. Oncaeidae	Cyclopoid copepod (Family)
13. Centropagidae	Calanoid copepod (Family)	45. Ostracoda	Crustacean (Class)
14. Cirrepedia	Barnacles	46. Paracalanidae	Calanoid copepod (Family)
15. Cladocera	Water fleas (Order)	47. Paguridae	Hermit crabs
16. Clausocalanidae	Calanoid copepod (Family)	48. Phaennidae	Calanoid copopod (Family)
17. Cephalopoda	Squids and octopuses	49. Pycnogonida	Sea spiders (Class)
18. Corycaeidae	Cyclopoid copepod (Family)	50. Platyhelminthes	Flatworms (Phylum)
19. Ctenophora	Sea gooseberries (Phylum)	51. Pontellidae	Calanoid copepod (Family)
20. Chaetognatha	Arrow worms (Phylum)	52. Radiolaria	Amoeboid protists
21. Unident. Cyclopoida	Cyclopoid copepod (Order)	53. Rotifera	Rotifers (Phylum)
22. Decapoda	Crabs, shrimps *et al.*,(Order)	54. Thaliacea	Salps (Class)
23. Echinodermata	Starfish/sea urchins	55. Scolecitrichidae	Calanoid copepod (Family)
24. Eucalanidae	Calanoid copepod (Family)	56. Siphonophora	Jellyfish, cnidarian (Class)
25. Euchaetidae	Calanoid copopod (Family)	57. Sapphirinidae	Cyclopoid copepod (Family)
26. Onychopoda	Cladoceran order Evadne	58. Spinocalanidae	Calanoid copepod (Family)

Scientific name	Common name	Scientific name	Common name
27. Foraminifera	Amoeboid protists	**59. Temoridae**	Calanoid copepod (Family)
28. Gastropoda	Molluscan class	**60. Tintinnida**	Tintinnids ciliates (Order)
29. Hydromedusae	Hydrozoan sub-class	**61. Tortanidae**	Calanoid copepod (Family)
30. Heliozoa	Amoeboid protists	**62. Unidentified organism**	Unidentified organism
31. Heterorhabdidae	Calanoid copepod (Family)	**63. Unident. Calanoida**	Unidentified calanoid (Order)
32. Ichthyoplankton	Fish eggs or larvae	**64. Unident. Harpacticoida**	Harpacticoid copepod (Order)
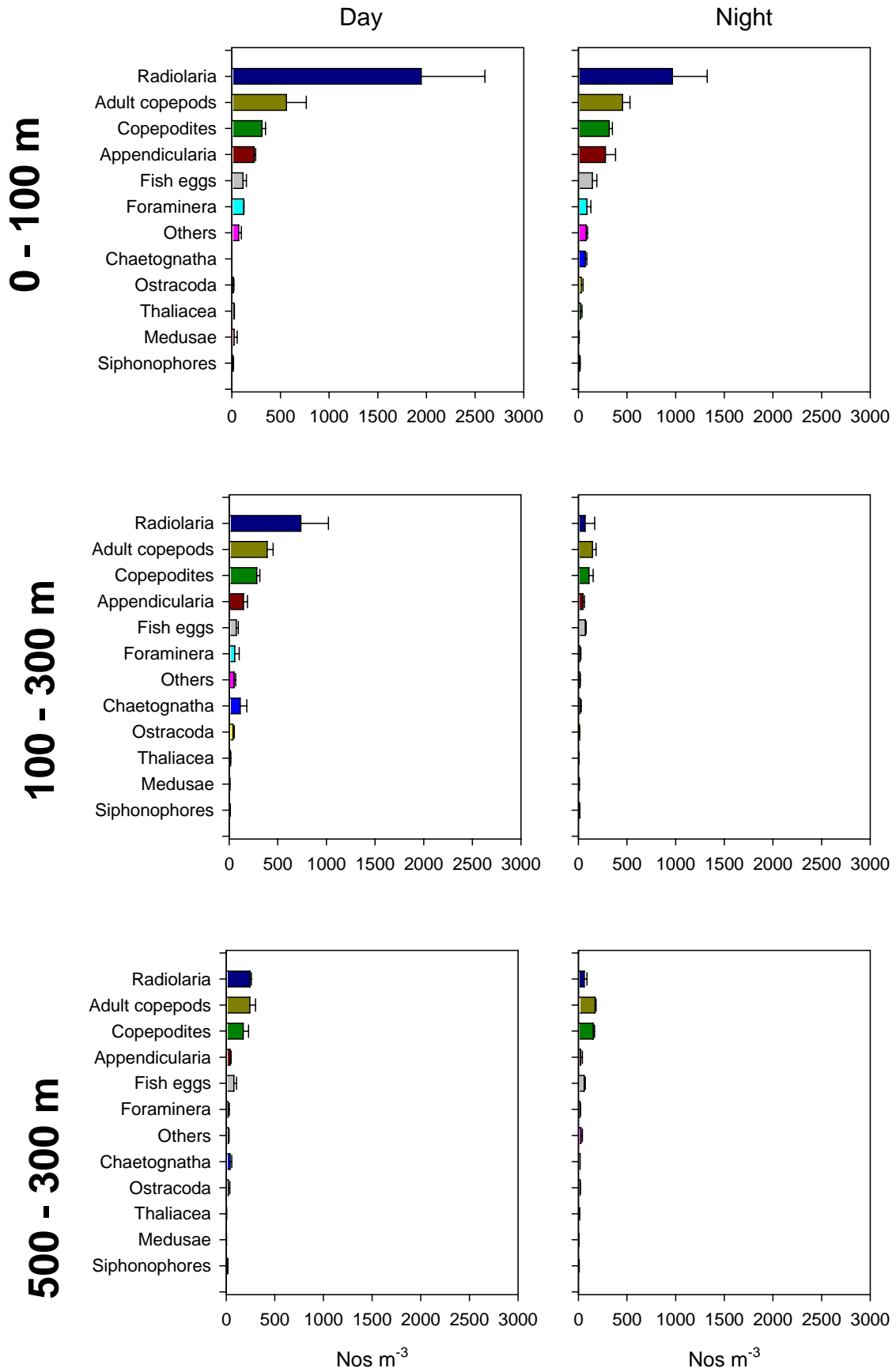
Figure 2.4.9.1 Day and night zooplankton abundance at station BC1.

Figure 2.4.9.2 Day and night zooplankton abundance at station BP1x.

2.4.10 Microplankton

The abundances of the major microplankton taxonomic groups at Basamuk are shown in table 2.4.10.1. The data were collected from only one station at 2 depths so present only a limited insight into the distribution and abundance of microplankton due to the small number of samples collected and lack of replication.

The microplankton community at all stations was dominated by diatoms (16 taxa) with much lower abundances of dinoflagellates and ciliates. Choanoflagellate abundance was also low. The diatom community was numerically dominated by *Pseudonitzschia delicatissima* (Appendix 6).

Table 2.4.10.1 Abundance (L^{-1}) of major microplankton taxa collected in samples from Basamuk

Station	Date	Depth	Diatoms	Dinoflagellates	Ciliates	Unknown Protists	Choanoflagellates
BP14	11/09/2008	10m	2040	180	100	320	80
BP14	11/09/2008	69m	3500	60	180	200	40

2.5 Analysis and discussion

2.5.1 Bathymetry and Acoustic Character

The steep and deeply incised continental slope reflects the high sediment supply from the Rai coast, predominately through supply from rivers. Gravitionally-influenced down-slope mass movement, such as turbidity currents and debris flows are the principal depositional processes. Evidence for these is shown in the v-shaped canyon heads on the upper slope (e.g. offshore from Basamuk) and in the echo-character of the basin sediments in the Vitiaz Basin. Echo-sounder profiles display an irregular and highly reflective seabed character with abundant hyperbolic echoes suggesting a hard or sandy seabed with outcrops of basement (Howe *et al*., 2007).

2.5.2 Physical Oceanography

For clarity, and to avoid repetition, the physical oceanography data are discussed together with the results in section 2.4.2

2.5.3 Sediment sampling and sedimentology

The origin of sediment in the Vitiaz Straits is predominantly terrestrial, supplied by riverine run-off. Density flows from the high-volume rivers supply sediment to the deep-sea through two mechanisms; bedload transport in canyons and channels on the margin and in dilute suspended plumes transported offshore to settle out in the water column. Direct evidence for these processes can be found in the presence of plant material and sand layers, interpreted as deposited from turbidity currents and density flows in the core samples. Once sediment has been deposited on the margin or basin floor, it can become subsequently resedimented by the strong contour currents (estimates of maximum velocities vary between 50-100 cm s^{-1}) (Murray, *et al.*, 1995) present in the Vitiaz Strait. Given the measured natural sediment mean grain size (varying between medium-coarse silts – 20-50 μm), this, and finer, grain sizes are easily carried in suspension in near-bottom flows, possibly as a benthic nepheloid layer. Suspended sediments, and hence future mine tailings, have the potential for a wide dispersal in the Vitiaz Strait notably towards to the NW, Madang and Karkar Island.

2.5.4 Sediment and Water Column Geochemistry

The geochemical results for the Basamuk study suggest different sediment sources are being supplied to the four transects, Astrolabe Bay, Basamuk, Helmholtz point and the eastern control transect. The largest differences are seen between the Astrolabe Bay and eastern control transects. Higher riverine or aeolian inputs occur at Astrolabe Bay compared to the eastern control transect with indications that the deepest station in the eastern control transect, BC4 is being influenced by Long Island.

The C:N ratios and organic carbon content indicate that the deeper stations are receiving a larger input of more labile marine derived organic carbon compared to the shallower stations which are receiving more refractory carbon. One exception to this generality is station BC12 at 1597m depth which contains a higher content of refractory carbon as indicated by the higher C:N ratios found at this station. This may indicate older more degraded carbon at this station.

The concentration and inventories of key major and minor elements at all the stations indicate that there are significant differences in the elemental signature of the sediments at the 4 transects confirming that the sources of sediment supply are different and that the shallowest station located in Astrolabe Bay is receiving significant inputs of riverine material.

The sediment mixing and accumulation rates were assessed at all the stations and the results from the ^{210}Pb activity profiles are in good agreement with the observations made of the sediment

benthos at the stations. As would be expected the most intense mixing is occurring at the coastal stations with less mixing occurring at the deeper stations. The sediment accumulation rates range from 0.02 to 0.1 g cm^{-2} yr^{-1}, with the highest rates occurring at the deeper stations.

The pore-water nutrient concentrations indicate that the whole region experiences low oxygen pore-water conditions with the Astrolabe Bay stations receiving the greatest nitrogen loading of the region. The N:P ratio of the pore-water decreases from Astrolabe Bay to the eastern control transect suggesting that there is an increase in the labile fraction of the organic material reaching the eastward located stations.

The trace element pore-water and solid phase profiles for the transect stations indicate that all the sediments are oxidising at the surface but do become anoxic at depth. Biogeochemical cycling is taking place at the stations and it is determining the distribution of elements between the sediment, pore-water and overlying water column. It is important that these processes are understood at the stations that will be impacted by mine tailings to ensure that any re-distribution of metals between the sediment and overlying water column can be predicted and any necessary mitigation procedures put in place.

The water column nutrient profiles at the shallower stations are characteristic of coastal zones experiencing high rainfall. The strong pycnocline caused by the surface runoff inhibits mixing of the nutrient rich waters giving rise to nutrient depleted surface waters along the transects. Ammonia is in measurable concentrations in the region probably suggesting productivity is reliant on this as a source of nitrogen however the dissolved organic nitrogen derived from fluvial sources may form the majority of the nitrogen pool.

The geochemical analysis of the suspended particulate material indicates that the depth profiles of mass and elemental concentrations exhibit complicated structures that may be explained by the effects of physical and chemical processes such as different water masses, currents and sediment supply. The highest amounts of SPM occur at the coastal station at Basamuk and the deepest eastern control station. The most striking feature of the SPM profiles is the sharp increase in concentration at depth at the BP stations. The increase in elemental concentrations at these stations may indicate resuspension of the floculant benthic nepheloid layer. If this is the case then the possible rsuspension of sediment within the tailings foot print must be considered.

2.5.5 Benthos

Among the three transects, only Basamuk Pipeline stations showed a consistent depth-related trend in faunal abundance, better-developed for meiofauna than macrofauna. The sharp decline in meiofaunal abundance from BP1x to BP4 is somewhat surprising, given that the depth range covered is not large (920 – 1598 m), and meiofauna typically show a less marked bathymetric gradient in numbers than macrofauna (Rex *et al*., 2006). The stations along the Astrolabe Bay and Basamuk Control transects showed no clear depth-related pattern.

In the steep, canyon-dissected slope habitat sampled along the Rai Coast, depth *per se* may be less important in determining faunal density and composition than the frequency and intensity of environmental disturbance by sediment slides and turbidity flows. The high meio- and macrofaunal densities recorded at BP1x are consistent with the relatively undisturbed appearance of the seabed at this station (see section 2.4.7). The single photograph obtained at the deeper station BP3 along the same transect may indicate a more recent disturbance event. If so, this could be related to the relatively low meio- and macrofaunal densities recorded here. A similar contrast was seen on the Eastern Control transect, where meiofaunal density was high at BC2, where no signs of recent disturbance were apparent on seabed photos, and lower at BC12, where the surface topography was suggestive of recent physical disturbance. The causal factors behind the extremely low faunal densities at station AB1 are uncertain as we have no seabed images from this transect.

The mean densities of meio- and macrofauna at each sampling locality are given in table 2.5.5.1 with individual stations aligned by water depth for ease of comparison.

Comparing the three transects together, the low faunal density at AB1 appears anomalous, although we have no stations at similar depth on the other transects to provide a comparison. Relatively high densities at BP1x, and low densities at BC1 are also apparent, but the remaining stations show a high level of agreement at comparable depths. This may be evidence that the environmental factors influencing benthic standing stock are similar across all three broad sampling areas.

Table 2.5.5.1 The mean (± SD) densities (ind. m^{-2}) of meio- and macrofauna (the latter in boldface font) at each sampling locality

Astrolabe Bay	Basamuk Pipeline	Basamuk Control
AB1 (762 m)		
Meio: 1612 ± 294		
Macro: 890 ± 583		
AB2 (902 m)	BP1x (920 m)	
Meio: 11310 ± 831	Meio: 18034 ± 958	
Macro: 5804 ± 1898	**Macro: 10631 ± 1260**	
AB3 (1155 m)	BP2 (1165 m)	BC1 (1190 m)
Meio: 11289 ± 3234	Meio: 11162 ± 4207	Meio: 4286 ± 2041
Macro: 5517 ± 1571	**Macro: 4859 ± 1178**	**Macro: 1868 ± 600**
		BC2 (1350 m)
		Meio: 9698 ± 2191
		Macro: 4521 ± 330
	BP3 (1420 m)	BC3 (1430 m)
	Meio: 6440 ± 1143	Meio: 5411 ± 1846
	Macro: 3756 ± 414	**Macro: 3024 ± 180**
	BP4 (1598 m)	BC12 (1597 m)
	Meio: 5347 ± 627	Meio: 5709 ± 4171
	Macro: 4775 ± 1278	**Macro: 4244 ± 0**

With respect to community composition, the most distinct pattern apparent in the data is the high abundance of small ampharetid polychaetes at the five stations in the 902 – 1190 m depth range. This family is much less prominent in the polychaete communities sampled at greater depths. Ampharetids are sedentary tube-builders which feed on organic particles at the sediment surface using a crown of long cephalic tentacles (Fauchald and Jumars, 1979). They are often common in deep-sea sediments.

2.5.6 Seabed photography

The seabed photographs at stations BP1x and BC2 show a diverse range of biogenic features superimposed on a fairly smooth, flat sediment surface. This topography suggests a relatively low-disturbance benthic environment. In contrast, the seabed at BC12 appeared much more disturbed, with an irregular physically-generated topography and less evidence of biological activity. This pattern may indicate that a downslope sediment transport event has taken place more recently at BC12 than at BP1x or BC2, although it is impossible to say whether this translates into a greater overall frequency or severity at the first station. The similarity of the single image from BP3 to the BC12 pattern may also be evidence of a relatively recent disturbance event.

The 18 photos from station BP1x showed a relatively large number of epifauna for such a small sample, consistent with the inference that this station has not been recently disturbed. The observations of an epifaunal elasipodid holothurian and a benthopelagic holothurian (if the latter is correctly identified) are interesting, as these animals are more typical of the Abyssal Zone (> 3500 m) than the shallower bathyal depths sampled here (Billett, 1991). Epifaunal enteropneust worms, and their distinctive faecal casts, are most often observed at abyssal depths but have also been recorded from the Bathyal Zone. These fragile worms are rarely collected intact and very little is known of their biology (Holland *et al.*, 2005; Smith *et al.*, 2005).

2.5.7 Zooplankton

The distribution of plankton in both the horizontal and vertical domains is usually patchy. Patchiness scales at multiple frequencies with the dominant modes typically between 200 km to a few centimeters. Organism counts within plankton samples are therefore usually variable with CVs in the order of 22-44% but can be as high as 100% (Cassie, 1968). The usual solution to increase the precision of the mean abundance estimates is to increase the number of replicate samples collected. However, because analysis of plankton samples still requires the work of a taxonomist using visual methods, there is a high cost to increasing the number of samples collected (although some progress has been made with automated systems they still do not give much speed advantage over the human analyst and usually require a long training period). In the present study, two or three replicates at each depth-band were collected, this being the maximum that could be accommodated with reasonable cost.

Given that not all the organisms collected in a net haul can be analysed, a further source of variation in the estimates of abundance comes from sub-sampling. The technique used (swirling flask and Stempel pipette) is a standard method. Assuming the organisms are randomly distributed in the swirling flask, the precision of the estimate of any one taxa will depend on the number of organisms counted. The precision will therefore be lower for rarer organisms in the sub-sample. For the common taxa, such as total adult copepods and radiolarians, generally more than 100 individuals were counted in a sub-sample and the precision will be better than +/- 20%.

The resulting standard deviations of the mean abundances, although relatively large, are not atypical of what would be expected for plankton abundances computed from this number of replicates.

It is generally expected in waters of this depth that the majority of planktonic organisms will be found in the upper part of the water column so the lower concentrations found deeper than 100

m are not unexpected. Many plankton exhibit vertical migrations and day-night differences in depth distribution are commonly observed. However, relatively fine-scale sampling is often needed to reveal such movements. Other observing methods which can resolve individuals such as high-frequency acoustics often provide stronger evidence for diel migrations compared with sampling with nets. The absence of strong day-night differences in the present samples may therefore reflect the relative thickness of the depth-bands sampled.

The wide representation of copepod families is also typical of tropical waters. A peak in copepod biodiversity as measured by taxa richness (apparent both at genera and family levels) is generally observed at the equator with a cline of decreasing richness moving north or south towards the poles (Woodd-Walker *et al.*, 2002).

2.5.8 Microplankton

The predominance of diatoms at station BP14, and their presence in relatively high numbers, suggests an environment characteristic of near-shore waters which are relatively rich in nutrients.

2.6 Summary

An extensive baseline survey has been carried out on the Rai coast at stations that are likely to be impacted by the proposed DSTP at Basamuk as well as at more distant stations in similar depths that are unlikely to be influenced by the tailings. This will allow future surveys to compare changes at impacted stations with the environmental conditions pertaining before impact and, by analysing changes at control stations over time will determine the level of natural temporal variability that will inform interpretation of the results at the impacted stations. This is the most comprehensive baseline study yet carried out for a DSTP mine in PNG and, as far as we know, in the world.

Detailed investigations have been made on benthic macro-and meiofaunal communities together with high resolution studies of both benthic and pelagic biogeochemistry. The physical oceanography of the area has been further characterised although there is much more that could be done to better understand the hydrodynamics of the region, especially relating to temporal variability.

The Basamuk site and the adjacent continental slope appear to confom to the fundamental requirements of a DSTP i.e. steeply sloping from close to the coast leading quickly into very deep

water. Provided the DSTP system is optimally specified and subsequently maintained it should perform as well as the system at Lihir (See section 3). However, there is always uncertainty in any prediction and a robust monitoring programme must be implemented once the DSTP becomes operational to ensure that the system performs as planned with minimal interaction with shallow water ecosystems.

3. Operations: the Lihir Study

3.1 Vital statistics of operations at Lihir

Lihir is a large scale, open pit gold mine located on the central east coast of Niolam Island, the main island in the Lihir Islands group, about 700 km north east of Port Moresby in PNG (Figure 3.1.1). The mine consists of two adjacent overlapping pits close to the shores of Luise Harbour. Niolam is a volcanic sea mountain emerging from greater than 2000 m depth. It consists of five Miocene-Pleistocene volcanic units, three of which are volcanic calderas and two are sequences of mafic volcanic rock that predate the three volcanoes. The volcanoes contain an abundance of hydrothermal breccias that are characterised by elevated levels of As, Cu, Mo and Pb (Muller *et al.*, 2002). The surrounding reef edge is narrow and grades steeply into deep water. Ocean depth increases to over 1500 m at a distance of 15 to 20 km from Luise Harbour. At that depth the submarine slopes grade more gently to a depth of 2000 m.
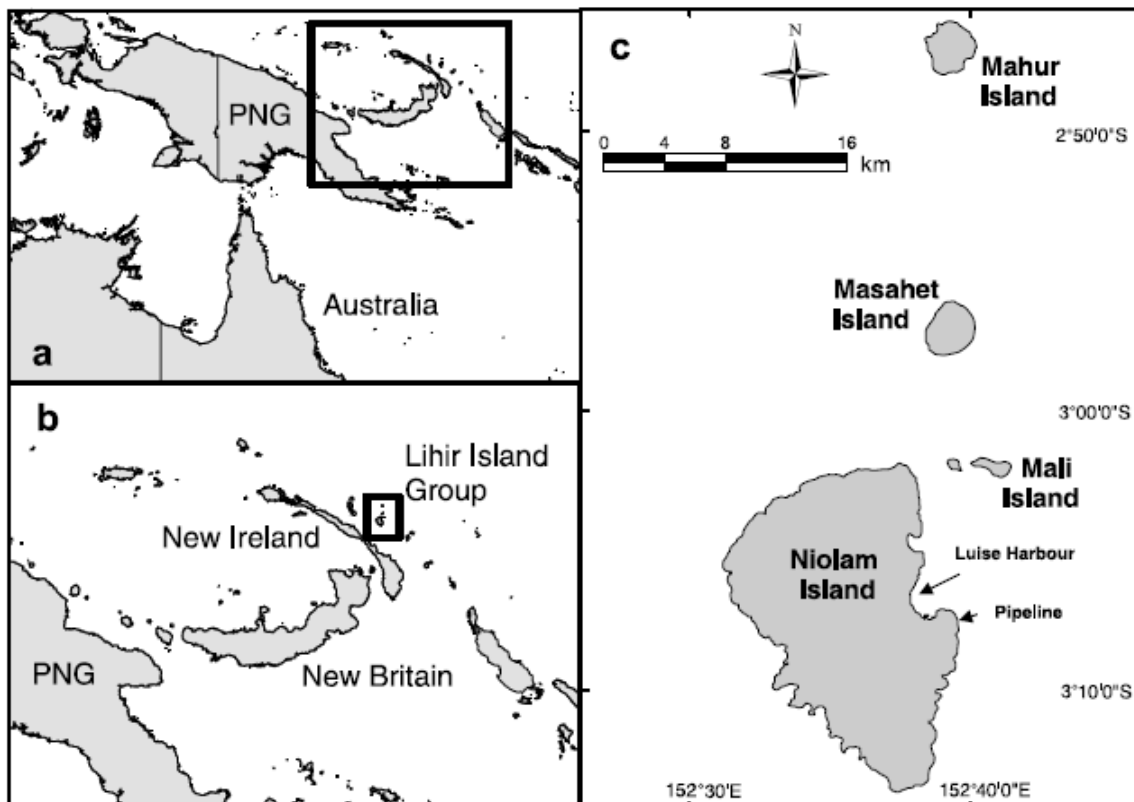
Figure 3.1.1 The Lihir Islands group off the coast of Papua New Guinea (a) and New Ireland (b), and the location of Lihir mine's DSTP pipeline on the east coast of Niolam Island (c) (source: Brewer et al., 2007).

Exploration of the area since 1983 identified several adjacent and partly overlapping gold deposits. Lihir gold mine has been in operation since 1996, and has a projected operational life of 44 years, with mining operations taking place until 2022 and processing of the stockpiled low-grade ore until 2040 (LGL, 2006)

The decision to use deep-sea placement of mine tailings waste in preference to land disposal at Lihir, was based on the same principles as those described for Misima (section 4.1). In short, it was reasoned that the steep terrain and the closeness to the shore did not provide any safe space for a terrestrial impoundment, which in any event would have been environmentally risky owing to the frequent earthquakes experienced at the site.

3.1.1 Deep-sea tailings disposal system at Lihir

The design of the DSTP system at Lihir is similar to that used at Misima. A diagrammatic representation of the water and tailings flows at Lihir is shown in Figure 3.1.1.1. All the outflow streams from the processing plant converge at a junction box, from which the combined flow enters a gravity fed pipeline to the tailings de-aeration tank (NSR, 2001).

Lihir processes the ore to recover the gold using whole-of-ore pressure oxidation followed by a carbon-in-pulp circuit, which involves the addition of a cyanide solution to the slurry of finely ground ore. The former process produces an acidic, metal-rich counter-current decantation (CCD) wash water, and the latter, an alkaline tailings slurry containing residuals quantities of cyanide and lime left over from the gold extraction process. Residual cyanide is treated in the detoxification plant by mixing the iron-rich and acidic CCD wash water with the alkaline tailings slurry. The treated tailings stream then flows to the tailings drop-box where it combines with the flow from the first CCD thickener to produce a dilute and acidic tailings slurry, which flows to the junction box and onward to the de-aeration tank. The tailings slurry is diluted with seawater cooling water before entering the de-aeration tank. The residence time of the tailings in the de-aeration tank allows trapped air bubbles to escape prior to being discharged through the tailings outfall pipeline at a depth of 115 m.
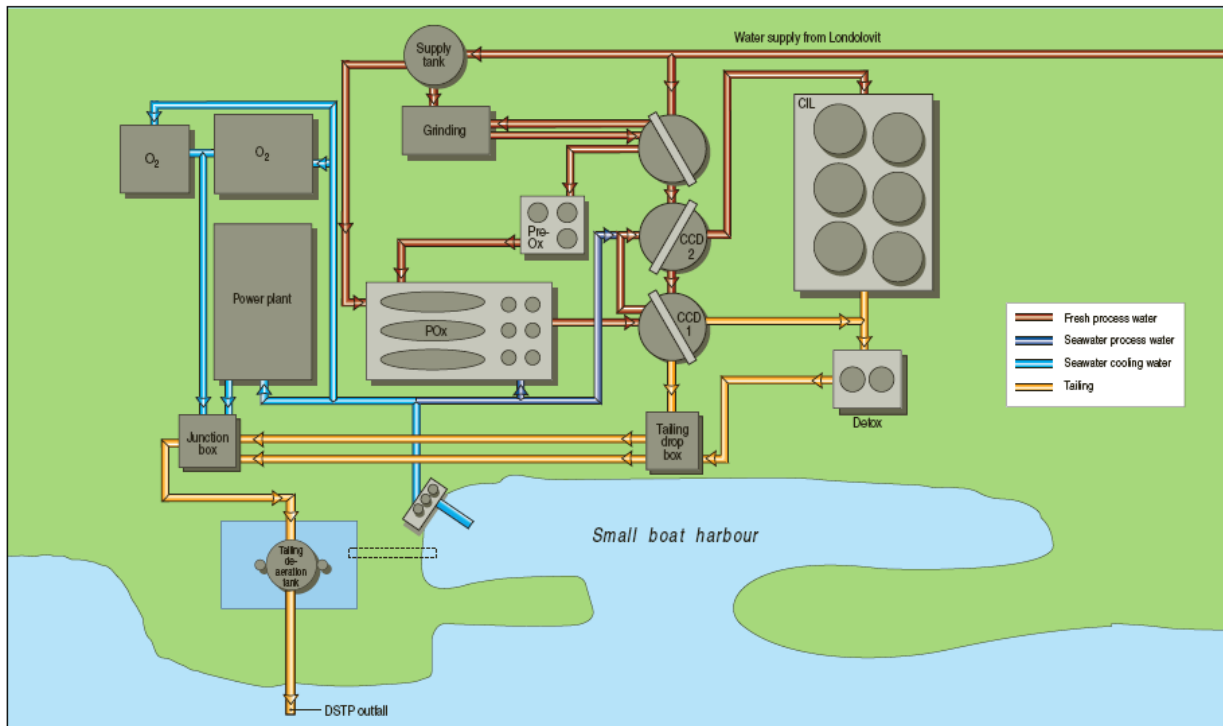
Figure 3.1.1.1 Schematic diagram of the layout of the DSTP system at Lihir showing the water and tailings flow within the processing plant (NSR, 2001).

The tailings waste is discharged onto the steep submarine slope via the DSTP pipeline which passes through an inclined hole drilled through the fringing coral reef and underlying basalt (Figure 3.1.1.2). The pipeline terminates at a depth of 115 m, below the euphotic zone at about 90 m and the deepest mixed layer at ~100 m. The tailings continue to descend down the submarine slope as a density current, eventually settling on the seabed at depths of between 900 m to 2000 m. Approximately 60 km^2 of the sea floor is impacted by probable mine derived sediments (LGL, 2005).

The DSTP system at Lihir is regulated through Water Use Permit (WUP) 29/990 granted by the Water Resources Board of PNG. The WUP specifies maximum permissible water quality concentrations at the discharge outfall and in the receiving ocean within the mixing zone boundary.

The boundary of the mixing zone, as defined in WUP 29/990, extends radially 1.8 km to the north and 2.3 km to the southeast of the outfall (Figure 3.1.1.3; NSR 2001).
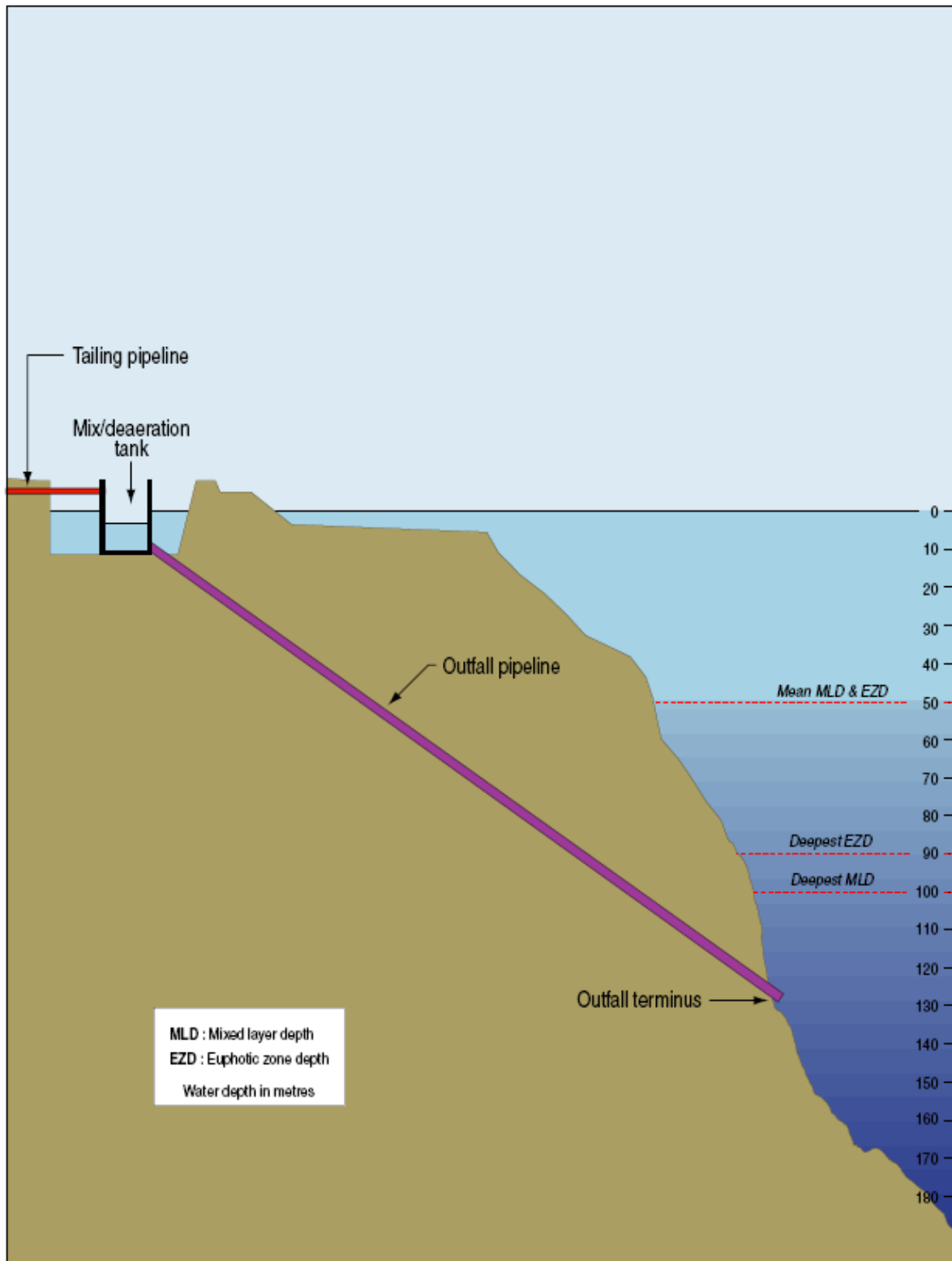
Figure 3.1.1.2 Schematic cross-section of the DSTP outfall pipeline at Lihir (NSR, 2001).
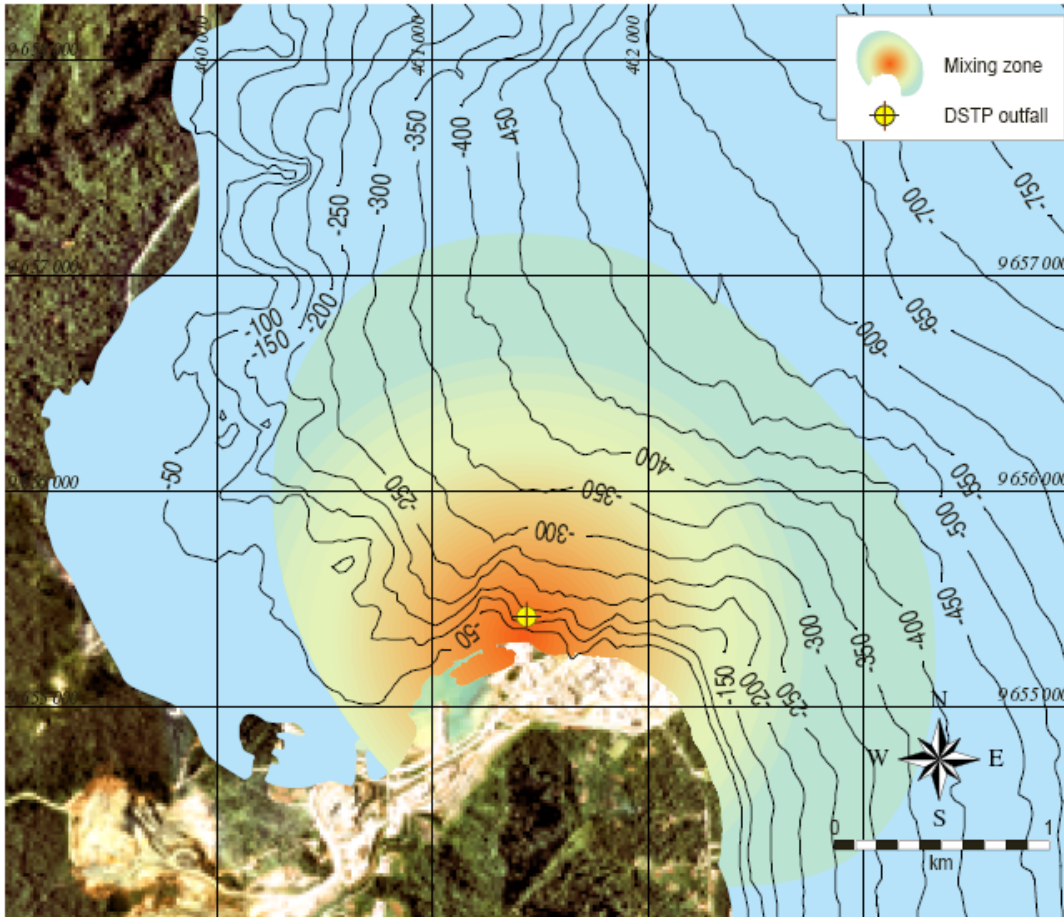
Figure 3.1.1.3 Lihir Gold Mine and the area of the allowable mixing zone for the DSTP outfall off Luise Harbour (NSR, 2001).

Lihir mine disposes of approximately 3.5 to 4.5 M t of tailings slurry to the marine environment each year (3.5 M t discharged in 2005, 4.2. M t in 2004, 3.9 M t in 2003). The tailings comprise a mixture of tailing solids (ca. 5% clay, 93% silt, and 2% fine sand), freshwater, seawater, dissolved metals (zinc, copper, arsenic, cadmium, mercury, lead, nickel, chromium and silver), and small amounts of process chemicals, including lime and weak acid dissociable cyanide. The tailings discharge has a pH of about 2.3 and a temperature of 34°C (LGL 2005).

Monitoring of the tailings stream chemistry and temperature are undertaken in accordance with the project's Environmental Monitoring and Management Plan (LGL 2004) and WUP 29/990. Analyses conducted by CSIRO (NSR 2001) and as part of the Environmental Impact Statement work scope (LGL 2005) show the tailings slurry to be compliant with the criteria established in WUP 29/990.

3.1.2 Environmental monitoring of DSTP at Lihir

The environmental monitoring programme detailed in Lihir's Environmental Monitoring and Management Plans (EMMPs) includes:

> Compilation of an environmental baseline with a range of variables describing background conditions. This commenced in 1984 with some variables and was completed after grant of the Special Mining Lease (SML), but before construction commenced (NSR 1996a).

> EMMP Monitoring During Construction (1995-May 1997) (NSR 1996b).

> EMMP Monitoring During Operations - for the first two and a half years of production (May 97 – Dec 99) (NSR/LMC 1998).

> Lihir EMMP Operations Phase (2000 – 2003).

Detailed procedures for the collection of data and samples, analysis, quality control, database management, and reporting for all elements of the EMMP are integrated into the Environmental Management System (EMS) prepared in accordance with (and externally audited against) the ISO14001 international standards for environmental management. The DSTP environmental monitoring programme at Lihir includes the following aspects:

Tailing stream chemistry and temperature

Routine monitoring of the tailing chemistry involves sampling of the tailing waste stream within the de-aeration tank prior to marine discharge. Samples are collected every two hours and combined over 12 hr, providing two composite samples per day. The composite samples are analysed for % solids, pH, conductivity, temperature, TSS, Fe, Mn, Al, Ag, Cu, Pb, Zn, Cd, Ni, As, Hg, Se, Cr, Co, total CN, WAD-CN, free CN. The results are used to characterise the physical and chemical composition of the tailing stream and ensure compliance with WUP 29/990 for tailing discharge. The criteria included in WUP 29/990 are used to ensure compliance with PNG Schedule 4 water quality criteria for marine waters at the mixing zone boundary.

Oceanic water quality

Monitoring is undertaken to assess compliance with PNG Schedule 4 water quality criteria at the mixing zone boundary. Collection of oceanic water samples initially relied on fixed-depth monitoring at all sites. Following an intensive oceanographic investigation into the transport of

sub-surface plumes during 1999 (NSR 2001), sampling was modified to target specific sampling depths and areas.

The surveys in 1999, using Acoustic Doppler Current Profilers (ADCPs), indicated that subsurface plumes varying in thickness from 10 to 200 m occur below the depth of the mixed layer to depths of 700 m (NSR 2001). The plumes generally occurred within the allowable mixing zone, however, some were found up to 4.4 km north of the discharge point (Figure 3.1.2.1). Approximately 10 to 30 % of the tailings waste was estimated to separate from the main density current as subsurface plumes (NSR 2001). The presence and dispersion of subsurface plumes increases the tailings deposition area from that initially predicted.

Chemistry and biology of ocean floor sediments

A distribution map of the tailings has recently been produced for Lihir (Figure 3.1.2.2).

The geographical extent of the tailings deposition area and its geochemistry is monitored. Benthic infaunal samples are collected to determine the impacts of habitat smothering and chemical toxicity arising from the deposited tailings waste.

Fish, shellfish and seagrass metal bio-monitoring

Metal concentrations in the tissues of fish, shellfish and seagrass are monitored to quantify long-term impacts and confirm initial predictions in the Environmental Plan that metal uptake is unlikely to be significant. Key organisms are monitored to provide integrated, long-term indicators of environmental health. Finfish, shellfish and seagrass (*Yelang* spp.) are collected annually.
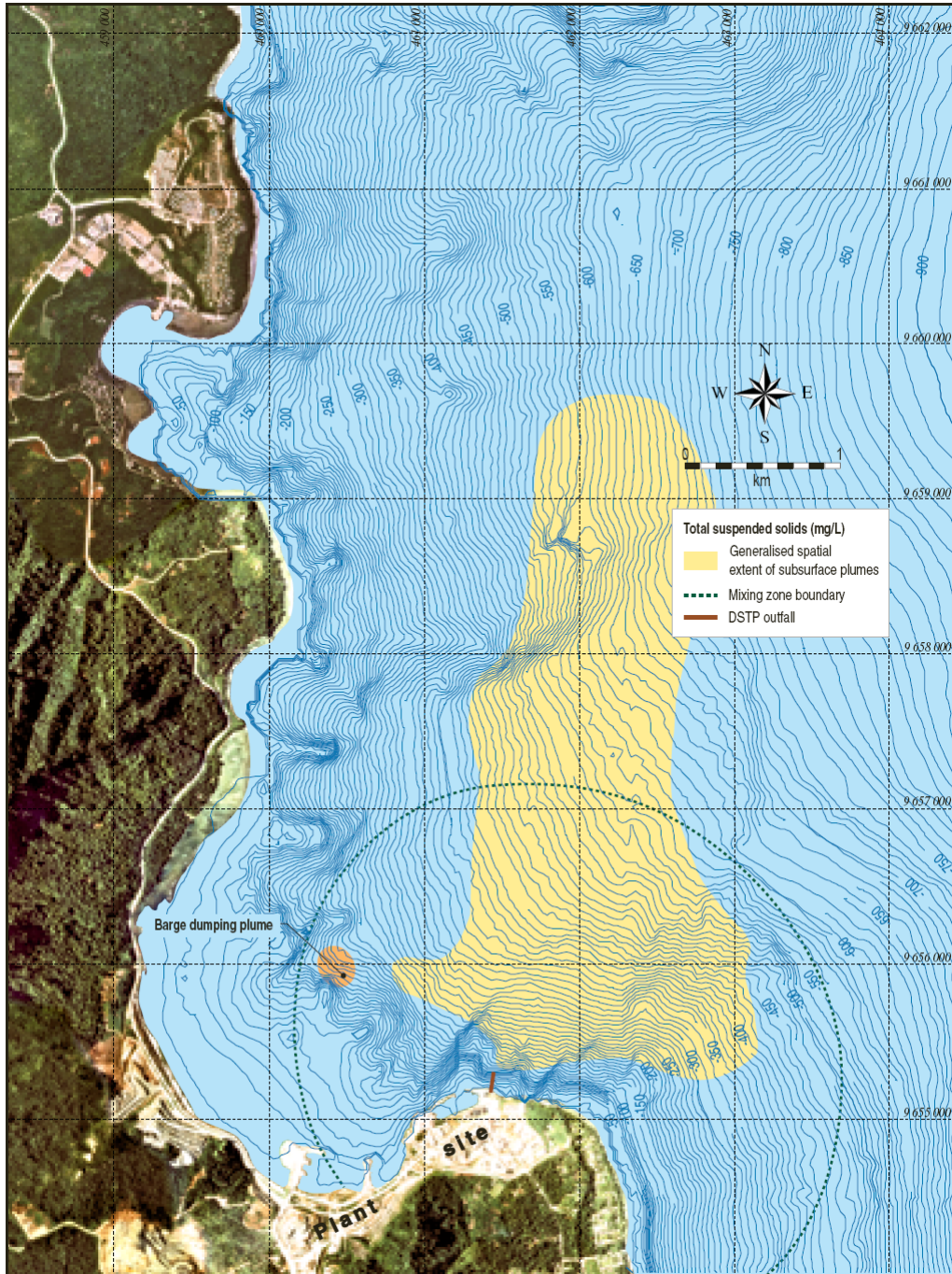
Figure 3.1.2.1 The spatial extent of observed subsurface tailings plumes arising from the DSTP outfall and tailings density current at Lihir from 23 to 31 January 1999 (NSR 2001).
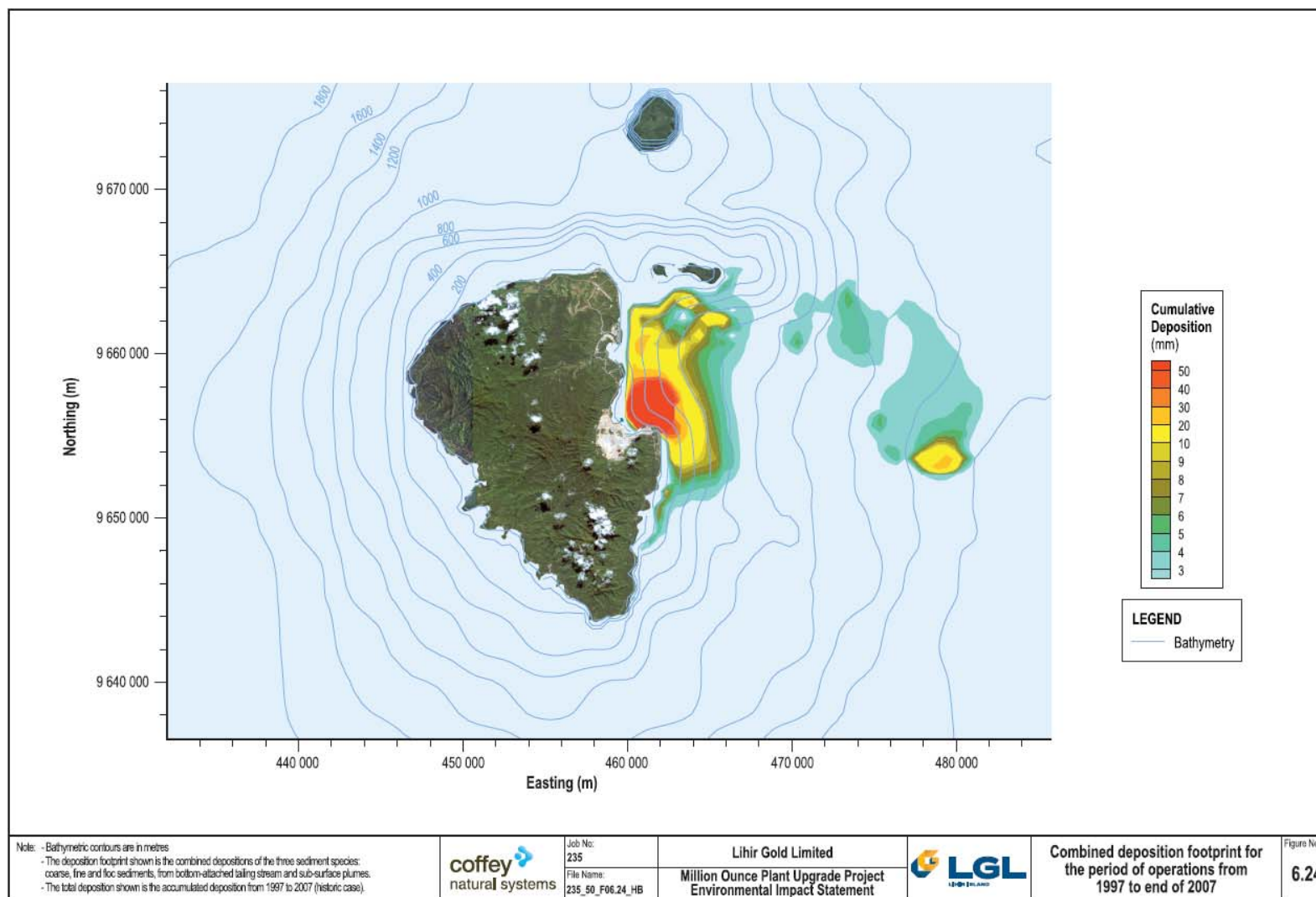
Figure 3.1.2.2 Estimated cumulative depositional tailings footprint to 2007 at Lihir (Coffey Natural Systems, 2009)

3.2 Environmental background

3.2.1 Geomorphology

Lihir geomorphology is controlled by the subduction of oceanic crust beneath continental plates. In the region of Papua New Guinea, the Australian Craton is actively over-riding the Pacific Plate producing a subduction zone, with an active island arc setting to the north of the island (White *et al*., 1995, Kamenov, 2004). This process has continued throughout the Cenozoic. At a regional scale, the tectonic setting is more complex with the interaction of a number of smaller plates. These are, from the north; (a) The Caroline Plate, presently undergoing crustal shortening via a transform faulted margin with the Australian Plate, (b) The Bismarck Plate, separated from the Pacific Plate by a youthful (3.5Ma) spreading ridge to the northeast and from the Australian Plate by a broad zone of faulting to the southwest and (c) The Solomon Plate which is presently being subducted beneath the New Britain Arc (Cullen and Pigott, 1989). Of particular note for this study is the location of Lihir Island in the main seismic zone, associated with the complex tectonics between the Solomon and Bimsark Plate. These interactions can develop earthquakes of up to magnitude 8 (Lihir Gold, 2005). Earthquakes result from vertical movements in steeply dipping reverse faults - this vertical motion can create tsunamis across the region.

Lihir Island is part of the Tabar-Lihir-Tanga-Feni (TLTF) island chain, itself part of the Bismarck Archipelago. The TLTF islands form part of the Western Pacific gold province, extending from Japan, the Philippines, Papua New Guinea, Solomon Islands, to Fijii and New Zealand (Kamenov, 2004, Kamenov *et al*., 2005). The Bismarck Archipelago is the result of subduction of the Pacific Plate under the Australian Plate and the TLTF region is subsequently dominated by alkaline volcanism. Lihir Island is composed of five volcanic blocks, two remnant; the Wurtol wedge and the Londolovit block and three Pleistocene stratovolcanoes, Huniho, Kinami and Luise. These three volcanoes are characterised by large debris avalanche amphitheatres. The Luise stratovolcano hosts the giant (44Moz) Ladolam epithermal gold deposit within the alkalic breccia of the collapsed caldera (White *et al*., 1995). Ladolam consists of four orebodies; Minifie, Lienetz, Kapit and Coastal. The gold is found in the refractory sulphide ores that occur as cement within hydrothermal breccias, which have average grades of approximately 5 g t^{-1} Au and are associated with pervasive adularia-pyrite alteration. Also present are quartz-calcite veins that can have gold grades of up to 120 g t^{-1} (White, *et al*., 1995). Mineralisation involved three distinct phases: (i) Early porphyry style biotite-feldspar alteration and minor copper-gold-molybdenum mineralization between 0.9 and 0.34 Ma (Moyle *et al*., 1990) (ii) Refractory pyrite ores associated with abundant hydrothermal breccias formed during the caldera collapse event. (iii) Low

sulfidation epithermal quartz-calcite veins which cross cut the refractory sulfides. The presence of the Luise volcano provides an active hydrothermal system consisting of hot mud pools, springs of chloride and acid sulphate water and low temperature fumaroles (Davies and Ballantyne, 1987; Welsh and McCulla, 1987; Plimer *et al.*, 1988; Moyle *et al.*, 1990).

The site of the DSTP, offshore from Luise Harbour, east of Lihir Island, is summarised by Thomas *et al.*, (2003). The authors describe the dump site as located between the coral reefs at Putput Point in the south and Kapit Reef in the north. The fringing reef is divided into two terraces, the upper one exposed at low tide and the lower one between 6-10m depth. The inshore zone is characterised by a gently sloping seabed of black basaltic sand, shelving gently to 40m. Below 40m the offshore geomorphology is more irregular, dominated by canyons and steep slopes. The seabed surrounding the harbour further offshore is characterised as young ocean crust, being highly irregular and containing active hydrothermal vents, these being found 8km to the south and 15km to the north of Lihir Island (Hargreaves and Associates, 2005).

3.2.2 Physical Oceanography

Lihir Island (152° 35' E, 3° 8' S) is located at the western end of 14,000 km of unbroken Equatorial Pacific Ocean (Figure 3.2.2.1). From an oceanographic point of view it is relatively small, with a major dimension of order 10 km, a very narrow shelf region surrounded by extremely steep bathymetric slopes leading very quickly to depths of 1000 m (well below the surface current system).

Lihir is exposed to the wind driven Equatorial current system that dominates the upper 200 m of this part of the Pacific Ocean. The nearby South Equatorial Current is, for most of the year, westward flowing with speeds of order 50 cm s^{-1}, although from December to February it is weak and variable (Admiralty, 1988).   Stronger currents are to be found at deeper depths. Just to the north of Lihir, centred on the Equator at a depth of about 200 m, is the eastward flowing Equatorial Under Current (EUC) with a core speed of > 50 cm s^{-1} at 156° E that diminishes to ~20 cm s^{-1} at 3 ° S (Johnson *et al.*, 2002). Off the northeast coast of New Ireland, across a section that ran very close to Lihir, Butt and Lindstrom (1994) reported a north-westward flowing current at a depth of 235 m , that had an approximate width of 40 km and speeds of ~ 60 cm s^{-1}, giving a total transport of ~2×10^{6} m^{3} s^{-1} (the New Ireland Coastal Undercurrent, NICU). To the north-east of Lihir velocities were significantly weaker and the current tended to flow north-eastward. This current and the NICU appear to feed into the EUC as they approach the Equator.

Butt and Lindstrom (1994) report that off Lihir temperature decreases from 13° C at 300 m to < 5° C at 1000 m, whilst over the same range salinity decreases from 35.0 to 34.6 at 500 m, with lower values below that depth. They also report that dissolved oxygen levels in the NICU core at 235 m are significantly lower (110 to 125 µmol l^{-1}) than they are at the Equator (130 µmol l^{-1}).

In the western Pacific this system is modulated on various timescales - particularly seasonal (due to movement of the Inter-Tropical Convergence Zone), and interannual (due to El Niño - Southern Oscillation, or ENSO, variability).
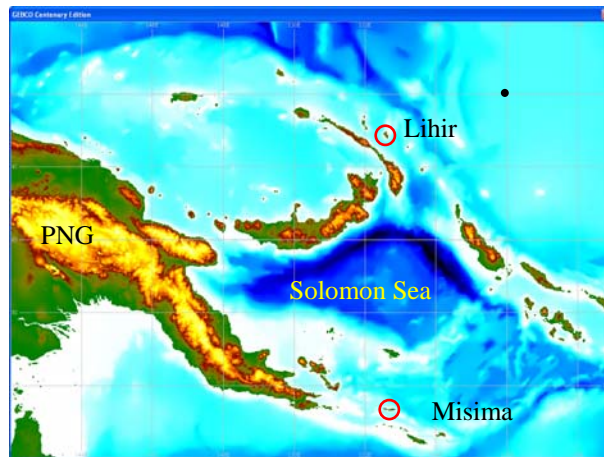
Figure 3.2.2.1 The Bismarck Archipelago and Solomon Sea showing the location of Lihir and Misima at the western end of the Equatorial Pacific. The black dot shows the position of buoy 2S156E. The Equator is at the top of the Figure.

3.2.3 Sediments

The water depths around Lihir Island increase to over 1500m 15-20km from Luise Harbour. Here the slope becomes gentler reaching water depths of 2000m. Further offshore a series of oceanic trenches (presumably young fracture zones) provide depths in excess of 3000m.

The multibeam bathymetric seabed survey data comprises opportunistic RV Sonne (1996 and 1999) and, specifically MV Western Venturer surveys (1997 and 2005) all these surveys reveal both the natural complex bathymetry and the impact of mining on the seabed of the region offshore of Lihir Island (Lihir Gold, 2005). These data are of very high quality and have been well-interpreted and are an essential baseline for further sampling and monitoring. In addition, acoustic seabed classification surveys were undertaken in 2005 to better map the extent of mine derived tailings in deep water, this study was experimental and more limited in its approach. Surveyed depths range from 10-2200m (Lihir Gold, 2005). The slopes of the island are mantled by radial-depositional fans extending over 10km out from the margin, produced by the mass-wasting

of steep slopes with a high sediment supply. Depositional processes that can contribute to these features are debris flows, slumps and turbidites producing downslope reworking of the slope through successive gravitationally and seismic-induced failure. Farther offshore are well-defined valley and ridge features, presumably thinly-sedimented ocean crust fractures. Hydrothermal vents are located 8km to the south and 15km to the north of the island, ample evidence of the active tectonic setting and production of young ocean crust in the region. It is not known if these vents are presently active (Hargreaves and Associates, 2005).

The area of interest, east of Luise Harbour displays a seabed modified by active downslope sedimentation, both natural and as a result of DSTP activity. Closest to the harbour, approximately 0.5-3km offshore, are two sediment mounds, interpreted as mounds from barge-dumped waste. The mounds are 35-55 m high and both display slide scars from gravity failures. The shore and ocean flanks of the mounds possess an angle of repose of 30°. At the base of the shore side of the mounds is a featureless plain of sediment, at 80m depth, thought to be the product of silt accumulating from dredging and discharging and unable to move offshore as the mound is blocking a submarine canyon (Hargreaves and Associates, 2005). The southerly mound has been known to be unstable. A small surge wave that occurred on October 13th, 2004 was produced by the failure of submerged rock waste from this mound into deep water. Lihir Gold Limited surveys of July, 2004 and again in October 2004 indicate the volume of waste rock in the mound had decreased by 5.1 Mm^3 (Lihir Gold, 2005).

The seabed levels survey indicates predominant deposition has occurred inshore on the flat margins of Luise Harbour whilst offshore is a zone of mixed erosion and deposition. The region of the mounds both show up as highly depositional although the collapsed SE flank of the southerly mound is presently erosional indicating downslope movement of sediment into deeper water.

The most profound seabed expression of the mining activities is the zone of smoothed seabed extending NE from the mounds into about 800m. This area of smoothed seabed is interpreted as the result of DSTP and waste rock disposal from barges. Of note in this area are the possible hydrothermal vents located 2km from the distal edge of the dumping zone.

The acoustic seabed survey of 2005 determined that mine derived tailings comprise 10.3% (approximately 60km^2) of the total survey region (Lihir Gold, 2005).

3.2.4 Benthos

There is relatively little published information on the deep-sea benthos of the western tropical Pacific (the Solomon and Coral Seas), and very little work has been done in the Lihir region. Shirayama (1984 a,b) sampled the deep-sea meiofauna at a range of depths in the western Pacific, with three stations located on the Solomon Rise to the north-east of the Lihir island group. These studies provide some baseline data on standing stocks of metazoan meiofauna and macrofauna in the region of interest, but none on the larger benthic animals (megafauna).

The Lihir island group lies within the *Western Pacific Archipelago Deep Basins* biogeochemical province defined by Longhurst *et al*.,(1995). Planktonic primary production in this area is estimated as ~ 100 g C m^{-2} year^{-1}, a relatively low Figure by global standards. The oligotrophic ocean environment around Lihir will be reflected in a low rate of flux of sinking organic matter to the deep-sea bed, although some additional input will be provided by terrestrial plant detritus. With the localized exceptions of hydrothermal vent and cold seep ecosystems, the deep-sea benthos is reliant on the supply of organic matter from surface waters and consequently benthic standing stock (abundance and biomass) typically declines with increasing water depth (Gage and Tyler, 1991). The gradient of the depth-biomass relationship varies according to body size, with numbers of larger animals declining more rapidly than smaller ones (Rex *et al*., 2006). Because of the limited organic input, the deep sea around Lihir would be expected to support a lower benthic standing stock than is found at comparable depths in more productive ocean regions such as the north-east Atlantic, with the contrast being most pronounced for megafauna and least for the smallest size classes of organisms.

Comparison of meiofaunal or macrofaunal densities recorded in different studies must be made with caution since results can be biased by sampling technique (Bett *et al*., 1994) and by the use of different sieve mesh sizes to define faunal categories (Gage *et al*., 2002). It is often not possible to make post-hoc 'corrections' for these confounding factors in the summary data presented by authors in their published work. With this caveat in mind, table 3.2.4.1 summarizes Shirayama's (1984a) data on densities of metazoan meiofauna and macrofauna at three deep-sea stations on the Solomon Rise. Values for the same depths predicted from empirical relationships based on global data compilations (Rex *et al*., 2006) are also shown for comparative purposes.

Table 3.2.4.1 Densities of metazoan meiofauna at three deep-se station on the Solomon Rise (Shirayama, 1984a) together with predictions from an empiricajl model (Rex *et al*., 2006).

Depth m	Meiofaunal density ind. 10 cm^{-2}	Rex et al.,(2006) prediction	Macrofaunal density ind. m^{-2}	Rex et al.,(2006) prediction
2090	434	318	1466	916
2230	552	311	1067	837
3600	138	251	100	346

Observed meiofaunal and macrofaunal densities are fairly consistent with the global bathymetric trend described by Rex *et al*.,(2006). Nematodes were the most abundant metazoan taxon, accounting for up to 80% of meiofaunal numbers at Shirayama's (1984a) stations. Shirayama (1984b) found the meiofauna to be heavily concentrated in the uppermost few centimetres of the sediment column, as would be expected in a food-limited deep-sea environment. Shirayama (1984a) listed values for total density and biomass of macrofauna at his stations (from single, unreplicated samples), but gave no details of community composition. As a result there is no published information on functional group composition, family or species-level diversity of the deep-sea macrofauna in the region.

Published information on the deep-sea megafauna around Lihir is confined to studies of hydrothermal vent fauna on Edison Seamount, a small volcanic cone on the southern flank of Lihir Island (Southward *et al*., 2002; Stecher *et al*., 2003; Tunnicliffe and Southward, 2004). These specialized chemosynthesis-based communities occupy a very different environment to the areas surveyed in this study and will not be considered further here.

3.2.5 Pelagic ecosystem

The main ecological concerns regarding disposal of mine waste into the marine environment are: (1) the potential uptake of bioavailable trace metals into the tissues of marine organisms, (2) bio-accumulation of these metal through food webs and into humans, (3) potential reduction in biodiversity and abundance of marine communities (Brewer *et al*.,2007). Most studies of these effects have focused on benthic communities and relatively little information is available on the

impacts of DSTP on pelagic communities, even though components of these communities (especially fish) are likely to be eaten by humans (Brewer *et al.*,2007).

Marine pelagic communities comprise the following functional groups of organisms: the phytoplankton (plants), bacterioplankton (bacteria), protozooplankton (herbivores and bacterivores), metazoan zooplankton (herbivores and carnivores), fish (herbivores and carnivores) and other higher predators including molluscs (squid), reptiles (turtles) and mammals (whales and dophins). Little information is available on the effects of DSTP on most of these groups except fish; however, a range of impacts can be anticipated. Impacts on phytoplankton may derive from enhanced heavy metals concentrations or from altered levels of photosynthetically available radiation and inorganic nutrient concentrations; however to our knowledge only one study, undertaken in temperate waters, has investigated effects of DSTP on phytoplankton primary production (Kessler 1986). Impacts on heterotrophic pelagic organisms are likely to derive from altered system productivity and bio-accumulation of heavy metals. The latter have been investigated in fish from tropical environments including studies from coastal waters of Papua New Guinea offshore from Lihir Island Group (Brewer *et al.*,2007) and Bougainville Island (Powell and Powell 2001) which observed little DSTP derived bio-accumulaton of heavy metals. It should be noted that the effects of DSTP on pelagic organisms may be relatively more difficult to discern in low productivity (i.e. oligotrophic) tropical environments due to potentially slower organism/community/ecosystem response.

3.3.1 Cruise summary

The purpose of the field work at Lihir was to collect physical oceanographic, sedimentological, geochemical, plankton/nekton and benthic biological samples and data with the specific objectives of assessing the quality of existing data and filling in gaps in knowledge to provide a better understanding of the impact of DSTP on the marine environment.

The cruise took place from 4th to 25th November 31st 2007 using the MV Miss Rankin equipped with a winch and crane supplied by Lihir Gold Limited.

The sampling at Lihir included the collection of 105 sediment cores for chemical and biological analysis from 8 stations. At 5 stations sediment cores were processed to extract pore-water which was collected to provide samples for nutrient and metal analysis. Water column sampling included 14 CTD casts, collection of 68 suspended particulate material samples from 7 stations and completion of 36 zooplankton (day and night) casts at 2 stations. In addition the water column

was sampled to provide nutrient, chlorophyll and salinity samples for calibration of the CTD sensors.

Seabed images were taken at a station known to be impacted by tailings and one that was believed to be non-impacted. The images were obtained using a Bed-hop camera which was deployed at stations L1 and L4.

3.3.2 Bathymetry and Acoustic Character

Seabed surveys were conducted using the Mk III Echotrack dual frequency (12 and 24 kHz) echo-sounder. The system was used in single frequency (12 kHz) mode from a pole mounted transducer from the starboard aft side. The analogue sounder had a thermal paper trace.

All stations were subject to a brief echo-sounder survey to enable the corer to be safely deployed in a known water depth. Also obtained were longer echo-sounder profiles used to develop a working model of the sedimentary setting of the margin and the seabed morphology. Typically these profiles were up to 10 km long and run either perpendicular or parallel to the slope

3.3.3 Physical Oceanography

CTD profiling

CTD data were collected using a Seabird SBE19*plus* equipped with a carousel of twelve 5-litre bottles and with sensors for light transmission, oxygen, chlorophyll, pressure, conductivity and temperature. Typically the instrument was deployed to a depth of 5 m and then switched on allowing the pump to the sensors to prime. Once the pump was activated the instrument was raised to just below the water surface and the data acquisition commenced. The rate of descent was kept to 0.5 m s^{-1} for the first 100 m and then approximately 0.75 m s^{-1} until close to the bottom. In general the descent was halted about 20m from the bed. Bottles were fired on the up-cast at depths determined by the display of sensor data indicating water-column features of interest. A total of 8 full depth CTD profiles were collected at Lihir at station locations given in table 3.3.3.1.

Table 3.3.3.1. CTD station summary at Lihir, 2007.

Sta.	Date	Latitude (S)		Longitude (E)		Depth	Conditions
		(°)	(min)	(°)	(min)	(m)	
L1	19 Nov	3	06.20	152	40.54	850	Confused sea
L2	22 Nov	3	07.00	152	46.37	1750	Large swell
L3	19 Nov	3	06.64	152	49.79	2020	Poor weather
L4	24 Nov	3	08.26	152	30.88	800	Improved weather
L5	25 Nov	3	00.36	152	26.07	1715	Improving weather
L6	25 Nov	2	56.90	152	22.27	2020	Improving weather
L7	20 Nov	3	06.89	152	39.36	300	Windy, swell
L8	20 Nov	2	57.68	152	40.88	600	Sheltered from swell

Salinity sample collection and calibration

Salinity samples were taken from the CTD at different depths within a cast. The depths were chosen to reflect different salinity values as indicated by the salinity sensor. The water samples were placed into calibrated, numbered glass bottles. Each bottle was rinsed 5 times with water from the CTD bottle before finally filling to the top with water. The bottles were then sealed and stored for return to the laboratory for analysis. Subsequently (back at SAMS) the CTD data were calibrated, validated, despiked and reformatted at 1 m intervals, see Figure 3.3.3.1
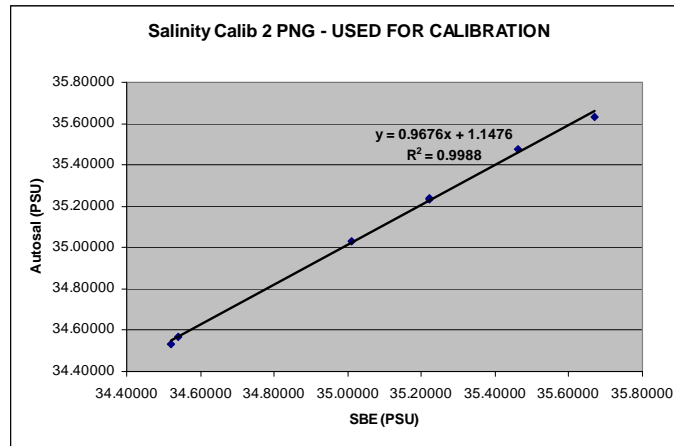
Figure 3.3.3.1. The calibration curve used for correcting salinity observations.

Oxygen calibration

The CTD oxygen sensor was calibrated at station L2 (event 87) using quintuplet analyses of standard followed by quintuplet analysis of water from 3 water depths of apparently significantly different oxygen concentration (Figure 3.3.3.2). Samples were drawn from the CTD bottles (one bottle per depth) directly into oxygen sample bottles of known volume using a silicon tube after excluding all bubbles. Samples were immediately fixed by the addition of manganese sulphate and alkaline iodide and then stored under water in an air conditioned room prior to analysis. Analysis was carried out using the standard Winkler method using an auto-titrator with potentiometric endpoint detection. The thiosulphate secondary standard was titrated against an iodate primary standard.
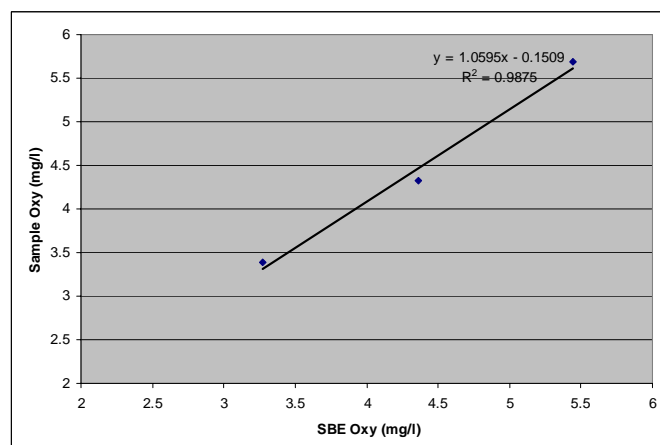
Figure 3.3.3.2. The calibration curve used for correcting oxygen observations.

3.3.4 Stations selected
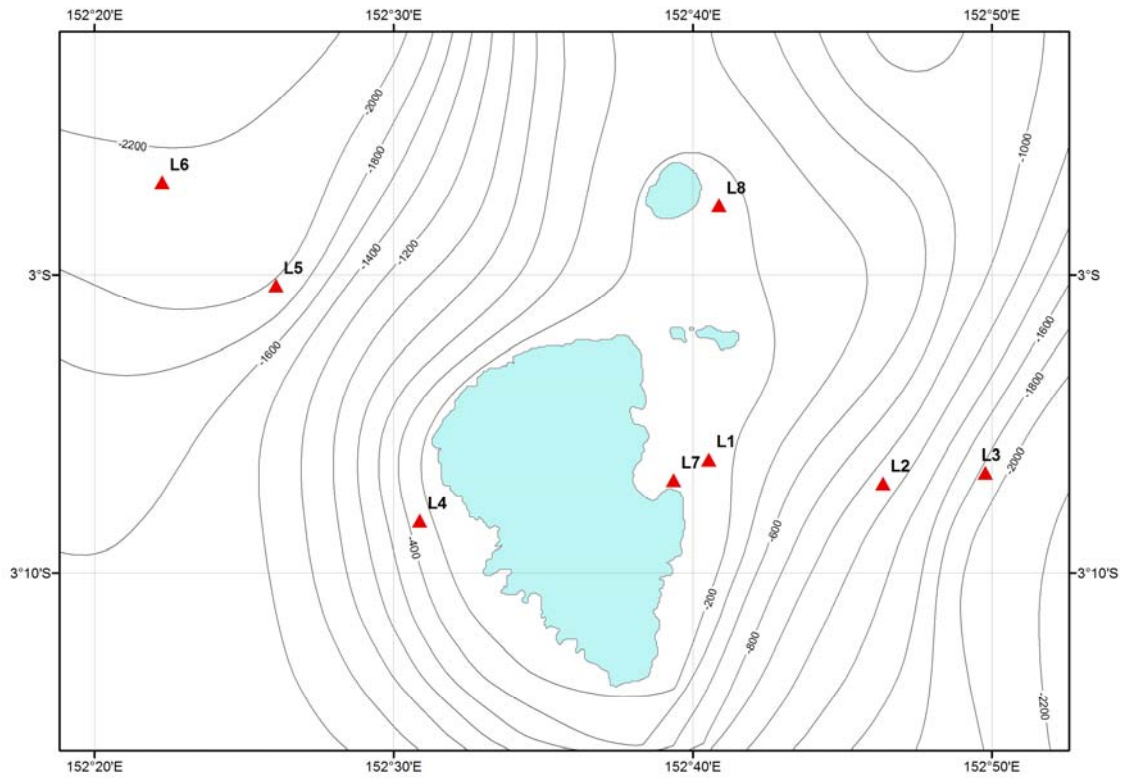
Figure 3.3.4.1 Chart of station positions at Lihir

Table 3.3.4.1 Station positions (conversion from WGS84 to AGD84 by Geocentric Translation (tx=134, ty=48,tz=-149) and depths (m).

Stn	WGS84		WGS84		Depth	AGD84 UTM56	
	Latitude deg	mins	Longitude deg	mins		Easting	Northing
L1	3	6.200	152	40.540	850	463858	9656824
L2	3	7.000	152	46.370	1750	474655	9655353
L3	3	6.640	152	49.790	2020	480988	9656018
L4	3	8.260	152	30.880	800	445970	9653022
L5	3	0.360	152	26.070	1715	437054	9667572
L6	2	56.901	152	22.266	2020	430005	9673941

Stn	WGS84 Latitude deg	mins	WGS84 Longitude deg	mins	Depth	AGD84 UTM56 Easting	Northing
L7	3	6.890	152	39.360	300	461673	9655552
L8	2	57.680	152	40.880	600	464483	9672521

All gear deployments were at the nominal station position. Station keeping was generally very good and always within 100m of the nominal station.

Table 3.4.3.2 Bedhop camera deployments

Station	L1	L4
Depth m	850	800
No. seabed contacts	25	25
Position, initial seabed contact	03^0 06.21' S 152^0 40.63' E	03^0 08.28' S 152^0 30.94' E
Position, final seabed contact	03^0 06.05' S 152^0 40.35' E	03^0 08.26' S 152^0 30.88' E
Results	25 seabed images	25 seabed images

3.3.5 Sediment sampling and sedimentology

All coring was carried out using the SAMS megacorer using the same methods given in section 2.3.5.

3.3.6 Sediment geochemistry

Sample collection and processing methods were identical to those described for the Basamuk study in section 2.3.6.

3.3.7 Water column geochemistry

Sample collection and processing methods were identical to those described for the Basamuk study in section 2.3.7.

3.3.8 Benthos

Sample collection and processing methods were identical to those described for the Basamuk study in section 2.3.8.

3.3.9 Seabed photography

Seabed photographs were taken using the "bed-hop" camera system as described in section 2.3.9. Successful deployments were made at stations L1 and L4. A third deployment was aborted as a result of heavy swell which made it difficult to detect contact with the seabed.

3.3.10 Zooplankton

See section 2.3.10 for sample collection and processing methods.

3.3.11 Microplankton

Microplankton samples were collected from 3 depths (10, 70, 150m) at 2 stations (L6 and L8). Water samples were collected during daylight hours by Niskin bottle, and 400 ml preserved with 1% final concentration formaldehyde. Analysis was as described in section 2.3.11.

3.4 Results

3.4.1 Bathymetry and Acoustic Character

The bathymetry of Lihir has been well-documented in previous studies, as outlined above (3.2.3), notably through the use of multibeam bathymetric sonar. The volcanic cone of Lihir Island is constantly undergoing submarine mass-wasting through debris flows, slides, turbidites and other associated gravitationally-induced sediment failures. These natural processes occur all around the margins of the island on the steep submarine slopes. The 2007 echo-sounder profiles illustrate these processes in and around the mine at Lihir. The seabed is typically smoothed but irregular, deeply incised by channels, 20-60m deep and up to 200m wide, radiating out from the island (Figure 3.4.1.1). The acoustic character is dominated by a persistent seafloor echo with little sub-bottom penetration. The only location where some sub-bottom geometry was noted is directly east of Luise Harbour in the vicinity of the tailings' discharge pipeline. Here in water depths of 800-1200m acoustically irregular to transparent clinoforms 50-150m long and up to 30m thick occur. Diffuse and hyperbolic reflectors were also observed, mostly confined to the flanks of the

slope and in channels. Farther offshore the seabed becomes more reflective, rougher and highly irregular.
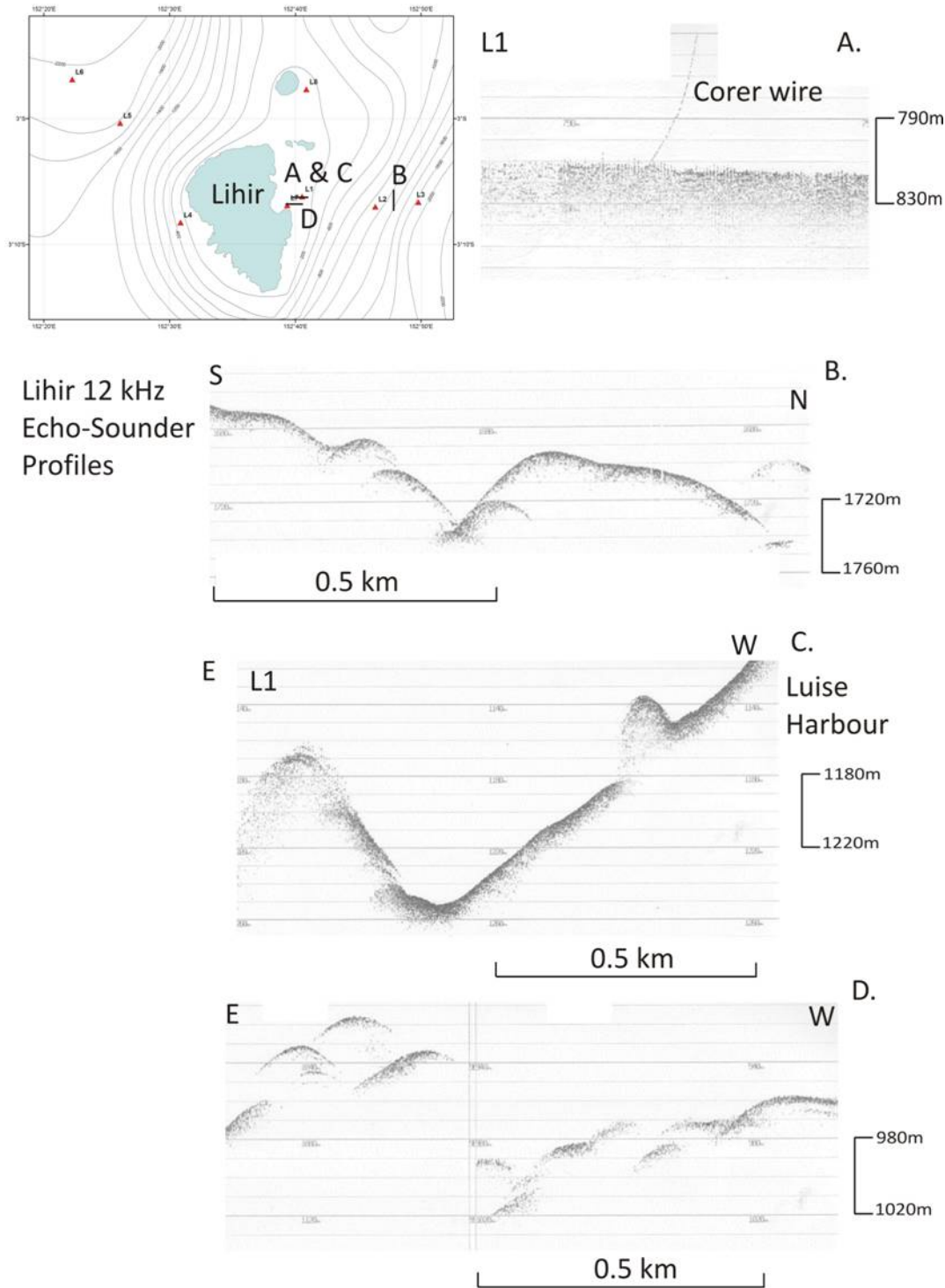
Figure 3.4.1.1 Examples of echo-sounder profiles, Lihir Island.

3.4.2 Physical Oceanography

Temperature (θ) and salinity (S)

At the time of the investigations at Lihir (and Misima) the Australian Bureau of Meteorology Southern Oscillation Index was positive (9.8) and increasing. This indicates that the Equatorial Pacific was in a La Nina cycle and should exhibit strong easterly trades forcing warm surface water westwards along the Equator towards the Bismarck Archipelago. However, La Nina conditions are not entirely reflected in the meteorological and sea surface conditions measured at the nearest functioning TAO/TRITTON buoy (2S156E) located at 156° E, 2° S, about 350 km ENE of Lihir (Figure 3.4.2.1).

Until 20 Nov the winds tended to blow from a south westerly direction and only after that did the SE Trade winds (mean speed ~6 m s^{-1}) appear although the wind direction had again turned SW by the 2nd week of December. Sea surface temperature was close to the winter mean, ranging between 29.4 and 30.2 °C, with the air temperature slightly cooler (between 26.5 and 29.5 °C).
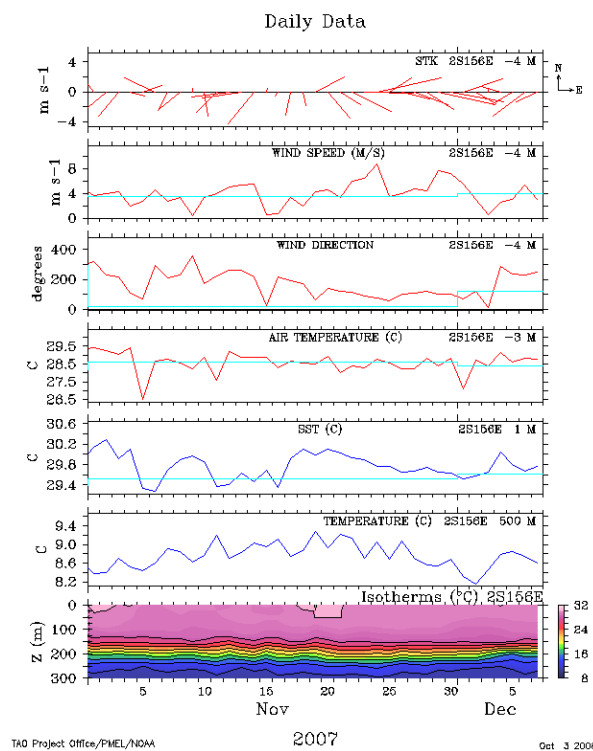
Figure 3.4.2.1.   Meteorological and surface oceanographic conditions at buoy 2S156E (for position see Figure 3.2.2.1). Source: http://www.pmel.noaa.gov/tao/jsdisplay/

Deep water

Below about 300 m (S = 35; θ = 12.5 °C) all CTD profiles reveal a very stable picture of the deeper waters of the central Pacific Ocean (see e.g. Figs 3.4.2.1 and 3.4.2.2). Temperature and salinity both decrease with depth along a TS curve that corresponds to Western South Pacific Central Water (WSPCW, S = 34.50; θ = 6.0 °C to S = 35.80; θ = 22.0° C, (Emery and Meincke, 1986)). A salinity minimum of about 34.55 is encountered at about 800 m, which can be attributed to the presence of Antarctic Intermediate Water (AAIW, which has temperatures ranging from 2 to 10° C, and salinities from 33.8 to 34.8). Below that salinity increases and temperature decreases as the presence of Circumpolar Deep Water (CDW, S = 34.62 to 34.73, θ = 0.1 to 2.0°C) becomes ever more apparent. The presence of AAIW and CDW, which have their origins at high latitudes to the south, indicates that these water masses (i.e. below 800 m) must be moving northward past Lihir.
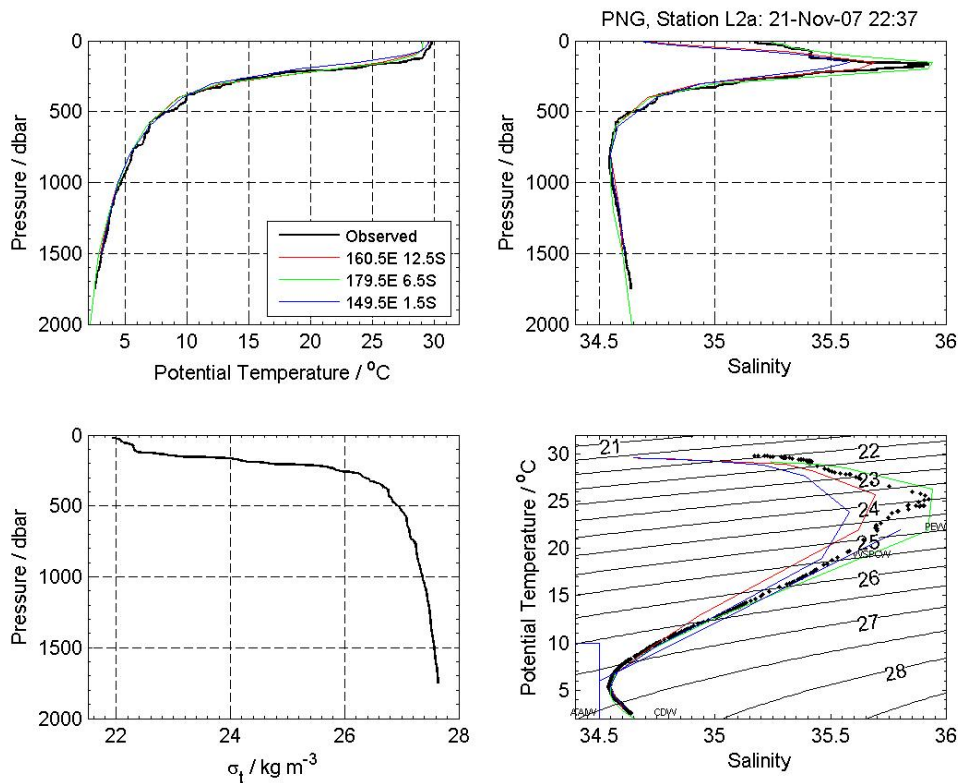
Figure 3.4.2.1. Temperature, salinity and σ_θ profiles; and θS plot at Sta. L2 with the water masses identified. Water masses are indicated on the θS plot. The red green and blue lines show climatological profiles at the locations in the vicinity of Lihir as indicated (http://ferret.wrc.noaa.gov/las/servlets/dataset)
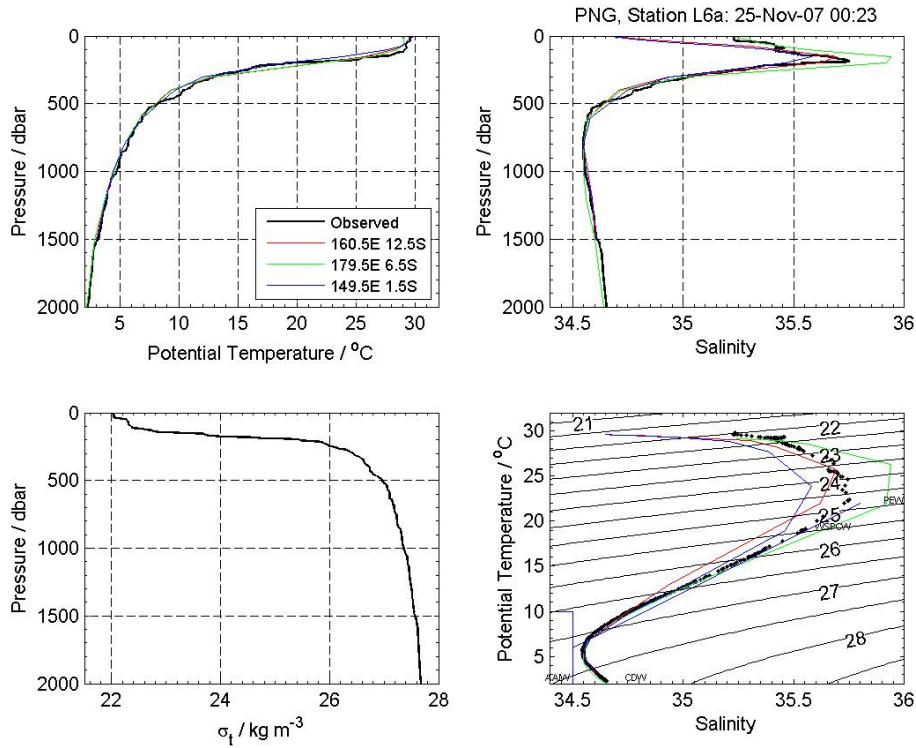
Figure 3.4.2.2. Temperature, salinity and σ_θ profiles; and θS plot at Sta. L6. See caption to Figure 3.4.2.1.
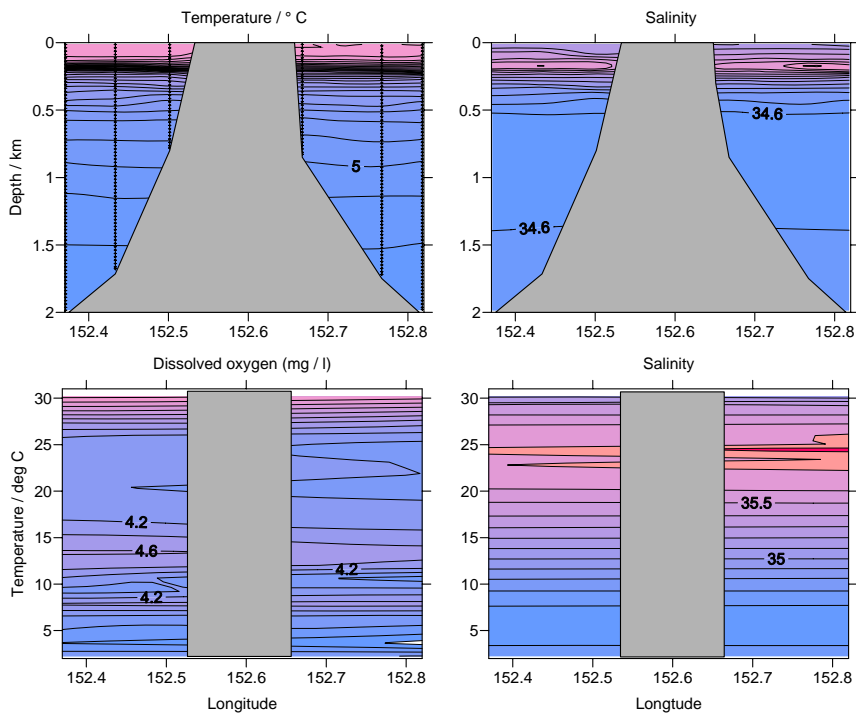
Figure 3.4.2.3. EW sections through Lihir from Sta. L6 to Sta. L3, through Stas L5, L4, L7, L1 and L2. Upper panels - temperature and salinity against depth. Lower panels - dissolved oxygen and salinity against temperature.

Intermediate water

Above 300 m lies water that has had more recent contact with the atmosphere. The highest salinities ($S \sim 35.7$) are encountered at about 180 m depth which is undoubtedly due to the influence of high salinity Pacific Equatorial Water (PEW, the lightest of which has $S = 36$; $\theta = 20°$ C, (Emery and Meincke, 1986). Temperature and salinity profiles from both sides of Lihir (Figs 3.4.2.1 and 3.4.2.2) and an EW section through the island (Figure 3.4.2.3), show quite clearly that PEW is more strongly present on the eastern side. These high salinities are also associated with low oxygen levels (3.8 mg L^{-1}). The fact that the θS plots at this depth change so greatly is a clear indication of the movement of different water masses at this level. The θS plots of Stations L2 and L6 (Figs 3.4.2.1 and 3.4.2.2) show how much closer to PEW is the water to the east of the island than the equivalent water to the west. Furthermore it is evident at both stations, but particularly Station L6, that the intermediate water there has a θS characteristic that is nearer to the climatology to the south, at 160.5° E, 12.5° S, than to the east, at 149.5° E, 1.5 S. This suggests that Lihir is located in a region where salty PEW from the east meets WSPCW from the south.

A small caveat to this description is that the θS plots at Stations L1 and L8 close to the eastern and northern sides of Lihir (Appendix 2A) indicate a stronger presence of 160.5° E, 12.5° S water than 8 km to the west at Station L2. Thus there may have been a front, or the boundary of an eddy, somewhere between Stations L1 and L2 during the cruise.

Surface water

The surface waters on both sides of the island have similar θS characteristics to the climatology at 179.5 °E, 6.5 °C in the central equatorial Pacific, than to the local climatology at 149.5 °E, 1.5 °S (see Figs 3.4.2.1 and 3.4.2.2). The observations are thus consistent with La Nina conditions and confirm the impression given by the θS plots of PEW migrating from the east at intermediate waters.

Other CTD parameters

Fluorescence

The fluorescence data are uncalibrated, and hence fluorescence levels can not be differentiated from bio-chemical (i.e. natural phytoplankton) sources or physio-chemical (in this context, largely due to deep sea tailings) sources. At nearly all stations below the photic zone (~ 200 m) fluorescent levels are at background voltages (typically 0.055 v). However at Sta. L1, just west of

the outfall, is a significant exception to this rule with maximum fluorescence levels of up to 0.18 v at a depth of 90 m. Equally significant is the fact that fluorescence levels remain close to 0.1 v throughout the rest of the water column down to 800 m (i.e. to depths well below photic zone), which indicates an anthropogenic source.

A surface plot of fluorescence levels at 90 m around Lihir (Figure 3.4.2.4) shows that such high fluorescence levels are only found on the eastern side of the island. Although Figure 3.4.2.5 is drawn from only a small number of stations, mainly along the section shown in Figure 3.4.2.3, the data shown in Figure 3.4.2.4 support evidence from elsewhere that the transport of this fluorescent peak is northward.
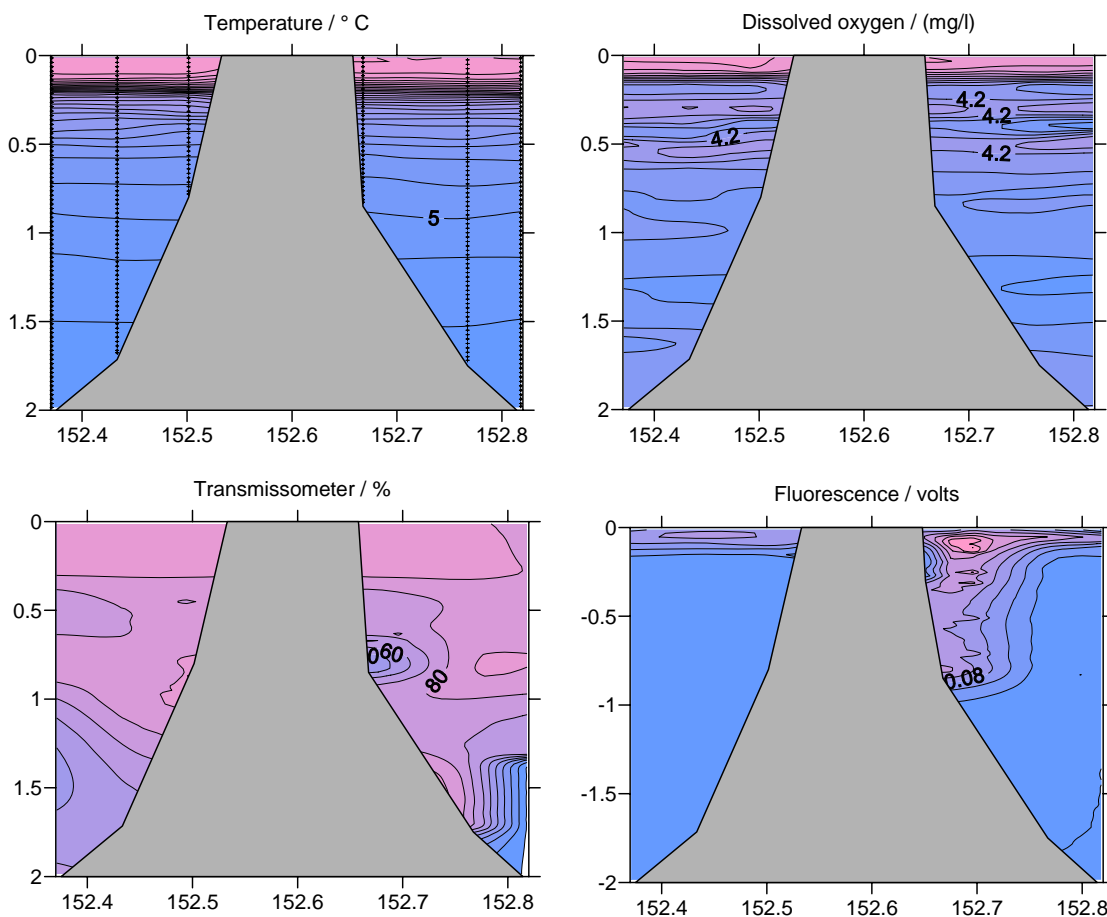
Figure 3.4.2.4. Temperature, dissolved oxygen, transmission and fluorescence sections through Lihir from Sta. L6 to Sta. L3.

Fluoresence (mg l^{-1}) at 90 m depth

Minimum transmission
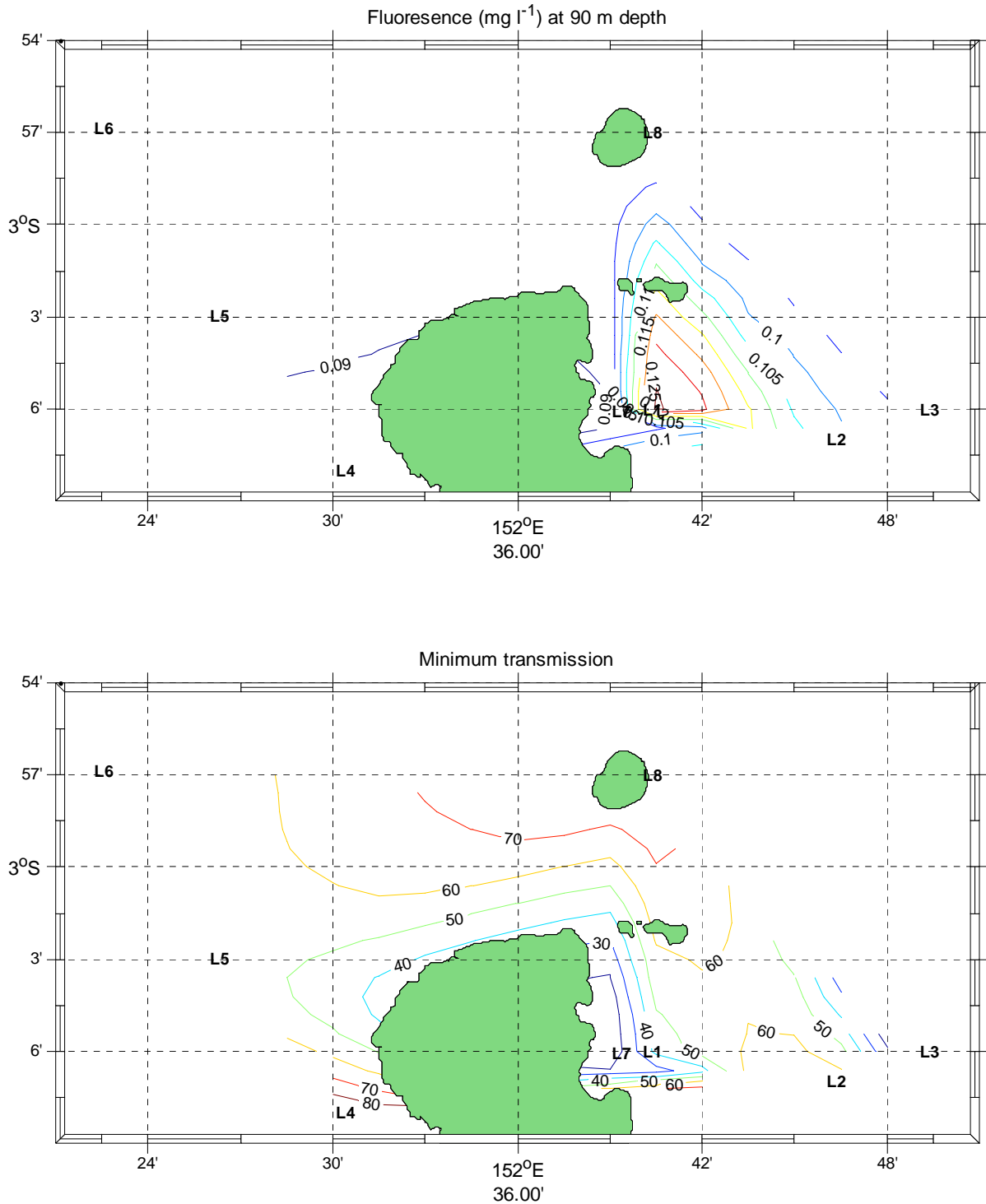
Figure 3.4.2.5. Upper panel: fluorescence levels at the depth of highest concentration at 90 m depth. Lower panel: Minimum transmission levels (% age) in the water column. There is evidence of enhanced fluorescence and suspended material in the water column on the east side of the island

Beam transmission

Beam transmission is a measure of the opaqueness of the water so low values indicate high turbidity. Although an obvious source of turbidity is mine tailings, natural sources are also likely, particularly near the sea bed where currents raise material into the water column. Calibration of the transmission data are unusual, because the data are very sensitive to local sources, and has not been undertaken here.

On the eastern side of the island beam transmission levels are lowest in the region - about 20% at a depth of 800 m at Sta. L1 (Figure 3.4.2.4). Elsewhere the lowest levels are generally found near the seabed, and these values are presented as a surface plot in Figure 3.4.2.5. The plot indicates that the lowest transmission levels are around the edge of Lihir. It is likely that, apart from the low levels along the east coast, most of this enhancement is due to increased bed stresses around the island margin, possibly due to tidal currents. The low levels near the harbour are almost certainly due to a combination of barge dumping and surface runoff from the shore based operations.

Dissolved oxygen (DO)

It was noted above that low DO levels at 200 m were associated with high salinity PEW pushing in from the east at intermediate depths (Figs 3.4.2.1, 3.4.2.2 and 3.4.2.3). At deeper depths there appears to be a DO maxima coincident with temperatures of 13 °C and 8 °C (Figure 3.4.2.3). The colder maximum occurs close to the deep minimum salinity and is probably associated with the formation of AAIW.

There appears little difference between the east and west sides of Lihir (Figure 3.4.2.6) with the exception of the ammonium concentrations which are noticeably higher on the eastern side. Ammonium concentrations tend to increase in surface waters due to zooplankton grazing of phytoplankton. The higher values of ammonium seen in mid and deeper waters on the east are just as likely to be due to analytical noise as to be real. The higher nutrient levels at Sta. L1 could suggest that the higher fluorescence levels observed on that side may have nothing to do with the mine discharge.
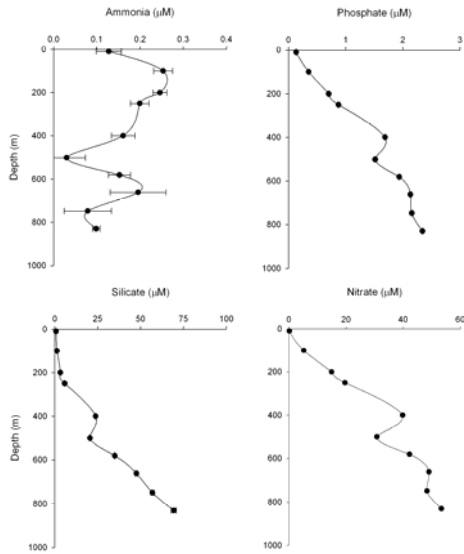
Figure 1: Water column nutrient concentration at Station L1
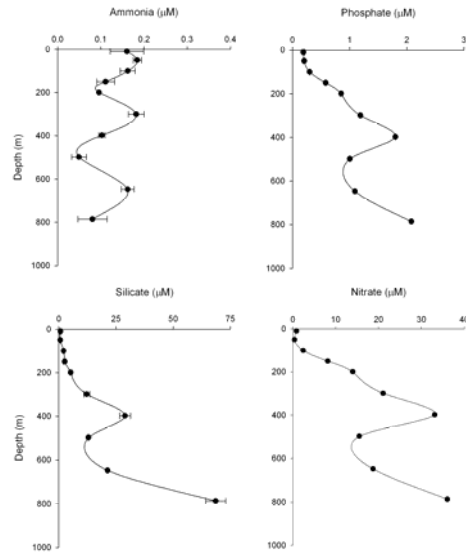
Figure 4: Water column nutrient concentration at Station L4

Figure 3.4.2.6 Nutrient levels at Sta. L1, to the east of Lihir, and L4 to the west.

There were also higher levels of nitrate and silicate in the mid and deep waters (>1000m) on the east side of the island with values exceeding 100 micromole for silica and 40 micromole for nitrate, which is due to the natural increase in nutrients in waters of Antarctic origin.

3.4.3 Stations selected

Stations for the main benthic and geochemical research were selected in order to conduct a control-impact study where likely impacted stations were matched in terms of depth with stations that were unlikely to have been affected by the mine DSTP (Figure 3.3.4.1). Stations L1, L2 and L3 were predicted to be impacted and this was shown to be the case by visual observation and subsequent analysis. Stations L4, L5 and L6 were chosen as the control (more properly: reference) stations and the predictions of low impact were supported by visual evidence and subsequent analysis. Staion L8 was chosen as a more accessible control station than L4 to conduct day and night zooplankton sampling paired with the L1 impacted station. Finally, station L7 was added mainly to collect high density suspended particulate material (SPM) data in order to both aid interpretation of other SPM data collected and to provide information on SPM densities near the DSTP outfall.

3.4.4 Sediment sampling and sedimentology

Core log sheets and particle size summary data tables are shown in Appendix 1.

Lihir Impacted Stations L1-L3

Station L1. East of Luise Harbour, 850m water depth. Sediments recovered from L1 were dominated by well-sorted brown and orange muddy sands. Two principal sediment units were present. An upper unit of <5 cm thick consisting of watery orange-coloured, poorly sorted fine-grained mud. This unit has a mean grain size of 34-41 µm (medium-coarse silt). Below the fine, orange mud, and across a sharp contact, occurs a thin (<1 cm) very well-sorted coarse sand layer, with mean grain sizes of >463 µm. Below 4 cm below sea floor the sediment consists of moderately well-sorted brown and orange, muddy sands with a mean grain size of between 85-263 µm (fine-medium sand). The sand content of the upper unit of orange mud is very low, <20%, below the orange mud the sand increase to >50%.

Station L2. Eastern Lihir, 1753m water depth. The sediments recovered from L2 consist of two sediment units. An upper 5 cm thick unit of poorly sorted fine-grained orange mud and a lower unit below 5 cm sediment depth of finely laminated sandy mud. The upper unit of orange mud has a mean grain size of between 15-27 µm (medium silt). The lower finely laminated brown and orange sandy mud has a mean grain size range of 19-218 µm (medium silt-medium sand). Sand contents in both units are highly variable between 2-11% in the upper orange mud to 4-62% in the sandy mud. The silt and sand composition is predominantly sub-angular quartz and pyrite grains.

Station L3. Eastern Lihir, 2020m water depth. As with the previous shallower two stations, L3 produced two distinct sediment units; an upper 3 cm thick unit of poorly sorted fine-grained orange mud and a lower unit of brown and orange sandy mud. These two units are separated by a 3 cm thin layer of very well sorted medium to coarse sands with sharp upper and lower contacts. The upper orange mud has a mean grain size of 21-46 µm (medium silt). The very well sorted sand layer has a mean grain size range of 113-228 µm (medium to coarse sand). Sand content is highly variable between the units, from <5% in the orange mud to up to 85% in the sand layer.

Lihir Control Stations L4-L6

Station L4. Western Lihir, 800m water depth. Sediments on the western margins of Lihir from L4 consist of homogenous shelly-rich muddy sands. The moderately well-sorted muddy sands have a mean grain size range of between 80-227 µm (fine-medium sand). Sand content is high throughout at >47%.

Station L5. Northwestern Lihir, 1715m water depth. Station L5 showed moderately well-sorted, homogenous muddy sands. Mean grain sizes range between 58-250 µm (coarse silt to medium sand). Sand content varies from 30-65%

Station L6. Northwestern Lihir, 2025m water depth. The farthest offshore control from Lihir contained homogenous, bioturbated moderately well-sorted muddy sands. Mean grain sizes are between 62-219 µm (coarse silt to medium sand). Sand content is 25-54%.

3.4.5 Sediment geochemistry

The sediments and pore-waters from Lihir were analysed for major, minor and trace elements and the combined data were used to evaluate sediment composition and provenance, identify biogeochemical controls and assess any post depositional mobility of elements within the marine environment surrounding Lihir Island.

The depth profiles of elemental concentrations for 33 elements within the solid phase and 24 elements in the pore-water of sediments collected from Lihir are presented in Appendix 4B. Depth plots of elemental concentrations for each core are presented in Appendix 4A.

The primary objective of the study was to provide a multi-element geochemical data set that could be used to determine the natural sediment signature, identify the tailings signature and assess the impact of the tailings on the marine environment surrounding Lihir Island.

There are no published papers on the geochemical composition of sediments surrounding Lihir and the only other data available are from an environmental baseline survey and post commissioning surveys initiated by Lihir Gold Ltd. The data are of limited use as is discussed in Appendix 9.

Marine sediments can be broadly described as being a mixture of lithogenic material, biogenic carbonate and silicate and organic matter. Element/Aluminium (Al) ratios can be used to indicate changes in sediment composition that are not caused by lithogenic dilution.

For example, Silicon (Si)/Al, Titanium (Ti)/Al, Magnesium (Mg)/Al can all be used as a proxy for aeolian inputs, Zirconium (Zr)/Al for sediment texture and reworking. However, in the context of Lihir this technique is only useful within the natural sediments as the mine tailings will have other controls determining the elemental/Al ratios of the sediment.

The major elemental/Al ratios for the surface sediments are given in Table 3.4.5.1. The ratios for the surface sediment indicate that Ca/Al, K/Al, Mg/Al ratios in the surface sediment form the impacted stations (L1-L3) have very different ratios to that of the control stations. The Ba/Al ratios at the impacted stations are generally higher than the controls and the Sr/Al ratios are lower than the controls. There is no obvious difference between the Fe/Al and Ti/Al ratios of the surface sediments at all the stations.

Table 3.4.5.1 Elemental/Al ratios in surface sediments for stations L1-L6

Stn.	Ba/Al	Ca/Al	Fe/Al	K/Al	Mg/Al	Mn/Al	Sr/Al	Ti/Al
L1	0.019	0.122	0.953	0.759	0.139	0.015	0.0075	0.070
L2	0.018	0.126	0.458	0.386	0.157	0.008	0.0076	0.027
L3	0.024	0.211	0.966	0.609	0.136	0.017	0.0094	0.089
L4	0.024	3.155	0.959	0.160	0.234	0.018	0.0329	0.074
L5	0.009	3.662	0.625	0.213	0.213	0.021	0.0180	0.053
L6	0.090	3.662	0.625	0.213	0.213	0.021	0.0180	0.053

In order to assess the rate of accumulation of the sediments at each of the stations the activity of the naturally occurring radionuclide ^{210}Pb was measured using gamma spectroscopy. See section 2.4.5 for a discussion of this technique.

The sediment accumulation rates (g cm^{-2} yr^{-1}) and the average linear sedimentation rates (mm yr^{-1}) are given in Table 3.4.5.2 along with the organic carbon content (% wt) and excess ^{210}Pb inventories (Bq cm^{-2}).

Table 3.4.5.2 Organic carbon content, extent of mixing, accumulation rate and excess ^{210}Pb inventories for stations L1 – L6.

Station Lihir	Depth m	Organic C (%)	Degree of mixing	mass accum. rate g cm^{-2} yr^{-1}	linear sed rate mm yr^{-1}	Surface xs ^{210}Pb Bq kg^{-1}	xs^{210}Pb-inventory Bq cm^{-2}
L1	850	>0.1 - 0.6	highly mixed and diluted	NA	NA	5	0.01
L2	1750	>0.1 - 0.15	highly mixed some dilution	NA	NA	180	2.21
L3	2020	0.2 - 0.8	Bioirrigation/ mixing top 1 cm	0.27	0.2	360	0.51
L4	800	0.15 - 0.45	no obvious mixing, possible bioirrigation at 4.5 cm	0.08	0.6	420	0.89
L5	1715	0.25 - 0.5	possible small amount mixing	0.05	0.3	1020	1.61
L6	2020	0.16 – 0.84	no obvious mixing	0.12	1.0	1100	2.15

The major element composition is shown in Figure 3.4.5.1. Stations L1-L3 are the stations on a transect moving eastward away from the mine and stations L4-L6 are on the westward side of the island and are assumed to be control stations.
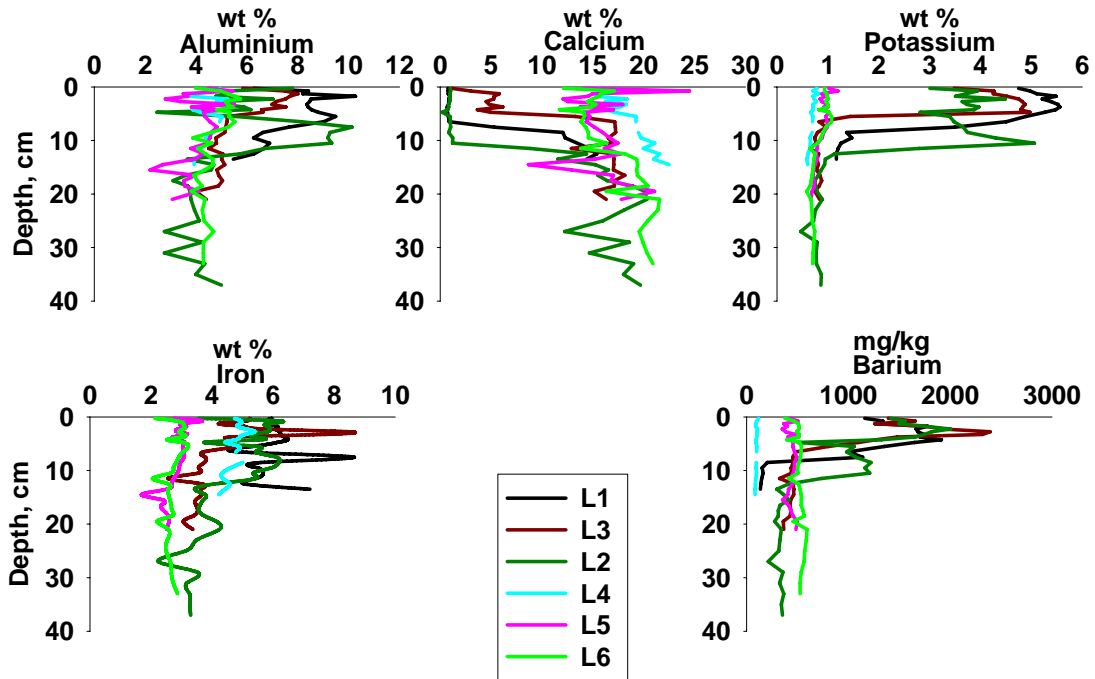
Figure 3.4.5.1 Major and minor elemental concentrations within sediment, L1-L6.

The concentrations of aluminium (Al), potassium (K), iron (Fe) and barium (Ba) are all higher within the top 5-10 cm of the impacted stations (L1-L3) when compared to the control stations (L4-L6). In contrast, calcium (Ca) concentrations are much lower in the impacted stations compared to that of the control stations.

Concentrations of the elements are all similar at depth indicating that the mine tailings slurry has at least twice the concentration of Al, four times the concentration of K, twice the concentration of Fe, three to five times the concentration of Ba and twelve to fifteen times lower concentration of Ca than the natural sediments of the area.

The concentrations of the minor and trace elements also vary between the impacted and control stations.

Table 3.4.5.3 indicates which elemental concentrations increase in the sediments from impacted stations compared to those of the control stations. Ca is the only element that shows a substantial decrease in concentration at the impacted stations in contrast to 21 elements which show an increase in concentration.

Table 3.4.5.3 Elemental concentrations of impacted stations (L1-L3) relative to control stations (L4-L6). Red signifies increase in concentration, blue a decrease in concentration and blank no discernible change in concentration.

Element		Element		Element		Element	
Ag		Cd	Red	K	Red	Rb	Red
Al	Red	Ce	Red	Li	Red	Sr	
As	Red	Co		Mg		Th	
Au		Cr	Red	Mn	Red	Ti	Red
B		Cs	Red	Mo	Red	Tl	Red
Ba	Red	Cu	Red	Na	Red	U	Red
Be	Red	Fe	Red	Ni		V	Red
Ca	Blue	Ga	Red	Pb	Red	Zn	Red

All elemental plots are given in Appendix 4A; however Figure 3.4.5.2 illustrates the differences between a number of elemental concentrations in sediments from the impacted station L2, 1750 m depth and L5, control station, 1715 m water depth. There are significant differences in concentrations of beryllium (Be), vanadium (V), copper (Cu), molybdenum (Mo) and Lead (Pb) between stations L2 and L5, with concentrations of all elements being higher at the impacted station, L2. However the concentrations of cobalt (Co) and nickel (Ni) are similar at both the impacted and control stations.
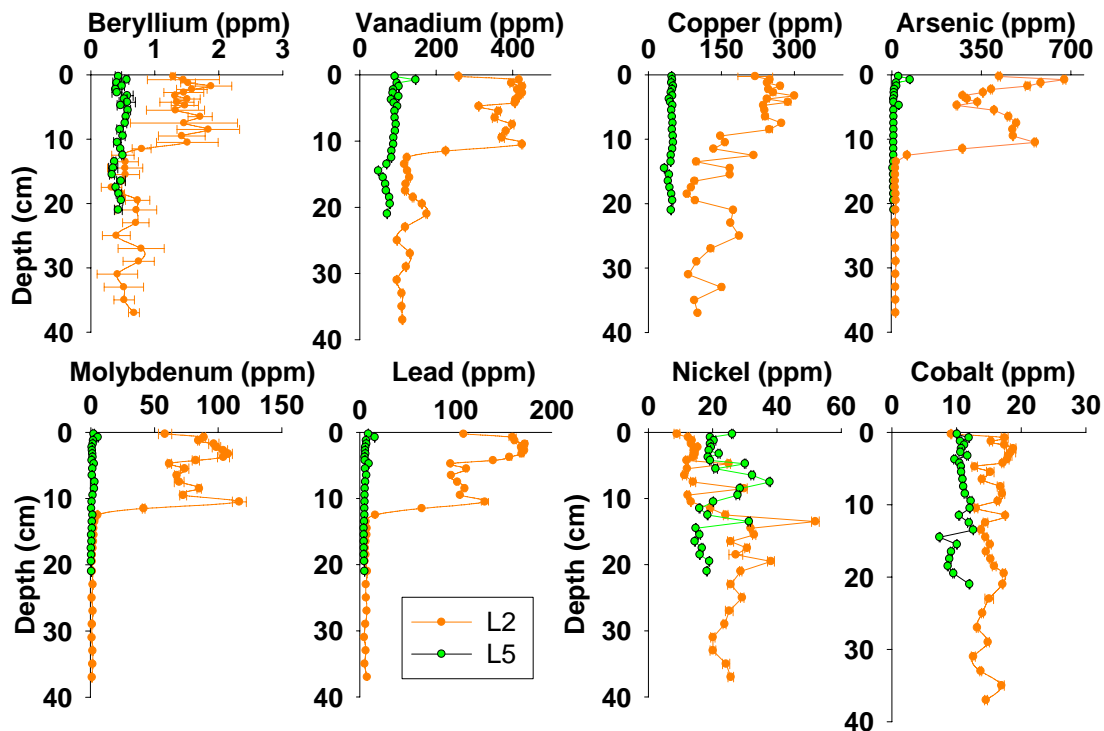
Figure 3.4.5.2 Minor and trace elemental concentrations within sediment, L2 (impacted, 1750 m) and L5 (control, 1715 m).

To investigate whether there is a statistical relationship of the elements with each other, Pearson Product Moment Correlation coefficients were calculated for sediment cores at each of the six stations. The pairs of elements that showed positive correlation coefficients above 0.7 and a P value below 0.05 were considered to increase together. For the pairs with negative correlation coefficients and P values below 0.050, one variable tends to decrease while the other increases.

The results of the Pearson Product Moment Correlation tests are given in Appendix 4B, tables 4B.201-209. The correlation coefficients were calculated on the complete data set for each core. In addition, for the impacted stations L1-L3, correlation coefficients were calculated for natural sediment that had not been impacted with tailings. The depth of tailings at each of the impacted stations was determined by observing the change in concentration of the major and minor elements.

The results of the Pearson Product Moment Correlation for station L1, considering the whole core to a depth of 14 cm, indicate that there are strong correlations amongst the majority of the metals with the exception of Co and Ni. There are a number of negative correlations between elements and Ca, Sr and organic carbon. It is interesting to note that Fe has no strong correlations; Mn only correlates strongly with Al, Ba and K and has a strong negative correlation with Ca.

The correlation coefficients for the natural sediment at L1 show a number of differences when compared to those calculated from the entire core. There are far less strong correlations between the metals and a larger number of negative correlations. Manganese indicates a strong correlation with Fe which was absent when considering the entire core, indicating that Fe and Mn have a strong association in the natural sediment which is missing when considering the impacted sediment. The organic carbon strongly correlates with Al, Mg, V, Cr and Co. In addition where the organic carbon had negative correlations with Al, Cu, Ga and Ce, these are all now positive and indicate that these vary together in the natural sediment, a relationship which is not apparent when considering the impacted sediment.

For station L2 the results for the whole core are similar with the notable exception that the organic carbon has strong positive correlations with Mg, Ti, V, Co and Ga and that some metals have a negative correlation with Ni.

The results for L2 below the depth of sediment impacted by tailings indicate less positive correlations between the metals and have less negative correlations than the natural sediment at station L1. In addition L2 has strong correlations between Pb , Cd and organic carbon in the natural sediment.

Station L3 has similar correlation coefficient results to that of L2 with a slightly lower number of positive correlations. When considering the non-impacted i.e. natural sediment there are a number of elements that vary differently in the natural sediment compared to the impacted sediment. These are As/Ba, U/Ba and V/Tl which all vary positively in the impacted sediment but have a negative correlation in the natural sediment. The reverse is true for K/Ca which has a negative correlation in the impacted sediment but a positive one in the natural sediment.

The control stations (L4-L6) were analysed using the entire core only as there was no evidence of tailings within these sediments. Of these stations L5 had the most positive correlations although this was still considerably less than any of the impacted stations. The only negative correlations at this station are with B /Ti and B/ Ga. Station L4 had considerably more negative correlations mainly with Ca and Sr and other elements. Finally station L6 had the least number of positive correlations and had negative correlations with K/Ca, Ce/Ca, Sr/Ce and Sr/Th.

To assess the impact of the tailings on stations L1-L3 the inventories of all elements for all cores L1-L6 were calculated and expressed as g/m^2 . The sediment cores collected at each station were different lengths and in order to compare the excess inventories of elements at all stations the depth range that the excess was calculated for was determined by the shortest length of core, in

this case this was station L1 at a depth of 14 cm. The total elemental inventories for cores at stations L1-L6 are given in Appendix 4B, tables 4B.189-200. Inventories have been calculated for complete cores as well as the top 14 cm at each station. The natural elemental baseline concentrations were calculated by using elemental concentrations of the deepest samples in the sediment cores.

The excess elemental inventories (g m^{-2}) for all stations are shown in Figure 3.4.5.3. The % excess elemental inventories are shown in Figure 3.4.5.4. Stations L1-L3 have significantly higher inventories of K, Ba, Rb, Pb, Tl, U, V, Zn, Cu and As than the control stations. They have higher inventories of Mo, Cd and Cs with the Be indicating that inventories are higher at the impacted stations than the control stations, however in this case the errors are greater. In contrast, Ca inventories indicate that there is a large deficit at stations L1-L3 ranging from -37% at L3 to -337% at L2. In most cases station L2 has either the largest excess or deficit of the three impacted stations.
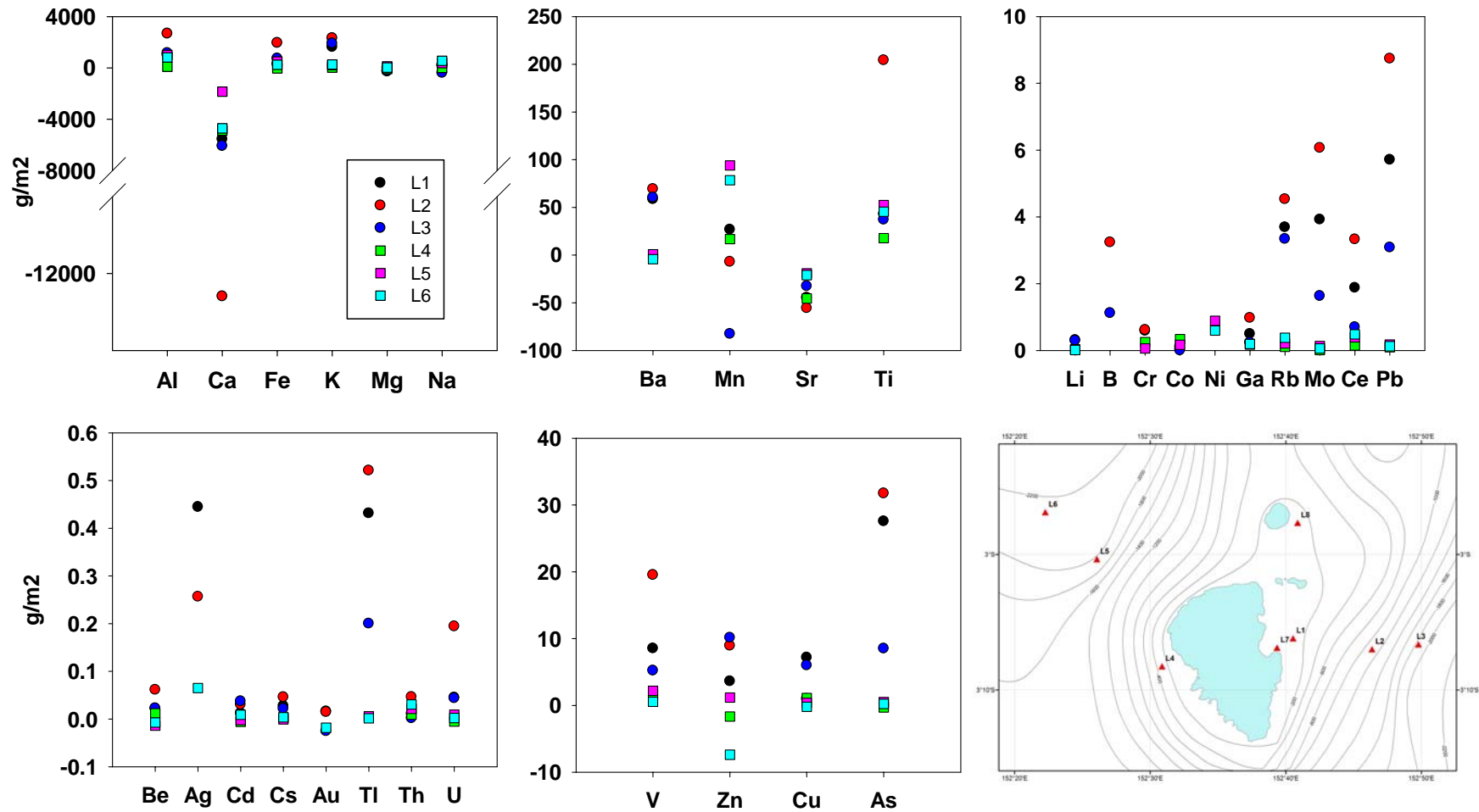
Figure 3.4.5.3 Excess inventory of elements (g m^{-2}) within the top 14 cm of Lihir station sediments

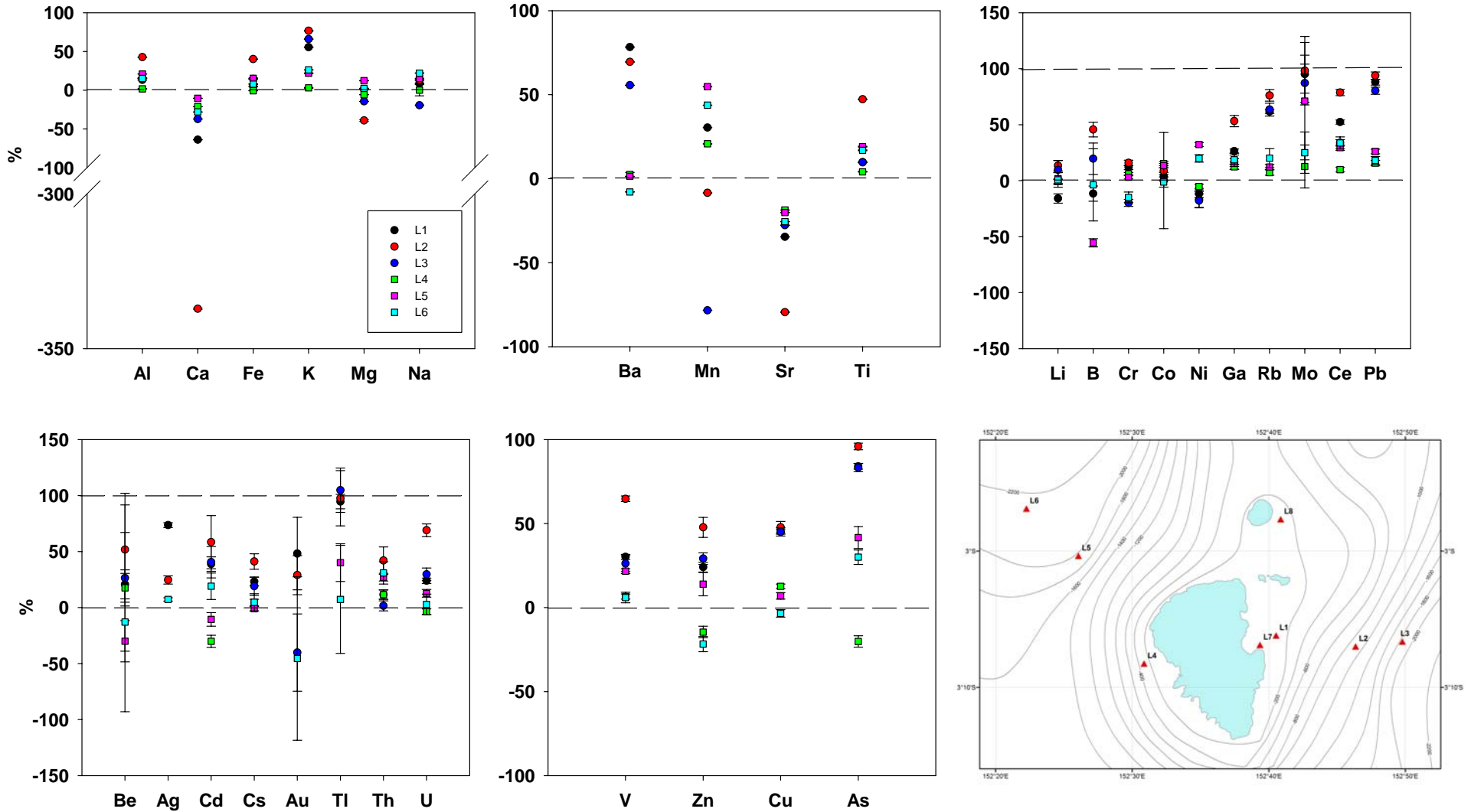**Figure 3.4.5.3 Excess inventories of elements (%) within the top 14 cm of Lihir Station sediments.**

Elemental concentrations within the pore-water samples of cores taken at each of the five stations L1-L4 and L6 are reported in Appendix 4B, tables 4B.77-91. No pore-water samples were obtained from station L5. Figures of the elemental depth profiles for each station are given in Appendix 4A, Figures 4A.46-60.

Pore-water nutrient concentrations were measured at 5 stations around the island of Lihir in order to characterise the upper-sediment biogeochemical processes occurring and to assess if mine tailings deposition had any detectable affect upon these processes. (Appendix 4B, tables 4B.26-40 and Appendix 4A, Figures 4A.10-14).

In general all nutrient concentrations are not atypical for sediment pore-water of equatorial oligotrophic oceans. From the limited dataset available nitrate values to the east of Lihir (Stations L1, L2 and L3) appear to reduce just below the surface more abruptly than those to the west. This may imply increased denitrification and hence oxygen consumption from a greater organic loading to the east of the island. Reduced subsurface nitrate concentrations are commonly associated with increasing ammonia concentrations and for the Lihir stations this is most easily seen at station L2 perhaps reinforcing the view that there is increased organic loading to the east of the island compared to the west. Generally, however, dissolved phosphate levels resulting from organic breakdown are comparable between all Lihir stations and do not show appreciable increase in depth suggesting that there is little degradable organic material penetrating into the sediment. Since silicate values do not significantly increase with depth around Lihir it can be assumed that there is little biogenic silica (diatom) production, deposition and its subsequent dissolution within this environment.

The solid phase and dissolved concentrations of Mn, Fe, Mo and U can be used to determine the redox state of sediment. The redox state of the sediment, either oxidising or reducing, will determine which biogeochemical processes will occur within the sediment environment and hence will give an indication of which elements may move within the sediment core through diffusion in the pore-water to be concentrated in oxidising surface sediments or alternatively released into the overlying water column. An example of this is Mn which is removed to the solid phase under oxidising conditions and is in the dissolved phase under reducing conditions. In comparison, U is soluble in oxidising conditions and removed to the solid phase in reducing conditions.

Figure 3.4.5.5 Mn, Fe, Mo and U solid phase (ppm or %) and pore-water (ppb) concentrations of L2 and L4.

Figure 3.4.5.5 illustrates the Mn, Fe, Mo and U solid phase and pore-water concentrations of an impacted station, L2 and a non impacted station L4. The solid phase concentrations of Mn are similar at both L2 and L4 with higher concentrations of Mn occurring at depth at station L2. In contrast the dissolved concentrations of Mn in L2 are two orders of magnitude higher (21 - 5645 ppb) than L4 (3 – 19 ppb). Solid phase concentrations of Fe are higher in L2 than L4, which is also reflected in the dissolved concentrations of Fe at both stations, L2 (6 – 9692 ppb) and L4 (0 – 1045ppb). The Mo solid phase concentrations of L2 are 35 times higher than those of L4. The dissolved concentrations of Mo also reflect large differences between the two stations with L2 Mo concentrations ranging from 0 to 317 ppb in comparison to L4 which has a concentration range of 8 to 100 ppb. U solid phase concentrations are 5 times higher in the surface sediment of L2 compared to L4 with dissolved concentrations of U at L2 ranging from 2.6 to 3.9 ppb and L4 ranging from 1.7 to 3.2 ppb. The dissolved concentrations of Mn, Fe and Mo are considerably higher in L2 than in L4, ranging from 5 times to 500 times higher in the impacted station when compared to a non-impacted station. Dissolved U concentrations are similar at both stations.

The above trends are generally reflected at the other stations with the impacted stations L1-L3 having higher concentrations of solid phase concentrations of Fe, Mo and U with all stations having similar Mn concentrations. Stations L1 and L3 have similar dissolved metal concentration trends as L2 and station L6 shows similar trends to those of L4.

To assess any impact of mine tailings on the marine environment of Lihir it is important to consider the redistribution of any elements that are considered to be toxic. By considering both the solid phase and pore-water distribution of such elements it is possible to assess whether redistribution is occurring and assess the likely fate of these elements. Figure 3.4.5.6 illustrates the solid phase and dissolved concentrations of As, Cu, Pb and Cd; all these metals are considered to be toxic to living organisms.
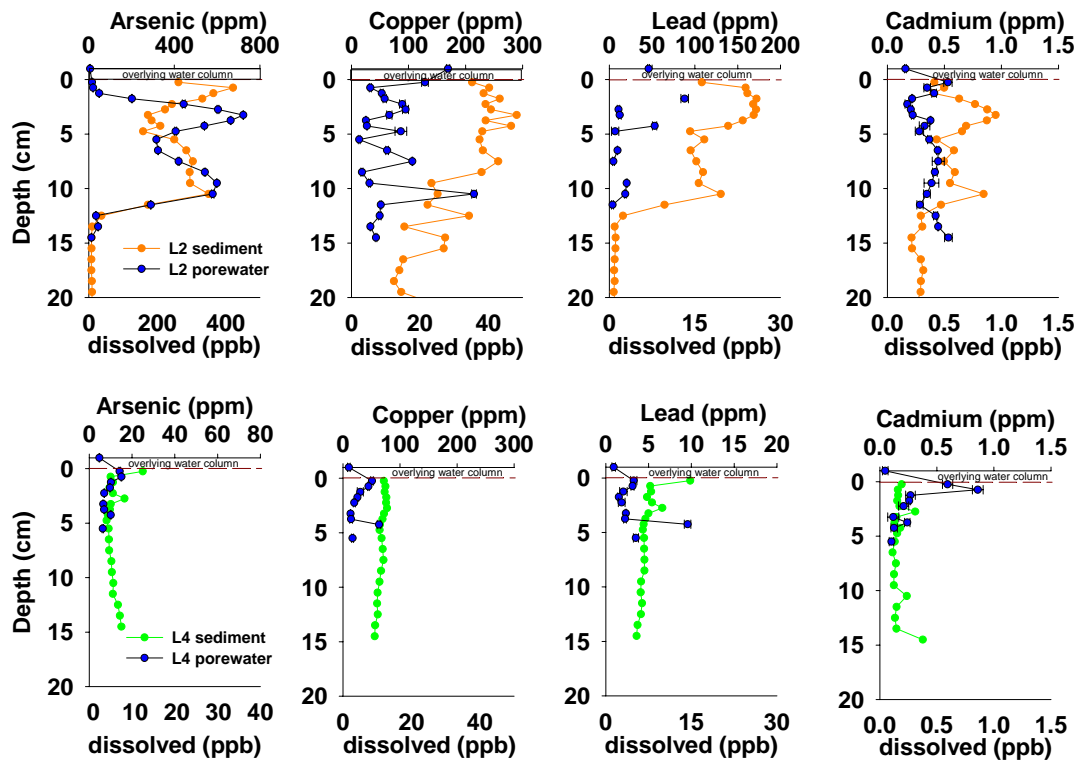
Figure 3.4.5.6 As, Cu, Pb and Cd solid phase and dissolved concentrations, L2 and L4.

The solid phase concentrations for As, Cu, Pb and Cd are all considerably higher at L2, the station impacted by tailings. The As concentration is 20 times higher, Cu, 4 times higher, Pb, 17 times higher and Cd, 5 times higher than the concentrations found in the sediment from the control station L4.

The dissolved concentrations of As, Cu and Pb are also considerably higher at the impacted station, L2, with the concentrations being 70, 3 and 3 times higher than those found at the control station L4. In contrast the dissolved Cd concentration found at L2 is half of that found at the control station L4.

The highest As concentration in sediment occurs at L1, 1124 ppm (Figure 3.4.5.7), with L2 having a maximum concentration of 675 ppm and L3 a maximum concentration of 508ppm. In contrast, the control stations L4-L6 have an order of magnitude lower concentrations with L5 and L6 having a maximum concentration of 70 ppm with the lowest As concentration of 25 ppm occuring at station L4.

The highest dissolved concentration of As occur at station L2 (621 ppb) decreasing to 110 ppb at L3 with L1 having the lowest concentration of dissolved As of the impacted stations. The dissolved As concentrations of the control stations (L4 and L6) are 6 and 11ppm respectively. In summary, the solid phase As concentration trend is L1>L2>L3>L5>L6>L4 with the dissolved As concentration trend L2> L3>L1>L6>L4.
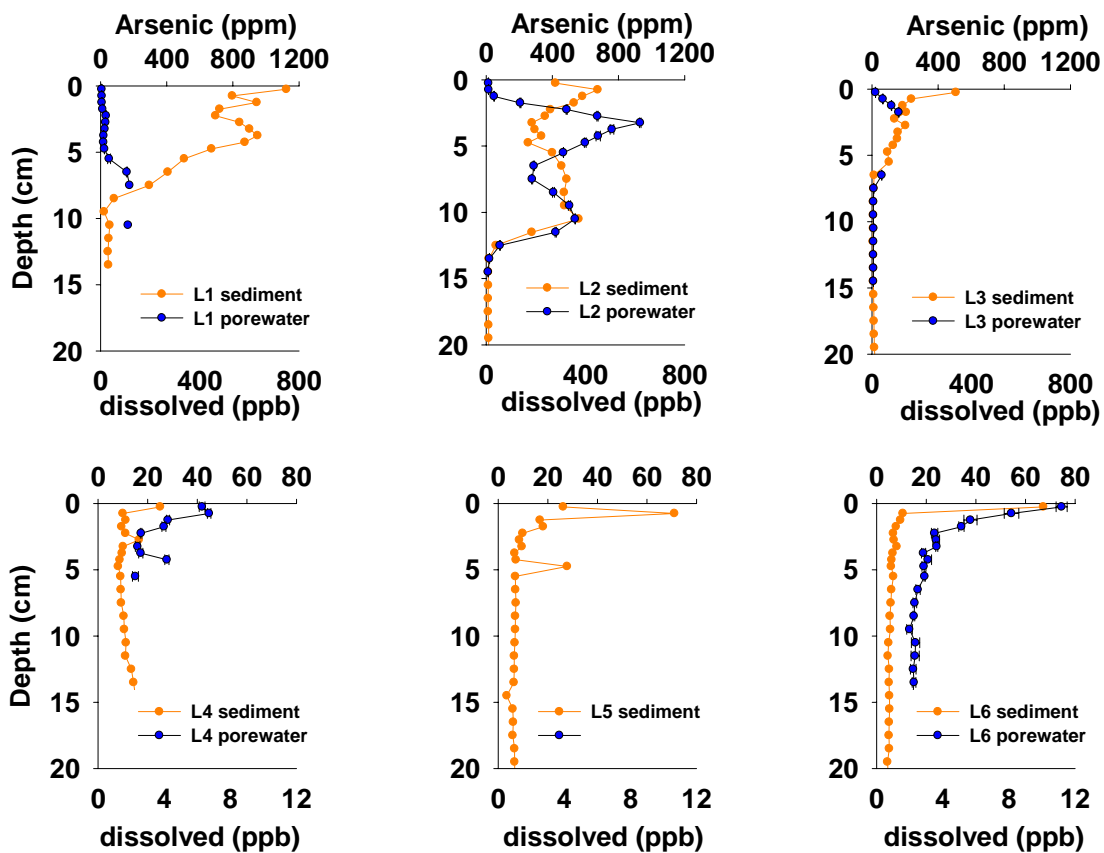
Figure 3.4.5.7 Solid phase and dissolved As concentrations for stations L1-L6

The production (dissolved element) and consumption (precipitated element i.e. removal from solution) of elements can be modelled from the dissolved profiles and the resultant flux to the sediment, or alternatively from the sediment to the pore-water or overlying water column, can be calculated. In this case the Berg model (Berg *et al.*, 1998) has been used to calculate the production or consumption of dissolved Fe, Mn and As at stations L2 and L6. In addition the fluxes of these elements to the sediment or pore-water have been calculated by the model and expressed as μmol m^{-2}d^{-1}.
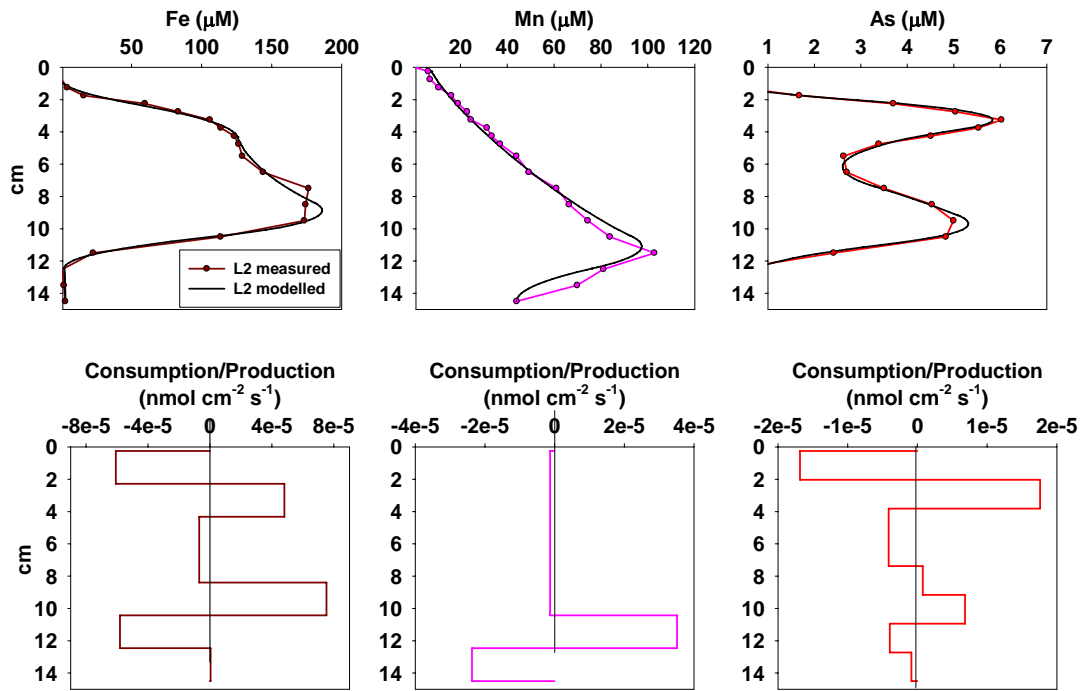
Figure 3.4.5.8 Measured and modelled pore-water (dissolved) concentration profiles for Fe, Mn and As, L2
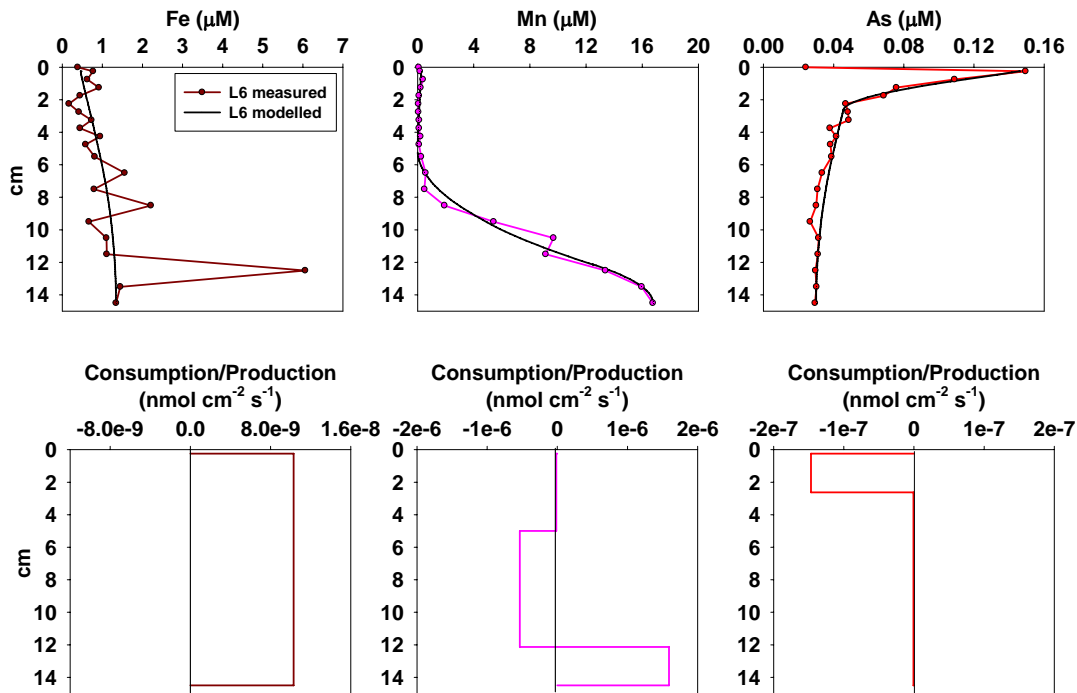
Figure 3.4.5.9 Measured and modelled pore-water (dissolved) concentration profiles for Fe, Mn and As, L6

Figures 3.4.5.8 and 3.4.5.9 show the modelled profiles and the consumption and production of Fe, Mn and As for L2 and L6 respectively. As discussed previously the dissolved Fe, Mn and As concentrations at L2 are higher than those at L6 by a factor of 30 for Fe, 10 for Mn and 40 for As. At L2 the modelling of the Fe profile produces 3 zones of consumption and 2 zones of production, resulting in an over all net flux of dissolved Fe of 16.3 µmol m^{-2} d^{-1}. The modelled profile (L2) of dissolved Mn indicates that there are 2 zones of consumption of Mn and one zone of production with an overall net removal of Mn to the sediment of 8.6 µmol m^{-2} d^{-1}. For As there are 4 zones of consumption and 3 zones of production with an overall net production of As to the pore-water of 7.2 µmol m^{-2} d^{-1}.

In comparison the modelling of dissolved Fe, Mn and As for L6 the control station, shows one zone of production for Fe with a modelled net removal of dissolved Fe of 0.13 µmol m^{-2} d^{-1} to the sediment. There is one zone of consumption and one of production for dissolved Mn with an overall net flux of dissolved Mn of 0.09 **µ**mol m^{-2} d^{-1} and there is a net flux of dissolved As of 0.31 mmol µ^{-2} d^{-1} (Table 3.4.5.4).

Table 3.4.5.4 Modelled flux rates of dissolved Fe, Mn and As at stations L2 and L6 (a negative number signifies a net consumption of dissolved species)

Station	Fe $\mu mol\ m^{-2}\ d^{-1}$	Mn $\mu mol\ m^{-2}\ d^{-1}$	As $\mu mol\ m^{-2}\ d^{-1}$
L2	16.34	-8.61	7.21
L6	-0.13	0.09	0.31

The solid phase and dissolved As concentrations indicate that the impacted stations have higher concentration of As within the sediment which is also reflected in higher dissolved concentrations of As. Compared to the control stations the solid phase and dissolved concentrations of As are an order of magnitude higher at the impacted stations.

Similar trends are also found in the solid phase for Cu, however, the dissolved Cu concentrations are similar between stations with L6 having the highest concentration of dissolved Cu. Excess inventories of Cu for stations L1-L3 are 45, 48 and 48% respectively. In comparison the control stations L4-L6 have excess Cu inventories of 13, 7 and -3% (Figure 3.4.5.4).

Pb concentrations in the sediment range from 100-200 ppm for stations L1-L3 with L2 having the highest concentration of Pb. The control stations L4-L6 have solid phase Pb concentrations an order of magnitude lower, ranging from 10 -20 ppm with L6 having the highest concentration. The percentage excess Pb inventories at stations L1-L3 are 88, 94 and 80% respectively, in comparison to 16, 26 and 18 % at the control stations, L4-L6. Dissolved Pb concentrations for all stations are in the range of 0-13 ppb with L2 having the highest concentration of 13 ppb.

Solid phase Cd concentrations range from 0.1 – 3 ppm with the deepest stations L3 and L6 having the highest concentrations. The dissolved Cd concentrations vary from 0 - 3 ppb with station L6 having the highest concentration. The excess inventories for stations L1-L3 range from 38- 58% with L2 having the greatest excess. The control stations range from -30 to 19 %.

Other metals worth considering are thallium (Tl), chromium (Cr), vanadium (V) and zinc (Zn) all of which can affect living organisms depending on their concentration and bioavailability.

Solid phase Tl concentrations are 10 times higher at the impact stations than the control stations with the percentage of excess Tl inventories at stations L1-L3 being 94, 97 and 100 % respectively.

Dissolved Tl was detected in a few samples of pore-water form stations L1, L2 and L6 and ranged from 0.05 to 0.3 ppb.

Concentrations of Cr range from 34 to 81 ppm for L1-L3 with station L1 having the highest concentration. The concentrations in the control stations range from 14 to 30 ppm, with L4 having the highest concentration. Concentrations of dissolved Cr for L1-L3 are below the detection limit with values in the control stations, L4 and L6, ranging from below detection limit to 2.6 ppb.

Concentrations of V range from259 - 368 ppm within stations L1-L2, in comparison to L1-L4 which range from 92 – 202 ppm. The percentage excess inventories of V in L1-L3 are 30, 65 and 26% respectively and 6, 22 and 6 % for L4 – L6. The dissolved V concentrations in the pore-water, for stations L1-L3, range from below detection limit to 44.8 ppb with the highest concentrations occurring at L3. Concentrations within the pore-water of the control stations range from below detection limit to 47.3 ppb.

Finally, Zn concentrations in L1 - L3 range from 196 – 300 ppb in comparison to L4 - L6 which range from 88 - 564 ppb with L6 having the highest concentration of Zn. Dissolved concentrations of Zn at stations L1-L3 range from below detection limit to 206.9 ppb, the highest concentration occurring at L1. The dissolved concentrations of Zn in L4 and L6 range from 5.1 to 143.8 ppb.

3.4.6 Benthos

Metazoan meiofauna

At all three depths sampled, mean values for total density of metazoan meiofauna were higher at control (unimpacted) than at tailings-impacted stations (Figure 3.4.6.1a). The differences were statistically significant at 800-850 m (2-sample t-test, $P < 0.01$) and 1715-1750 m ($P < 0.05$), but there was no signficant difference at 2020 m.

The metazoan meiofauna at all three tailings-affected stations (L1, L2, L3) was numerically dominated by harpacticoid copepods, with this group making up > 70% of the total at L1 and L3, and comprising almost the entire fauna at L2 (Figure 3.4.6.2a) In contrast, at the three Control stations (L4, L5, L6) nematodes and harpacticoid copepods were approximately equal in abundance, each comprising 40-50% of the community (Figure 3.4.6.2b). Ostracods and minor metazoan groups were rare at all stations.
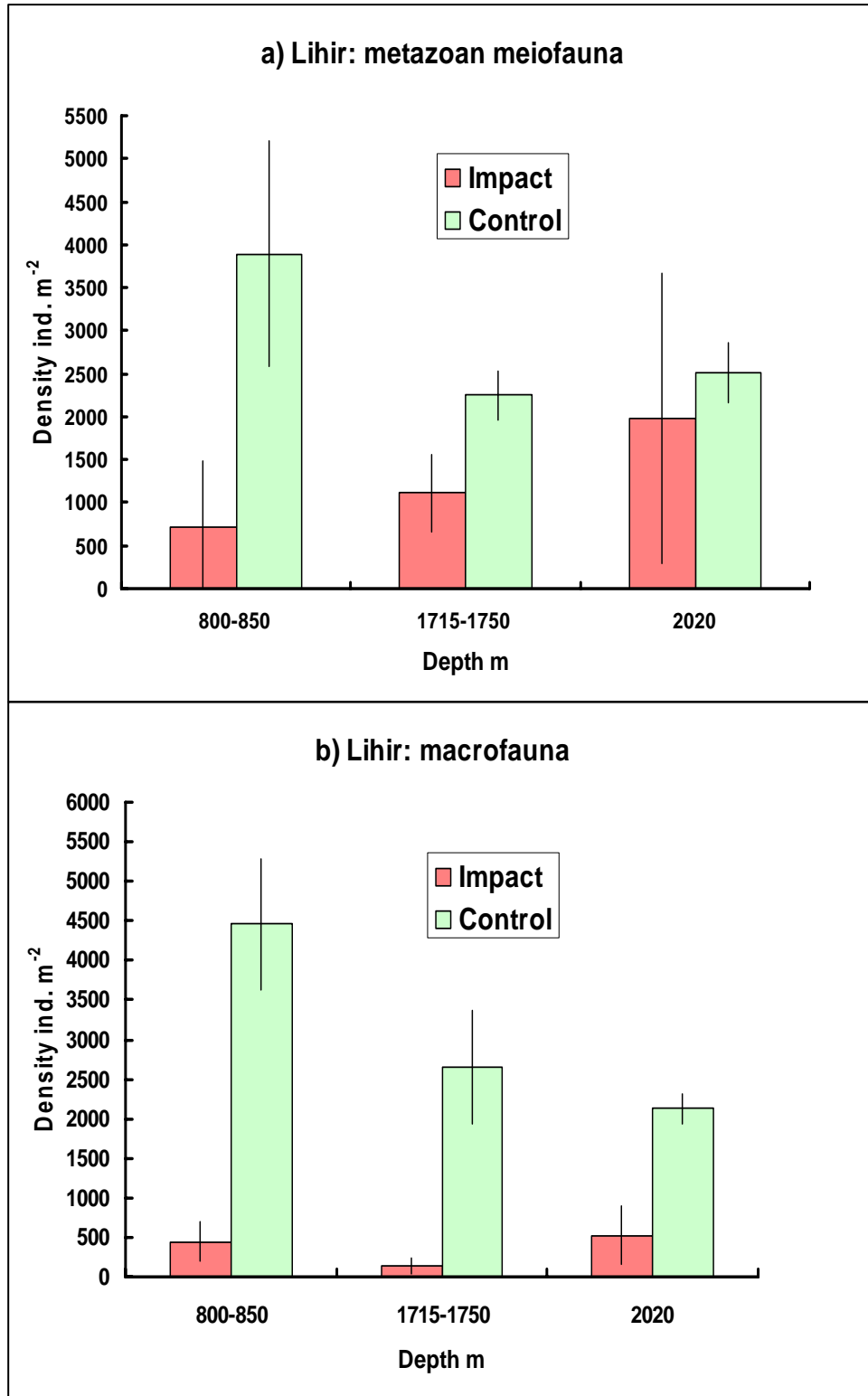
Figure 3.4.6.1. Histograms showing mean densities of (a) metazoan meiofauna and (b) macrofauna (> 250 μm) at Impact (L1, L2, L3) and Control (L4, L5,L6) stations off Lihir. Stations are grouped according to water depth. Bars represent mean values (± SD) for each station with individual corer drops as replicates. Numbers refer to the upper 10 cm of the sediment column.

Figure 3.4.6.2. Histograms showing percentage contribution of major taxa to the metazoan meiofaunal community (> 250 μm) at (a) Impact and (b) Control stations off Lihir. Bars represent mean values (± SD) for each station with individual corer drops (n = 1 core per drop) as replicates.

Foraminifera

Living benthic Foraminifera were entirely absent from the 500 μm and 250 μm sieve fractions at L1 and L2. At the third tailings-affected station, L3, living forams (all calcified species) were present at low density. Living forams were present in samples from all three Control stations off Lihir and included both calcified and organic-walled (allogromiid) species. Mean densities are shown in table 3.4.6.1.

Table 3.4.6.1 Mean densities of living forams were present in samples from all three control stations off Lihir

Station	Depth m	Calcified forams ind. m^{-2}	Organic-walled forams ind. m^{-2}
L4 (Control)	800	1146 ± 441	382 ± 459
L5 (Control)	1715	2504 ± 1396	425 ± 294
L6 (Control)	2020	297 ± 265	297 ± 194
L3 (Impact)	2020	297 ± 321	None

At 2020 m, mean density of calcified forams was identical at Impact (L3) and Control (L6) stations, but the Impact station differed in the absence of organic-walled taxa.

Macrofauna

At all three depths sampled, mean values for total density of macrofauna were much higher at Control (unimpacted) than at tailings-impacted stations (Figure 3.4.6.1b). The differences were statistically significant at all three depths (2-sample t-test P < 0.001 at 800-850 m and 2020 m, P < 0.05 at 1715-1750 m).

The sparse macrofauna at the Impact stations consisted almost entirely of small polychaetes, accounting for 83-97% of the total community. Only one or two polychaete families were represented at each station (Spionidae and Dorvilleidae at L1, Cossuridae and Paraonidae at L2, Paraonidae at L3). Bivalves and peracarid crustaceans (tanaids and amphipods) were present in very low numbers. In contrast, the Control stations supported more diverse communities in which

Polychaeta was the most abundant major group (58-64% of the total) but did not dominate to the extent seen at the Impact stations. Crustaceans and molluscs were well-represented at all three Control stations. The number of polychaete families represented at the control stations ranged from 17 (L6) to 27 (L4). In terms of higher-taxon composition, the macrofaunal communities at L4, L5 and L6 were indistinguishable (Figure 3.4.6.3).

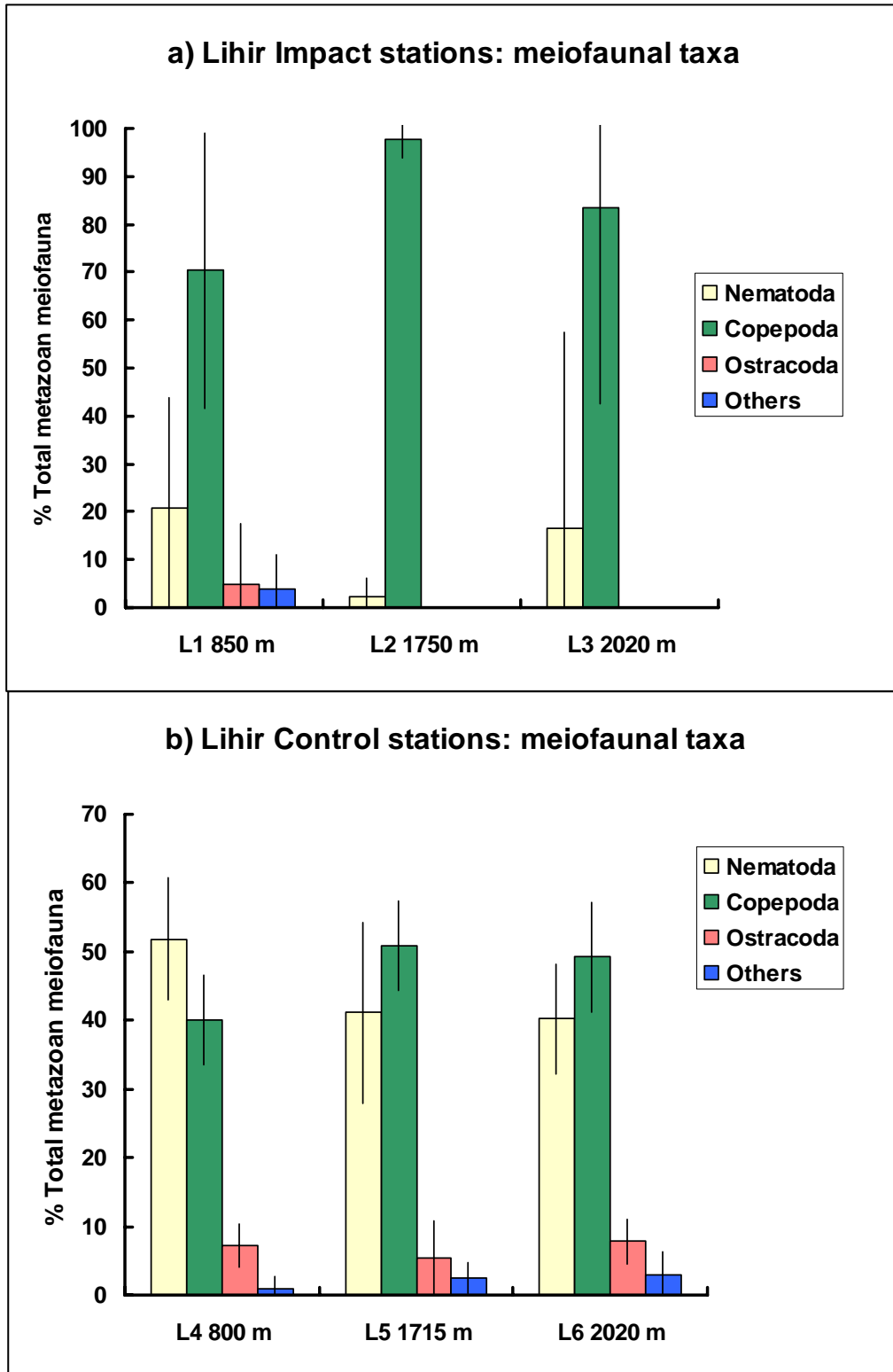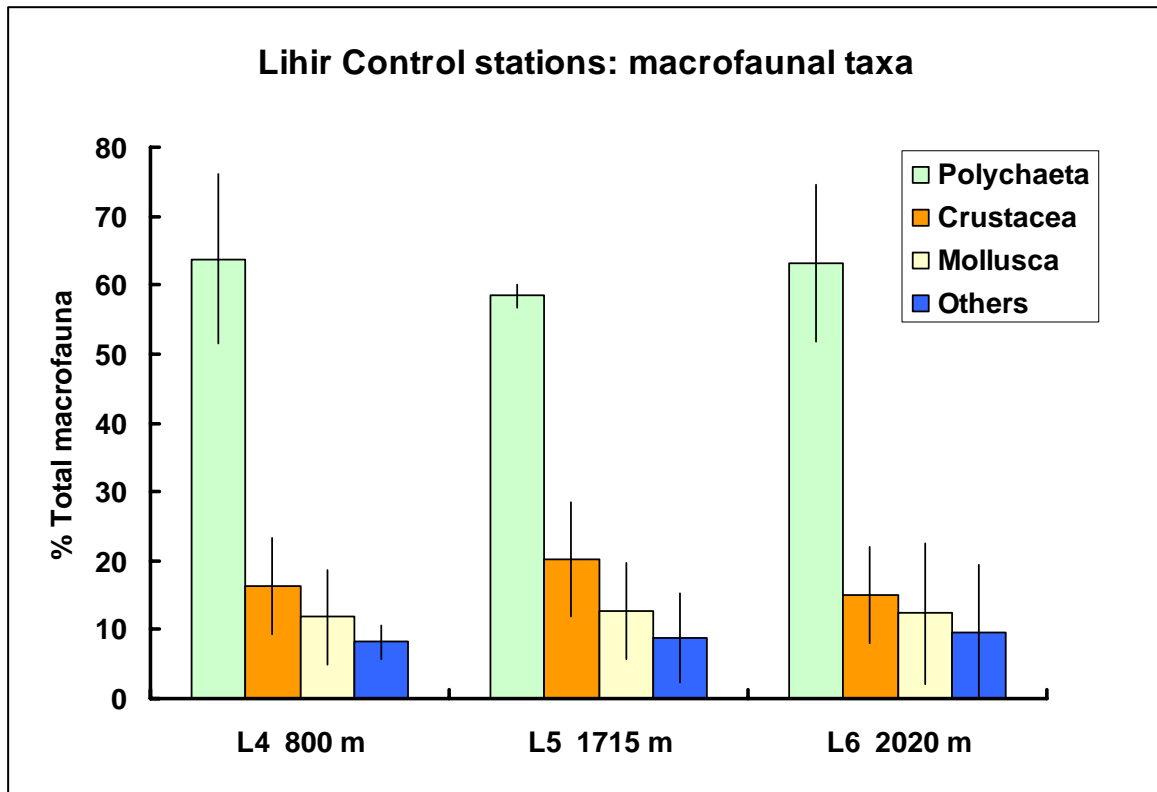**Figure 3.4.6.3. Histogram showing percentage contribution of major taxa to the macrofaunal communities (> 250 μm) at Control stations off Lihir. Bars represent mean values (± SD) for each station with individual corer drops as replicates.**

Faunal depth distribution in the sediment column

In all samples, both meio- and macrofauna were virtually absent in the 5-10 cm depth horizon of the sediment column. In a typical core only isolated individuals, and often none at all, were found below 5 cm depth. At water depths of 1715-1750 m and 2020 m metazoans were heavily concentrated in the 0-1 cm horizon of the sediment (> 70% total individuals) (Figure 3.4.6.4b, c), with a steep decline in occurrence below this. At shallower water depths (800-850 m), metazoans were more evenly distributed across the upper 5 cm of the sediment column, although still with highest abundance in the surface layer (Figure 3.4.6.4a). There was no significant difference

between control and impact stations at any water depth. The few calcified Foraminifera recorded at Impact station L3 were all found in the uppermost 0-1 cm sediment horizon.
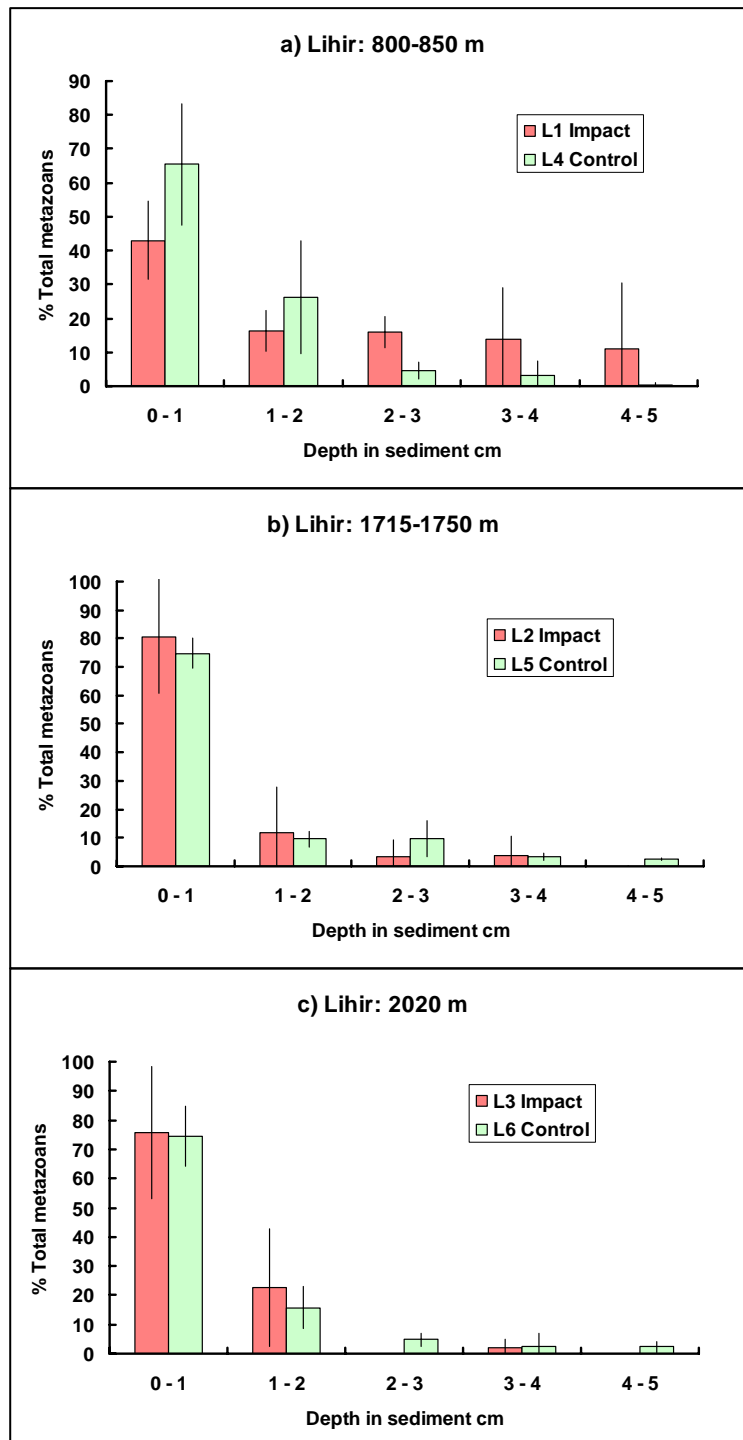
Figure 3.4.6.4. Histograms showing percentage ocurrence of metazoans (> 250 μm) in 1 cm-deep sections of the upper 5 cm of the sediment column at Control and Impact stations off Lihir. Bars represent mean values (± SD) for each station with individual corer drops (n = 1 core per drop) as replicates.

3.4.7 Seabed photography

Station L1 Twenty-five photographs were obtained at L1. In all cases the seabed was obscured by a dense haze of suspended particles (Figure 3.4.7.1). The seabed is faintly visible on photo 009, but no details can be made out. The turbidity of the bottom water is not the result of silt clouds raised by accidental contact of the camera frame with the seabed, as this artefact is easily recognizeable when it occurs. Bottom water turbidity must be a feature of the ambient environment at the time the photographs were taken.

Station L4. Twenty-five images were also obtained at L4. In the early section of the deployment (photos 001-008) the seabed topography appears to be irregular and steep in places, with expanses of sediment-draped rock. Possible worm tubes and other small encrusting fauna are seen in places, with a group of large stalked crinoids (sea lilies) clearly visible on photo 007 (Figure 3.4.7.2). From photo 009 onwards, the camera covers a seabed of flat sediment with a limited amount of biogenic topography (small burrow openings and fine trails). Terrestrial leaves are visible on the sediment surface in several photos. No animals can be seen.

Figure 3.4.7.1. "Bed-hop" camera image taken at Lihir station L1, showing the seabed obscured by a dense haze of suspended particles. Width of image at lower edge approximately 1m, depth of field approximately 2.5 m.

Figure 3.4.7.2. "Bed-hop" camera image taken at Lihir station L4, showing an irregular seabed possibly consisting of sediment-draped rock. Several stalked crinoids are clearly visible at far left and just below the compass head. Width of image at lower edge approximately 1m, depth of field approximately 2.5 m. In this photograph the compass arm has been bent back towards the camera by accidental impact on the seabed.

3.4.8 Water column geochemistry

Water column nutrient concentrations are reported in Appendix 3B, tables 3B.11-17. Figure 3.4.8.1 illustrates the water column nutrient concentrations for Lihir. The results indicate little difference between the nutrient concentrations in the water column to the east and west sides of Lihir with exception of ammonium concentrations which are noticeably higher on the eastern side. Ammonium concentrations increase in surface waters due to zooplankton grazing of phytoplankton. If phytoplankton levels are higher, the subsequent grazing and ammonium release is also higher.   There are also higher levels of nitrate and silicate in the mid and deep waters (>1000m) on the east side of the island with values exceeding 100 micromole for silica and exceeding 40 micromole for nitrate.

.
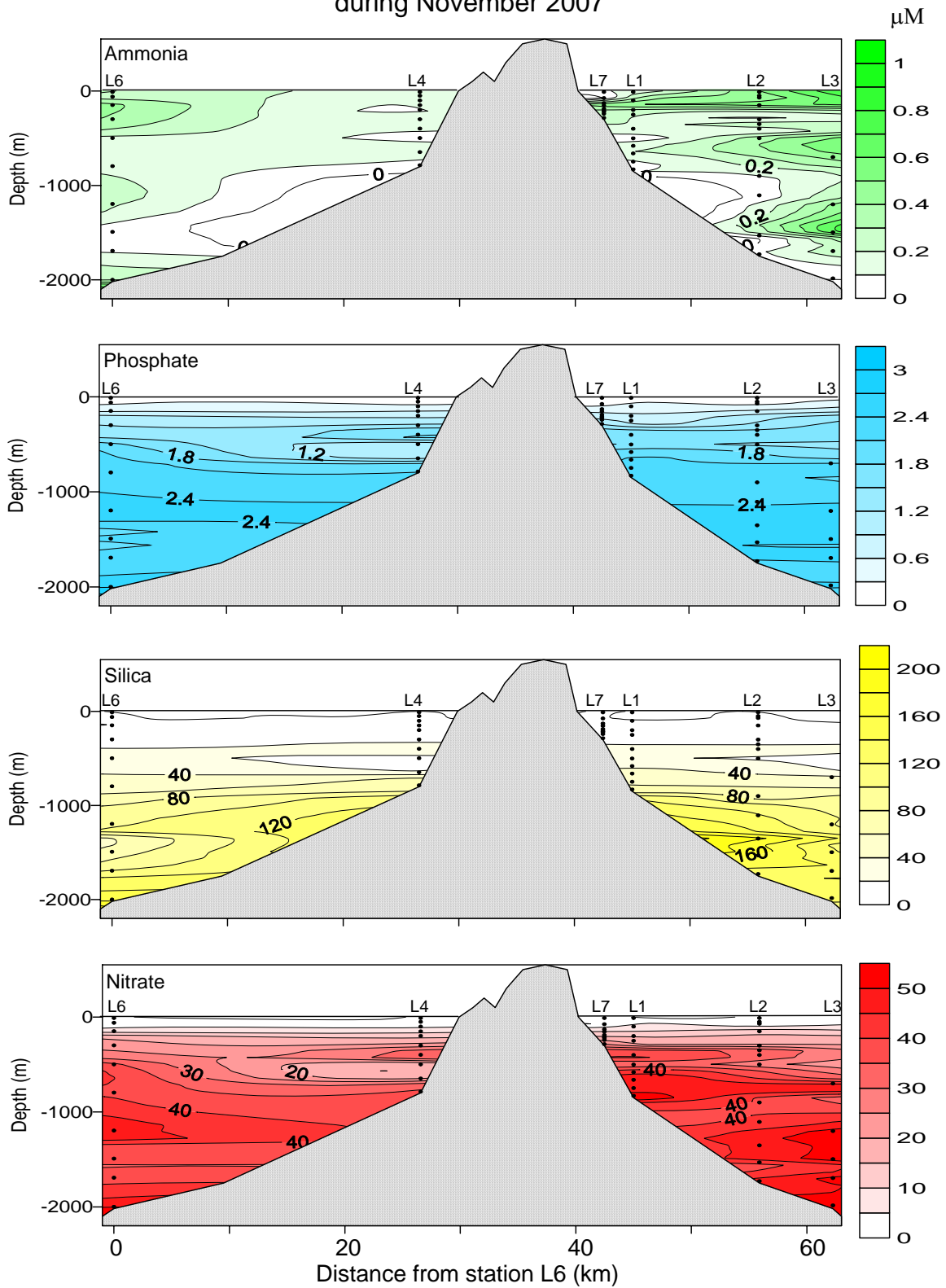
Figure 3.4.8.1 Water column nutrient concentrations, Lihir

Suspended particulate material (SPM) was collected at stations L1-L4, and L6 , in addition two further stations were sampled for SPM, station L7 close to the mine tailings discharge pipe and L8 located offshore from Masahet Island (Figure 3.3.4.1)

The elemental concentration data for each station are given in Appendix 3B, tables 3B.50-68. The Figures of the depth profiles of elemental concentrations are given in Appendix 3A, Figures 3A.49-58.

Table 3.4.5.5 gives the maximum concentration of SPM and the depth at which it occurs at each station. The concentration of SPM is highest at L7, the station closest to the outfall from the DSTP pipe, with maximum concentration occurring at 14.5 mg L^{-1} at a depth of 285 m. The next highest concentration of SPM occurs at station L1, 5.7 mg L^{-1}, at a depth of 748m. L2 has a concentration of 0.5 mg L^{-1} with the two control stations having a maximum SPM concentration of 0.15 and 0.16 mg L^{-1}. L8, at Masahet Island has a concentration of 0.26 mg L^{-1} which is higher than the control stations similar to L3 and lower than L1 and L2.

Table 3.4.5.5 Depth of maximum suspended material at Lihir stations

Station	L1	L2	L3	L4	L6	L7	L8
Maximum (mg L^{-1})	5.72	0.50	0.23	0.15	0.16	14.56	0.26
Depth of maximum (m)	830	1352	150	200	1693	285	10
Depth of water column (m)	850	1750	2020	800	2020	300	600

The depth profiles of SPM (Figure 3.4.8.2) show some structure which is related to the distance from the discharge pipeline and the physical structure of the water column with the stations in shallower water depths having more complex profiles.

The SPM depth profiles show highest metal concentrations at the stations closest to the mine with concentrations decreasing with distance from the mine. The two control stations L4 and L6 generally have the lowest concentrations of metals within the suspended particulate material.
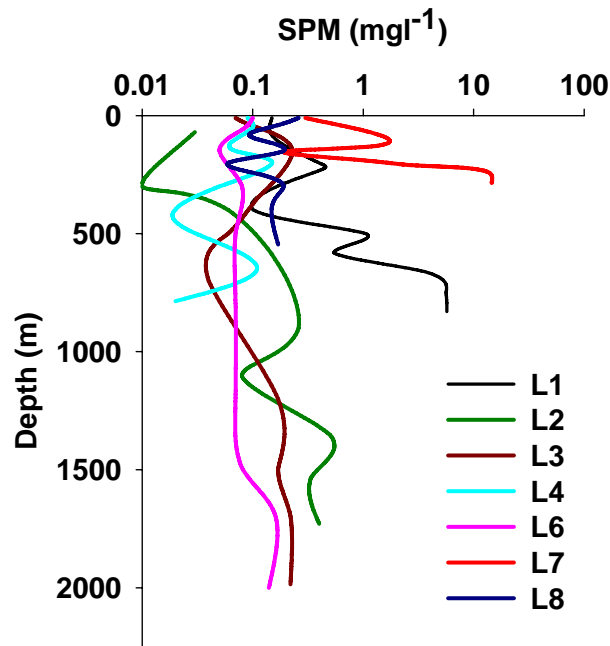
Figure 3.4.8.2 Weight of suspended particulate material per litre of water at Lihir stations

The correlation coefficients for all the samples (Appendix 4B, tables 4B.64-68) indicate strong correlations between large numbers of the elements. However, Ni, Zn and Cu have correlation with B and Au shows a correlation with B, Zn, Cs and Ba. The correlations for the impact stations L1-L3 and L7 are very similar to those coefficients when all the samples are considered. The correlation coefficients for the control stations L4 and L6 indicate obvious differences. Neither Li or Sr have strong correlations with any other elements, the relationship between Ni, Zn, Cu and B is absent, there are less correlations of Tl with other elements and Be has no correlation with Li although there is a very strong correlation between Be and Li in the correlations when all samples are considered, when the impact stations are considered and when L8 and L7 are considered on their own.

Station L7, the station closest to the discharge pipe, also shows some differences to the correlations with all impact stations. The main differences in this case are that the correlations between Fe and Li, Be, Al, V and Mn are absent as are a number of the correlations with As and Tl. In this case As shows a very strong correlation with Fe as do Mo, Ba and Tl.
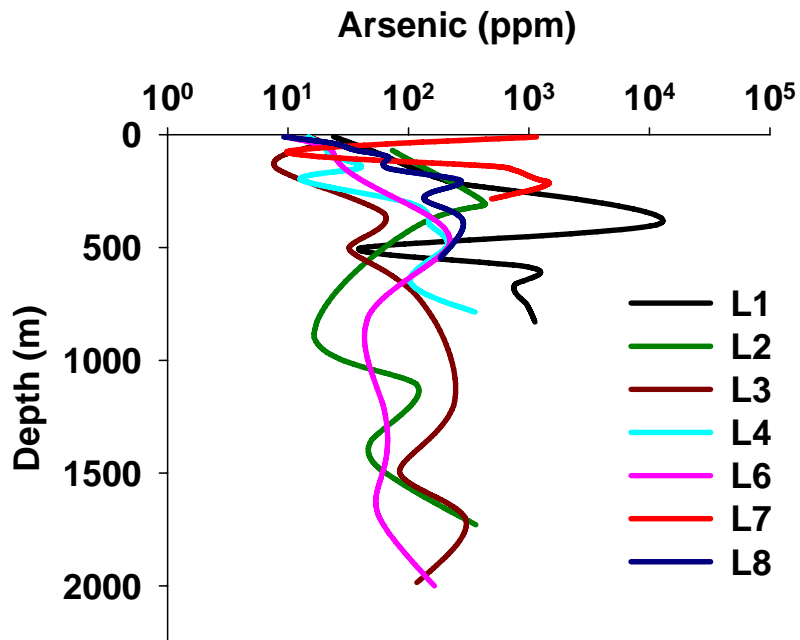
Figure 3.4.8.3 Arsenic concentrations within the suspended particulate material at Lihir

The As concentrations in the SPM are high (Figure 3.4.8.3) with the highest concentration of 11540 ppm occurring at L1, at a depth of 400m. L7 has a maximum concentration of As of 1435 ppm at 209m depth and the surface concentration is also high at the surface with a concentration of 1156 ppm. The SPM at stations L2 and L3 have maximum As concentrations of 423 ppm and 294ppm and station L8 at Masahet Island has a maximum As concentration of 282 ppm at a depth of 380m.

The control stations L4 and L6 have maximum As concentrations of 357 ppm and 214 ppm at depths of 786 and 498 m respectively. The SPM As concentrations indicate that stations L1, L2 and L7 have higher concentrations of As than the control stations.

Stations L1-L3 have maximum Be concentrations 29.2, 5.4 and 0.6 ppm (Figure 3.4.8.4), L7 has a maximum Be concentration of 6.3ppm and L8, has a similar Be concentration to L3 of 0.7 ppm Be. The SPM at the control stations L4 and L6 have no detectable levels of Be.
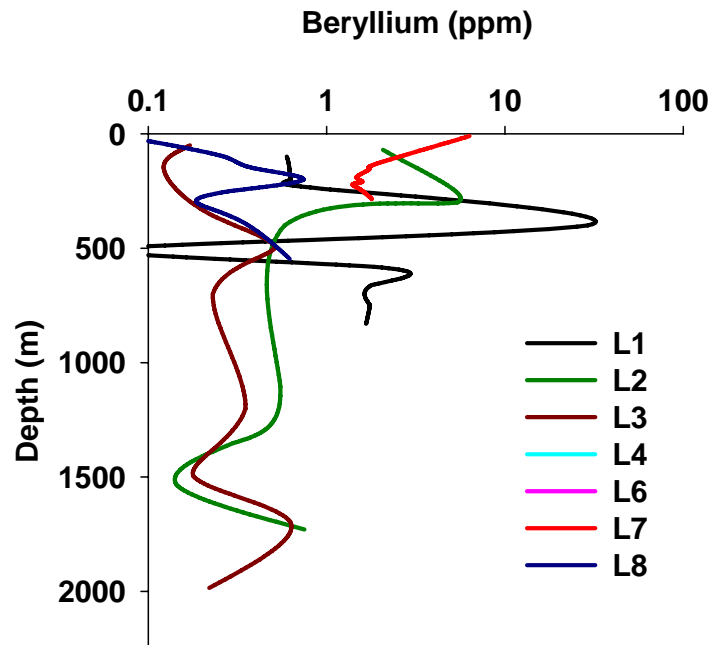
Beryllium (ppm)

Figure 3.4.8.4 Beryllium concentrations within the suspended particulate material at Lihir

3.4.9 Zooplankton

The number of organisms identified from each station at Lihir ranged from 114-648 (cf. 232-968 at Basamuk 2.4.9). Across both Lihir and Basamuk a total of 65 taxa were identified (Table 2.4.9.1). At Lihir the average taxa concentrations as number of organisms per m^3 were similar at both stations 1 and 8. Considering the most abundant taxa, the concentration of organisms was highest in the upper sampled depth band (100 to 0 m) with little obvious change between day and night (Figure 3.4.9.1 and 3.4.9.2). Radiolarians and adult copepods (grouping all families) were most abundant followed by the copepodite stages of copepods. Fish eggs were also an important constituent of the plankton in this depth-band. Less abundant but still significant taxa included appendicularians, forams, various medusae, ostracods, chaetognaths, tinitinnids and siphonophores. The 'others' category included a range of organisms including amphipod and caridean shrimps, ctenophores and echinoderm larvae. All taxa in this category were present at concentrations of less than 17 organisms m^{-3}. The general spread of taxa was reflected in the lower depth-bands sampled but with much reduced abundances. The naupliar stages of copepods were always found at low concentrations but this likely reflects size selectivity due to the 200 μm mesh net used rather than their true abundance.
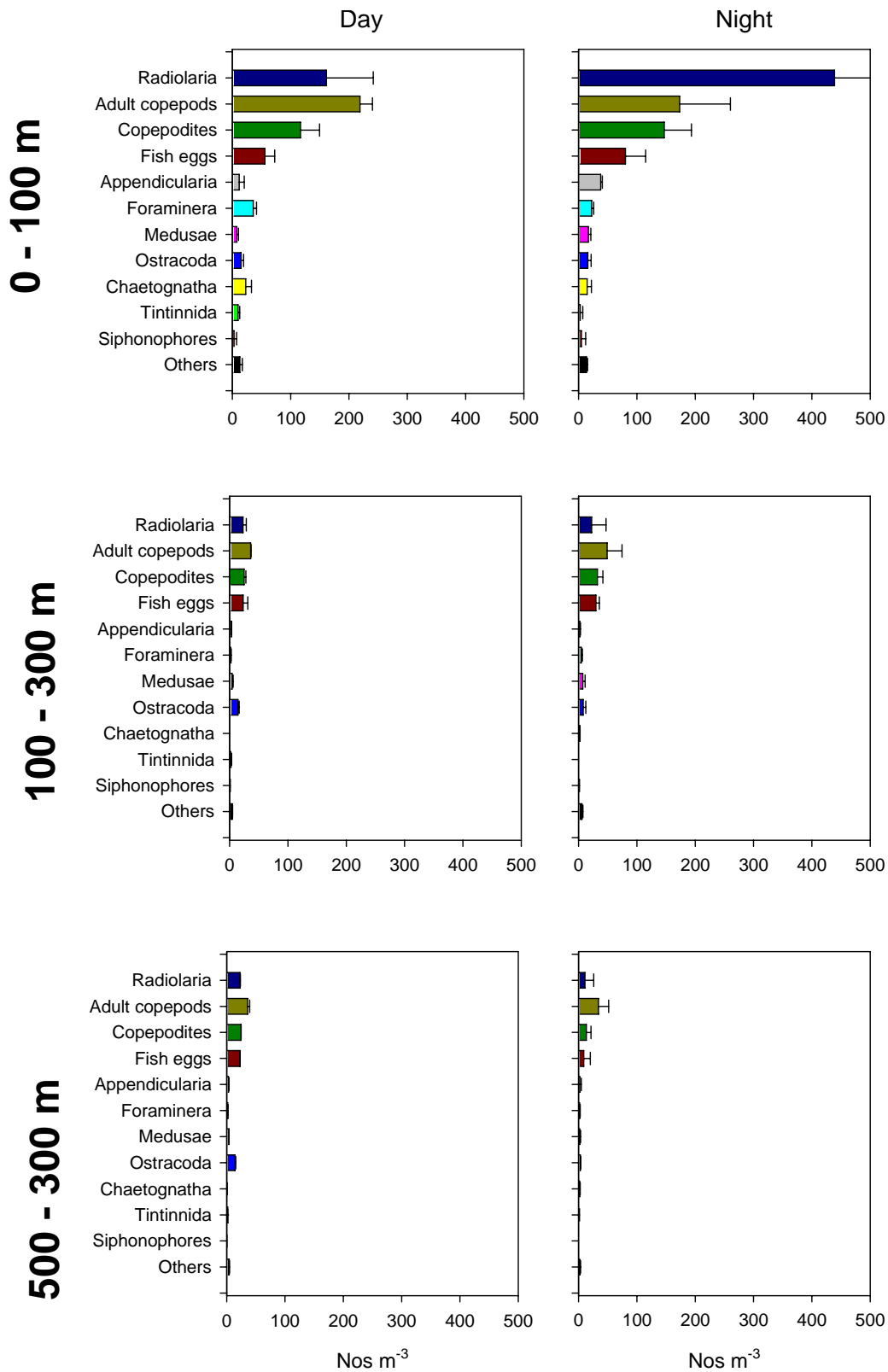
Figure 3.4.9.1 Day and night zooplankton abundance at station L1.
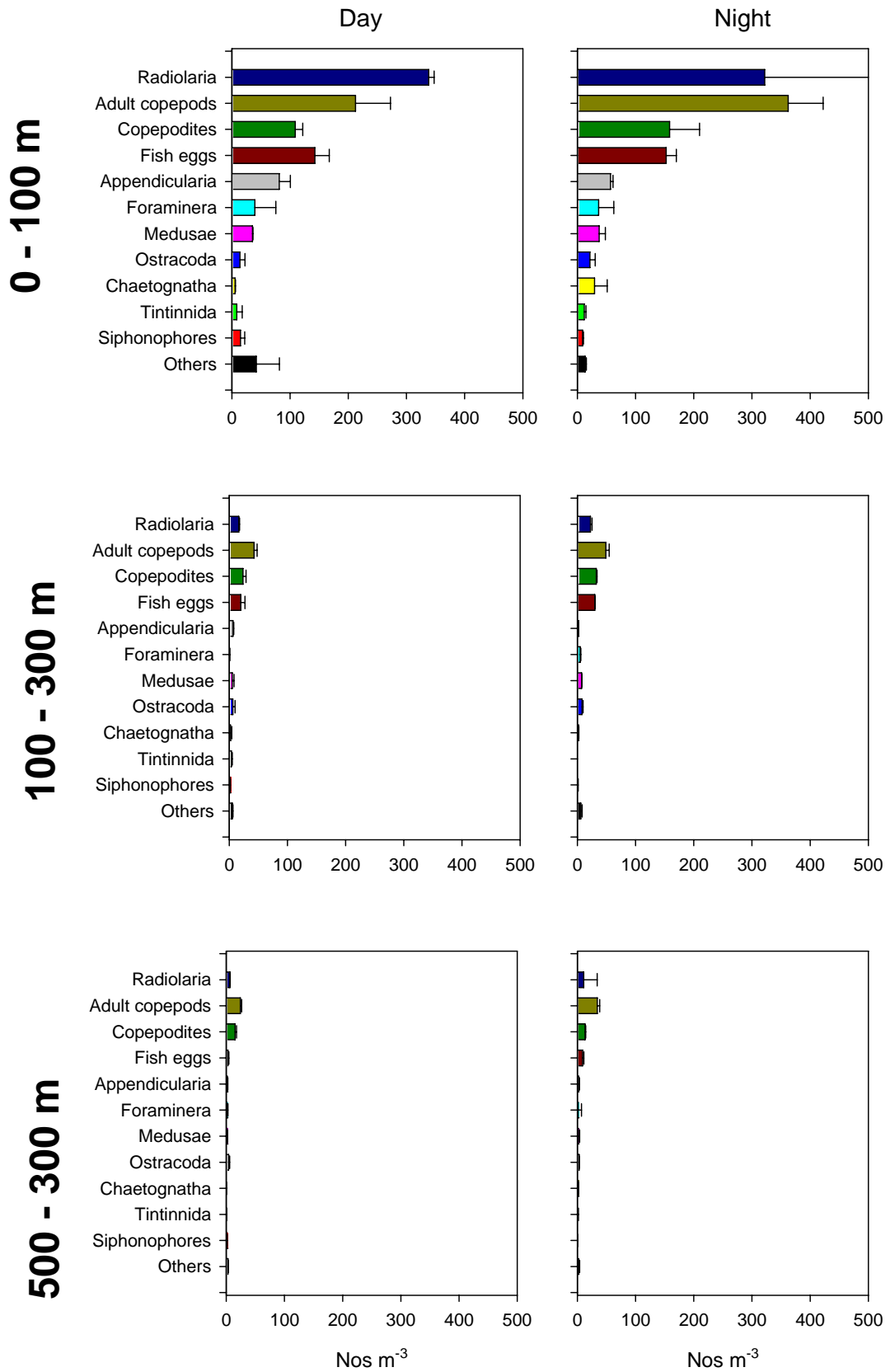
Figure 3.4.9.2 Day and night zooplankton abundance at station L8.

3.4.10 Microplankton

The abundances of the major microplankton taxonomic groups at Lihir are shown inTable 3.4.10.1. The data were collected from only 2 stations at 3 depths each so presents only a limited insight into the distribution and abundance of microplankton due to the small number of samples collected and lack of replication.

The microplankton community at almost all stations was dominated by diatoms (19 taxa) with much lower abundances of dinoflagellates and ciliates. Abundances were, as expected, highest in the surface 70 m at all three stations reflecting the surface euphotic zone. Choanoflagellate abundance was also low except at 10 m depth at station L6. The diatom community was numerically dominated by *Pseudonitzschia delicatissima* at station L8 (see Appendix 6).

Table 3.4.10.1 Abundance (L^{-1}) of major microplankton taxa collected in samples from Lihir.

Station	Date	Depth	Diatoms	Dinoflagellates	Ciliates	Unknown Protists	Choanoflagellates
L6	25/11/07	10m	1720	260	240	560	3100
	25/11/07	70m	1220	40	60	80	200
	25/11/07	150m	100	20	40	0	20
L8	20/11/2007	10m	1700	180	220	60	40
	20/11/2007	70m	1500	20	60	60	100
	20/11/2007	150m	100	40	0	40	0

3.5 Analysis and discussion

3.5.1 Bathymetry and Acoustic Character

The echo sounder survey revealed nothing unsurprising about the nature of the seabed to the east of Lihir. Given the detailed survey work that had been undertaken previously this is to be expected. In summary the results of the echo sounder survey suggest that proximal to the tailings outfall there are thick accumulations of soft tailings and barge dump rock waste that have been, or are becoming remobilised down-slope, most probably by gravity. Notable from the echo

sounder profiles in the vicinity of station L1 are debris flows, the down-slope movement of sediment slurries, recognised by their transparent internal acoustic character and clinoform geometry (Stoker 1997). Farther offshore the acoustic character is more uniform with a reflective acoustic character and an irregular morphology. The floor of the submarine channels are more reflective that the surrounding seafloor, suggesting these are the main conduit for the coarser, sandier sediments from Lihir, both tailings waste and natural in origin.

3.5.2 Physical Oceanography

For clarity, and to avoid repetition, the physical oceanography data are discussed together with the results in section 3.4.2

3.5.3 Sediment sampling and sedimentology

The core sampling and subsequent sediment particle size analysis provide evidence for the main sediment types and depositional processes occurring around Lihir. The sampling stations east of Luise Harbour and the tailings outfall all display sediments wholly containing mine tailings with mine-derived waste found >30km away from the outfall. Mine tailings are recognised both by their distinctive orange-brown colour and by their quartz and pyrite composition. All three stations east of Lihir displayed a thin surface layer of fine-grained orange mud with orange-brown sandy mud and muddy sands beneath, sometimes laminated. This is interpreted as coarser sediments deposited as bedload from density currents, most probably turbidity flows flowing down-slope principally confined to channels (Stow and Piper, 1984). Within the channels the coarser sediments dominate, but overspill and lofted plumes of sediments deposit material between channels. The result of this process is visible in the cores from station L2 where a series of sand laminations are interpreted as repeated turbidites. The ubiquitous surface layer of orange mud is interpreted as fine-grained mine-derived waste deposited from a plume, evidence for this plume is seen in the camera deployments at station L1, closest to the outfall. In contrast the control samples all exhibit homogenous muddy sands, suggesting that, west of Lihir the depositional environment is less dynamic and not dominated by down-slope sedimentation, as there is little evidence for coarse-grained turbidites. The lack of turbidites in the control samples might be the result of either; a) a different source of sediment, being mostly finer-grained, and/or b) a decrease in sediment supply, i.e. down-slope sedimentation is not as frequent as offshore eastern Lihir and therefore not observed in the short cores obtained in this survey.

3.5.4 Sediment and water-column geochemistry

The geochemical results for the sediment samples around Lihir indicate that the discharge of mine tailings is impacting on the sediment regime of the marine environment east of Lihir. The stations L1-L3 have all been impacted by the discharge of the tailings. The sedimentation rates at these stations are higher than would be expected for typical deep sea sediments at these water depths and, although there is a low abundance of bioturbating fauna, the ^{210}Pb profiles indicate highly mixed sediments over the top 5-10 cm at L1 and L2 indicating a rapid input of sediment particles with low activities of ^{210}Pb. There is evidence of mixing at L1 but this is restricted to the top 1 cm.

The chemical analyses of the sediment cores show elemental depth profiles which penetrated below the mine tailings at the impacted stations. These profiles indicate that the mine tailings composition is significantly different from the naturally occurring sediments and can be identified by their geochemical signature. The mine tailings are contributing to the metal content of the sediments at the impacted stations yielding significantly higher inventories of K, Rb, Ba, Cu, Zn, V, As, Pb, Tl and U.

The inventories of excess As at the impacted stations (L1-L3) range from 8.5 g m^{-2} to 27.6 g m^{-2} compared to the control stations (L4-L6) which range from -0.3 to 0.5 g m^{-2}. Pb behaves similarly, with excess inventories ranging from 3.1 to 8.7 g m^{-2} at the impacted stations compared to 0.09 to 0.18 g m^{-2}. at control stations. Other metals follow this trend. In addition to the solid phase increase in metal concentration there is also an increase in dissolved metals. The pore-waters of the impacted stations show elevated levels of dissolved metals with dissolved As levels at the impacted stations being at least an order of magnitude higher at the impacted stations compared to the control stations. The solid phase and pore-water profiles of Fe and Mn suggest that the dissolution of Fe and Mn oxyhydroxides is releasing As and other metals into the pore-waters of the sediment.

The analysis of suspended particulate material (SPM) indicates that the maximum concentration of suspended particulates occurs at the station closest to the discharge pipe, with the concentration of particulates in the water column decreasing with increasing distance from the mine. The distribution of particulates throughout the water column shows some structure suggesting that the particulates are being influenced by the physical properties of the water column as well as the distance from the pipe. Metal concentrations of the SPM are highest at the stations closest to the mine with concentrations decreasing with increasing distance from the mine. The control stations have the lowest concentrations of metals within the SPM.

The As concentration of the SPM at the stations closest to the discharge pipe L7 and L1 are high with the highest concentrations occurring at L1. In addition to high concentrations of As in the SPM at depth in the water column at L7 there are also high concentrations of As in SPM at 60m depth which is 50 m above the depth of the discharge pipe. It is not possible to say whether this is coming from surface run off from acid rock drainage or whether this is particulate material being entrained into the surface waters. The concentration of Be was also measured in the SPM and the highest concentrations were detected at the impacted stations (L1-L3 and L7). The highest concentration was measured at L1 at a depth of 400m. Be was not detected in either of the control stations, however it was detected in L8, Masahet Island, suggesting that the finest particulate material being discharged from the mine is travelling large distances before settling out. As with the Arsenic profile, SPM Be concentrations at station L7 are also high in the surface waters but decrease with depth, suggesting that this is indeed land runoff, however further work will need to be carried out to determine the source of particulate metals, including As, V, Cu, Ga, Cd, Tl, Pb and U, to the upper water column.

The combination of the geochemical analysis of the suspended particulate material, the sediment and the pore-waters allow us to construct a picture of the movement and impact of the mine tailings within the environment of Lihir. The tailings are contributing a significant amount of material to the immediate marine environment and further afield. The material being discharged contains a significant amount of heavy metals with the finer particulate material having higher specific concentrations of metals. These fine particulates are being distributed widely and the inventories and concentrations measured at L2 suggest that the area is a sedimenting environment where particulates are settling out. In addition the results suggest that Be can be used as a tracer for mine tailings as no Be was found in any of the SPM samples from the control stations but was found in all other samples including those from L8, Masahet Island indicating that the mine tailings are reaching this area.

3.5.5 Benthos

The results show clearly that mine tailings deposition east of Lihir has a significant impact on macrofaunal communities at all three sampled depths. Macrofaunal numbers and diversity were very low relative to unimpacted stations at comparable depths to the west of the island. Macrofaunal abundance in natural sediments at the Control stations showed the expected pattern of decline with increasing water depth (Rex *et al*., 2006). Metazoan meiofaunal abundance appeared also to be depressed by tailings deposition, with the magnitude of impact inversely correlated with water depth. The contrast between Impact and Control stations was greatest at

800-850 m and lower at 1715-1750 m, although still statistically significant. At 2020 m there was no significant impact of tailings on total abundance of metazoan meiofauna. However, an effect at 2020 m was still apparent in meiofaunal community structure, with L3 sharing the copepod-dominated pattern seen at L1 and L2. Tailings deposition at L1 and L2 was associated with a complete absence of living benthic Foraminifera in sieve fractions > 250 μm. At 2020 m, numbers of calcified Foraminifera did not differ between Control and Impact stations but organic-walled taxa were absent from the tailings-affected station.

There are no previous published studies of biological responses to DSTP but some comparisons can be made with studies of shallow-water communities exposed to tailings deposition. Studies in Greenland and Chile have both shown significant effects of tailings deposition on coastal meiofaunal communities. Meiofaunal taxa show differential responses to tailings, and both physical and chemical effects can be identified. In northern Chile, meiofauna at tailings-affected littoral stations were significantly less abundant and diverse than at reference stations (Lee and Correa, 2005). In fjordic sediments heavily impacted by discharges from the Black Angel Mine in western Greenland, benthic Foraminifera disappeared almost completely during the period of tailings disposal, but recolonisation was rapid after the termination of mining activity (Elberling *et al*., 2003). The absence of forams from stations L1 and L2 is consistent with this pattern, while results from L3 suggest that calcified taxa may be more rapid colonizers of tailings-impacted sediment than organic-walled species.

Recently-published results of shallow-water field experiments using tailings from the Batu Hijau copper/gold mine in Indonesia showed that meiofaunal abundance returned to levels statistically indistinguishable from natural unaffected controls after 203 days (Gwyther *et al*., 2009). Harpacticoid copepods were the most rapid initial colonizers, probably reaching the sediment mesocosms on drifting debris. Nematodes had returned to community dominance after 203 days. The results from Lihir are fully consistent with this pattern. Copepod dominance was found at all three tailings-affected stations, contrasting with the more even nematode/copepod community in natural sediments.

Shallow-water studies of macrofaunal community responses to tailings deposition agree in showing significant declines in total abundance and diversity in heavily-impacted areas (Olsgard and Hasle 1993; Burd *et al*., 2000; Lancellotti and Stotz, 2004). Impacts seem to be largely attributable to the physical effects of smothering and sediment instability, with little evidence of any additional effect of heavy metals or other toxic contaminants. Results from Lihir indicate a

major impact of DSTP on macrofaunal communities, with numbers and diversity being significantly depressed relative to natural sediments even at the greatest depth sampled (2020 m).

Distribution of metazoans across the upper 5 cm of the sediment column did not appear to be significantly affected by tailings at any station. The occurrence of > 70% of the total fauna in the surface 0-1 cm layer at 1715-1750 m and 2020 m is a typical pattern for deep-sea sediments, arising from the dependence of the biota on organic matter settling from the overlying water column (Shirayama, 1984b). At L1 (850 m), the apparently more even depth distribution of metazoans may be a consequence of rapid burial at this station closest to the tailings outfall. It is also possible that the apparent distribution may be partly an artefact. It was difficult to avoid some disturbance to the thick layer of unconsolidated surface material when removing tubes from the corer and setting them on the processing stand, and tiny infauna could easily have been redistributed in the highly fluid sediment.

The reader is directed to section 4.5.6 for a comparison of impacted stations at Lihir and Misima.

3.5.6 Seabed photography

The images from station L1 indicate high water column turbidity associated with the tailings outfall further up-slope, and are consistent with the thick layer of fresh tailings found on cores from this station. The invisibility of the seabed in this deployment prevents any visual assessment of the large-scale distribution of tailings across the seabed. Additional deployments of a photographic system would be necessary to determine whether high turbidity is a permanent or intermittent feature at this depth.

The "bed-hop" camera system is not designed or well-suited for use on steep, rocky or irregular seabeds, but the images obtained from L4 provide some information on the benthic environment at a depth similar to station L1 but not affected by tailings deposition. As would be expected, the seabed appears to be patchy and irregular, with expanses of muddy or sandy sediment and localized steeper slopes or outcrops of silty bedrock. The presence of terrestrial plant debris on the seabed is to be expected given the steep gradient and dense vegetation along the western side of Lihir island. The stalked crinoids visible in one photograph are characteristic inhabitants of hard substrata at bathyal depths in the tropical western Pacific (Ameziane and Roux, 1997).

3.5.7 Zooplankton

The discussion of the zooplankton results is identical for both Lihir and Basamuk (section 2.5.7) and is not repeated here.

3.5.8 Microplankton

The predominance of diatoms at stations L6 and L8, and their presence in relatively high numbers, suggests an environment characteristic of near-shore waters which are relatively rich in nutrients. The presence of substantial numbers choanoflagellates at 10 m depth at station L6 indicates the presence of an abundant population of bacterivores.

3.6 Summary

This is the first replicated study of the benthic and seabed geochemical impacts of a DSTP system using state-of-the-art sampling and analytical equipment in the world. This study has revealed the extent of the difference in the biological assemblages present in impacted versus references stations. In short, the differences are very large and profound. However, it is interesting that despite the very high flux of tailings to the sea bed there are still measurable numbers of meiofauna in the surface layers of the sediment, increasing at the more distant impacted stations.

The sedimentary geochemistry of the impacted stations is profoundly altered from reference conditions with much higher concentrations of a broad suite of metals in both solid phase and pore-waters including some ecotoxic elements such as copper, cadmium and arsenic.

Suspended particulate material was found at several depths within the water-column to the east of Lihir with quite high levels of particulate arsenic especially at the stations near to the DSTP discharge point. High levels of suspended particulate materal found in the surface layers of the water column are more likely to have come from surface runoff from the mine rather than from the mine tailings.

4. After DSTP: the Misima Study

4.1 History of operations at Misima

Misima Mine was a large scale, open pit, gold and silver mine, located at the eastern end of Misima Island, within the Louisiade Archipelago, 600 km east of Port Moresby in Papua New Guinea (Figure 4.1.1). Misima Island is a large mountain jutting out of the sea with fringing coral reefs very close to the shore, and steep submarine slopes to the south that extend down to a depth of 1500 m in the Bwagaoia Basin. Alluvial gold was discovered on the island in 1888, and between 1889 and 1989, approximately 250,000 ounces of gold were produced from alluvial and underground workings (Misima Mines Ltd 2000).

Placer acquired an interest in the deposit in 1977 and began exploration. Environmental monitoring projects were initiated in 1982 by NSR environmental consultants and a final environmental plan was completed early in 1987. Government approval for the mine was granted in 1987 under the terms of the *Environmental Planning Act* 1978, and a Water Use Permit for DSTP under the *Water Resources Act* 1982 was obtained. Construction of Misima mine began in 1988 and mining operations commenced in 1989 (Misima Mines Ltd 2003). The mine closed in May 2004 following depletion of the mineable reserves, and the decommissioning and deconstruction process is still ongoing.

In the context of DSTP, Misima was the first case outside Canada (Island Copper and Kitsault Molybdenum mines) in which DSTP was publicly documented from conception, through construction, to operations (Jones and Ellis 1994). The mine at Misima was the first waste disposal system to use 'very deep' tailings disposal, with the bathyal plain (1000-1500 m) in Bwagaioa Basin as the target area for its final tailings deposition zone (Jones and Ellis 1994; NSR 1997).

Figure 4.1.1 Location of Misima Island and Misima mine site, including the location of the DSTP pipeline on Misima Island (source: Misima Mines Ltd, 2003)

The decision to allow DSTP was made after a comprehensive evaluation of alternative waste disposal options. Factors considered in the selection of deep ocean disposal as the preferred waste disposal option included:

- Flat and gentle sloping land suitable for waste impoundment structures was in productive agricultural use, supporting the island's subsistence gardeners.

- Waste impoundment structures had to be located in the forested and mountainous hinterland to avoid use of agricultural land.

- Impoundment structures in mountainous terrain had to withstand severe seismic activity and cyclonic rainfall events.

- Impoundment structures in the mountainous hinterland posed a safety risk to the coastal villages below.

- The steep drop-off near shore on the south coast of Misima allowed discharge of tailings to the deep ocean floor.

- Fishing was limited to the shallow-water reef, with no deep-water fishery development.

- The risk of tailings upwelling to the surface waters could be minimised by locating the tailing outfall terminus below the mixed layer depth (MLD).

4.1.1 Deep-sea tailings disposal system at Misima

Tailings from the mill's carbon-in-pulp tanks were pumped to a counter-current decantation circuit that thickened the slurry. Within the circuit, the tailings were washed with freshwater to recover as much as possible of the dissolved cyanide and metals. An automatic sampling device in a small compartment located within the tailings collection tank monitored the tailings for metallurgical and compliance sampling. Seawater was added to the thickened tailings in the collection tank to produce a slurry (50% solids by weight), which then flowed though a pipeline to the mixing/de-aeration tank, where it mixed with seawater drawn from a depth of 82 m to obtain a nominal ratio of seven parts seawater to one part tailings slurry. The resultant mixture had a density of about 1.08 g cm^{-3}, compared with ca. 1.02 g cm^{-3} for seawater density (NSR 1987). The development of the density differential drives the discharge through the outfall pipeline, which terminated at a depth of 112 m on the steep submarine slope (>45°), approximately 200 m offshore from the mixing tank (Figure 4.1.2). The outfall terminus was located below the euphotic zone (80 m) and deepest mixed layer depth (95 m) to minimise the risk of tailings upwelling to the surface.
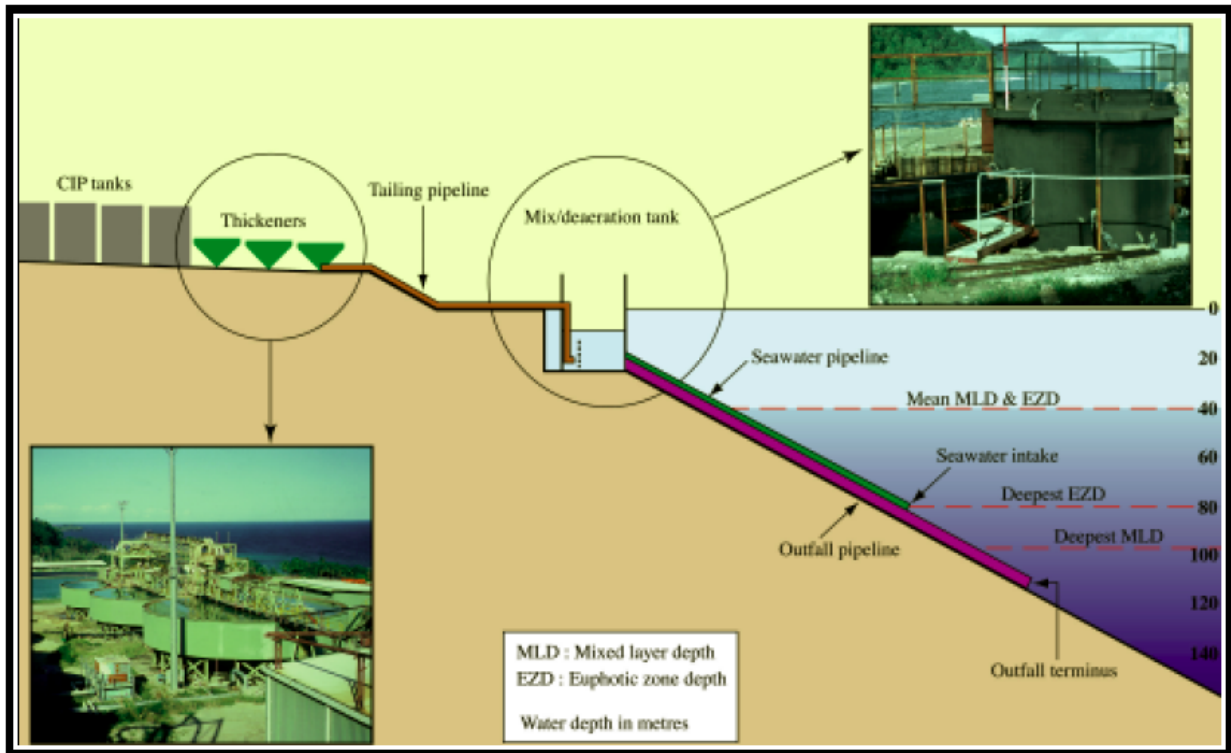
Figure 4.1.2 Schematic cross section of the DSTP system at Misima (source: NSR 1997).

The tailings exited the outfall as a turbulent jet and continued to flow down the slope, eventually forming a coherent density current. Additional dilution of the tailings is achieved by seawater being entrained within the density current as it flows down the slope. Modelling work predicted that the discharged tailings should be diluted 3000 to 5000 fold on reaching the 1200 m mixing zone compliance boundary (Hay and Co. 1997, cited in Misima Mines Ltd 2000). Although the bulk of the tailings discharge was predicted to remain as a bottom attached density current until reaching the floor of the Bwagaoia Basin, dilute mid-water plumes did break off from the main current, particularly along areas of strong density discontinuities at depths of 250 to 450 m (NSR 1996). Seismic profiling located the main tailings deposition zone between 950 and 1500 m below sea level, covering an area of approximately 20 km^2 (Figure 4.1.3). The thickness of the tailings deposited within this area ranged from 1.5 to 75 m deep.
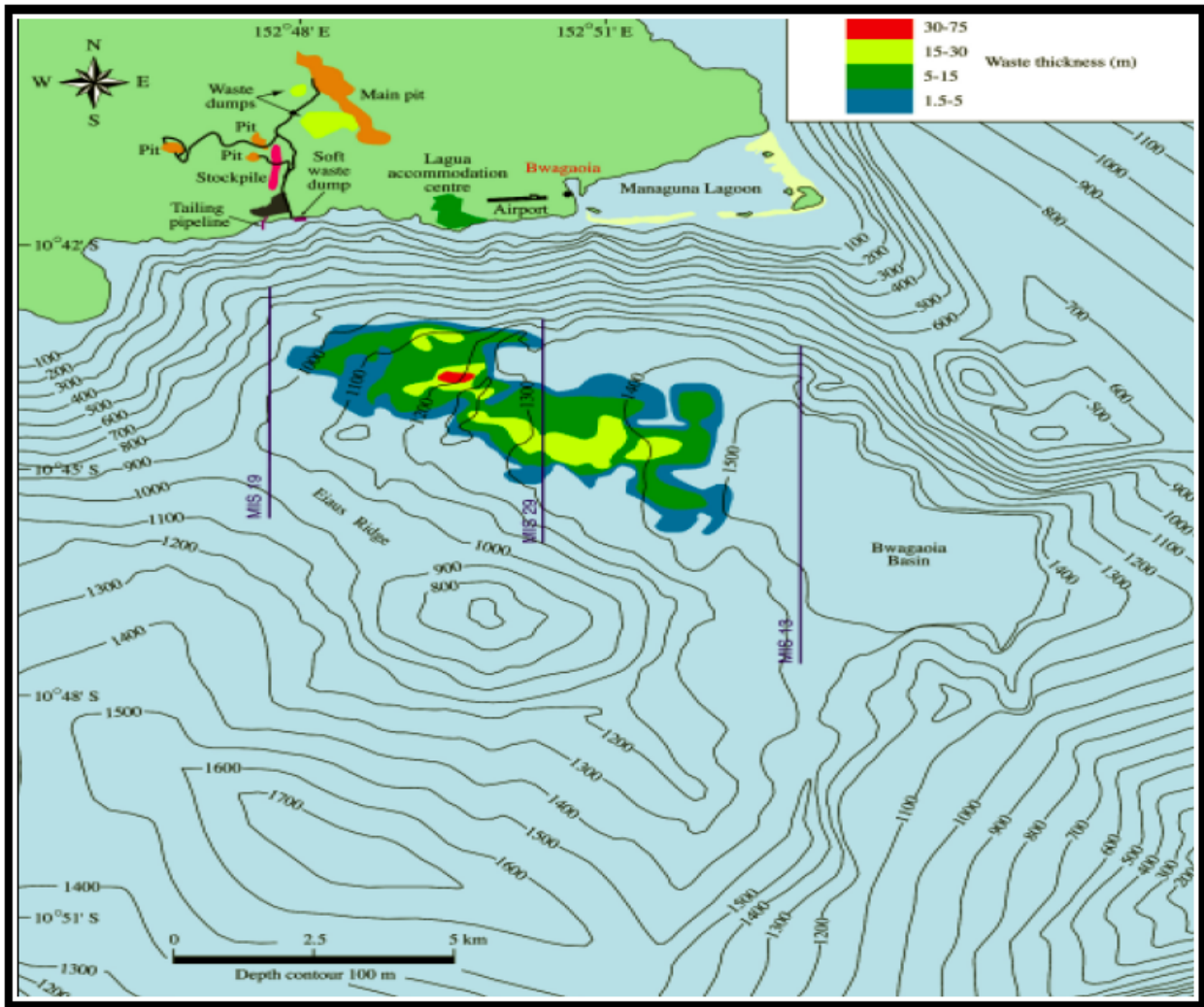
Figure 4.1.3 Bathymetry of the Bwagaoia basin showing the area and thickness of tailings and soft waste deposition from Misima Mine (source: Misima Mines Ltd, 2000; NSR, 1996).

The gold extraction process involved cyanide leaching, so residual quantities of cyanide were present in the tailing effluent. Before being released into the sea the tailings were diluted on shore with seven parts of seawater to one part tailing in an engineered "mixing tank" to reduce the concentration of residual cyanide and other contaminants to a level acceptable for deep ocean discharge. Following dilution, cyanide concentrations in the tailings still remained higher than Papua New Guinea's water quality criteria for seawater. Consequently, Placer Dome was granted a very large area in the sea around the outfall of the pipe, the mixing zone, within which concentrations of cyanide and other chemicals exceeded the water quality criteria. The mixing zone extended 42 m above the pipe terminus (at a depth of 112 m), and 488 m below the pipe (Figure 4.1.4 and 4.1.5). The mixing zone was about 2.5 km wide at the top, tapering down to about one km wide at the bottom.
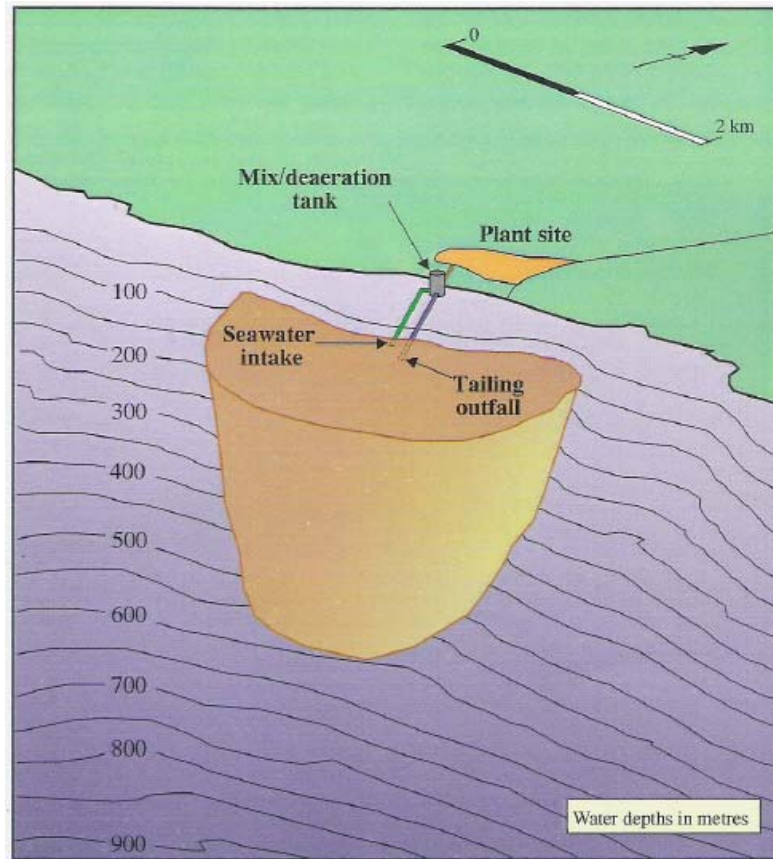
Figure 4.1.4 Three-dimensional projection of the allowable mixing zone for submarine tailings disposal at Misima. The upper surface is 70 m below the ocean surface and the vertical component is at a radius of 1200 m from the mixing/de-aeration tank (source: NSR 1997).
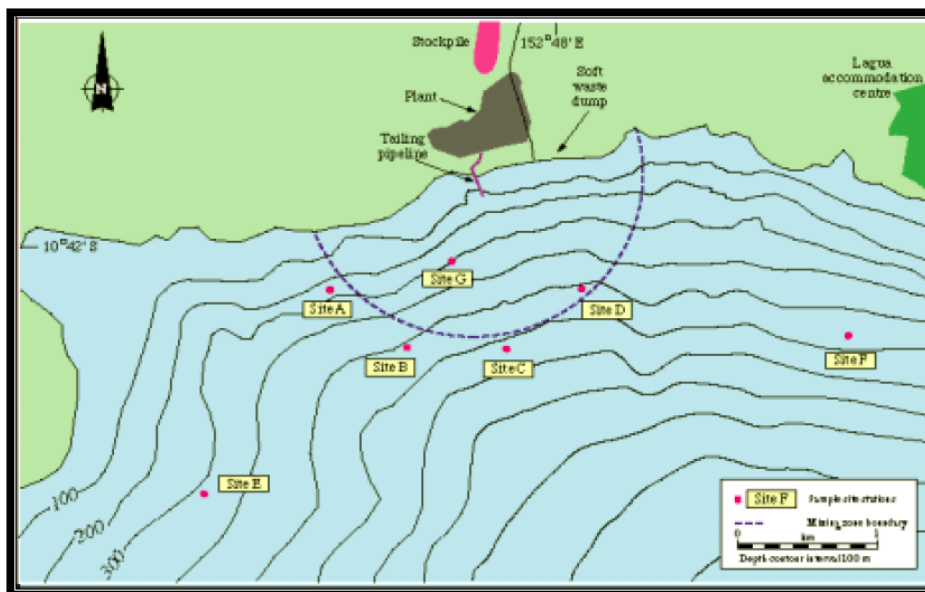
Figure 4.1.5 Location of the mixing zone boundary and monitoring stations at Misima Mine (Misima Mines Ltd, 2000).

Between 1989 and June 1996, Misima Mine discharged more than 42 M tonnes of tailing via the deep sea tailings pipeline (Figure 4.1.6). Mining ceased in 2001 but processing of stockpiled ore continued until May 2004 when a total of 90 M tonnes of tailing had been discharged.
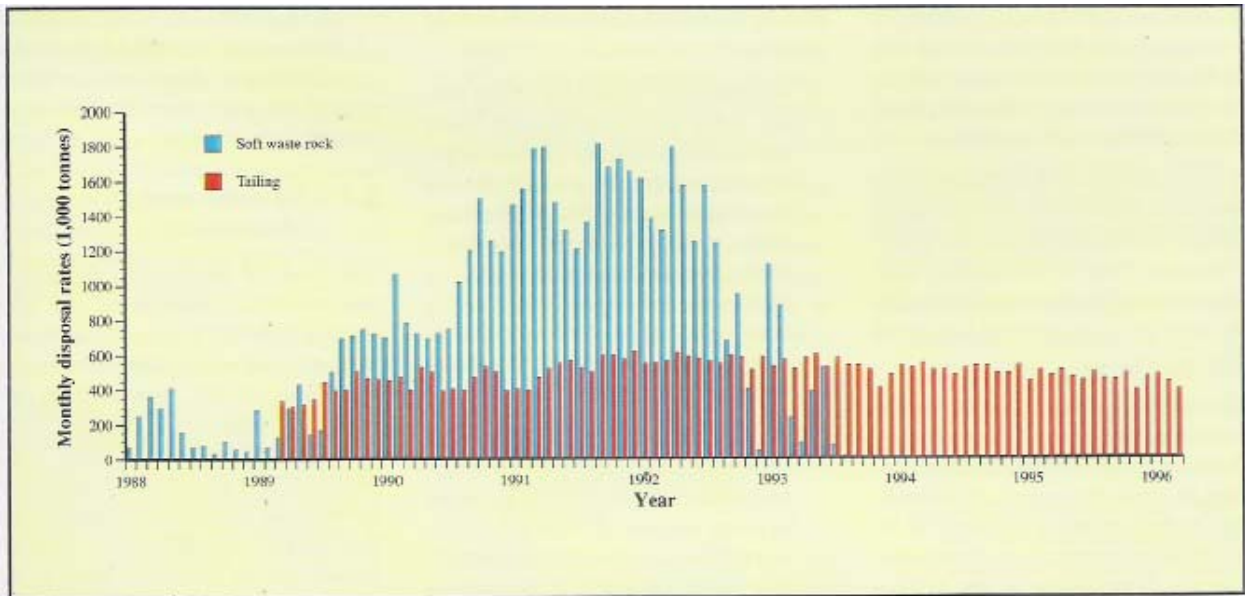
Figure 4.1.6 Monthly ocean disposal rates of waste rock and tailings from Misima Mine between 1988 and 1996 (NSR 1996).

4.1.2 Environmental monitoring of DSTP at Misima

A five year environmental impact programme prior to construction of the mine established the existing environmental conditions at Misima (NSR 1988). Emphasis was placed on monitoring marine impacts and focused on fringing coral reefs as fisheries at Misima are exclusively in shallow water (NSR 1988). An intensified monitoring programme during mine construction focussed on sedimentation impacts resulting from increased erosion from disturbed areas (NSR 1988, 1989).

Monitoring during mine operations included compliance validations of the DSTP system: (i) fortnightly analysis of the tailings effluent prior to mixing with seawater; (ii) monthly determination of the mixed depth layer (MDL) to determine its depth in relation to the deep-sea pipe terminus to assess the possibility of tailings upwelling into shallow water; and (iii) quarterly sampling of the mixed layer for physico-chemical parameters (metals, cyanide, TSS).

Concentrations of dissolved metals in 24 h composite samples of tailings effluent were generally orders of magnitude below compliance levels (Misima Mines Ltd., 2003). Concentrations of copper

and cyanide were the only parameters in the tailings discharge that approached, and occasionally exceeded, compliance limits during the operational life of the mine (Figure 4.1.2.1).

Deep-sea pipe incidents at Misima

In July 1997, the deep sea tailings pipe broke at a depth of 55 m due to a submarine landslide caused by localised failure of the steep submarine slope. The pipe continued to discharge tailings at this depth until it was fixed six months later.

In December 2001, the deep-sea pipe was damaged at a depth of 14 m, approximately 90 m from the shoreline, releasing tailings into the shallow euphotic zone through a split in the pipe (Misima Mines Ltd, 2001). The majority of the escaped tailings were reported by the mine company to behave in the normal manner, forming a density current that flowed down the submarine slope to depth. The processing plant was shut down after discovery of the split and re-started with the tailings system operating in reverse so that tailings were deposited at a depth of 60 m on the submarine slope using the seawater intake pipe. Normal operations using the deep-sea pipe recommenced in February 2002.

In 2002, tailings were again discharged down the seawater intake pipe for several weeks while the deep-sea pipeline was re-sleeved with a smaller diameter pipe.
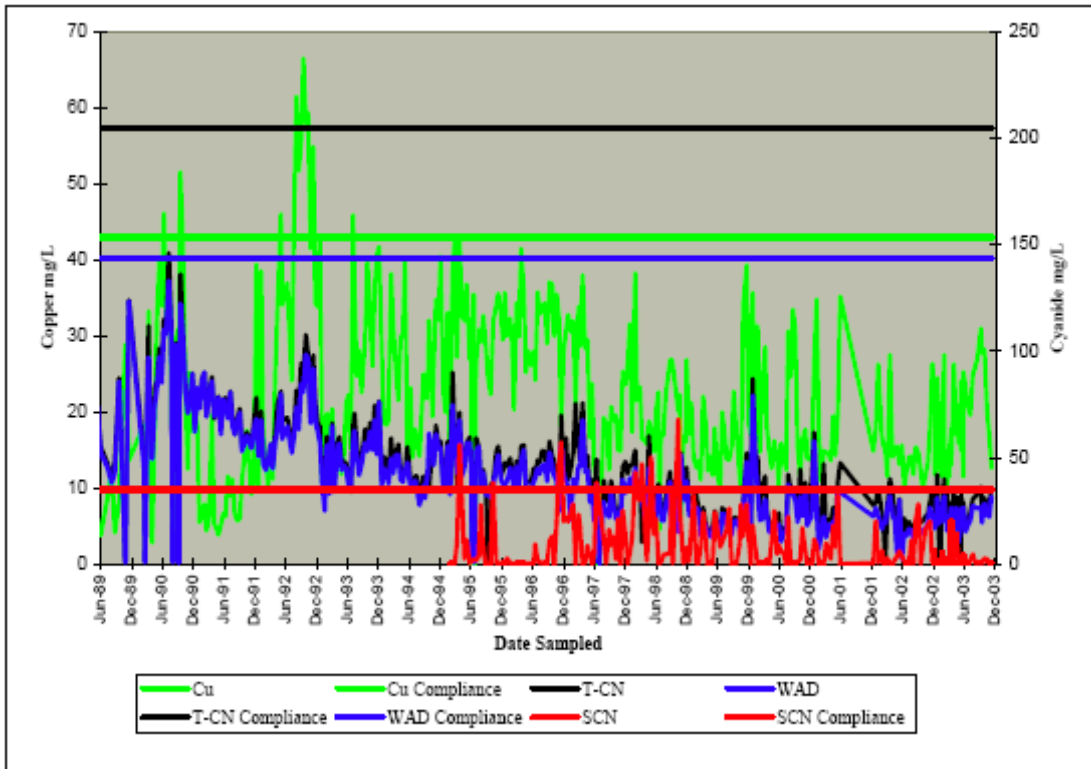
Figure 4.1.2.1 Copper and cyanide species concentrations in tailings discharge from Misima Mine from June 1989 to December 2003 (Misima Mines Ltd 2003). Total cycanide (T-CN), Weak acid dissociable cyanide (WAD), Soluble cyanide (SCN).

4.2 Environmental background

4.2.1 Geomorphology

In contrast to the dynamic collisional tectonic setting of Lihir Island, Misima Island formed as part of rifted continental crust, the eastward extension of the Papuan Peninsula. The crust in this region has been stretched, separated and extended by active sea floor spreading in the Woodlark Basin, north of Misima (Taylor, *et al*., 1995, Hall, 2002). Spreading is suggested to have begun about 6Ma, with ocean crust formation, rifting of the Papuan Peninsula and the development of the metamorphic core complexes of the D'Entrecasteaux islands (Taylor *et al*., 1995 and 1999). Metamorphic rocks comprise the majority of Misima Island, being mostly greenschist facies associations of Cretaceous-age psammopelitic metasediments enclosing Miocene-age mafic igneous rocks (Clarke *et al*., 1990, White *et al*., 1995). The epithermal Umuna gold and silver deposit on Misima Island is hosted within a 100-300 m wide zone of fractures, veins, anastomosing shears and breccia sheets that can be traced over a 3 km strike length. Estimated gold grades of 1.4 g t^{-1} and silver grades of 21 g t^{-1} have been reported (White *et al*., 1995, Clarke *et al*., 1990 and Lewis and Wilson, 1990).

The Misima DSTP was located off the southeast coast of the island. This area of seafloor is characterised by a steep submarine slope, to the south and east, descending to over 1200m 5km offshore. The deepest point of the margin has been informally termed the Bwagaoia Basin (NSR, 1996 and 1997). The southern boundary of the basin is formed by the ridge termed the Eiaus Ridge trending east-southeast from Eiaus village and extending to Renard Island. The eastern boundary is formed by a broad un-named ridge between the southeast tip of Misima Island and the Renard Islands. The inshore region of the island is dominated by a fringing reef typically less than 100m wide. At peak production, the Misima mine produced 20,000 tonnes of tailings per day.

4.2.2 Physical Oceanography

Like Lihir, Misima Island (152° 45' E, 10° 40' S) is located at the western end of 14,000 km of unbroken Equatorial Pacific Ocean. From an oceanographic point of view it is relatively small, with major dimension of order 10 km (much less than the internal Rossby radius), and a very small shelf regions surrounded by extremely steep bathymetric slopes leading very quickly to depths of 1000 m (well below the surface current system).

The island is located on the southern edge of the Solomon Sea in a region of weak and variable flow throughout the year.   Much less appears to be known about the deep sea oceanography along the southern side of the Solomon Sea near Misima than is the case for Lihir. In the absence of reports to the contrary it has been assumed that the oceanic conditions near Misima are not dissimilar to those at Lihir, with the caveat that Misima is significantly further from the Equator and so the Earth's rotation will play a bigger role in determining the local ocean structure.

One difference that may have a bearing on the observations at Misima is the nearby presence of the islands of the Louisiade Archipelago and the shallow reefs between some of them which may give rise to significant internal tides and local internal mixing.

4.2.3 Sediments

A short (<1m) gravity corer was deployed at Misima (1994) by the University of Sydney in order to confirm the results of the seismic survey and define the extent of the mine-derived sediment accumulations. Unfortunately the maximum length of core recovered was only 0.6m, compared to the thinnest sediments identified from the seismic reflection profiles being 1.5m thick. Therefore the core samples could not be used to map the extent and thickness of the mine-derived sediment. A thin (<0.1m) deposit was identified from the cores as a surficial layer throughout the Bwagaoia Basin. The mine-derived tailings, determined from gravity cores were soft, brown muds

readily distinguished from the green-grey carbonate ooze of the natural underlying ocean sediments (NSR, 1997).

4.2.4 Benthos

Published information on the deep-sea benthos of the Misima region is very limited. Standing stocks of benthic bacteria, micro- and meiofauna on the Queensland continental slope and Coral Sea Plateau were described by Alongi (1987) and Alongi and Pichon (1988). Alongi (1990, 1992) later extended this work to a series of stations from the Coral Sea to the Woodlark Basin off the eastern tip of Papua New Guinea. Collectively these studies provide baseline data on standing stocks of the smallest size fractions of the deep-sea benthos (bacteria to metazoan meiofauna) in the region of interest. They provide very limited information on the macrofauna, but none on the largest benthic animals (megafauna).

Misima island lies within the *Western Pacific Archipelago Deep Basins* biogeochemical province defined by Longhurst *et al*. (1995). Planktonic primary production in this area is estimated as ~ 100 g C m^{-2} year^{-1}, a relatively low figure by global standards. The oligotrophic ocean environment around Misima will be reflected in a low rate of flux of sinking organic matter to the deep-sea bed, although some additional input is provided by terrestrial plant detritus carried in riverine outflow from New Guinea (Alongi, 1990). With the localized exceptions of hydrothermal vent and cold seep ecosystems, the deep-sea benthos is reliant on the supply of organic matter from surface waters and consequently benthic standing stock (abundance and biomass) typically declines with increasing water depth (Gage and Tyler, 1991). The gradient of the depth-biomass relationship varies according to body size, with numbers of larger animals declining more rapidly than smaller ones (Rex *et al*., 2006). Because of the limited organic input, the deep sea around Lihir and Misima would be expected to support a lower benthic standing stock than is found at comparable depths in more productive ocean regions such as the north-east Atlantic, with the contrast being most pronounced for megafauna and least for the smallest size classes of organisms.

Sediments in the deep Coral and Solomon Seas are moderately/poorly-sorted calcareous oozes mainly of pteropod and foraminiferal origin (Shirayama, 1984a; Alongi, 1990). Organic carbon content is relatively low (0.3 – 0.6%) and varies little with depth (Alongi, 1992). Alongi (1987) proposed that the low sediment organic content, combined with high densities of Foraminifera and other protists, are indicative of rapid microbial activity and detrital turnover in surface sediments, resulting in very low rates of carbon burial.

Comparison of meiofaunal or macrofaunal densities recorded in different studies must be made with caution since results can be biased by sampling technique (Bett *et al*., 1994) and by the use of different sieve mesh sizes to define faunal categories (Gage *et al*., 2002). It is often not possible to make post-hoc 'corrections' for these confounding factors in the summary data presented by authors in their published work. With this caveat in mind, table 4.2.4.1 summarizes available data on densities of metazoan meiofauna and macrofauna at deep-sea stations in the Coral Sea (Alongi, 1992). Values for the same depths predicted from empirical relationships based on global data compilations (Rex *et al*., 2006) are also shown for comparative purposes.

Table 4.2.4.1 Densities of metazoan meiofauna and macrofauna at deep-sea stations in the Coral Sea (Alongi, 1992) with values for the same depths predicted from empirical relationships based on global data compilations (Rex *et al*., 2006).

Location	Depth m	Meiofaunal density ind. 10 cm^{-2}	Rex et al.,(2006) prediction	Macrofaunal density ind. m^{-2}	Rex et al.,(2006) prediction
Papuan Slope, northern Coral Sea	695	1580	344	736	2251
Coral Sea Plateau	1454	194	351	120	1380
Queensland Trough	2256	172	310	280	823
Woodlark Basin	2395	172	303	316	752
Papuan Slope, northern Coral Sea	2426	181	301	273	737
Woodlark Basin	2775	106	285	87	589
Woodlark Basin	2800	131	284	173	579
Papuan Slope, northern Coral Sea	3264	151	264	134	430
Coral Sea Basin	4008	126	235	56	266
Coral Sea Basin	4350	99	223	163	213

With the exception of Alongi's (1992) 695 m station on the Papuan Slope, which supported an extremely high density of turbellarian flatworms, observed meiofaunal densities are fairly consistent with the global bathymetric trend outlined by Rex *et al*.,(2006). Apparent differences

are mostly in the direction of lower densities in the Coral Sea, possibly reflecting the oligotrophic environment of the region. With the exception of the turbellarian-dominated station noted above, nematodes were the most abundant metazoan taxon at most localities. Alongi (1992) reported that meiofauna were heavily concentrated in the uppermost few centimetres of sediment, again with the exception of the relatively shallow (695 m) station on the Papuan Slope.

Observed macrofaunal densities are generally lower than predicted by the global data compilation of Rex *et al*.,(2006), probably as a consequence of the oligotrophic environment of the Coral Sea. Alongi (1992) recorded only the percentage representation of polychaetes, crustaceans and bivalves in his samples. As a result there is no published information on functional group composition, family or species-level diversity of the deep-sea macrofauna in the Misima region.

4.3 Methods

4.3.1 Cruise summary

The sampling and measurement at Misima was undertaken within the same cruise that was used to obtain the Lihir samples (Appendix 7) and measurements. Please see section 3.3.1 of this report for details of the section of the cruise pertaining to the Misima sampling.

The cruise took place from 25th November to 9th December 2007 using the MV Miss Rankin equipped with a winch and crane supplied by Lihir Gold Limited.

The sampling at Misima included the collection of 108 sediment cores for chemical and biological analysis from 6 stations. At 4 stations sediment cores were processed to extract pore-water which was collected to provide samples for nutrient and metal analysis. Water column sampling included 8 CTD casts and collection of 17 suspended particulate material samples from 2 stations. In addition the water column was sampled to provide nutrient and chlorophyll samples for calibration of the CTD sensors.

On the 7th December at station M1, Misima, the winch rectifier failed on the second drop of the CTD with 200m wire out. The CTD was recovered using manual un-braking. After contacting LGL, it became apparent that no spare rectifier had been left with the winch. Therefore no further sampling was possible and the ship prepared for transit back to port in Port Moresby.

As a consequence, at Misima approximately 85% of the planned sampling was completed. The sediment sampling was 100% completed but only 2 stations were sampled for water column measurements and no zooplankton sampling was possible at this site.

4.3.2 Bathymetry and Acoustic Character

Seabed surveys were conducted using the Mk III Echotrack dual frequency (12 and 24 kHz) echo-sounder. The system was used in single frequency (12 kHz) mode from a pole mounted transducer from the starboard aft side. The analogue sounder had a thermal paper trace. All stations were subject to a brief echo-sounder survey to enable the corer to be safely deployed in a known water depth. Also obtained were longer echo-sounder profiles used to develop a working model of the sedimentary setting of the margin and the seabed morphology. Typically these profiles were up to 10 km long and run either perpendicular or parallel to the slope.

4.3.3 Physical Oceanography

The methodologies for taking physical measurements at Misima were the same as those for Lihir (see Section 3.3.3).

4.3.4 Stations selected
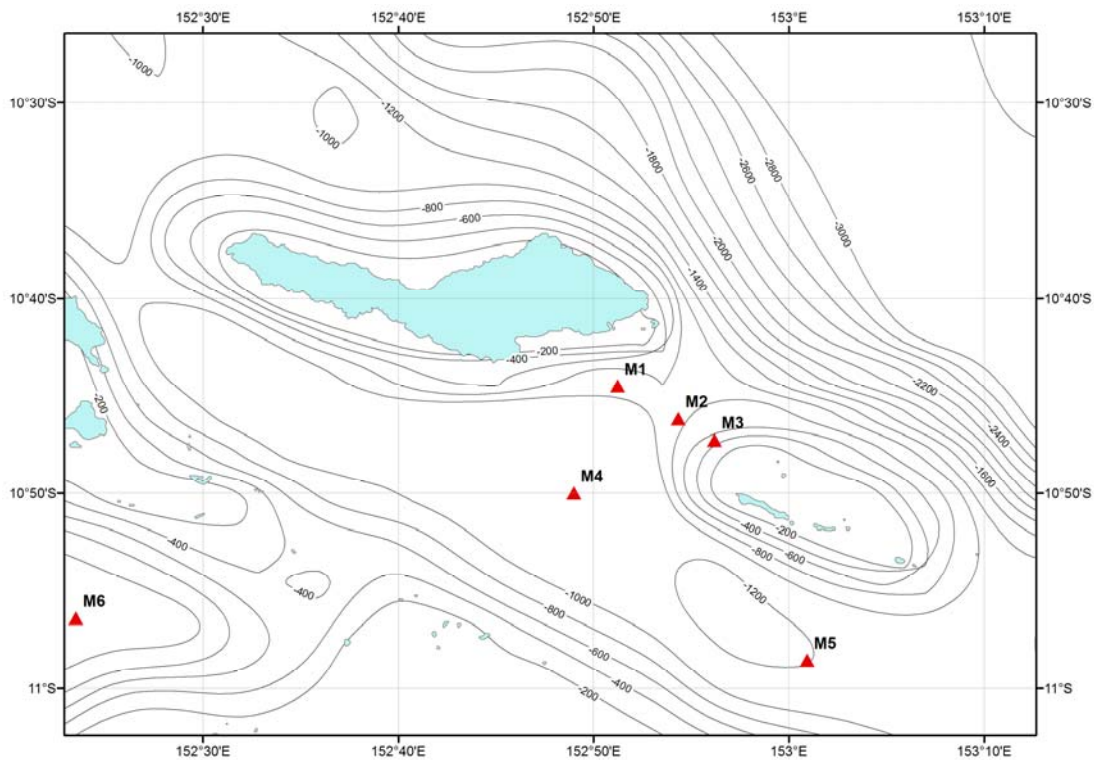
Figure 4.3.4.1 Chart showing station positions at Misima

Table 4.3.4.1 Station positions (conversion from WGS84 to AGD84 by Geocentric Translation (tx=134, ty=48,tz=-149) and depths (m).

	WGS84		WGS84			AGD84 UTM56	
Stn	Latitude deg	mins	Longitude deg	mins	Depth	Easting	Northing
M1	10	44.500	152	51.242	1380	483936	8812412
M2	10	46.184	152	54.356	1461	489612	8809311
M3	10	47.280	152	56.210	1467	492991	8807292
M4	10	50.000	152	49.000	1793	479857	8802274
M5	10	58.561	153	40.943	1704	501613	8786503
M6	10	56.425	152	23.503	1250	433430	8790373

All gear deployments were at the nominal station position. Station keeping was generally very good and always within 100m of the nominal station.

Table 4.3.4.2 Bedhop camera deployments

Station	M1	M5
Depth m	1380	1704
No. seabed contacts	25	24
Position, initial seabed contact	10^0 44.70' S 152^0 51.08' E	10^0 58.50' S 153^0 00.94' E
Position, final seabed contact	10^0 44.56' S 152^0 50.94' E	10^0 58.41' S 153^0 00.79' E
Results	22 seabed images	24 seabed images

4.3.4 Sediment sampling and sedimentology

All coring was carried out using the SAMS megacorer using the methods outlined in section 2.3.5.

4.3.5 Sediment geochemistry

Sample collection and processing methods were identical to those described for the Basamuk study in section 2.3.6.

4.3.6 Benthos

Sample collection and processing methods were identical to those described for the Basamuk study in section 2.3.8.

Polychaete community structure at the Family level was compared at the six Misima stations using individual corer drops as replicates. Corer drop abundance data for each family were standardized to ind. m^{-2} to correct for differences in the number of individual cores analyzed per drop. Communities were compared using hierarchical cluster analysis of Bray-Curtis similarities and non-metric multidimensional scaling (nMDS), all carried out using PRIMER^{TM} version 5 (Clarke and Warwick, 2001). Correlations between polychaete community structure and a range of environmental variables were examined using the BIO-ENV procedure in PRIMER^{TM}. The variables chosen were water depth and a range of important sediment properties including mean grain size, and percentage nitrogen and organic carbon as indices of sediment nutritional quality. Pore-water concentrations of metals known to have toxic effects (As, Cu, Pb, Cd) were included, along with solid-phase indicators of tailings (Be, Ca, K).

The polychaete family-level composition data were included in the BIO-ENV analysis along with geochemical data measured in one sediment core from each station. Solid-phase and pore-water metal concentration data were available for cores from stations M1, M3, M4 and M5. Only solid-phase metal data were available for M2 and M5. Mean sediment grain size, percentage nitrogen and percentage organic carbon data were available for all stations. For each variable, data were taken from successive 0.5 cm slices extending from the sediment surface to 4.75 cm depth and a mean value calculated for this depth range. This corresponds to the 0-5 cm horizon containing virtually all the sediment biota.

The table below lists the environmental variables used in the BIO-ENV analysis. Metal concentration data are for pore-water concentrations ($\mu g\ L^{-1}$), unless indicated as solid-phase data

by (SP). Solid-phase beryllium is measured in mg kg^{-1} dry sediment, solid-phase calcium and potassium as percentage weight in dry sediment.

BIO-ENV analysis for all six stations was carried out using the variables water depth, mean grain size, % nitrogen, % carbon, and the three solid-phase metal concentration. Pore-water metals could not be used in the six-station analysis as no data were available M2 and M5. In line with recommendations of Clarke and Warwick (2001), % nitrogen, % carbon and metal concentration data were log-transformed. Water depth and mean grain size were not transformed. Environmental data for the six stations were analyzed in BIO-ENV along with family abundance Figures for each station from all corer drops combined and standardized for area (ind. m^{-2}).

Table 4.3.6.1 The environmental variables used in the BIO-ENV analysis

	M1	M2	M3	M4	M5	M6
Core	**MC64-6**	**MC67-4**	**MC47-3**	**MC56-1**	**MC58-6**	**MC63-4**
Depth m	1380	1461	1467	1793	1704	1250
Mean grain size μm	45	30	30	32	60	50
% N	0.020	0.019	0.043	0.085	0.065	0.125
% C$_{org}$	0.266	0.257	0.393	0.620	0.706	1.446
As	2.689		2.387	7.323		6.748
Be (SP)	0.886	1.066	1.026	0.571	0.173	0.109
Cd	11.956		7.166	1.119		0.572
Ca (SP)	3.860	3.998	4.940	18.520	22.058	22.987
Cr	0.526		0	5.764		4.018
Cu	14.728		10.477	16.602		16.463
Fe	155.975		45.025	314.856		121.161

Core	M1 MC64-6	M2 MC67-4	M3 MC47-3	M4 MC56-1	M5 MC58-6	M6 MC63-4
Pb	9.813		3.120	2.017		0.609
Mn	7408.471		4673.193	1319.355		170.091
K (SP)	1.221	1.411	1.346	0.786	0.422	0.508

4.3.7 Seabed photography

Seabed photographs were taken using the "bed-hop" camera system as described in section 2.3.9. Successful deployments were made at stations M1 and M5. A third deployment was aborted as a result of a re-positioned compass arm causing interference with the altimeter beam and preventing assessment of distance from the seabed.

4.3.8 Water column geochemistry

Sample collection and processing methods were identical to those described for the Basamuk study in section 2.3.7.

4.4 Results

4.4.1 Bathymetry and Acoustic Character

The most notable feature of the bathymetry south of Misima is the steep submarine slope. Slope angles of an average of 13° can be encountered. With such steep slopes, combined with a large sediment supply, the natural depositional process will inevitably be down-slope, gravitationally-influenced. During the 2007 survey, it was realised that the bathymetry of the Bwagaoia Basin is poorly known being much more complex than previously surveyed. Unfortunately a detailed bathymetric survey of the region was beyond the scope of this survey. The acoustic character of the margin south of Bwagaoia is characterised by a steep, reflective slope with irregular to transparent, lens-shaped sub-bottom reflectors, approximately 10-15m thick and between 100-300m long (Figure 4.4.1.1). Hyperbolic and faint, diffuse reflections are common on the slope above 1300m water depth. This acoustic character is indicative of debris flows and slumps, possibly relating to the submarine slide in 1997. Below 1400m water depth the basin floor

contains channels with well defined, mounded levees. The channel floors are highly reflective suggesting the presence of coarser sediment.
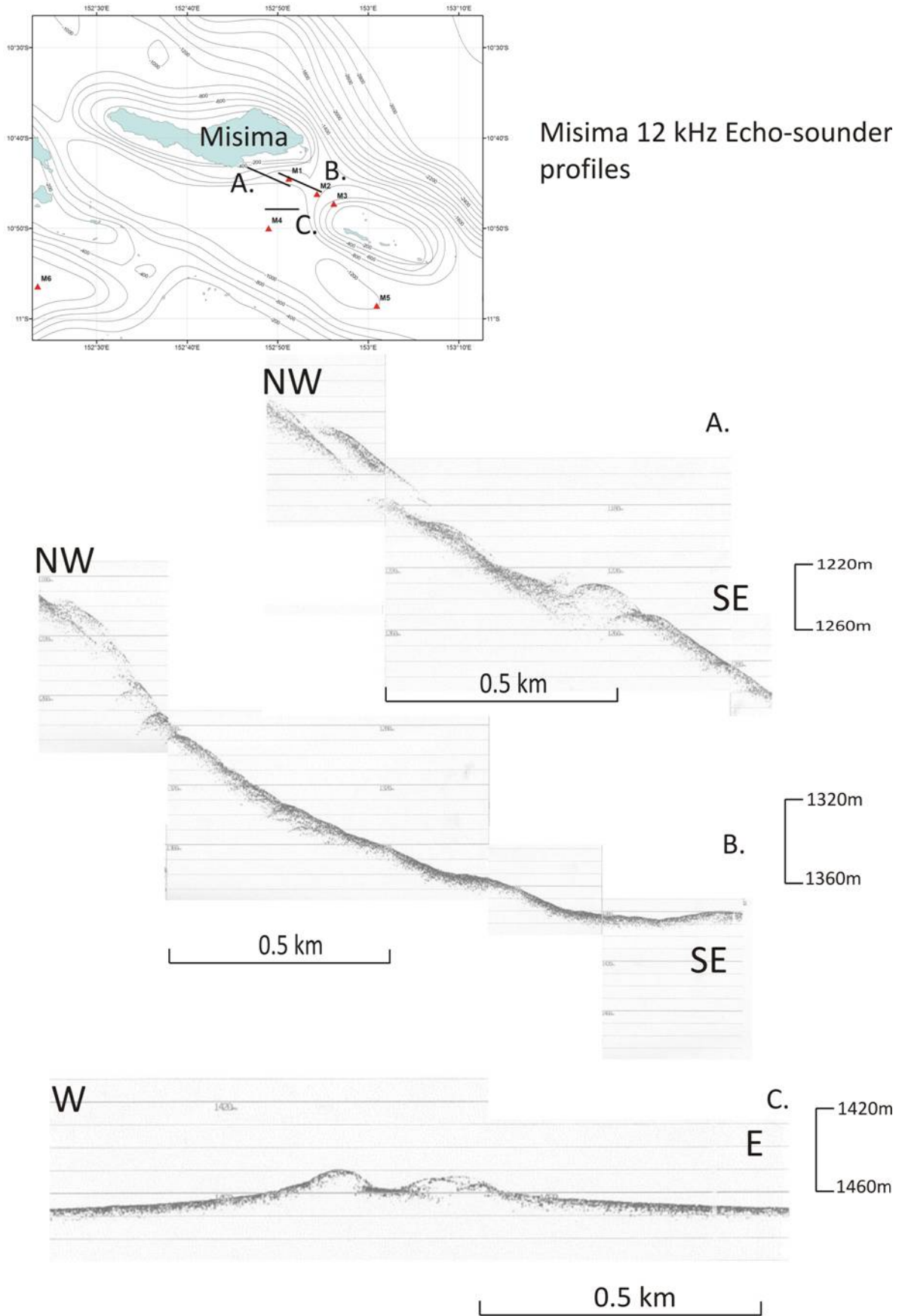
Figure 4.4.1.1 Examples of echo-sounder profiles south of Misima Island.

4.4.2 Physical Oceanography

Only 3 CTD profiles were completed before the winch failed (Table 4.4.2.1)

Table 4.4.2.1 CTD Staion positions at Misima, 2007

Station		Latitude (S)		Longitude (E)		Depth
		(°)	(min)	(°)	(min)	(m)
M1	7 Dec	10	44.50	152	51.24	1380
M2	5 Dec	10	46.18	152	54.35	1461
M5	6 Dec	10	58.56	153	40.94	1704
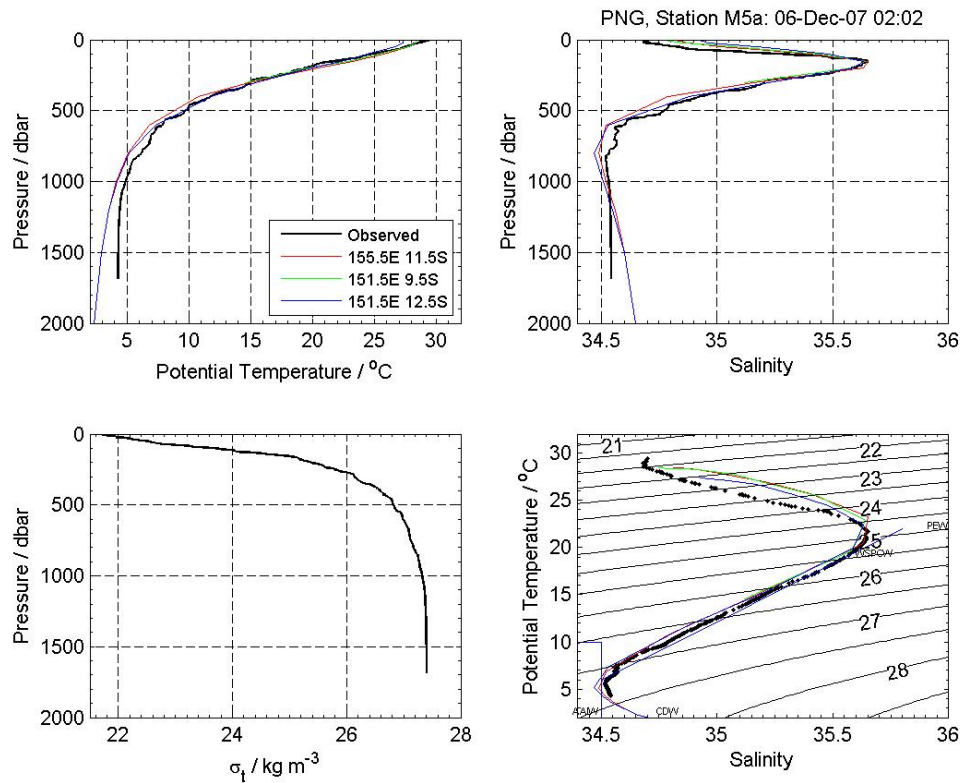
Figure 4.4.2.1 Temperature, salinity and σ_θ profiles at Sta. M6. Also shown is the θS plot.   The red green and blue lines show climatological profiles at the locations in the vicinity of Misima as indicated (http://ferret.wrc.noaa.gov120/las/servlets/dataset)

The climatology profiles, which are taken from deep water locations that bracket Misima, show very little regional variation (Figure 4.4.2.1), although this lack of variation may to some extent reflect a paucity of historical observational data. Down to 1000 m the CTD profiles follow the climatology very closely, although the surface waters are a little fresher. However, the bottom 500 m of the water column is almost isothermal and isopycnal, with the deepest water at 1684 m being 4.25 °C and 34.54 salinity units. Thus the bottom waters are very different from the climatological profiles. It is suggested that this well mixed layer, which was seen at all three stations, may be due to tidal and internal tidal mixing at the seabed, and thus be indicative of strong bottom currents.

4.4.3 Stations selected

Station M1 was selected on the basis of its proximity to the bottom of the slope immediately below the expected route of the tailings outfall. The disturbed and rugged nature of the seabed on the slope above that was apparent from the echosounder profiles precluded coring at shallower depths. M2 and M3 were chosen as representing conditions in the middle and near the end of the long, smooth, tailings-filled Bwagaoia basin (see Figure 4.1.3). Interestingly, although Figure 4.1.3 (taken from Misima Mines Ltd, 2000; NSR, 1996) shows a depth contour at 1500 m, we did not find any depths greater than 1470 m, suggesting that the basin contains a considerable depth of tailings. M4 was chosen as the first control station but visually the cores looked very similar in colour and consistency to the tailings recovered at stations M1-M3. We therefore sought a more distant control station M5 but again we were not able to visually confirm the absence of tailings. It should be borne in mind that whereas at Lihir the tailings have a strong orange colour, the Misima tailings are olive grey and not easy to distinguish visually from natural sediments. In order to be sure of a true reference station, our final station, M6, was located at some distance from the mine and separated by a coral island chain (The Calvados Islands) where no known process could have transported mine tailings. The information that was gained from subsequent benthic and geochemical analysis, present in the following sections, was necessary for *post hoc* discrimination between control and impacted stations.

4.4.4 Sediment sampling and sedimentology

Core log sheets and particle size data summary tables are given in Appendix 1.

Misima Stations M1-M6

Station M1, southeast of Bwagaoia, 1380m water depth. Sediments from station M1, closest to the site of the original tailings discharge (<5km), comprise moderately well-sorted laminated

sands with a sharp contact with poorly-sorted olive, grey sandy mud. Mean grain sizes range from 30 to 80 μm (medium silt to fine sand) in the sandy mud to up to 150 μm in the sandy horizons (medium sand). Sand content is highly variable from 12-80%. Some cores from this station displayed contorted and overturned sand layers (i.e. showing negative grading).

Station M2, southeast of Bwagaoia, 1461m water depth. The sediments at station M2 are homogenous, moderately well-sorted, olive grey sandy mud. Mean grain sizes range from 22 to 77 μm (medium silt to fine sand). Sand content is variable from 4-51%.

Station M3, southeast of Bwagaoia, 1467m water depth. Station M3 produced poorly-sorted, faintly laminated pale brown sandy mud. Mean grain sizes range from 17 to 76 μm (medium silt to fine sand). Sand contents are between 2-43%.

Station M4, south of Bwagaoia, 1793m water depth. The sediments recovered from M4, on the floor of the Bwagaoia Basin were poorly-sorted pale grey sandy mud and bioturbated brown sandy mud. The grey sandy mud occurs as thin (1 cm) horizons within the brown sandy mud. Mean grain sizes range from 17 to 55 μm (medium silt to fine sand). Sand contents are low, between 4-23%.

Station M5, southeast of Bwagaoia, 1704m water depth. Station M5, the most distant from the Bwagaoia site, produced poorly-sorted, pale grey muddy sand with thin well-sorted muddy sand horizons. Mean grain sizes range from 14 to 308 μm (medium silt to medium sand). Sand contents are between 15-30% in the sandy mud but higher and more variable across the sand horizons between 27-73%.

Station M6, southwest of Misima, 1250m water depth. M6, located away from Misima beyond the Calvados Islands to the south, produced very poorly-sorted homogenous pale grey sandy mud. Mean grain sizes range from 38 to 58 μm (medium to coarse silt). Sand content is low at 16-22%.

4.4.5 Sediment geochemistry

The sediments and pore-waters from Misima were analysed for major, minor and trace elements and the combined data were used to evaluate sediment composition and provenance, identify biogeochemical controls and assess any post depositional mobility of elements within the marine environment surrounding Misima Island.

The depth profiles of elemental concentrations for 33 elements within the solid phase and 24 elements in the pore-water of sediments collected from Lihir are presented in Appendix 4B. Depth plots of elemental concentrations for each core are presented in Appendix 4A.

The primary objective of the study was to provide a multi-element geochemical data set that could be used to identify the tailings signature and assess the impact of the tailings on the marine environment surrounding Misima Island and determine if possible, any post depositional mobility of elements associated with the tailings.

There are no published papers on the geochemical composition of sediments surrounding Misima and no analysis was carried out as part of the baseline study before tailings deposition began. As a result the data presented here represent the most comprehensive study of the sediments within the area surrounding Misima Island.

Marine sediments can be broadly described as being a mixture of lithogenic material, biogenic carbonate and silicate and organic matter. Element/Aluminium (Al) ratios can be used to indicate changes in sediment composition that are not caused by lithogenic dilution.

For example, Silicon (Si)/Al, Titanium (Ti)/Al, Magnesium (Mg)/Al can all be used as a proxy for aeolian inputs, Zircronium (Zr)/Al for sediment texture and reworking. However, in the context of Misima this technique is only useful within the natural sediments as the mine tailings will have other controls determining the elemental/Al ratios of the sediment.

The major elemental/Al ratios for the surface sediments are given in Table 4.4.5.1. The ratios for the surface sediment indicate that Ca/Al ratios in the surface sediment vary considerably between stations (0.7 – 57) with stations M2 and M3 having similar ratio of 0.7 and M1 having a higher ratio of 1.05. However stations M4 –M6 have a range of Ca/Al ratios from 4 to 57 with the two control stations M5 and M6 ratios being much higher than the other stations. The K/Al, Mg/Al and Sr/Al ratios also have a wide range with M5 and M6 having the highest ratios and M1-M3 the lowest in all cases. M4 has a ratio higher than M1-M3 but lower than M5-M6. Fe/Al ratios vary from 0.4 to 0.7 with M4 having the lowest ratio. The Ba/Al ratios are very similar at all stations and range from 0.017 to 0.022. Mn/Al ratios are lower for stations M1-M4 than the control stations, M5 and M6.

It is obvious from the surface elemental /Al ratios that stations M5 and M6 are quite different in sediment composition from stations M1-M4 with the Ca/Al, K/Al, Mg/Al and Sr/Al ratios all being considerably higher in the control stations. These stations were located within areas that had a

number of small islands with coral reefs and the elemental ratios would suggest that the material depositing at these stations is being influenced by the coral ecosystems.

Table 4.4.5.1 Elemental/Al ratios in surface sediments for stations L1-L6

Major elemental/ Al ratios in surface sediment

	Ba/Al	Ca/Al	Fe/Al	K/Al	Mg/Al	Mn/Al	Sr/Al	Ti/Al
M1	0.020	1.049	0.660	0.198	0.305	0.023	0.013	0.086
M2	0.018	0.667	0.722	0.210	0.361	0.033	0.007	0.078
M3	0.017	0.704	0.703	0.195	0.371	0.023	0.008	0.073
M4	0.022	4.002	0.618	0.237	0.488	0.021	0.051	0.065
M5	0.017	18.984	0.420	0.440	0.799	0.090	0.344	0.075
M6	0.018	57.135	0.680	0.779	2.365	0.061	0.844	0.058

In order to assess the rate of accumulation of sediments at each of the Misima stations the activity of the naturally occurring radionuclide ^{210}Pb was measured using gamma spectroscopy. A more detailed discussion of this technique is given in section 2.4.5.

The sediment accumulation rates (g cm^{-2} yr^{-1}) and the average linear sedimentation rates (mm yr^{-1}) are given in Table 4.4.5.2 along with the organic carbon content (% wt) and excess ^{210}Pb inventories (Bq cm^{-2}).

Table 4.4.5.2 Organic carbon content, extent of mixing, accumulation rate and excess ^{210}Pb inventories for stations M1 – M6.

Station Misima	Depth m	Organic Carbon %	Degree of mixing	mass accumulation rate g cm^{-2} yr^{-1}	average linear sedimentation rate mm yr^{-1}	xs Pb210 @ surface Bq kg^{-1}	xsPb-210 inventory Bq cm^{-2}	flux Bq g^{-1}yr^{-1}
M1	1380	0.2 - 0.3	mixed but sed rate assessed	0.16, however mixing apparent	1.00	100	1.08	
M2	1461	0.1 - 0.4	mixed, bioturbation or slumping of sediment	NA	NA	200	1.15	
M3	1467	0.2 - 0.5	mixed, peak of Pb-210 at 2-3 cm	NA	NA	30	0.65	
M4	1793	0.6 - 1.0	no obvious mixing	0.17	1.5	880	3.46	20.35
M5	1704	0.6 - 1.5	signs of mixing/bioturbation	0.3	2.0	340	2.13	7.10
M6	1250	0.6 - 1.5	mixing at very surface	0.09	0.8	580	1.88	20.93

The organic carbon content of the sediment varies from 0.1 to 1.5% with stations M1-M3 having the lowest concentrations and M5 and M6 the highest, M4 has an organic content which is higher than M1-M3 but lower than M5 and M6. The higher organic content of the control stations may be influencing the Mn/Al ratios at these stations as a result of biogeochemical cycling.

The major element composition is shown in Figure 4.4.5.1. Stations M1-M3 are the stations on a transect moving eastward away from the mine, station M4 is located south westward of M2. Station M5 is located south eastward from the transect with M6 located south westward from Misima Island (Figure 4.3.4.1). M5 and M6 are assumed to be control stations.
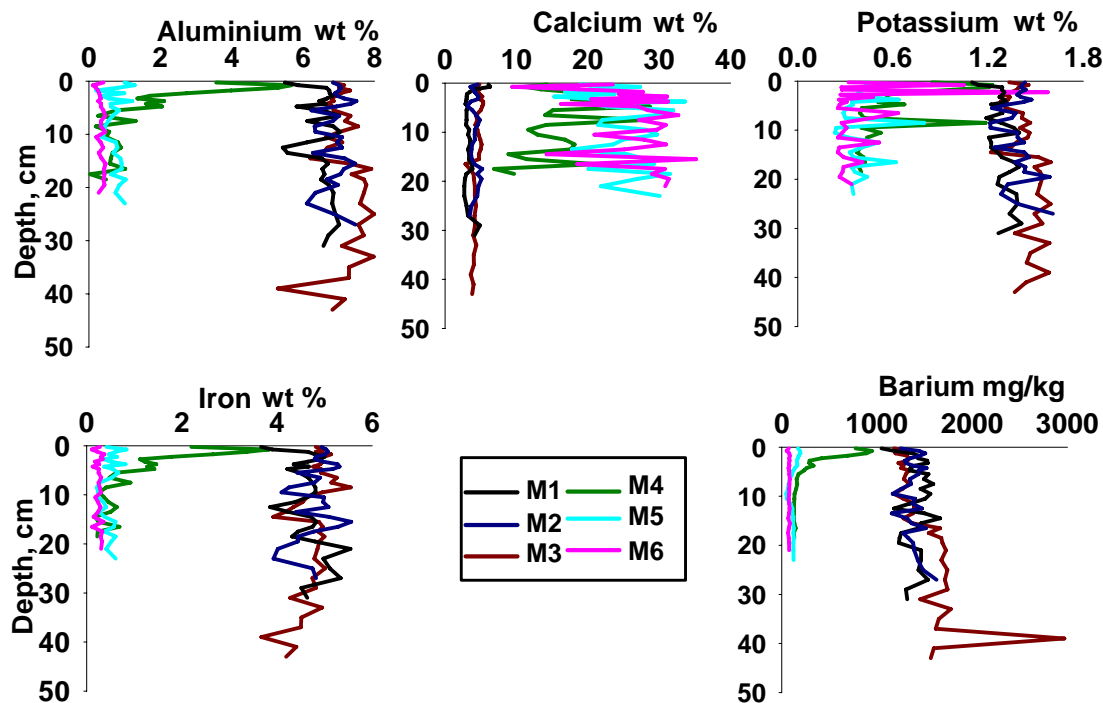
Figure 4.4.5.1 Major and minor elemental concentrations within sediment, M1-M6.

The concentrations of aluminium (Al), potassium (K), iron (Fe) and barium (Ba) are all higher within the complete length of the core for the impacted stations (M1-M3) when compared to the control stations (M5-M6) indicating that only sediment impacted by mine tailings were sampled at these stations. M4 has high concentrations in the top 5 cm of the core after which the concentrations decrease to similar values observed in the control stations M5-M6. In contrast, calcium (Ca) concentrations are much lower in the impacted stations compared to that of the control stations.

Ca concentrations are three to five times lower at M1-M3 than the sediments of the control stations (M5-M6) with maximum concentrations of 5%. The Ca concentrations of M4 are similar to those of M5 and M6 having a maximum concentration of Ca of 28% compared to 34 and 35% for M5 and M6 respectively.

Concentrations of the elements within the sediment from the impacted stations have concentrations of Al that are ten times higher, K, five times higher and Ba, fifteen times higher than the concentrations found at the control stations. Stations M1-M3 have Al concentrations which range from 5.3 to 8 % in comparison to M5 and M6 which have a range of 0.1 to 1.3% with M4, Al concentrations from 0.04 to 5.7% . The concentration of K ranges from 1.0 to 1.6% for M1-M4 in comparison to the control stations which generally have K concentrations below 0.6%. The Fe concentrations for the impacted stations M1-M3 range from 3.7 to 5.6% with the concentrations at the control stations being 0.1 to 0.8%. M4 has an Fe concentration of 0.2 to 3.8%. Finally Ba concentrations at stations M1-M3 range from 1085 to 2970 ppm which contrasts with the control stations (M5-M6) which have Ba concentrations in the range of 49 to 196 ppm. Once again M4 has higher concentrations at the surface with Ba concentrations from 124 to 948 ppm.

The range of concentrations within the sediment of the six stations suggests that the impacted stations (M1-M3) have a different chemical signature to the control stations (M5 and M6) and that M4 has a signature that varies between that of the impacted and control stations.

The concentrations of the minor and trace elements also vary between the impacted and control stations.

Table 4.4.5.3 indicates which elemental concentrations increase in the sediments from impacted stations compared to those of the control stations. Ca and Sr show a substantial decrease in the impacted stations in contrast to 23 elements which show an increase in concentration.

All elemental plots are given in Appendix 4B; however Figure 4.4.5.2 illustrates the differences between a number of elemental concentrations in sediments from the impacted station M1, 1380 m depth and M6, control station, 1250 m water depth. There are significant differences in concentrations of beryllium (Be), vanadium (V), copper (Cu), Arsenic (As), Lead (Pb), Nickel (Ni) and cobalt (Co) between stations M1 and M6, with concentrations of all elements being higher at the impacted station, M1.

Table 3.4.5.3 Elemental concentrations of impacted stations (M1-M3) relative to control stations (M5-M6). Red signifies increase in concentration, blue a decrease in concentration and blank no discernible change in concentration.

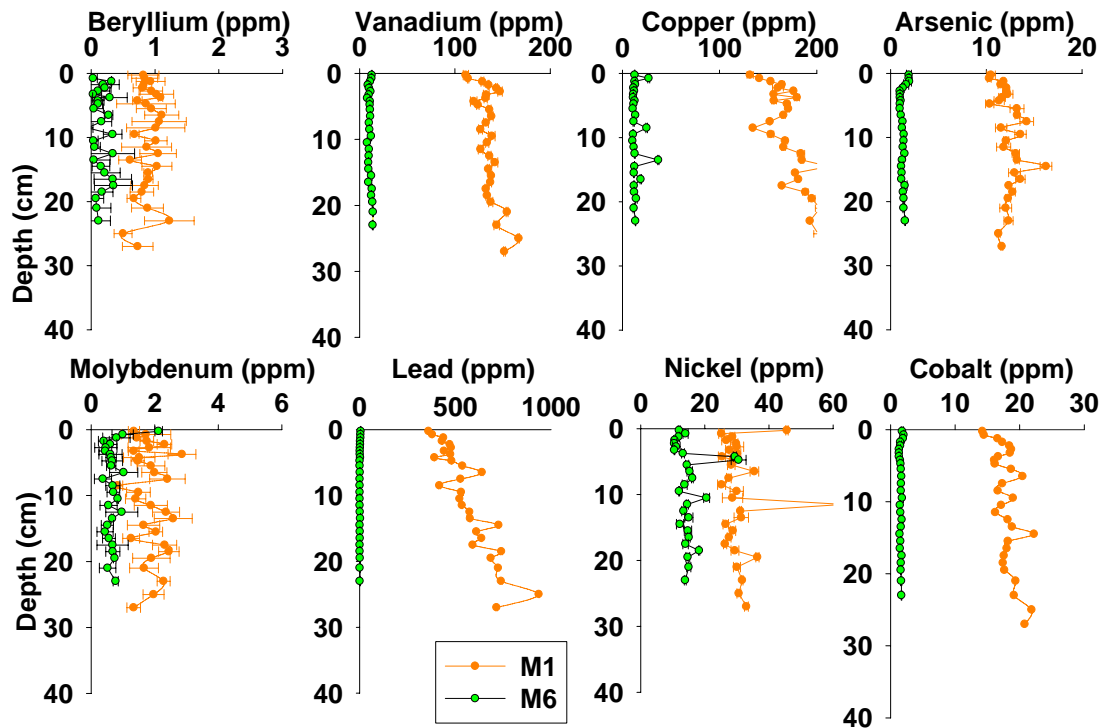| Element		Element		Element		Element	
Ag		Cd	🟥	K	🟥	Rb	🟥
Al	🟥	Ce	🟥	Li	🟥	Sr	🟦
As	🟥	Co	🟥	Mg	🟥	Th	🟥
Au		Cr	🟥	Mn		Ti	🟥
B		Cs	🟥	Mo		Tl	🟥
Ba	🟥	Cu	🟥	Na		U	🟦
Be	🟥	Fe	🟥	Ni	🟥	V	🟥
Ca	🟦	Ga	🟥	Pb	🟥	Zn	🟥

Figure 4.4.5.2 Minor and trace elemental concentrations within sediment, M1 (impacted, 1380 m) and M6 (control, 1250 m).

To investigate whether there is a statistical relationship of the elements with each other, Pearson Product Moment Correlation coefficients were calculated for sediment cores at each of the six stations. The pairs of elements that showed positive correlation coefficients above 0.6 and a P value below 0.05 were considered to increase together. For the pairs with negative correlation coefficients and P values below 0.050, one variable tends to decrease while the other increases.

The correlation coefficients were calculated on the complete data set for each core. In addition, for station M4, correlation coefficients were calculated for the top 5 cm that appeared to be impacted by tailings. The depth of tailings at M4 was determined by observing the change in concentrations of the major and minor elements. The results of the Pearson Product Moment Correlation tests are given in Appendix 4B, tables 4B:234-240.

The results of the Pearson Product Moment Correlation for station M1, considering the whole core to a depth of 27 cm, indicate that there are strong correlations with a number of the metals. Zn, Cu, V, Cr, Co, Pb Ti and Fe all show strong positive correlations with each other. There are also strong correlations with Ag, K, Zn, Cu and Cd. In addition Ag indicates a positive correlation with B. There are a number of negative correlations between elements and Ca, Sr, Fe and organic carbon. In addition, organic carbon has a negative correlation with Cd and Zn. It is interesting to note that Mn has no strong correlations.

For station M2 the results for the whole core are generally similar with the notable exception that the organic carbon does not have negative correlations with Cd and Zn. The strong correlations between Co, Cr, V, Zn and Cu are also absent. As has correlations with K and Ba.

Station M3 has more negative correlations than either M1 or M2. The negative correlations are between Ti, Sr, Co, Ni, Cs and Ce. There is also a negative correlation between U and Th , Cr, Mg and Fe. As has correlations with Li, Be, V, Zn and Cu.

Station M4 was the only core to have large number of significant Pearson correlations for both the whole core and the top 2.5 cm, the depth identified as having possible tailings impact from the elemental profiles.

The results for the whole core indicate a far larger group of positive correlations between elements than M1, M2 or M3. There are also strong negative correlations with organic carbon and U and Sr. At this station there is also a strong correlation of Be with a large number of the metals and both V and Ni do not have any strong correlations with any other element. The correlation tables suggest that the sediment at M4 is different from stations M1-M3.

The correlation results for the top 2.5 cm have less positive and negative correlations with no positive correlations of Tl with other elements, as was seen in the correlations obtained for the whole core. The difference between the top 2.5 cm correlations and the whole core suggests that the sediment in the top 2.5 cm of the core is different to that at depth.

The correlation coefficients for station M5 are different than M1-M4. There are more correlations than M1-M3. This is indicated by more positive correlations for As, Ni, Zn, Cu, Rb, Ag and Mo. In contrast, to M1, station M5 has a larger number of negative correlations of organic carbon with metals with the exception of Sr which has a positive correlation.

Station M6 has the least number of positive correlations of any of the stations indicating positive correlations between Sr, Ba, Ca, Fe, Mg and Ti. There are also strong correlations between V and Cr and, Ba, Ca, Fe, Mg, Sr and Ti. There are negative correlations between organic carbon and Pb and As, Ag with B and Zn and finally U with Pb and Na.

Using the correlation coefficients the stations can be grouped, stations M1-M3 are broadly similar with M3 having the greatest number of positive and negative correlations of the three stations. M4 has the greatest number of strong positive correlations of any station. M5 has fewer correlations and M6 has the least number of correlations of any station.

The elemental concentrations of the stations suggest that M1-M3 have been impacted by tailings, M4 profiles suggest that only the top of the sediment core may be impacted by either direct input of tailings or the re-deposition of tailings from and impacted area. M5, a control station, has a different elemental signature to stations M1-M4 and is considered to be free from tailings. Station M6 is different from M5 and the elemental concentrations suggest that this core has a predominance of Ca material probably originating from surrounding coral reefs.

To assess the impact of the tailings on stations M1-M3 the inventories of all elements for all cores M1-M6 were calculated and expressed as g m$^{-2.}$ The sediment cores collected at each station were different lengths and in order to compare the excess inventories of elements at all stations the depth range that the excess was calculated for the top 10 cm of each core. Cores from stations M1-M3 have high elemental concentrations of major elements through out the core indicating that these cores are composed of tailings and that the tailings were too deep to allow the natural sediment to be sampled. In this case the average background of core M4 has been subtracted from concentrations observed in the sediment at these stations, to allow excess inventories to be calculated.

The total elemental inventories for cores at stations M1-M6 are given in Appendix 4B, tables 4B.221-233. Inventories have been calculated for complete cores as well as the top 10 cm at each station.

The excess elemental inventories (g m^{-2}) for all stations to a depth of 10 cm are shown in Figure 4.4.5.3. The % excess elemental inventories are shown in Figure 4.4.5.4.

From the graphs it can be seen that stations M1-M3 have significantly higher inventories of Al, Fe, Mn, Pb, Cd and Zn. Other elements that show an excess inventory are K, Mg, Cr, Be, Cs, V and Cu. The data also indicates that stations M1-M3 have a deficit of Ca, Sr and U compared to stations M4-M6.

Figure 4.4.5.4 displays the percentage excess of elements at each of the stations. These figures illustrate the trends seen in the total excess inventories. In addition As, Cr, Co, Rb and Cs all have % excess inventories in stations M1-M3 above the levels observed at the control stations. It is interesting to note that inventories of metals within the sediment at M4 lie between the control and impacted stations suggesting that station M4 has been impacted by tailings to some degree.
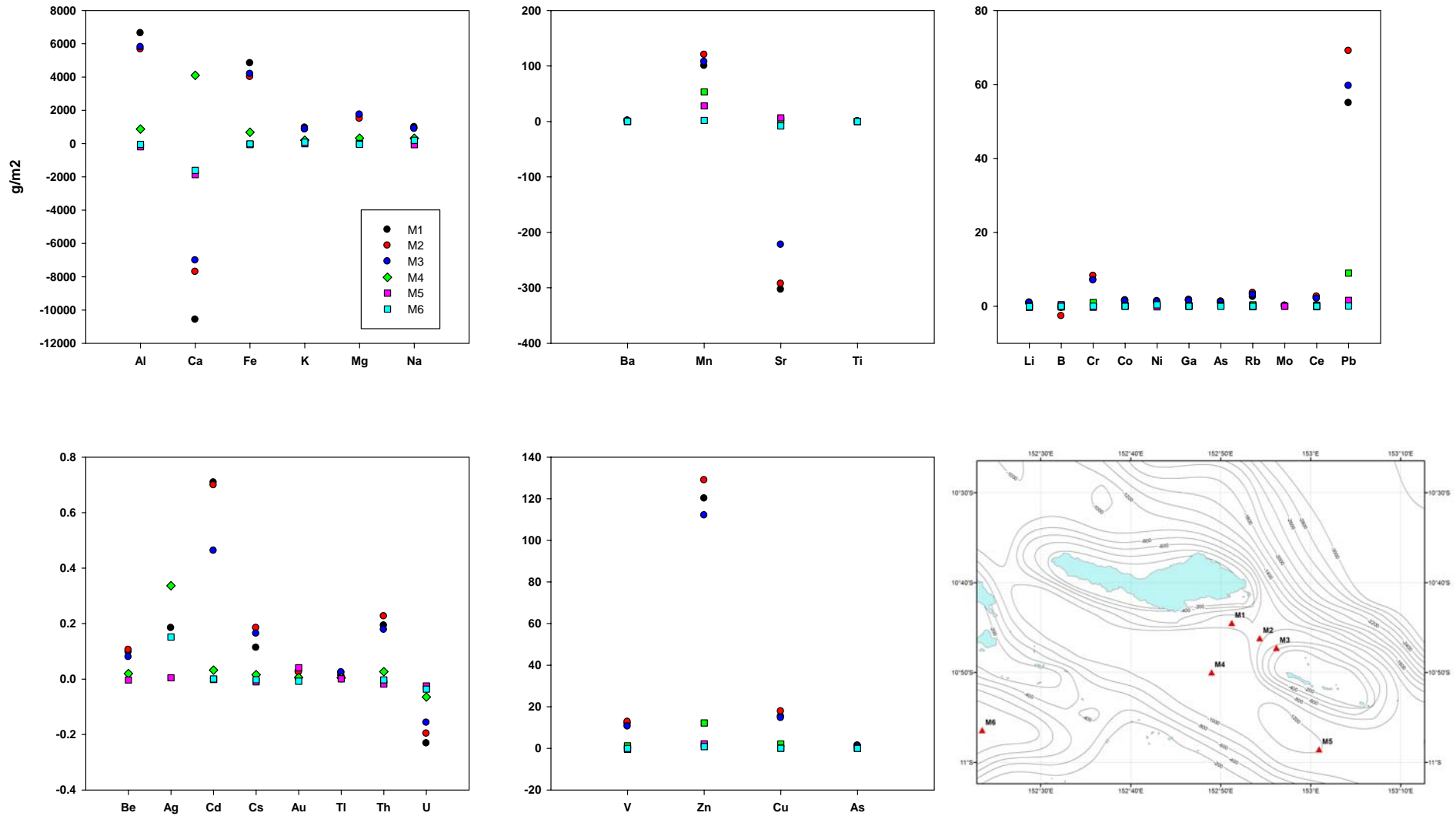
Figure 4.4.5.3 Excess inventory of elements (g m^{-2})within the top 10 cm of Misima sediments
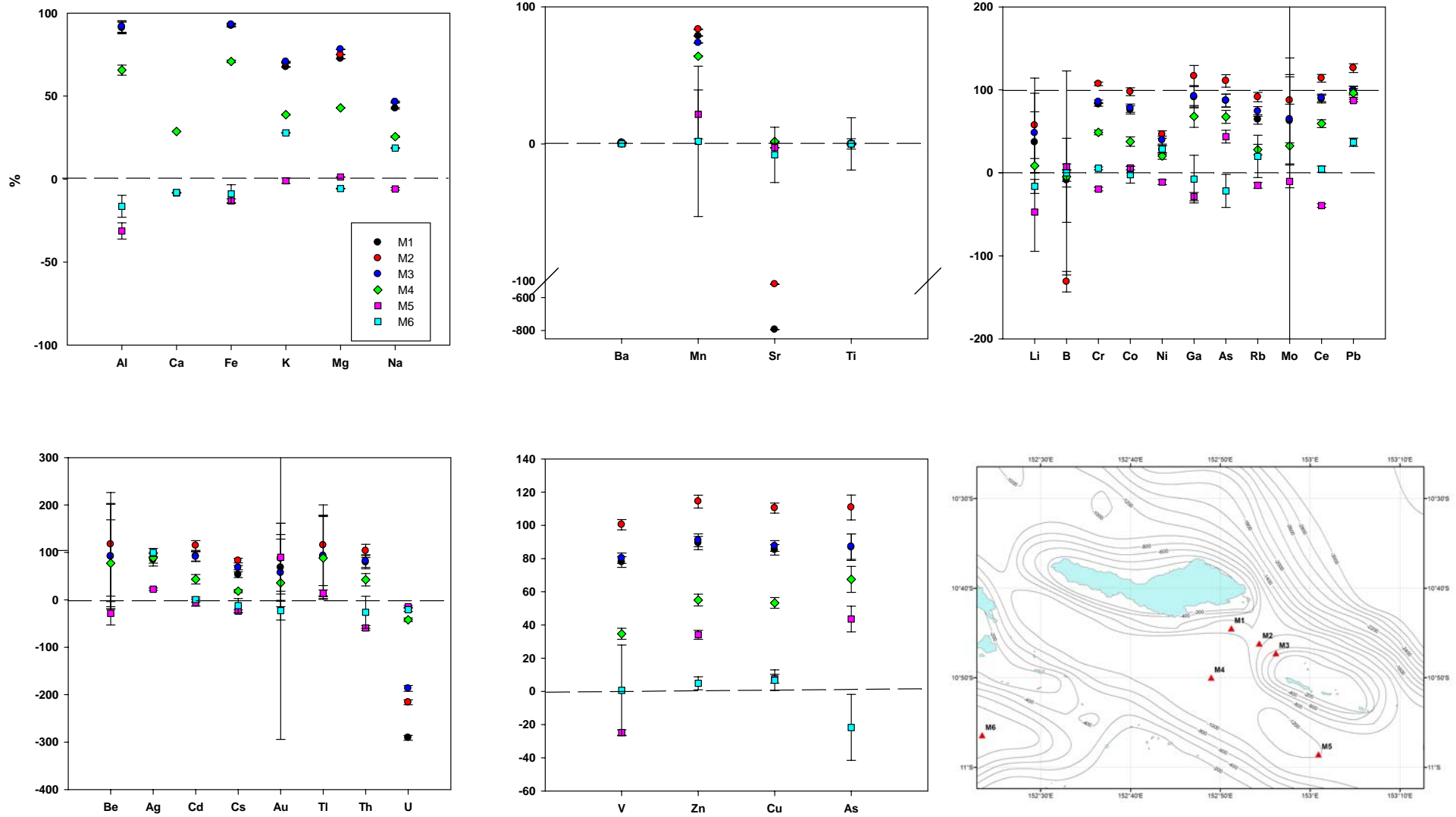
Figure 4.4.5.4 Excess inventory of elements (%) within the top 10 cm of Misima sediments

The dissolved nutrient and elemental concentrations within the pore-water samples of cores taken at each of four stations M1, M3, M4 and M6 are reported in Appendix 4B, tables 4B.41-52 and 4B.92-103. No pore-water samples were obtained from station M2 or M5. Figures of the elemental depth profiles for each station are given in Appendix 4A, Figures 4A.61-72.

Pore-water nutrient concentrations were measured at 4 stations in order to characterise the upper-sediment biogeochemical processes occurring and to assess if historic mine tailings deposition had any detectable affect upon these processes.

In general all nutrient concentrations are not atypical for sediment pore-water of equatorial oligotrophic oceans. The Misima stations pore-water data profiles show very close comparison between cores from each individual station possibly indicating that there was little mega-faunal bioturbation activity disturbing the diffusion profiles. All Misima stations exhibit a subsurface ammonia minimum that is probably attributable to anoxic ammonia oxidation by NO_2^-, NO_3^- and/or MnO_2; the anammox reaction, (Rysgaard et al., 2004, Thamdrup et al., 2006). The anammox zone appears to deepen with increasing water depth, from station M1 to Station M6. Below the anammox zone the ammonia values increase more steeply in the shallower water stations, M1 and M3 which would suggest greater denitrification due to an increased organic loading at the shallower depths. The dissolved phosphate levels do not show appreciable increase with depth suggesting that there is little degradable organic material penetrating into the sediment. However the deepest station, M6, exhibits the greatest dissolved phosphate concentration. This may be the result of a greater input of inorganic phosphate or refractory organic material to this station compared to the other locations. Dissolved silicate concentrations at the Misima stations increase with increasing water depth, suggesting dissolution of biogenic silica at stations M4 and M6.

Figure 4.4.5.5 illustrates the Mn, Fe, Mo and U solid phase and pore-water concentrations of an impacted station, M1 and a non impacted station M6.
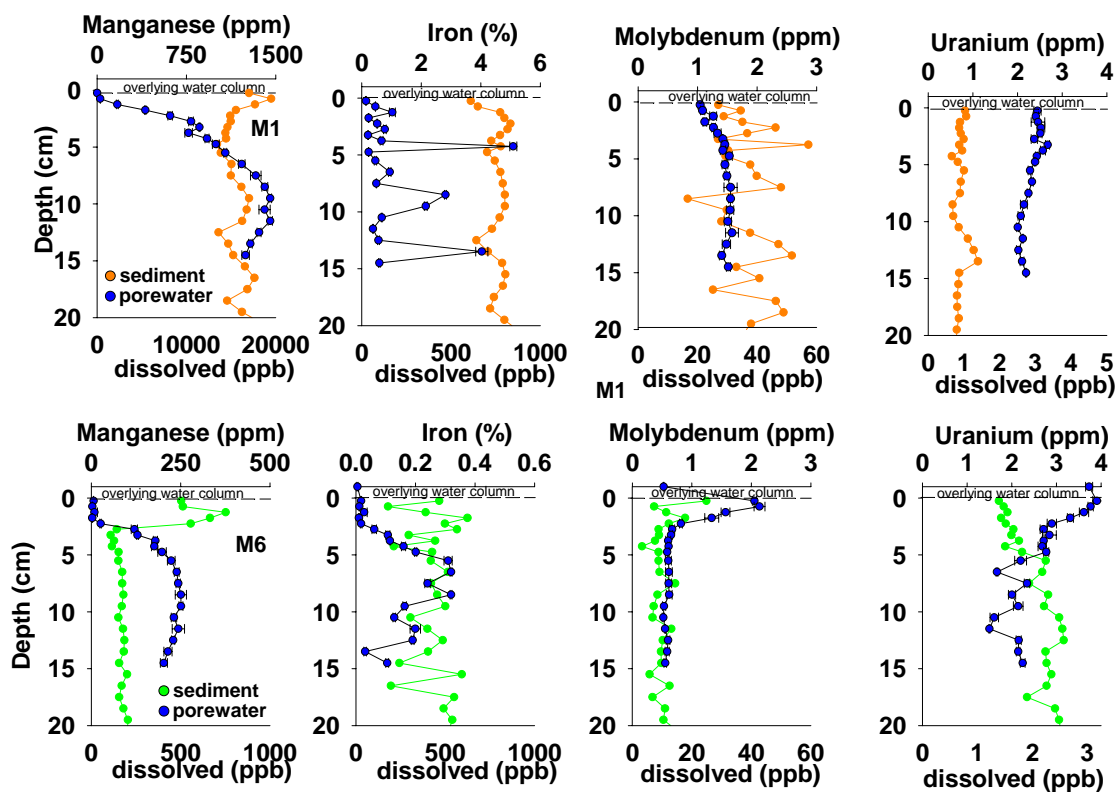
Figure 4.4.5.5 Mn, Fe, Mo and U solid phase (ppm or %) and pore-water (ppb,) concentrations of M1 and M6.

The dissolved Mn concentration at M1 indicates that dissolution of Mn is occurring at depth in the core with Mn being oxidised and removed to the sediment towards the surface of the sediment core. The solid phase concentrations of Mn at M1 are three times higher than those at M6 however dissolved concentrations of Mn are 20 times higher at M1 compared to M6. Station M6 Mn solid phase and dissolved profiles have a similar structure to M1. Mn is released into the water column when the redox conditions of the sediment are such that Mn^{4+} is reduced to Mn^{2+}, the dissolved species then migrate towards the surface of the core where they react with oxygen and precipitate as oxyhydroxides.

The Fe profiles for M1 indicate that solid phase concentrations are higher than at M6 by a factor of 10 and dissolved concentrations are within the same range for both stations. The dissolved phase profile for the control station, M6, once again indicates a classic dissolved Fe profile found in sediments with a dissolved Fe maximum at the redoxcline, the concentration decreasing towards the surface within the oxygenated zone of the sediment.

For Mo the solid phase and dissolved concentrations are similar for both stations with the M1 dissolved profile of Mo being similar to Mn suggesting that the Mo profile is influenced by the Mn geochemistry. The dissolved Mo profile for M6 increases towards the surface indicating a release of Mo from the solid phase in the oxygenated surface sediment.

Finally solid phase U concentrations at M1 are approximately half that of M6. The dissolved concentrations are similar but there is a decrease in concentration with depth at M6 indicating that U is being removed from solution at depth as it is reduced.

The solid phase and dissolved profiles of M1 suggest that the core is oxidising at the surface, however, the cycling of elements in the pore-water is being influenced by the Mn geochemistry. The control station (M6) solid phase and dissolved profiles indicate that the sediment is reducing at approximately 3 cm depth and the dissolved profiles of all four elements reflect this with the Mn being reduced first followed by Fe, deeper in the sediment column. The U profile also confirms that the sediment is reducing at approximately 3 cm depth, where U reduction and removal to the sediment is taking place. The organic carbon content of M6 is higher (0.6 – 1.5%) compared to M1 (0.2-0.3 %) which will influence the redox cycling within the sediments.

Figure 4.4.5.6 illustrates the solid phase and dissolved concentrations of As, Cu, Pb and Cd; all these metals are considered to be ecotoxic.
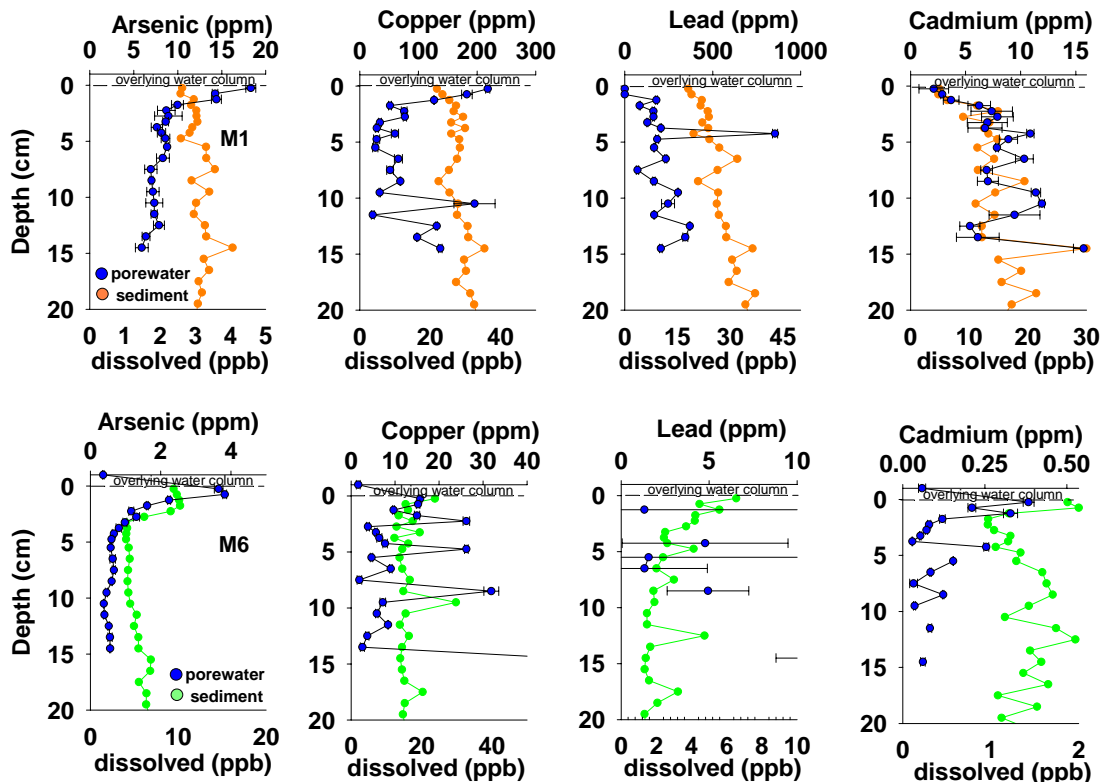

Figure 4.4.5.6 As, Cu, Pb and Cd solid phase and dissolved concentrations, M1 and M6.

The solid phase concentrations for As, Cu, Pb and Cd are all considerably higher at M1, the station impacted by tailings. The As concentration is 5 times higher, Cu, 10 times higher, Pb, 50 times higher and Cd, 5 times higher than the concentrations found in the sediment from the control station M6.

The dissolved concentrations of As is 3 times higher at the control station, M6, than the impacted station, M1 even though the solid phase concentration is higher by a factor of 5 at M1.

The dissolved Cu concentrations are similar at both stations in comparison to the solid phase which is 10 times higher at M1.

The dissolved Pb concentration at the impacted station is higher with only a few samples of pore-water from M6 having detectable levels of dissolved Pb.

Dissolved Cd concentrations are approximately 5 times higher at station M1 compared to the control station M6. The dissolved phase profiles of As and Cu at M1 suggests that there maybe a supply of these elements to the overlying water column with Cd being removed from the dissolved phase towards the surface of the core.

The dissolved concentration profiles of As and Cd at M6 suggest that there may be a release of these metals to the overlying water column at this control station.

The highest solid phase concentration of As occurs at M3, 17.4 ppm, with the lowest occurring at M6, 2.6 ppm. The highest dissolved concentration of As occur at station M4 and M5 (17 and 15 ppb) decreasing to 3 ppb at M1 with M3 having the lowest dissolved arsenic concentration at the surface. At M3 the dissolved arsenic concentration remains relatively constant down the length of the core.

In summary the solid phase As concentration trend is M3>M1>M2>M4>M5>M6 with the dissolved As concentration trend M4> M5>M1>M3. It is clear that at the Misima site, the historically impacted stations do not have the high solid phase and dissolved As concentrations that were seen at impacted stations at Lihir (Figure 3.4.5.7).
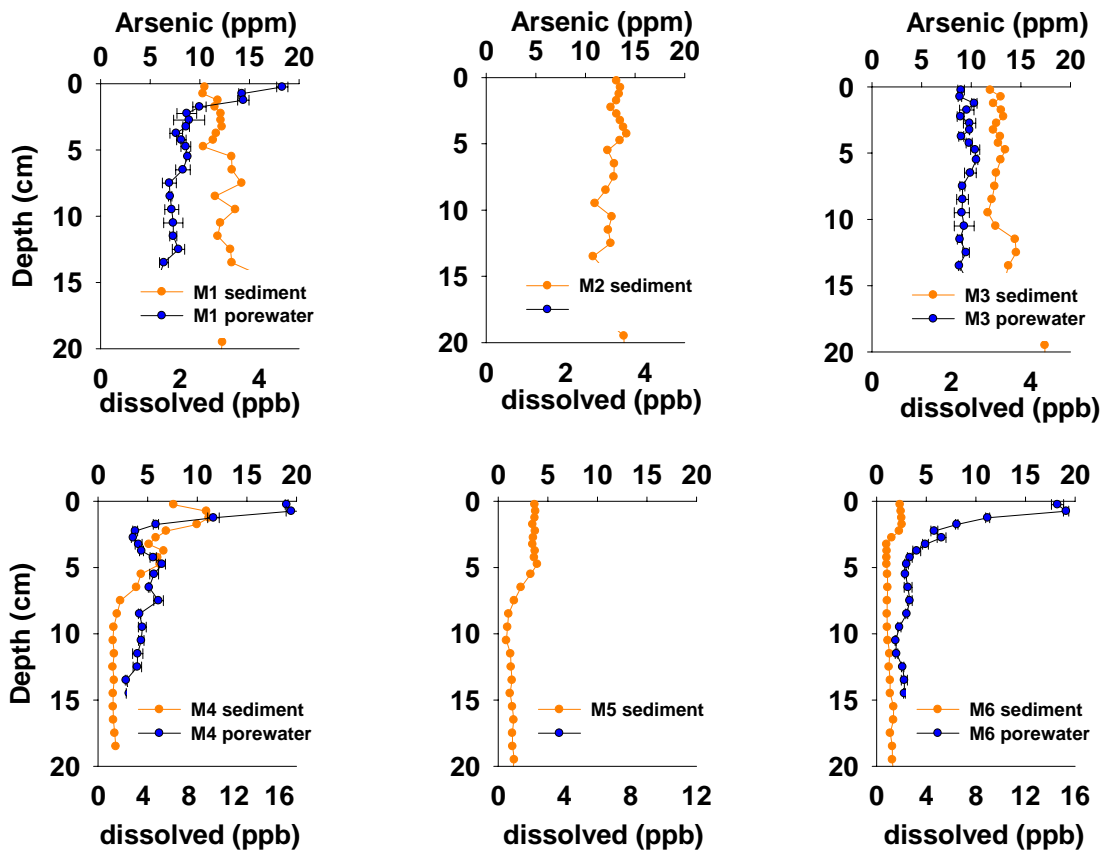
Figure 4.4.5.7 Solid phase and dissolved As concentrations for stations M1-M6

The production (dissolved element) and consumption (precipitated element i.e. removal from solution) of elements can be modelled from the dissolved profiles and the resultant flux to the sediment, or alternatively from the sediment to the pore-water or overlying water column, can be calculated. In this case the Berg model (Berg *et al*., 1998) has been used to calculate the production or consumption of dissolved Fe, Mn and As at stations M1, M4 and M6. In addition the fluxes of these elements to the sediment or pore-water have been calculated by the model and expressed as μmol m^{-2}d^{-1}.

Figure 4.4.5.8 Measured and modelled pore-water (dissolved) concentration profiles for Fe, Mn and As, M1

Figure 4.4.5.9 Measured and modelled pore-water (dissolved) concentration profiles for Fe, Mn and As at station, M4
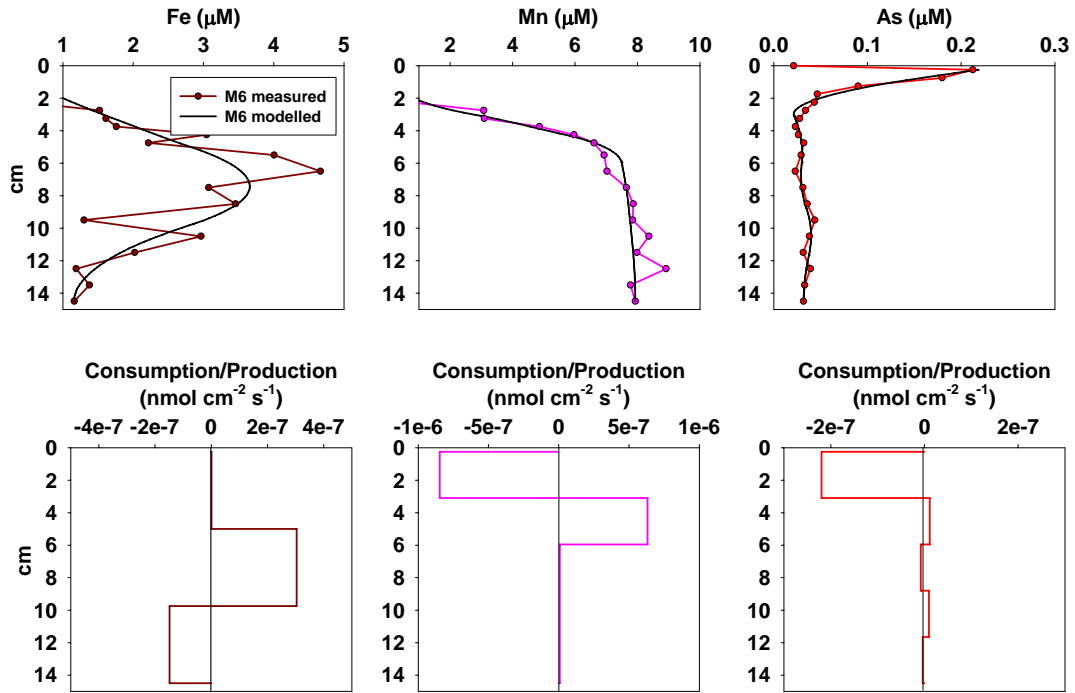
Figure 4.4.5.10 Measured and modelled pore-water (dissolved) concentration profiles for Fe, Mn and As, M6

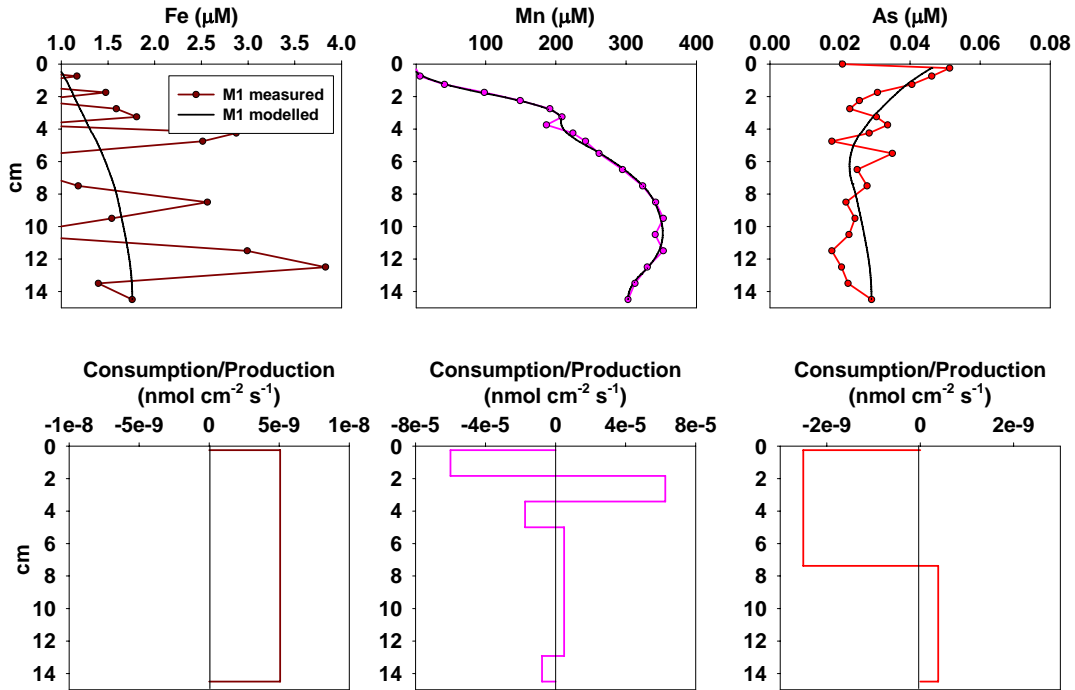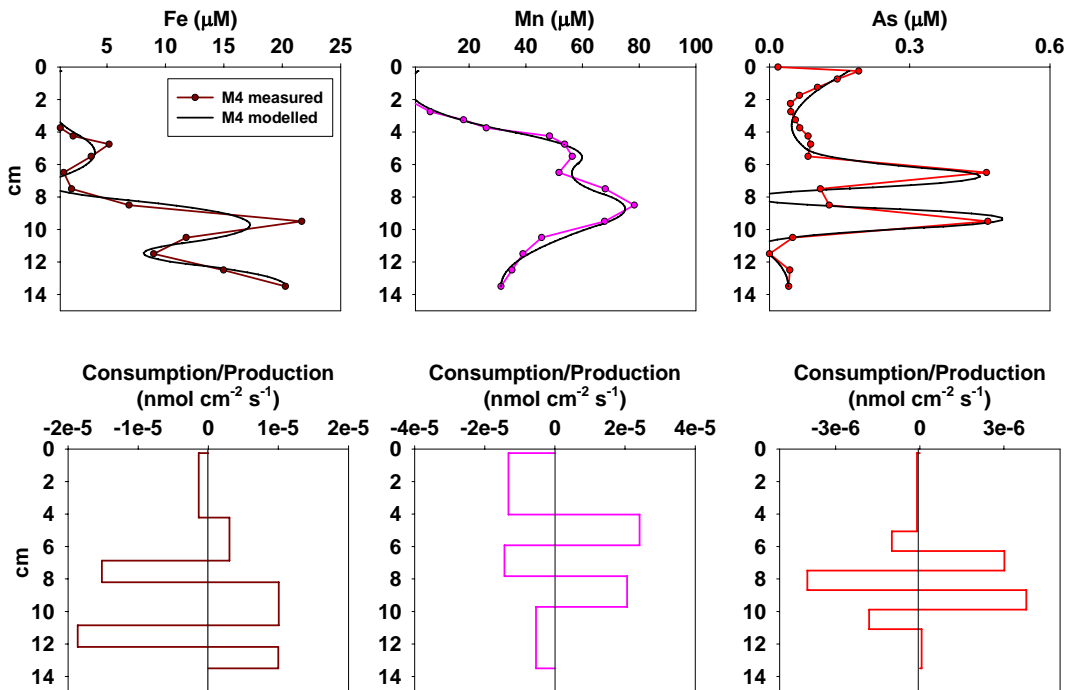Figures 4.4.5.8 to 4.4.5.10 show the modelled profiles and the consumption and production of Fe, Mn and As for M1, M4 and M6 respectively. The modelling of dissolved Fe, Mn and As profiles for M1 indicates that there is one zone of production for Fe, two zones of production and three of consumption for Mn and one zone of production and one for consumption for As. The overall net removal of Fe from pore-water to the sediment of 0.06 µmol m^{-2} d^{-1}, with the net removal of Mn to the sediment being 2.56 µmol m^{-2} d^{-1}, finally the net flux of As from the sediments to the pore-water is 0.01 µmol m^{-2} d^{-1}.

At station M4, the modelling indicates three zones of production for Fe and three zones of consumption with a modelled net flux of dissolved Fe 1.97 µmol m^{-2} d^{-1} to the sediment. There are three zones of consumption and two of production for dissolved Mn with an overall flux of Mn to the pore-water of 11.28 µmol m^{-2} d^{-1}. The modelled As profile shows three zones of consumption and 2 of production with a net flux of dissolved As of 0.29 µmol m^{-2} d^{-1}.

Finally at the control station, M6, the modelling of the dissolved Fe gives one zone of production and one zone of consumption resulting in an overall net flux of Fe from the pore-water to the sediment of 0.64 µmol m^{-2} d^{-1}. The Mn modelled results also give one zone of consumption and

one of production resulting in a net flux from the sediment to the pore-water of 1.02 µmol m^{-2} d^{-1}. The As modelled results indicate that there are two zones of consumption and two zones of production of As resulting an overall flux of As from the sediment to the pore-water of 0.52 µmol m^{-2} d^{-1}.

Table 4.4.5.4 Modelled flux rates of dissolved Fe, Mn and As at stations M1, M4 and M6 (negative number signifies a net consumption of dissolved species)

Station	Fe (µmol m^{-2} d^{-1})	Mn (µmol m^{-2} d^{-1})	As (µmol m^{-2} d^{-1})
M1	-2.56	-0.06	0.01
M4	1.97	11.28	0.29
M6	1.02	-0.64	0.52

The solid phase As , Cu, Pb and Cd concentrations at the impacted stations (M1-M3) all have maximum concentrations higher than M4 which has higher concentrations than the control stations (M5, M6) indicating that the stations have been impacted by the mine tailings deposition from Misima.

The dissolved Cu concentrations are highest at M1 and M4 with M3 and M6 being similar and lower in concentration.

Stations M1-M3 have maximum Pb concentrations ranging from 360 – 1092 ppm, with M4 having a Pb maximum of 531 ppm and M5 and M6 a maximum Pb concentration an order of magnitude lower, ranging from 6-56 ppm. Dissolved Pb concentrations for M1 and M3 range from 0-18 ppb with M4 and M6 dissolved Pb concentrations being below detection limit.

Maximum solid phase Cd concentrations occur at M1- M3 with maximum concentrations ranging from 11.5 – 16 ppm. Station M4 has a maximum Cd concentration of 3.5 ppm with the control station M5 and M6 being 0.6 and 0.5 ppm respectively.

Other metals worth considering are thallium (Tl), chromium (Cr), vanadium (V) and zinc (Zn) all of which can affect living organisms depending on their concentration and bioavailability. The

maximum solid phase Tl concentrations range from 0.4 to 1 ppm at M1-M3, 0.3 ppm at M4 and 0.1ppm at the control stations M5 and 6. Dissolved Tl was detected at M1 at a concentration of 0.3 to 2.7 ppb. The only other detectable dissolved Tl was found in a few samples from M6.

Maximum solid phase Cr concentrations in M1-M3 range from 96 – 108 ppm. In comparison, M4 has a maximum Cr concentration of 71 ppm and M5 and M6 15-20 ppm. Concentrations of dissolved Cr for M1 range from 0.26 – 1.24 ppb but are below the detection limit for M3 and are only detectable in the top 2.5 cm of M4 (1.6 – 21.8 ppb) . M6 has dissolved concentrations of Cr ranging from 0.2 to 14 ppb.

Maximum concentrations of solid phase V range from 158 - 167 ppm at stations M1-M3, , 113 ppm at M4 and 15 – 32 ppm at M5-M6. The dissolved V concentrations in the pore-water range from 1.5 to 9.8 ppm for stations M1-M3, 2- 78 ppb at M4 and 3-120 ppb at M6 which had the highest concentrations.

Finally, solid phase maximum Zn concentrations in M1 - M3 range from 1833 to 1893 ppm in comparison to M5-M6 which range from 158-556 ppm with M4 having a maximum concentration of 1367 ppm. Dissolved concentrations of Zn are highest at M3 and M6 (45-586 ppb) and lowest at M1 by a factor of 10.

4.4.6 Benthos

Metazoan meiofauna

Mean densities of metazoan meiofauna showed wide variation among the six Misima stations (Figure 4.4.6.1a). Densities were much higher at M6 than at any other station. Very low densities were recorded at M1, with slightly higher Figures at M2 and M3. Values at M4 and M5 were intermediate between these stations and M6. One-way ANOVA with Fisher's multiple comparisons test showed that the three station groupings of (M1, M2, M3), (M4, M5) and M6 were significantly different from each other (P< 0.001). With respect to higher-taxon community structure, M3, M4, M5 and M6 were broadly similar in showing high nematode abundance with harpacticoid copepods as the second most-abundant taxon and a small representation of ostracods and minor metazoan groups (Figure 4.4.6.2). At M1, copepods were approximately twice as abundant as nematodes and other metazoan groups were absent. The meiofaunal community at station M2 had a higher ostracod component (> 20%) than any other station, but in common with M1 harpacticoid copepods were the most abundant group, acounting for 52% of total individuals.

Foraminifera

Living benthic Foraminifera were present at all Misima localities but total densities and community structure varied considerably among the stations (Figure 4.4.6.3). Stations M4, M5 and M6 all supported a mixture of organic-walled (allogromiid) and calcified forams with no single taxon predominating. In contrast, M1, M2 and M3 were characterized by high densities of individual foraminiferan taxa. M1, M2 and M3 all showed high densities of a porcelaneous calcified foram belonging to the Order Miliolida, (possibly a species of the genus *Quinqueloculina*). This foram occurred at very similar high densities at M1, M2 and M3 but was absent or very rare at the other three stations. A hyaline-walled calcified foram of the Order Buliminida (genus unidentified) also occurred in large numbers at stations M1 and M2, where it was the most abundant foraminiferan. This species was absent or very rare elsewhere.
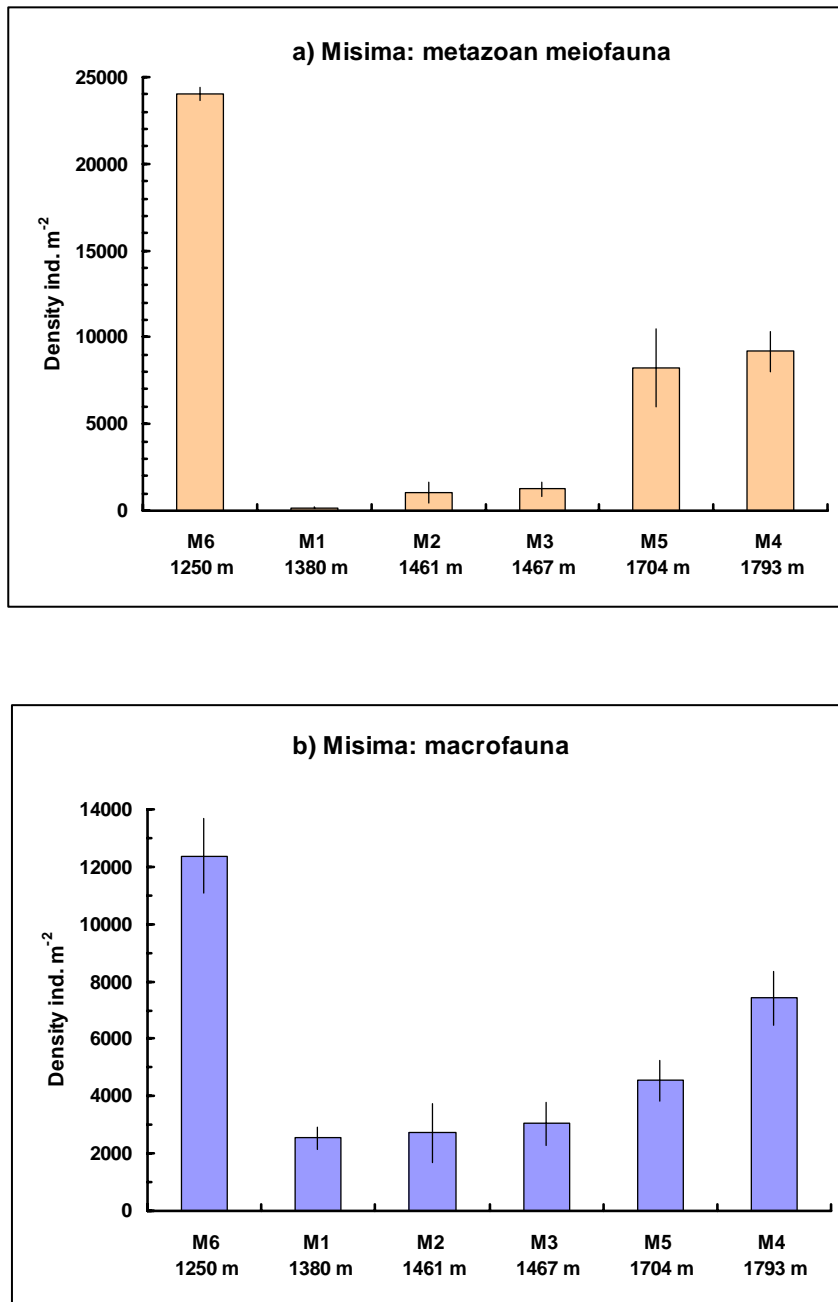
Figure 4.4.6.1. Histograms showing mean densities of (a) metazoan meiofauna and (b) macrofauna (> 250 μm) at the six Misima stations arrayed in order of increasing water depth. Bars represent mean values (± SD) for each station with individual corer drops as replicates. Numbers refer to the upper 10 cm of the sediment column.

Figure 4.4.6.2. Histogram showing percentage contribution of major taxa to the metazoan meiofaunal community (> 250 μm) at Misima stations arrayed in order of increasing water depth. Bars represent mean values (± SD) for each station with individual corer drops (n = 1 core per drop) as replicates.

Macrofauna

Mean macrofaunal density was considerably higher at M6 than at any other Misima station (Figure 4.4.6.1b). Means for stations M1-M5 showed a gradational increase with water depth, with lowest values at M1 and highest at M4. One-way ANOVA with Fisher's multiple comparison test showed that differences were statistically significant (P < 0.001) and that station groups (M1, M2, M3), (M4), (M5) and (M6) could be identified as significantly different. This is the same pattern as found for metazoan meiofaunal density, with the exception of a significant difference between M4 and M5 for macrofauna.

With respect to higher-taxon community structure, Polychaeta was the largest single group at all stations (Figure 4.4.6.4), but stations differed in representation of some other taxa. Notably, peracarid crustaceans (amphipods, isopods, cumaceans and tanaids) were relatively common at

M4, M5 and M6, but very rare or absent at M1, M2 and M3. Station M1 was distinctive in showing a high abundance (18.4% of total macrofauna) of echiuran worms, a group either absent or at most a very minor community element at the other five stations. Bivalve molluscs were also only slightly less abundant than polychaetes at M1 (35.5% versus 43.2%), while at all other stations the Polychaeta accounted for a much higher percentage of the total.
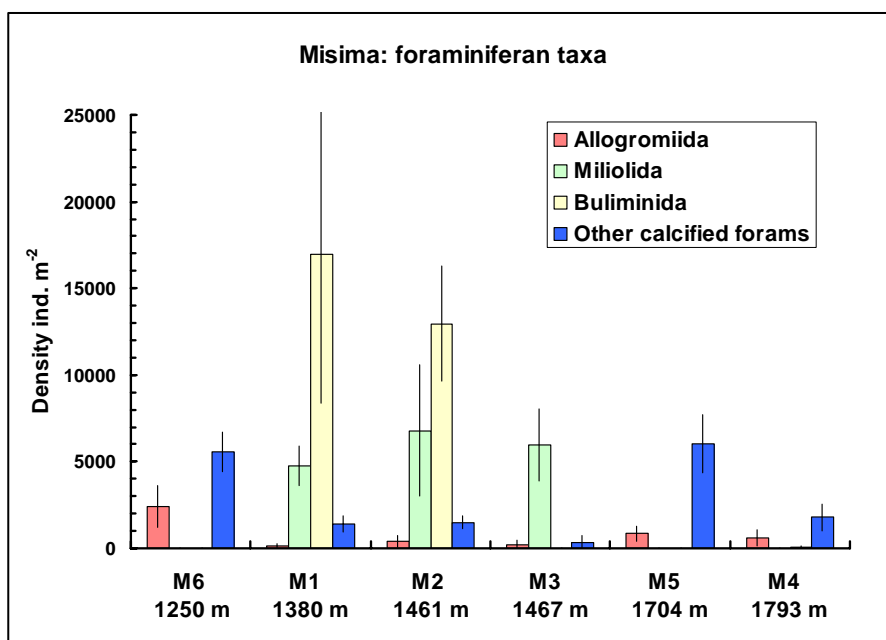
Figure 4.4.6.3. Histogram showing densities of major benthic foraminiferan taxa (> 250 μm) at Misima stations arrayed in order of increasing water depth. Bars represent mean values (± SD) for each station with individual corer drops (n = 1 core per drop) as replicates.
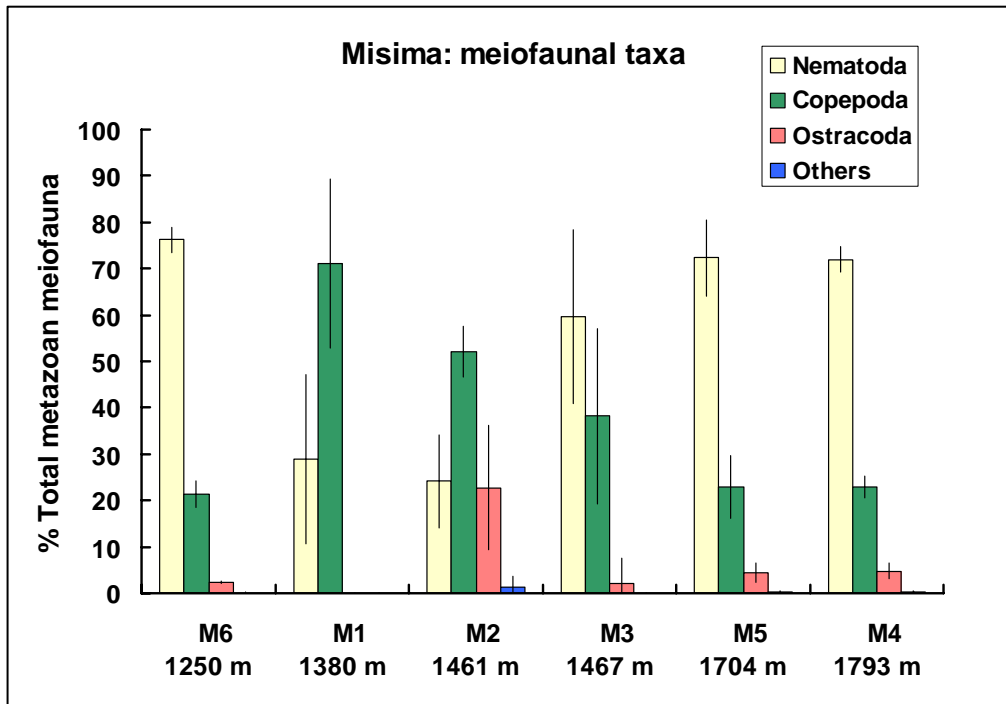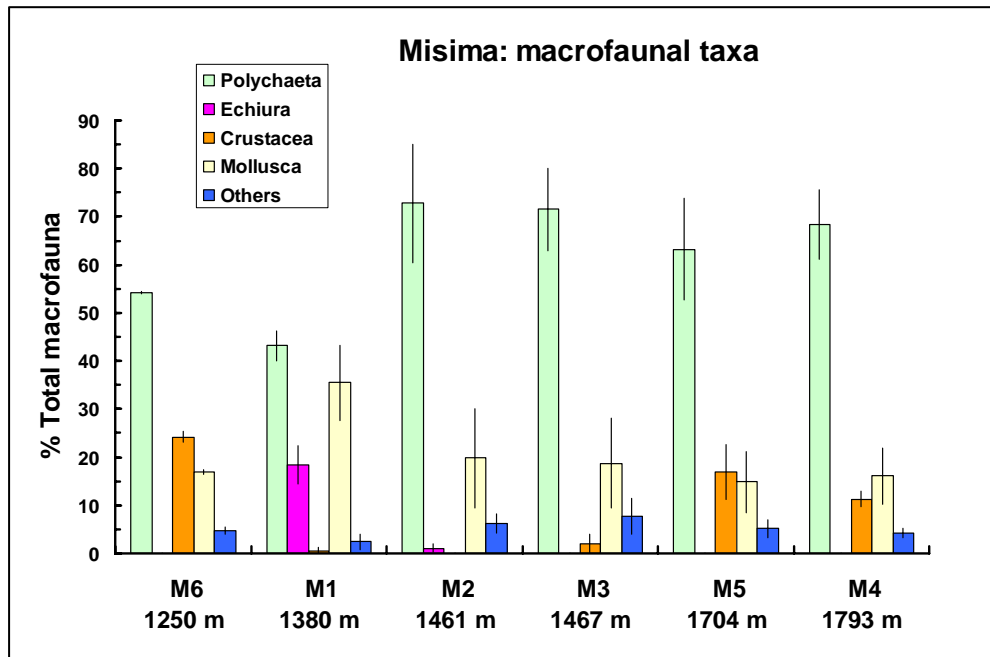
Figure 4.4.6.4. Histogram showing percentage contribution of major taxa to the macrofaunal communities (> 250 μm) at Misima stations arrayed in order of increasing water depth. Bars represent mean values (± SD) for each station with individual corer drops as replicates.

Polychaete community structure

In addition to being the largest single contributor to macrofaunal abundance, the Polychaeta includes species representing a wide range of lifestyles and ecological roles. The structure of the Misima polychaete communities was therefore analysed in more detail at the Family level. The number of families represented ranged from 14 (M1) to 32 (M6). The percentage contribution of the five most abundant families at each station is shown in Figure 4.4.6.5. Spionidae was the most consistently-abundant family, ranking among the top five at all stations. Paraonidae and Cirratulidae were major families at five out of six stations. Stations M1, M2 and M3 were distinguished by the high abundance of Lumbrineridae, which accounted for 18-30% of the total polychaete community.

Cluster analysis of Bray-Curtis similarities using untransformed data (Figure 4.4.6.6) showed a primary division between stations (M1, M2, M3) and (M4, M5, M6). This pattern was confirmed by the non-metric multidimensional scaling (nMDS) plot. Analysis of Similarity (ANOSIM) showed that these two clusters were signficantly different (Global R = 0.797, P = 0.001). Within the two primary

clusters there were no significant differences among stations M1, M2 and M3. Within the second group, M5 was signficantly different from both M4 and M6.

The PRIMER[TM] SIMPER routine on unstandardized family data (i.e. using absolute abundance) showed that the five most important contributors to the overall dissimilarity between the two main station clusters were Spionidae (15.0%), Paraonidae (12.7%), Syllidae and Cirratulidae (both 9.6%) and Lumbrineridae (9.1%). On standardized family data (ie. using percentage contribution rather than absolute abundance) Lumbrineridae was by far the largest contributor, accounting for 22.6% of the overall dissimilarity between stations (M1, M2, M3) and (M4, M5, M6), with the second-largest contributor (Paraonidae) accounting for 8.1%.

Correlation between community patterns and environmental variables

Preliminary analysis of the sediment core data in PRIMER[TM] showed that % nitrogen was highly correlated with % carbon (0.957). To simplify the analysis, % nitrogen was removed from the dataset, leaving % carbon as the indicator of food availability.

BIO-ENV analysis with the simplified dataset gave a best correlation with polychaete community patterns of 0.775 for Log Ca alone. This suggests that the primary division in the polychaete data between stations (M1, M2, M3) and (M4, M5, M6) is associated with the concentration of tailings in the sediment. This is apparent from the data in the table in section 4.3.7, where Ca levels in sediment at stations M1, M2 and M3 are much lower than at the other three stations, indicating greater dilution of Ca by tailings. Percentage organic carbon alone also had a relatively high correlation (0.621) with community patterns, indicating that food availability may also contribute to the clustering of stations.

Faunal depth distribution in the sediment column

Metazoan depth distribution in the sediment column was fairly uniform at the six Misima stations (Figure 4.4.6.7a). Between 48% and 66% of all animals were found in the surface 0-1 cm layer, with numbers decreasing steadily below this. In most samples only a few individuals, mostly larger polychaetes, were found in the 5-10 cm depth horizon. Foraminiferan depth distribution was more variable (Figure 4.4.6.7b). Stations M4, M5 and M6 were all very similar and showed the same pattern as the metazoans.
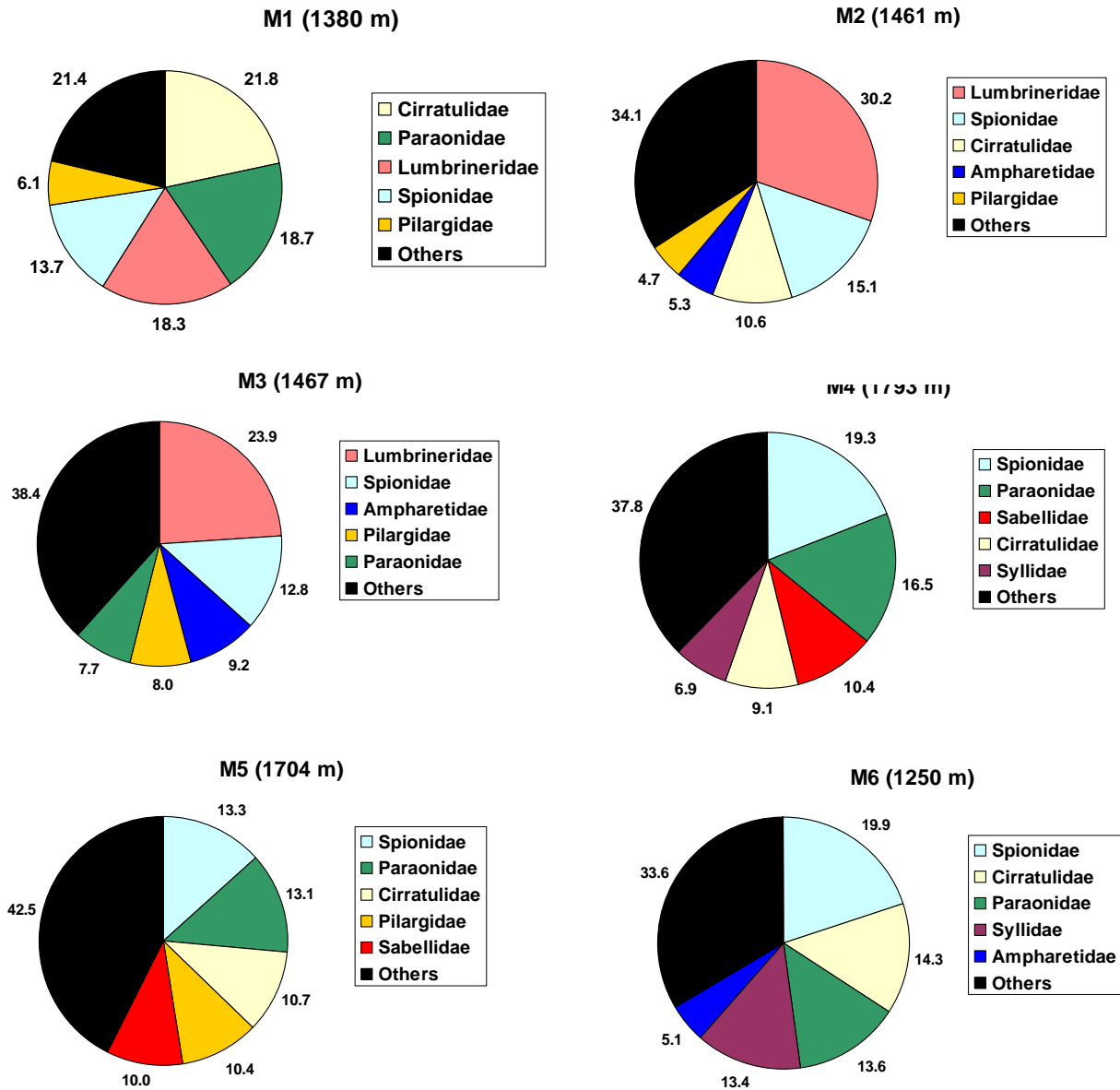
Figure 4.4.6.5. Polychaete community structure at the six Misima stations. Charts show the mean contributions of the five most abundant families at each station as a percentage of total polychaete abundance. Juvenile polychaetes not firmly identified to Family level are excluded from the analysis.

At M1, numbers of forams were approximately equal in the 0-1 and 1-2 cm layers, with a sharp decrease below this, while at M2 significant numbers of forams occurred down to 4 cm. Station M3 was distinctive in that foraminiferans were almost entirely located in the uppermost sediment horizon with virtually none found below 1 cm depth.

Misima polychaete families
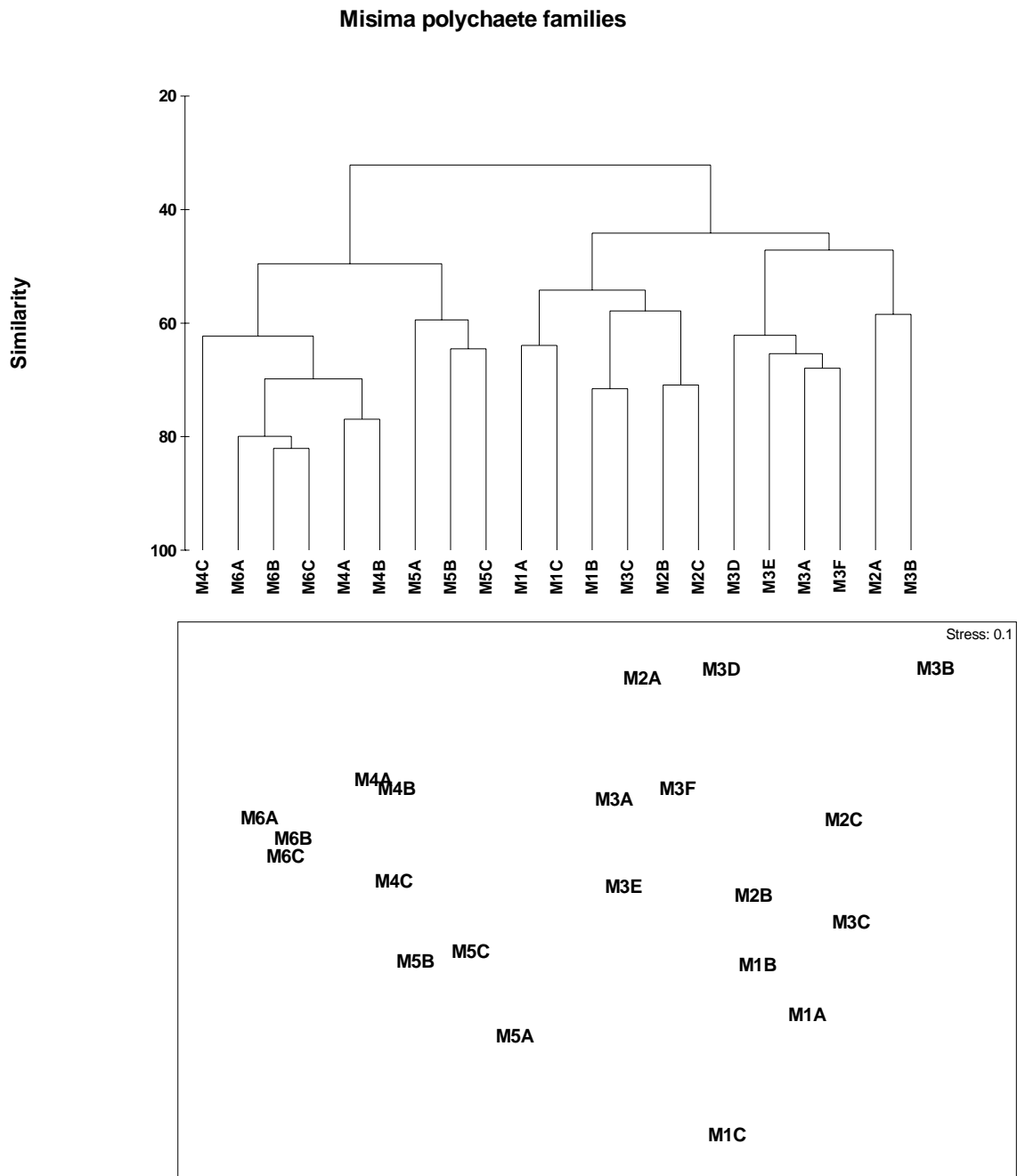
Figure 4.4.6.6. Hierarchical cluster analysis and non-metric multidimensional scaling (nMDS) plots of Misima samples using untransformed polychaete family abundance data. Samples are differentiated by station number (M1, M2, M3 etc.) with letters indicating individual corer drops. Abundance data for corer drops are standardized to ind. m^{-2} to correct for variation in the number of individual cores per drop.
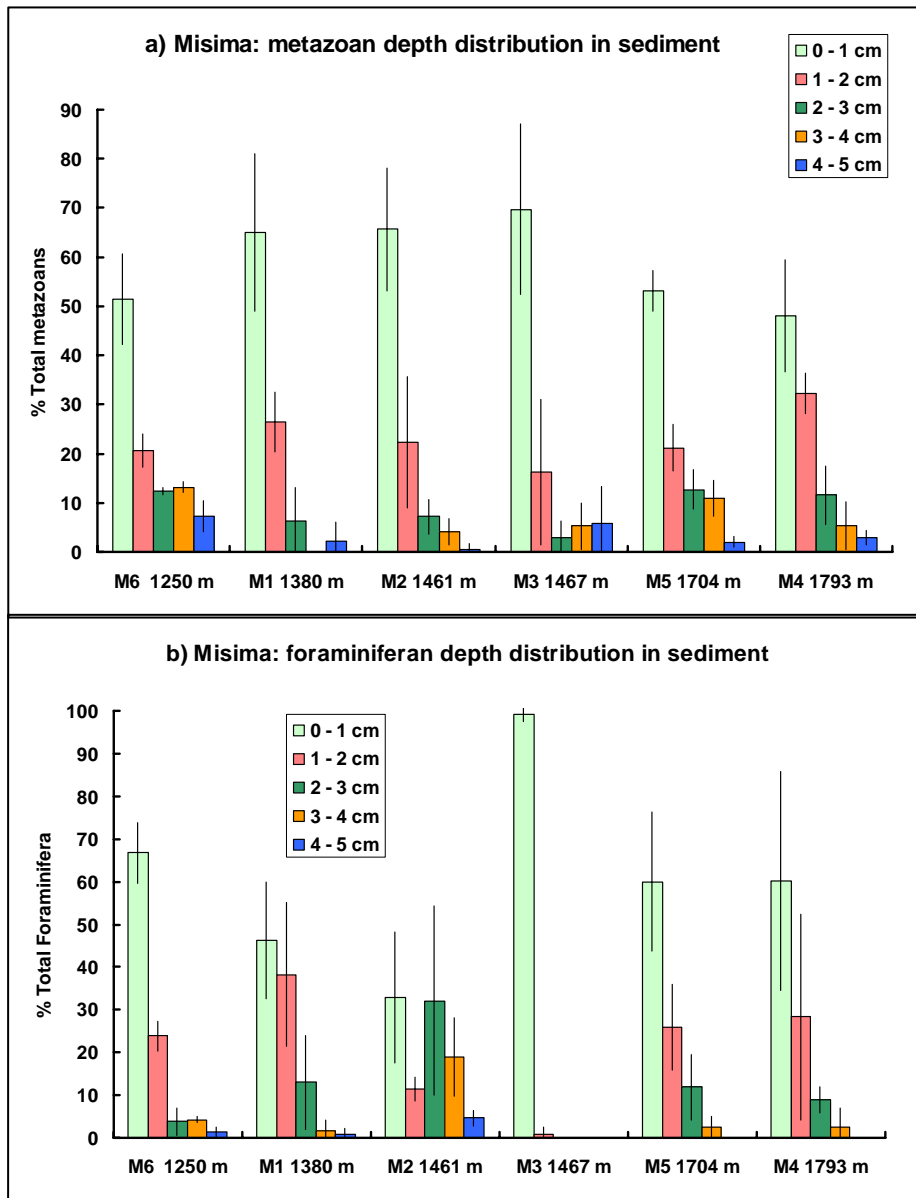
Figure 4.4.6.7. Histograms showing percentage ocurrence of (a) metazoans and (b) foraminiferans (> 250 µm) in 1 cm-deep sections of the upper 5 cm of the sediment column at Misima stations arrayed in order of increasing water depth. Bars represent mean values (± SD) for each station with individual corer drops (n = 1 core per drop) as replicates.

4.4.7 Seabed photography

Station M1

Twenty-two seabed images were obtained at station M1. The seabed type is uniform throughout, with a distinctive rough topography created by a high density of small hummocks and ridges (Figure 4.4.7.1). These do not appear to be biogenic in origin. Probable seagrass blades can be seen on the sediment surface in a few photos (e.g. 007, 011). There are no visible animals, burrows or any other clear evidence of biological activity.
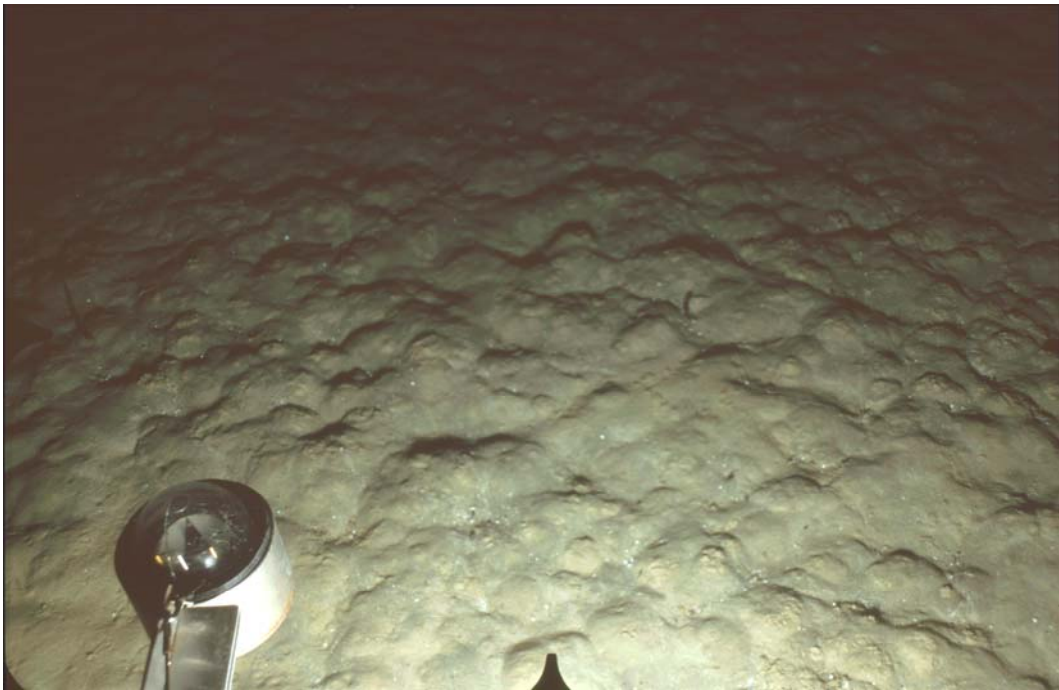
Figure 4.4.7.1. "Bed-hop" camera image taken at Misima station M1, showing an irregular seabed topography of small hummocks and ridges. Width of image at lower edge approximately 1m, depth of field approximately 2.5 m.

Station M5

The 24 images from M5 show a largely flat seabed of fine sediment, with a small-scale topography dominated by features of biological origin. The visible features include many typical deep-sea animal traces such as burrow openings, small mounds, linear trails, "spoke burrows", faecal casts and imprints made by resting seastars. Very few animals are visible, the clearest example being photo 021, which shows a red squat lobster (possibly *Munidopsis* sp.) and a red shrimp swimming just above the seabed (Figure 4.4.7.2).

Figure 4.4.7.2. "Bed-hop" camera image taken at Misima station M5. The flat seabed shows much evidence of biological activity in the form of small mounds, burrow openings and linear trails. A red squat lobster is visible at the lower centre of the image, with at lower right a red shrimp swimming above the seabed. Width of image at lower edge approximately 1m, depth of field approximately 2.5 m. The compass arm was not fitted to the camera frame on this deployment.

4.4.8 Water column geochemistry

Water column nutrient concentrations are reported in Appendix 3B, tables 3B.18-19. Due to the failure of the winch the water column sampling was limited at Misima. For a full explanation see the cruise report, Appendix 7. Samples were obtained from M 1, M2 and M5, with only 2 depths being sampled at M1.

Suspended particulate material (SPM) was collected at stations M1, M2 and M5 (Figure 4.4.8.1). The elemental concentration data for each station are given in Appendix 3B, tables 3B.69-77. The Figures of the depth profiles of elemental concentrations are given in Appendix 3A, Figures 3A.69-77.
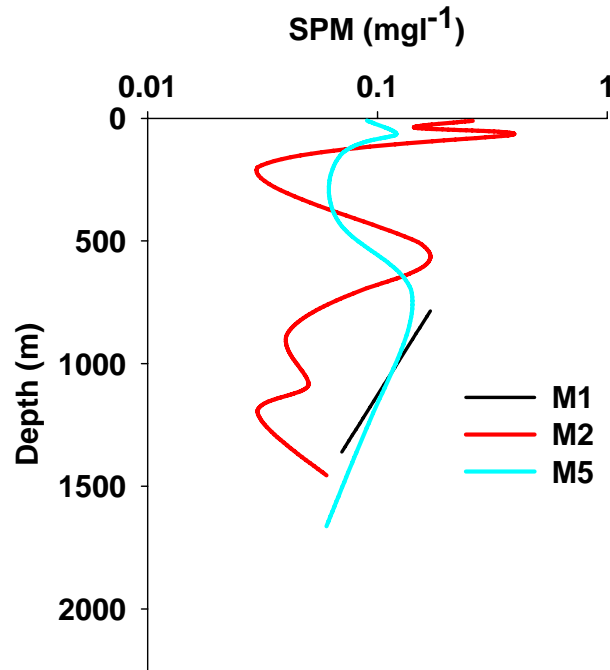
Figure 4.4.8.1 Weight of suspended particulate material per litre of water at Misima stations

The depth profiles of SPM (Figure 4.4.5.1) show some structure which is related to the inputs of particulates and the physical structure of the water.

Table 4.4.8.1 gives the maximum concentration of SPM and the depth at which it occurs at each station. Note this is not reported for M1 as only 2 depths were sampled. The concentration of SPM is highest at M2 with maximum concentration of 0.37 mg L^{-1} occurring at a depth of 70 m.

Table 4.4.8.1 Depth of maximum suspended material at Misima stations

Station	M1	M2	M5
Maximum (mg L^{-1})	NA	0.37	0.14
Depth of maximum m)	NA	70	698
Depth of water column (m)	1380	1461	1704

The SPM depth profiles show highest metal concentrations at depth at station M2. Concentrations at the surface for both M2 and M5 are similar for Ba, Mn and Fe with Al being higher at M5 and Sr lower at M5 (Figure 4.4.8.2). As and Tl show maximum concentrations in SPM at 1200m depth

whereas Ag, Cd and Pb have maximum concentrations at a depth of 890m. The Cu maximum within the SPM occurs at a depth of 70m (Figure 4.4.8.3).
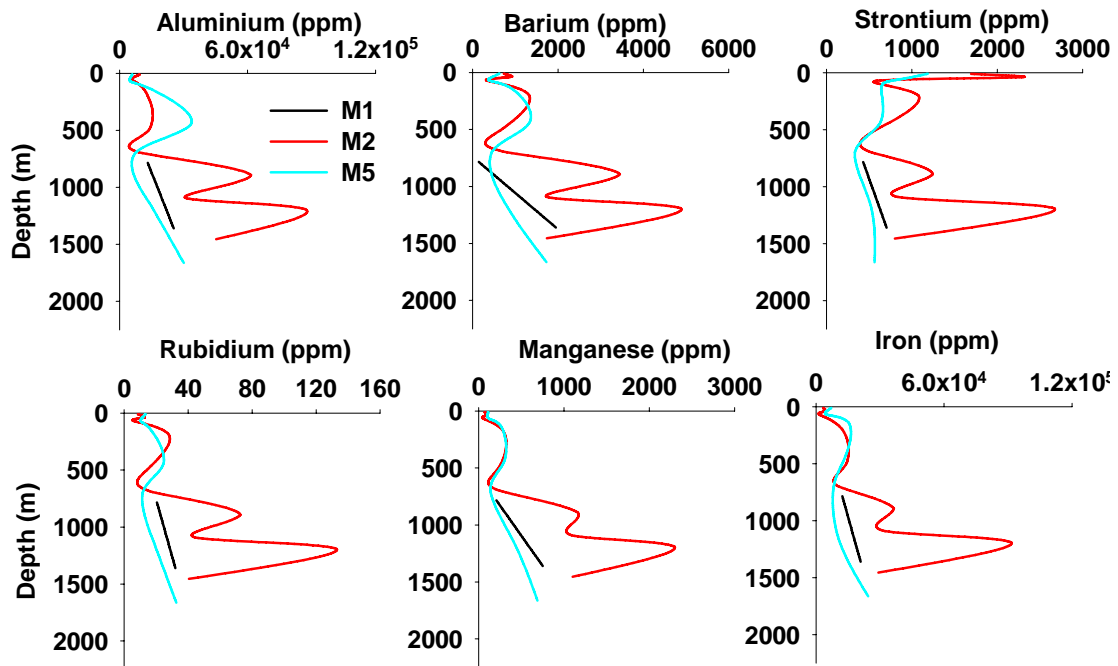
Figure 4.4.8.2 Al, Ba, Sr, Rb, Mn, and Fe concentrations within the suspended particulate material at Misima

The correlation coefficient tables for the SPM are given in Appendix 4B, tables 75-77.

The correlation coefficients for all the samples show a large number of positive correlations. The noteable exceptions are Cu which has only one strong correlation with Au and B which has correlations with Ba, Pb and Th. Ag only has correlations with Al, Cr and Co and Cd with Cr, Co and Ni.

When this is compared to M5 we can see that M5 has many fewer correlations with one negative correlation between Tl and Al. The main differences are the reduced number of correlations with Sr, Ni, Co,Zn, As, Ga, Rb and Mo as well as Au, Tl, Pb and U.
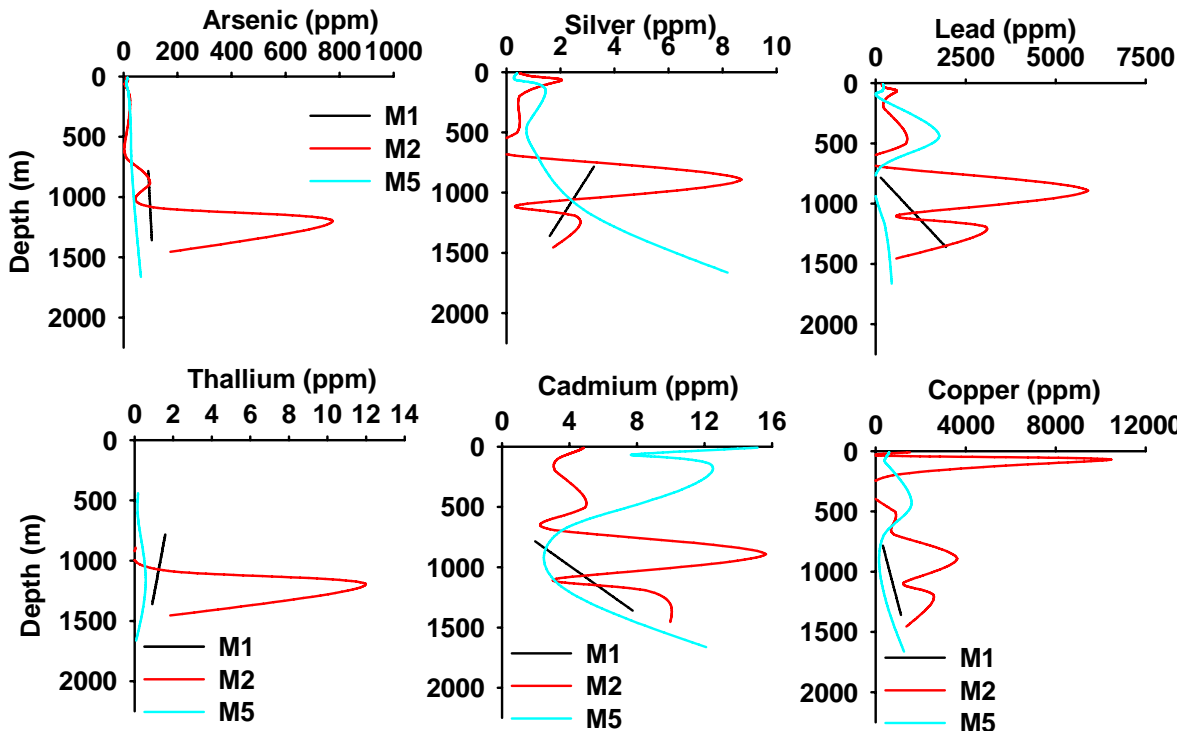
Figure 4.4.8.3 As, Ag, Pb, Tl, Cd and Cu concentrations within the suspended particulate material at Misima

4.5 Analysis and discussion

4.5.1 Bathymetry and Acoustic Character

Much of bathymetry south of Misima, towards the Calvados Islands and in particular the Bwagaoia Basin remains unknown. As stated earlier the predominant depositional process is down-slope, as indicated from the acoustic character of the slope being steep and reflective with irregular to transparent, lens-shaped sub-bottom reflectors. This is attributed to debris flows, possibly the product of the 1997 earthquake remobilising the slope and redepositing the sediments on the floor of the basin. The existence of the submarine channels with marked levees on the basin floor suggests persistent down-slope sedimentation in the form of turbidity flows. As observed in Lihir the reflective floors of the channel indicating the coarser sediments carried by bedload from concentrated density flows originating on the slope. It is assumed that the sediments in this area are a combination of both natural and mine-derived waste.

4.5.2 Physical Oceanography

The most interesting observation from the limited physical oceanographic measurements made is the presence of a well mixed deep bottom layer indicative of strong bottom currents perhaps capable of resuspending and redistributing tailings.

4.5.3 Stations selected

Given the paucity of previous work in the area, and poorly characterised bathymetry, station selection had a trial and error component. This has allowed us to sample three impacted sites (M1 -3), a site which has likely had some impact from mine tailings (M4) and 2 sites that are unimpacted by the mine (M5, 6).

4.5.4 Sediment sampling and sedimentology

When compared to Lihir the most fundamental problem when interpreting the Misima sediment samples, is discriminating between natural sediment and mine-derived waste. Sediments in the Bwagaoia Basin and on the slope toward to north display highly mixed deposits of both natural, pale carbonate-rich sands and terrigenous grey-olive-grey sands of metamorphic origin, presumably mine waste. Stations close to the mine, principally station M1 produced core samples displaying highly disturbed sediments with slumps, turbidites and overturned beds common. This indicates mobile sediments becoming redeposited down-slope under the influence of gravity (Stow, 1986). Given the small size of Misima (approximately <90km^2) and low elevation (<600m) a high sediment supply would not be typical on the submarine slope.

4.5.5 Sediment geochemistry

The geochemical results for the sediment samples around Misima indicate that the past discharge of mine tailings has impacted on the sediment regime of the marine environment surrounding Misima. The geochemical signature and elemental inventories of stations M1-M3 indicate that these stations have been impacted by tailings and continue to have high concentrations of metals within the sediments. The two control stations M5 amd M6 have lower concentrations of metals and in addition M6 differs in composition from M5, possibly being influenced by a high Ca supply from surrounding coral reef areas. Station M4 has a similar chemical signature in the top 2.5 cm of the core to sediments at stations M1-M3.

The sedimentation rates at these stations are higher than would be expected for typical deep sea sediments at these water depths and although the rates calculated may be indicative of the rate of sediment supply at these stations, it must also be remembered that bioturbation can also produce similar depth profiles and the profiles might in fact represent different degrees of mixing at each station.

The chemical analysis of the sediment cores produced elemental depth profiles which indicate that the mine tailings composition is significantly different from the naturally occurring sediments

and can be identified by their geochemical signature. However as a comprehensive baseline study was not undertaken before the start of operations then it has been assumed that the sediment of M4 below 2.5 cm is representative of natural sediment below the tailings at stations M1-M3. The mine tailings are contributing to the metal content of the sediments at the impacted stations which have significantly higher inventories of Al, K, Fe, Mg, Ti and a deficit in Ca and Sr. These stations also have higher inventories of V, Cr, Ni, Zn, Cu, As, Pb and Cd and a deficit of U.

The inventories of excess As at the impacted stations (M1-M3) range from 1.0 g m^{-2} to 1.3 g m^{-2} compared to the control stations (M5-M6) which range from 0 to 0.1 g m^{-2}. Pb also follows this trend with excess inventories ranging from 55 to 60 g m^{-2} at the impacted stations compared to 0.1 to 1.6 g m^{-2}. Other metals also follow this trend. In addition to the solid phase increase in metal concentration there is also an increase in dissolved metals. The pore-waters of the impacted stations show elevated levels of dissolved metals, however, dissolved As levels at the impacted stations are lower than the control stations. The solid phase and pore-water profiles of Fe and Mn suggest that the dissolution of Fe and Mn oxyhydroxides is releasing As and other metals into the pore-waters of the sediment.

The sediment and pore-water analysis indicates that the sediments of Misima have been impacted by mine tailings discharge and the results for M4 suggest that this station is also affected by the tailings but this is limited to the upper 2.5 cm of sediment at this station. The two control stations are unaffected by mine tailings and the two controls have different sediment composition indicating that the sediment supply is different to these two stations.

The analysis of suspended particulate material (SPM) indicates that the impacted station M2 has higher concentrations of metals within the SPM than the control station M5. However, this may also indicate that there is a different source of sediment supply to these two stations as mining discharge had ceased 3 years before sampling. However, the higher concentrations are seen at depth in the water column and could be due to resuspension of fine material.

The combination of the geochemical analysis of the suspended particulate material, the sediment and the pore-waters allow us to construct a picture of the impact of the mine tailings within the environment of Misima. The tailings are contributing a significant amount of material to the immediate marine environment and further afield. The geochemical signature of station M4 indicates that the top 2.5 cm of the sediment core contains mine tailings. If the average sedimentation rate of 1.5 mm y^{-1} is applied then the tailings layer represents a time span of 17 years which indicates that the mine tails reached this area around 1990 which is in excellent

agreement with the start of mining in 1989. Mine tailings discharge ceased in 2004 and the samples were collected in 2007, a 3 year time span equating to 6 mm of sediment deposition. It is therefore unlikely that a decrease in the mine tailings would be seen in the sediment archive due to biological and physical mixing processes, however, it is highly probable that the area most severely impacted by mine tailings discharge is now the source of contaminated sediment to station M4.

When compared to the impacted stations at Lihir it is obvious that heavy metals such as As, Pb and Cd are at much lower levels in the Misima sediments. As there are no baseline sediment geochemcistry data for Misima it is not possible to determine how much, if any, of these metals have been lost to the water-column.

4.5.6 Benthos

Detection of DSTP impacts at Misima

In the following discussion of DSTP impacts at Misima it is important to bear in mind that the benthic communities were analyzed at a relatively coarse taxonomic level, with the Family (for Polychaeta) being the lowest unit employed. In the published literature there has been much discussion of the validity of "Taxonomic Sufficiency" (TS) as a tool in marine ecological research. This method, originally defined by Ellis (1985), is based on the concept that anthropogenic impacts can be detected using coarse taxonomic resolutions, avoiding the need for costly and time-consuming species-level identification of benthic fauna. Several authors have cautioned against the use of TS, arguing that full species-level identification remains essential in baseline biodiversity studies, especially in poorly-known environments (Maurer, 2000; Narayanaswamy *et al*., 2003; Terlizzi *et al*., 2003). On the other hand, TS has been found to provide an acceptable level of sample discrimination in several studies related to monitoring of pollution or other anthropogenic impacts (Dauvin *et al*., 2003; Gomez Gesteira *et al*., 2003; Bertasi *et al*., 2009). In this study we limited the scope of our faunal analysis to the higher taxon and Family level partly for logistical reasons set by the project timetable, and partly because our objective was to test the effects of a large-scale environmental impact, for which community analysis above the species level has been shown to be effective. The following discussion attempts a broad categorization of the Misima stations according to degree of impact. This does not preclude the possibility that more subtle differences within station groups might also be detected with community analysis at the species level.

Station groupings and degrees of impact

The summary table (4.5.6.1) suggests that the six stations fall into two broad groupings of (M1, M2, M3) and (M4, M5, M6). The analysis of polychaete family-level community structure shows that this primary clustering of stations is highly-correlated with an indicator of sediment tailings content (low solid-phase Ca). The low metazoan densities and distinctive community patterns at M1, M2 and M3 are thus likely to indicate a persistent impact of tailings, 3 years after the cessation of DSTP at Misima. With respect to density of metazoan meiofauna, station M1, closest to the outfall station, appears to be the most heavily-impacted. Mean metazoan meiofaunal density at M1 (164 ± 43 ind. m^{-2}) is comparable to that recorded at Lihir station L1 (715 ± 778 ind. m^{-2}), where heavy deposition of fresh tailings is still taking place. Station M1 also shows the copepod-dominated community structure found at stations L1, L2 and L3 in the Lihir DSTP "footprint". Stations M2 and M3 both support a higher meiofaunal density than M1 (> 1000 ind. m^{-2}). Harpacticoid copepods are still the most abundant meiofaunal higher taxon at M2, while M3 approaches the nematode-dominated community pattern seen at M4, M5 and M6. The metazoan meiofaunal communities at stations M1, M2 and M3 therefore show a degree of impact consistent with their respective distances from the DSTP outfall.

The benthic foraminiferan communities at stations M1, M2 and M3 were distinctive in being dominated by large numbers of one or two calcified taxa. A gradation of community structure with distance from the DSTP outfall is again apparent, with the buliminid foram species superabundant at M1, slightly less abundant at M2 and absent at M3. The miliolid foram species was abundant at all three stations. The occurrence of highest foram densities at the most tailings-affected stations at Misima contrasts with the situation at Lihir, where living forams were entirely absent at stations L1 and L2, and present only in low numbers at L3. Elberling *et al.*,(2003) found that forams were eliminated from tailings-affected sediment in a Greenland fjord but that recolonization was rapid once tailings deposition had ceased. A similar pattern seems to operate at Lihir and Misima, with forams being absent from Lihir stations still receiving large quantities of fresh tailings but numerous at Misima where fresh deposition is no longer occurring.

Table 4.5.6.1 Broad patterns of Misima station groupings arising from the main components of the benthic faunal analysis

Metazoan meiofaunal density	M6 >> (M4, M5) >> (M1, M2, M3)
Metazoan meiofaunal community composition	M4, M5, M6: nematodes >> copepods
	M3: nematodes approx. = copepods
	M1, M2: copepods > nematodes
Foraminiferan density and composition	M4, M5, M6: similar density, no taxa dominating
	M1, M2: Miliolida and Buliminida abundant
	M3: Miliolida abundant
Macrofaunal density	M6 > M4 > M5 > (M1, M2, M3)
Macrofaunal community composition (higher taxa)	M4, M5, M6: peracarid crustaceans common
	M2, M3: peracarids very rare
	M1: peracarids very rare, echiurans common
Polychaete community composition (Family-level)	Primary division between (M1, M2, M3) and (M4, M5, M6)

At the higher-taxon level, the macrofaunal communties at M1, M2 and M3 were all distinguished by the absence or rarity of peracarid crustaceans. The relative abundance of echiuran worms at M1 was a notable feature unique to that station.

Within the "low-impact" group of stations (M4, M5, M6), sediment granulometry and geochemical data provided no evidence of tailings at M5 and M6. This is consistent with the distance of M6 from the DSTP outfall and the tailings depocentre in the Bwagaoia Basin. Results from M6 are therefore the best available indicator of the natural state of bathyal communities at this depth in the Misima region. With respect to community composition, stations M4, M5 and M6 showed close agreement (at the taxonomic levels investigated), but significant differences were found in

total densities of metazoan meio- and macrofauna. Sediment geochemical evidence for presence of tailings in the top few centimetres at M4 is clear (section 4.4.5). Depth-dependent food input is considered to be the primary cause of the global bathymetric gradient in benthic abundance and biomass in the deep sea (Rex *et al*., 2006). Stations M4 and M5 lie in deeper water than M6 (by 454 and 543 m respectively) and would be expected to support a lower benthic standing stock for this reason alone. Sediment organic carbon and nitrogen content was higher at M6 than at M4 or M5, reflecting the greater flux of organic material from the surface. The possible contrasts between M4, M5 and M6 in tailings exposure are therefore confounded with food availability, making it difficult to assess the relative importance of the two factors.

Causal factors behind tailings impacts

The correlation of community patterns with an indicator of tailings content does not in itself identify the particular causal factor (or factors) behind the observed differences. Manipulative experiments, such as those performed in shallow-water settings (Lee and Correa, 2004; Lee *et al*., 2006; Gwyther *et al*., 2009), would be necessary to distinguish between the effects of the wide variety of contaminants present in the mine tailings.

Studies of tailings impacts in shallow water indicate that metazoan meiofauna are sensitive both to physical changes in sediment grain size and to pore-water toxin concentrations (Lee and Correa, 2004, 2005, 2007; Lee *et al*., 2006). Sediments in the upper 5 cm of the six Misima stations were all sandy muds with no sharp contrast in mean grain size between high- and low-impact station groups. Sediment data tabulated in section 4.3.7 show elevated concentrations of pore-water cadmium and lead, both potential toxins, at stations M1 and M3 compared with M4 and M6. There was little difference in pore-water copper, while arsenic was actually present at higher levels at M4 and M6. Pore-water concentrations of cadmium and lead are therefore correlated with the low meiofaunal densities in the Bwagaoia Basin, but without manipulative experiments we cannot conclude that a cause-and-effect relationship exists.

Studies of coastal macrofaunal community responses to tailings deposition agree in showing significant declines in total abundance and diversity in heavily-impacted areas (Burd *et al*., 2000; Burd, 2002; Lancellotti and Stotz, 2004). In contrast to the meiofaunal pattern, impacts have been largely attributed to the physical effects of smothering and sediment instability, with little evidence of any additional effect of heavy metals or other toxic contaminants (Olsgard and Hasle, 1993; Kline and Stekoll, 2001). In the Cassidaigne Canyon on the French Mediterranean slope, reduced macrofaunal densities in areas receiving discharges of "red mud" were also attributed to

smothering (Dauvin, 2010). Recolonization of tailings-affected sediments by macrofauna is generally rapid once deposition has ceased and the substratum has stabilized (Ellis, 2000; Burd, 2002; Dauvin, 2010). Core data and seabed photographs show that sediments at M1 are unstable and affected by downslope debris flows and turbidites, processes that would be expected to depress the numbers of both meio- and macrofauna. Persistent toxic effects of tailings may also contribute to the low macrofaunal densities and community patterns across all three Bwagaoia Basin stations (M1, M2, M3). In a West Greenland fjord affected by tailings from the Black Angel lead/zinc mine, Josefson *et al*.,(2008) found that recolonization of tailings-affected sediments was slow, and impacted areas were still dominated by opportunistic macrofaunal species 15 years after mine closure. A correlation was found between community diversity and sediment solid-phase lead content, with effects apparent above a threshold of ~ 200 mg Pb kg^{-1} sediment. Table 4.5.6.2 shows values for solid-phase lead from cores at the six Misima stations. Lead levels at stations M1, M2 and M3 are clearly far above Josefson *et al*.'s threshold value for macrofaunal community impacts. Station M4 sits almost on the 200 mg kg^{-1} threshold, while M5 and M6 are well below it.

Table 4.5.6.2 Solid phase lead from Misima (0 – 5 cm)

Station	Core	Solid-phase Pb mg kg^{-1} (mean value 0 – 5 cm)
M1	MC 64-6	434.7
M2	MC 67-4	630.2
M3	MC 47-3	612.0
M4	MC 56-1	238.7
M5	MC 58-6	42.1
M6	MC 63-4	4.0

Caution must be exercised in applying the findings of one shallow-water impacts study to the very different environmental setting at Misima, but Josefson *et al*.'s (2008) results suggest that

persistent contaminants from mine tailings may be a factor influencing macrofaunal abundance and community structure at M1, M2 and M3.

Prior to this study there were no reliable pre-impact biological data to indicate the natural state of deep-sea benthic communities off Misima. In addition, the full spatial extent of tailings dispersal was uncertain, although the Bwagaoia Basin depocentre had been identified. In contrast to Lihir, *a priori* designation of sampling stations as "impacted" and "non-impacted" was not possible at Misima for areas outside the Bwagaoia Basin. Our assessment of the scale of biological impacts is therefore based on correlations between benthic community abundance and composition, and geochemical indicators of sediment tailings content. This work leads to the conclusion that stations M1, M2 and M3 are still significantly impacted by tailings 3 years after the cessation of DSTP at Misima. In terms of benthos only, Stations M4 and M5 show little evidence of tailings effects and are closely similar to station M6, which is the best available indicator of the natural, unimpacted deep-sea ecosystem in this area. At this stage it is premature to consider the Misima stations in terms of "recovery" from the impacts of tailings. We do not know whether the heavily-impacted community states observed at M1, M2 and M3 form part of a continuum that will change over time towards the more natural benthic conditions seen at M4, M5 and M6, or whether they represent quasi-stable states that will remain in their present condition for many years. Future time-series sampling will be necessary to answer this question.

Comparison of tailings-impacted stations at Lihir and Misima

Assessment of benthic community recovery at Misima is hampered by the lack of any baseline, pre-DSTP data for the area. Some inferences can be drawn by comparison of stations showing the clearest geochemical signals of sediment tailings content (M1, M2, M3) with those showing less impact (M4, M5, M6). The effects of ongoing tailings deposition can also be evaluated by comparing community patterns at Lihir (where DSTP is still in progress) and Misima (3 years after cessation of DSTP). Table 4.5.6.3 summarizes key biological parameters at the three tailings-impacted stations at Misima with those at Lihir stations L1 and L2, which bracket the Misima stations with respect to water depth.

Table 4.5.6.3 Key biological parameters at impacted Misima stations in comparison to impacted Lihir stations

	L1 850 m	M1 1380 m	M2 1461 m	M3 1467 m	L2 1750 m
Fresh tailings deposition	Active	Ceased	Ceased	Ceased	Active
Metazoan meiofauna ind. m^{-2}	715 ± 778	164 ± 43	1040 ± 605	1245 ± 426	1116 ± 450
Meiofaunal community	Copepod-dominated	Copepods > Nematodes	Copepods, Nematodes, Ostracods	Copepods = Nematodes	Copepod-dominated
Macrofauna ind. m^{-2}	446 ± 250	2532 ± 388	2715 ± 1014	3038 ± 749	136 ± 103
Foraminifera	Absent	Abundant	Abundant	Abundant	Absent

The summary table shows that abundance of metazoan meiofauna is not obviously depressed by active tailings deposition at L1 and L2, relative to the stations that have been free from fresh tailings input for approximately 3 years. However, the meiofauna present at L1 and L2 consists almost entirely of copepods, contrasting with the more even occurrence of major taxa at M2 and M3. Station M1 shows an extremely low meiofaunal density even compared with the Lihir stations that still receive fresh tailings. This may be a physical disturbance effect as indicated by the photographic evidence of sediment instability at M1. Macrofaunal and Foraminiferan densities show a more consistent effect of fresh tailings deposition, with both groups showing greatly reduced abundance at L1 and L2. These summary data lead to the following conclusions regarding the impacts of tailings deposition and the extent of benthic recovery at Misima:

- Rapid colonization of fresh tailings by harpacticoid copepods means that total metazoan meiofaunal densities are not significantly depressed at L1 and L2 relative to the three Misima stations.
- In the 3-year period following cessation of DSTP, meiofaunal community structure at M2 and M3 has moved closer to the nematode-dominated pattern typical of deep-sea sediments.
- Station M1 still shows a meiofaunal community dominated by copepods, possibly as a consequence of physical disturbance by downslope sediment slides.

- Active deposition of fresh tailings leads to virtual elimination of benthic Foraminifera and severely reduced abundance of metazoan macrofauna. Three years after cessation of DSTP at Misima, stations M1, M2 and M3 show high densities of benthic forams, primarily resulting from "blooms" of one or two calcareous taxa. Densities of metazoan macrofauna have also partially recovered, but are still significantly reduced in comparison with the low-impact stations M4, M5 and M6.

4.5.7 Seabed photography

The distinctive, irregular lumpy appearance of the seabed at M1 is consistent with the core evidence of downlope sediment slides and turbidity flows. A high frequency and intensity of physical disturbance would be expected to depress the numbers and diversity of sediment infauna and this pattern was observed in the biological core data from this site. The seabed topography at M1 appears to be largely imposed by physical processes, obscuring any smaller-scale biogenic features created by the sparse infauna.

In contrast, station M5, in deeper water further from the mine outfall, showed a seabed environment typical of lower bathyal depths, with a varied biogenic topography of mounds, burrow openings, linear trails and other animal traces. The scarcity of animals actually visible on the seabed is entirely normal for a small sample of images from this depth range, and is not to be taken as evidence of mine-related impacts. A much more extensive photographic survey, in the order of hundreds of images (at least), would be required to provide an accurate estimate of epifaunal abundance and diversity.

4.6 Summary

This is the first ever replicated study of the benthic and sediment geochemical environment after the closure of the DSTP system and was carried out with the state-of-the-art benthic sampling equipment and analytical methods. Despite the lack of background information, stations were selected that allowed characterisation of both impacted and reference stations. In contrast to the operational site at Lihir, where extreme differences between benthic assemblages at control and impacted sites rendered statistical analysis redundant, impacted stations showed some degree of post-impact recolonisation. None-the-less, detailed analysis of both the benthic faunal assemblage and the dominant metal concentrations revealed very clear differences between stations. Three stations in the basin adjacent to the Misima DSTP were very clearly impacted by mine tailings, a fourth station was determined to be partially impacted but possibly indirectly through post depositional resuspension and re-deposition.

5. Integration: what have we learned during the 3 studies?

      5.1 What are the effects of DSTP on deep benthos?

This study has provided the first detailed quantitative survey of the effects of mine tailings placement on deep-sea benthic communities. Replicated samples collected using state-of-the-art methods were processed and the data analyzed to the standards demanded by modern deep-sea ecological research, thus providing a solid basis for assessment of impacts and a baseline for monitoring of future changes. The major achievements in each of the three study areas were as follows:

Basamuk: Benthic environments, meio- and macrofaunal communities have been characterized at stations along the projected tailings "footprint", and at control stations to the east and west of the outfall. This establishes a quantitative baseline for monitoring of future impacts off the Basamuk DSTP outfall and assessment of tailings dispersal and environmental impacts along the Rai Coast.

Lihir: A detailed comparison of depth-matched stations to the east and west of Lihir island provides an unambiguous demonstration that ongoing DSTP has major impacts on the abundance and community structure of meio- and macrofauna, extending to water depths of at least 2020 m.

Misima: Our results demonstrate that three stations in the Bwagaoia Basin differ significantly in abundance and community structure of benthic Foraminifera, metazoan meiofauna, and macrofauna in comparison with three stations outside the basin. Integration of biological, sedimentological and geochemical data shows that the observed differences are correlated with sediment tailings content. It can therefore be inferred that significant tailings impacts are still apparent 3 years after the cessation of DSTP at Misima.

5.2 What effect do mine tailings have on sedimentary geochemistry?

The discharge of mine tailings alters the natural sediment geochemistry at affected stations at both Lihir and Misima. Consideration of the geochemistry of the suspended particulate material, the sediments and their pore-waters allows detailed examination of the main biogeochemical processes involved.

The sedimentation rates at stations impacted by tailings are much higher than would be expected for typical deep sea sediments at these water depths. The chemical analysis of the sediments indicates that the mine tailings composition is significantly different from naturally occurring

sediments and can be identified unambiguously by their geochemical signatures. This was to be expected at Lihir as the method of extraction of the gold or silver uses excess quantities of iron to neutralise any unused cyanide that may be present in the tailings after the precious metal has been extracted but is also the case at Misima where dilution was used to reduce cyanide concentrations. The pH of the tailings is also increased which results in the formation of iron, manganese and aluminium oxides and oxyhydroxides as fine flocculent materials. The solid phase and pore-water profiles of iron and manganese suggest that the dissolution of iron and manganese oxyhydroxides release arsenic and other metals into the pore-waters of the sediment. This process is well known and occurs naturally as the redox conditions of the sediment change. However, the direct input of the tailings hydroxides affects the sediment geochemistry by inputting increased amounts of scavenged metals to the system by pre-concentration of these within the tailings slurry.

The mine tailings contribute to the metal content of the sediments at the impacted stations yielding significantly higher inventories of heavy metals. The pore-waters of the impacted stations show elevated levels of dissolved metals with dissolved arsenic levels at the impacted stations of Lihir being at least an order of magnitude higher compared to the control stations. In contrast, dissolved arsenic levels at the impacted stations of Misima were lower than at control stations indicating either that original arsenic concentrations much were lower at Misima than at Lihir or that arsenic has been lost to the water-column.

At Misima, sediment biogeochemistry is dominated by a combination of iron and manganese cycling and the amount of organic carbon within the system. Dilution by tailings reduces the concentration of organic matter in sediments at the impacted stations altering the rates of diagenetic processes. The concentration of metals by iron and manganese oxyhydroxides is the major process of removal of dissolved species, however, at the impacted sites there is an increase in iron and aluminium which may also influence metal speciation within the environment - either removing dissolved metals to the solid phase or releasing them to the dissolved phase. The results presented here indicate that heavy metals are being released as the iron and manganese oxydroxides are dissolved but further work is required to ascertain whether the biogeochemical processes within the impacted sites have the potential to release heavy metals to the water column or whether these metals are being locked in the sediment system and buried with natural sedimenting material. The Misima results suggest that concentrations of arsenic, copper and vanadium increase in the pore-water towards the surface of the sediment whereas at Lihir, where dissolved and solid phase concentrations are much higher, the heavy metal concentrations in the

pore-water decrease towards the sediment surface, being removed as dissolved iron and manganese are reoxidised. The difference in metal behaviour between Lihir and Misima is likely to be because of the non-steady state at Lihir as further, oxidised tailings are continuously added to the surface diluting the natural supply of organic matter. In contrast, several of the stations at Misima receive intermittent fresh supplies of likely anoxic material caused by slope failures whereas others receive an undiluted organic matter supply. The amount and type or organic material within each system, both dissolved and particulate is important in determining the fate of metals within the tailings impacted sites.

5.3. The fate of suspended material within the water column following a release from a DSTP in the Western Equatorial Pacific (WEP)

These comments relate to the situation that prevails along the north coast of PNG and in the islands to the east of it. The peculiar conditions of this region are: relatively weak winds (generally less than 5 m s^{-1}); steep deep slopes; and proximity to the Equator (resulting in a weak Coriolis force). The comments do not apply to locations where any one of these conditions does not hold, for example the shallow Coral Sea which is also further from the Equator.

As was discussed earlier the surface and intermediate waters of the WEP are swept by large and persistent ocean currents that have been driven westward by prevailing oceanic conditions to the east. There is thus good overall long term flushing of the region such that any suspended material will be transported generally northward towards the Equator. However, the vertical redistribution of material within the water column is not so certain and needs further comment. There are two fundamental processes that cause the re-distribution of material in the sea - advection and diffusion, which in the present context translate into coastal upwelling and vertical mixing. We consider vertical mixing first.

It is generally accepted that water at the upper level of Pacific Equatorial Water and below (i.e. below the salinity maximum at about 250 m) mixes very slowly in the Pacific, so that it retains its identity over very long distances. Whilst no direct measurements of vertical mixing were made in the upper layers, its general strength can be inferred from the intensity of stratification, with strong stratification indicating weak (or slow mixing). During the cruises, the surface waters were invariably stratified by a salinity gradient, although the temperature profile was more generally uniform to as deep as 80 m. The intensity of stratification below 80 m (here and throughout the Equatorial Pacific) is so great that it is inconceivable that suspended material released below the

thermocline (say 100 m) could diffuse vertically back to the surface, whether from wind induced surface mixing or internal wave mixing, anywhere in the vicinity of a DSTP. The strength of stratification between 80 m and the salinity maximum also indicates weak mixing.

Thus if suspended material is to be lifted to the surface it would require a horizontal (wind forced) divergence of the surface currents, leading to upwelling. Along a long coastline such divergence usually occurs when a steady and strong wind blows parallel to the coast in such a direction that the surface Ekman layers of the ocean are driven offshore. In temperate latitudes upwelling tends to occur on the Eastern side of an ocean where strong winds blow towards the Equator (e.g. along the coasts of South America or Portugal, see Figure 5.3.1). On or very close to the Equator such winds would need to be directed offshore. Along the northern coast of PNG upwelling favourable winds come from the NE, or possibly offshore since the significance of Coriolis acceleration it is not immediately obvious at such low latitudes. However, such winds are generally too weak.
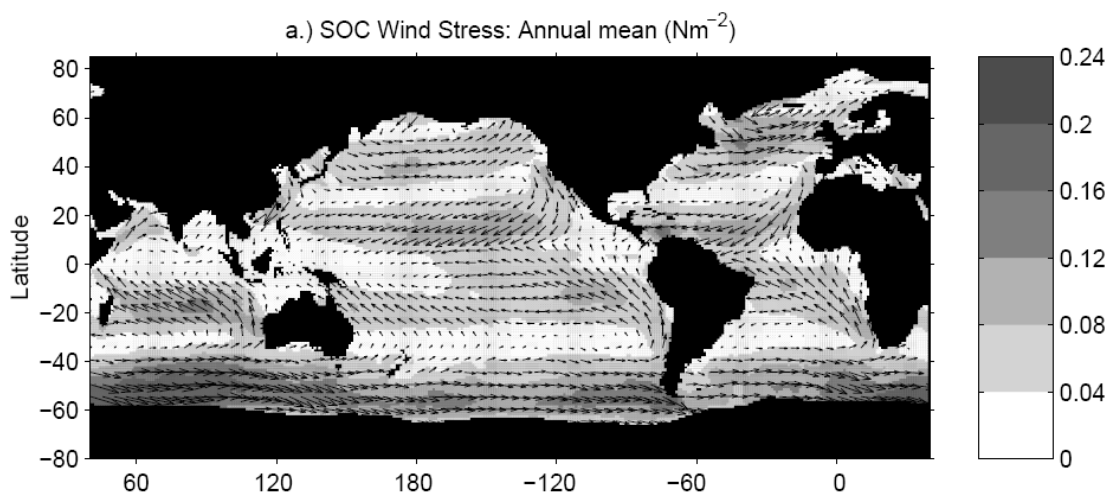

Figure 5.3.1. Mean wind stress in the world ocean. The figure shows that upwelling favourable winds (strong, with Coriolis directed offshore) tend to be found at temperate latitudes on the eastern sides of the major oceans (Josey et al. 2002)

Since the coasts of Lihir and Misima are too short to allow upwelling divergence to occur, and during the survey of the Vitiaz Basin there was no evidence of any upwelling isopycnals . Furthermore, even in the most intense of upwelling regions such as the west coast of South America the upwelled waters come from fairly shallow depths (i.e. less than 150 m, *Tomczak, M. and J S. Godfrey (2003), Regional Oceanography: an Introduction, Daya Publishing House*). It thus seems very unlikely on either observational or theoretical grounds that upwelling from below the depth of the salinity maximum (250 m) is a significant process in the WEP.

6. Research gaps

6.1 Physics

A comprehensive understanding of the dynamic regime of any of these sites is lacking. However, given the daily, seasonal and interannual / decadal variability of the far field system, it is difficult to see how a comprehensive evaluation of the full physical regime can be determined within a realistic timescale. It is also not clear whether such an exercise would throw much additional light on the impact of a DSTP on the environment.

A full scale dynamical ocean model could be applied but inevitably this would be very expensive and require boundary conditions that were established from existing operational models of the Equatorial Pacific. It would be advisable that consideration should be given to modelling the whole of the north and eastern sides of the PNG archipelago in one go in order to provide results that could be applied to any future DSTP sites. The model should also investigate seasonal and ENSO variations in the offshore currents. Such an exercise should only be done by an established and experienced ocean modelling group with access to operational model boundary conditions.

6.2 Benthos

Basamuk: At present we have very limited information on larger benthic animals (megafauna) in the study areas. These animals are not represented in small-volume benthic core samples and can only be effectively surveyed by seabed photography. The 2008 cruise allowed only limited opportunities for seabed photography, and a more thorough survey would be highly desirable. Given the steep and irregular topography of the Rai continental slope, a deep-water remote operated vehicle (ROV) would be the most appropriate platform for a camera survey.

Lihir: The 2007 cruise demonstrated that tailings impacts are detectable to the east of the island to depths of at least 2020 m. It would be desirable to achieve a more precise estimation of the spatial extent of biological impacts by sampling in deeper water further to the east, and by sampling along transects running north-south through the tailings "footprint". This would allow identification of any geochemical thresholds associated with biological impacts.

As mentioned for Basamuk, we did not have the capacity to survey the benthic megafauna off Lihir on the 2007 cruise. The Lihir DSTP "footprint" covers a very large area, mostly over a gentle bathymetric gradient, and in this setting a towed, off-bottom seabed photographic system such as WASP or SHRIMP (Jones *et al.*, 2009) would be the most effective survey method.

Misima: It would be valuable to carry out a more comprehensive photographic survey of benthic environments and megafaunal communities at stations off Misima. A deep-water ROV would be needed to survey the steep slope close to the outfall position, but for stations with more level topography an off-bottom towed system would allow greater areal coverage.

Species-level identification of benthic fauna collected in 2008 was not feasible within the timeframe of this project. It would be valuable to continue analysis to this level for finer-scale discrimination of stations and assessment of DSTP impacts on benthic biodiversity.

6.3 Geochemistry

Basamuk: The results of sediment and water column geochemistry analyses at sites within the Vitiaz Basin (encompassing Astrolabe Bay and Pommern Bay, Basamuk) provide an overview of the geochemistry of the area. However, with regards to the site at Basamuk where the discharge pipeline will be situated, it would be advantageous to understand the sediment transport dynamics in greater detail. The vertical distribution of suspended particulate material in the water-column indicates that particulate matter concentration is primarily determined by the character of the different water masses and currents that are present. Large amounts of particulate material from land runoff are likely to be very important in this area and therefore better understanding of both the influence of land runoff and its seasonal changes in sediment transport is desirable. This would also increase knowledge of the predominant mechanisms influencing the extent of future tailings transport and the effects of natural sediment input in the area.

Misima: The results from the Misima study indicate that the sediments closest to the mine remain impacted by the mine tailings. The combined pore-water/sediment studies indicate that biogeochemical cycling is taking place and that some elements are being redistributed between the sediments and pore-water and overlying water. In addition the sediments at Misima are being redistributed due to physical instability on the steep submarine slopes bordering the island. This affects biogeochemical processes and rates occurring within this system. Additional sampling using *in-situ* landers to monitor biogeochemical processes on the seabed would add to the information gathered and would help understand the long term effects of mine tailings on similar marine systems.

The physical oceanography results suggest that there is a likelihood of bottom sediment resuspension. This will have an impact on the redistribution of contaminants within the marine system of Misima and therefore the establishment of a number of stations that would be

monitored long-term to assess the redistribution of sediment and suspended particulate material is recommended.

Lihir: The geochemical analysis of sediments and pore-waters at sites impacted with tailings indicate the accumulation of heavy metals. The analysis of the water-column suspended particulate material indicates that mine tailings are being transported further afield by the ocean currents. As with Misima it would be advisable to set up a number of long term monitoring stations that could be used to monitor sediment and contaminant transport. It would be important to choose these stations to allow the important physical and chemical factors to be measured, including *in-situ* measurement of biogeochemical cycling and measurement of suspended particulate material. Technology has advanced in recent years and intelligent moorings could be used to provide a large amount of data. In many cases this data could be obtained in real time giving the added advantage providing an early warning system to the mine itself of any unusual events which would allow early intervention and mitigation.

Further investigation of the extent of transport and deposition of the mine tailings should be made, including an assessment of the amount of tailings being distributed in the far field caused by advection of sub-surface plumes of fine tailings material.

7. Literature cited

Admiralty, 1988. Pacific Islands Pilot, NP 60. Hydrographer of the Navy.

Alongi, D.M. and Pichon, M., 1988. Bathyal meiobenthos of the western Coral Sea: distribution and abundance in relation to microbial standing stocks and environmental factors. Deep-Sea Research 35: 491-503.

Alongi, D.M., 1987. The distribution and composition of deep-sea microbenthos in a bathyal region of the western Coral Sea. Deep-Sea Research 34: 1245-1254.

Alongi, D.M., 1990. Bacterial growth rates, production and estimates of detrital carbon utilization in deep-sea sediments of the Solomon and Coral Seas. Deep-Sea Research 37: 731-746.

Alongi, D.M., 1992. Bathymetric patterns of deep-sea benthic communities from bathyal to abyssal depths in the western South Pacific (Solomon and Coral Seas). Deep-Sea Research 39: 549-565.

Ameziane, N. and Roux, M., 1997. Biodiversity and historical biogeography of stalked crinoids (Echinodermata) in the deep sea. Biodiversity and Conservation 6, 1557-1570.

Apte, S.C. and Kwong, Y.T.J., 2004. Deep sea tailings placement: critical review of environmental issues. Review undertaken by CSIRO Australia and CANMET Canada, 94 pp.

Asmund, G., Bollingberg, H.J. and Bondam, J., 1975. Continued environmental studies in the Qaumarujuk and Agfardlikavsa fjords, Marmorilik, Umamak district, Central West Greenland, Geol. Surv. Greenland Rep. 80: 53-61.

Asmund, G., Broman, P.G and Lindgren, G., 1994. Managing the environment at the Black Angel mine, Greenland. International Journal of Surface Mining, Reclamation and Environment 8, 37-40.

Berg, P., Risgaard-Petersen, N. and Rysgaard, S., 1998. Interpretation of measured concentration profiles in sediment pore water. Limnology and Oceanography 43, 1500-1510.

Berkun, M., 2005. Submarine tailings placement by a copper mine in the deep anoxic zone of the Black Sea. Water Research 39, 5005-5016.

Bertasi, F., Colangelo, M.A., Colosio, F., Gregorio, G., Abbiati, M. and Ceccherelli, V.U., 2009. Comparing efficacy of different taxonomic resolutions and surrogates in detecting changes in soft bottom assemblages due to coastal defence structures. Marine Pollution Bulletin 58, 686-694.

Bett, B.J., Vanreusel, A., Vincx, M., Soltwedel, T., Pfannkuche, O., Lambshead, P.J.D., Gooday, A.J., Ferrero, T. and Dinet, A., 1994. Sampler bias in the quantitative study of deep-sea meiobenthos. Marine Ecology Progress Series, 104: 197-203.

Billett, D.S.M., 1991. Deep-sea holothurians. Oceanography and Marine Biology Annual Review 29, 259-317.

Blott, S.J. and Pye, K., 2001. GRADISTAT: a grain size distribution and statistics package for the analysis of unconsolidated sediments. Earth Surface Processes and Landforms 26, 1237-1248.

Bollingberg, H.J. and Johansen, P., 1979. Lead in spotted wolfish, *Anarhichas minor*, near a zinc-lead mine in Greenland. Journal of the Fisheries Research Board of Canada 36, 1023-1028.

Boltovskoy, D., 2005. Zooplankton of the South Atlantic Ocean, ETI Bioinformatics.

Boxshall, G.A. and Halsey, S.H., 2004. An Introduction to Copepod Diversity. The Ray Society, 421 pp.

Brewer, D.T., Milton, D.A., Fry, G.C., Dennis, D.M., Heales, D.S., and Venables, W.N., 2007. Impacts of gold mine waste disposal on deepwater fish in a pristine tropical marine system. Marine Pollution Bulletin. 54:309-321.

Bruns, W., Herzog, J. and Galkin, S.V., 1997. Megafauna associated with hydrothermal vents in the Manus Back-Arc Basin (Bismarck Sea). Marine Geology 142, 197-206.

Burd, B., 2002. Evaluation of mine tailings effects on a benthic marine infaunal community over 29 years. Marine Environmental Research 53: 481-519.

Burd, B., Macdonald, R. and Boyd, J., 2000. Punctuated recovery of sediments and benthic infauna: a 19-year study of tailings deposition in a British Columbia fjord. Marine Environmental Research 49: 145-175.

Butt, J., Lindstrom, E., 1994. Currents off the east-coast of New Ireland, Papua New Guinea, and their relevance to regional undercurrents in the western Equatorial Pacific Ocean. Journal of Geophysical Research-Oceans 99 (C6), 12503-12514

Cassie, M.R., 1968. Sample design. In: Zooplankton sampling. UNESCO monographs on oceanographic methodology, 2. UNESCO (ed.) Paris: United Nations Educational, Scientific and Cultural Organization, pp. 105-144.

Clarke, D.S., Lewis, R.W., and Waldron, H.M., 1990. Geology and trace-element geochemistry of the Umuma gold-silver deposit, Misima Island, Papua New Guinea. Journal of Geochemical Exploration, 36, 201-223.

Clarke, K.R. and Warwick, R.M., 2001. Change in Marine Communities: an Approach to Statistical Analysis and Interpretation, 2nd Edition. PRIMER-E, Plymouth.

Coffey Natural Systems, 2007. Environmental Baseline Report, Ramu Nickel Project CR 161_33_v2

Coffey Natural Systems, 2009. Environmental Impact Statement Lihir Gold Limited, Main Report, Million Ounce Plant Upgrade Project, Summary Report Volume 2 , October 2009 CR235-50-v4, Coffey Natural Systems.

Coffey Natural Systems, 2007. Environmental Baseline Report, Ramu Nickel Project. Volume A, Main Report, 34 pp.

Cullen, A.B. and Piggot, J.D., 1989. Post-Jurassic tectonic evolution of Papua New Guinea. Tectonophysics, 162, 291-302.

Dauvin, J.C., 2010. Towards an impact assessment of bauxite red mud waste on the knowledge of the structure and functions of bathyal ecosystems: the example of the Cassidaigne canyon (north-western Mediterranean Sea). Marine Pollution Bulletin 60, 197-206.

Dauvin, J.C., Gomez Gesteira, J.L. and Salvande Fraga, M., 2003. Taxonomic sufficiency: an overview of its use in the monitoring of sublittoral benthic communities after oil spills. Marine Pollution Bulletin 46, 552-555.

Davies, R.M. and Ballantyne, G.H., 1987. Geology of the Ladolam gold deposit, Lihir Island, Papua New Guinea. In: Proceedings Pacific Rim Congress, Australasian Institute of Mining and Metallurgy, 943-949.

Donato, D.B., Nichols, O., Possingham, H., Moore, M., Ricci, P.F. and Noller, B.N., 2007. A critical review of the effects of gold cyanide-bearing tailings solutions on wildlife. Environment International 33, 974-984.

Egbert, G.D., Erofeeva, S.Y., 2002. Efficient Inverse Modeling of Barotropic Ocean Tides. Journal of Atmospheric and Oceanic Technology 19 (2), 183-204

Elberling, B., Knudsen, K.L., Kristensen, P.H. and Asmund, G., 2003. Applying foraminiferal stratigraphy as a biomarker for heavy metal contamination and mining impact in a fiord in West Greenland. Marine Environmental Research 55, 235-256.

Ellis, D. and Ellis, K., 1994. Very deep STD. Marine Pollution Bulletin 28, 472-476.

Ellis, D., 1985. Taxonomic sufficiency in pollution assessment. Marine Pollution Bulletin 16, 459.

Ellis, D., 2006. A short history of submarine tailings placement (STP) in the context of lessons learned for subsequent sustainable development at a mining site (Update #8). Manuscript Report, 42 pp.

Ellis, D.V., 2000. Effect of mine tailings on the biodiversity of the seabed: example of the Island Copper Mine, Canada. In: Sheppard, C. (ed.), Seas at the Millennium: An Environmental Evaluation. Elsevier. pp. 235-246.

Emery, W.J., Meincke, J., 1986. Global water masses: summary and review. Oceanological Acta 9 (4), 383 - 391

ENESAR, 2007. Environmental Baseline Study, Ramu Nickell Project, Ramu NiCo Management Limited. 61 pages.

Erickson, K.L., Macko, S.A. and Van Dover, C.L., 2009. Evidence for a chemoautotrophically based food web at inactive hydrothermal vents (Manus Basin). Deep-Sea Research II 19-20, 1577-1585.

Fauchald, K. and Jumars, P.A., 1979. The diet of worms: a study of polychaete feeding guilds. Oceanography and Marine Biology: an Annual Review, 17, 193-284.

Fleming, C.A., 1992. Hydrometallurgy of precious metals recovery. *Hydrometallurgy* 30, 127-162

Gage, J.D. and Tyler, P.A., 1991. Deep-Sea Biology: a Natural History of Organisms at the Deep-Sea Floor. Cambridge University Press, 504 pp.

Gage, J.D., Hughes, D.J. and Gonzalez Vecino, J.-L., 2002. Sieve-size influence in estimating biomass, abundance and diversity in samples of deep-sea macrobenthos. Marine Ecology Progress Series, 225: 97-107.

Galkin, S.V., 1992. The benthic fauna of hydrothermal vents in the Manus Basin. Oceanology 32: 768-774.

Garcia, R., Koho, K.A., De Stigter, H.C., Epping, E., Koning, E. and Thomsen, L., 2007. Distribution of meiobenthos in the Nazaré Canyon and adjacent slope (western Iberian Margin) in relation to sedimentary composition. Marine Ecology Progress Series 340, 207-220.

Gomez Gesteira, J.L., Dauvin, J.C. and Salvande Fraga, M., 2003. Taxonomic level for assessing oil spill effects on soft-bottom sublittoral benthic communities. Marine Pollution Bulletin 46, 562-572.

Gwyther, D., Batterham, G.J., Waworuntu, J., Gultom, T.H., Prayogo, W. and Karnan, S., 2009. Recolonisation of mine tailings by meiofauna in mesocosm and microcosm experiments. Marine Pollution Bulletin 58, 841-850.

Hall, R., 2002. Cenozoic geological and plate tectonic evolution of SE Asia and the SW Pacific: computer-based reconstructions, model and animations. Journal of Asian Sciences, 20, 353-431.

Hargreaves, I., and Associates, 2005. Production Improvement Program: Environmental Impact Statement: Physical Marine Investigations.

Harris, R.P., Wiebe, P.H., Lenz, J., Skjoldal, H.R. and Huntley, M., 2000. ICES Zooplankton Methodology Manual. Amsterdam: Elsevier Academic Press, 684 pp.

Hellerman, S., Rosenstein, M., 1983. Normal Monthly Wind Stress Over the World Ocean with Error Estimates. Journal of Physical Oceanography 13 (7), 1093-1104

Holland, N.D., Clague, D.A., Gordon, D.P., Gebruk, A., Pawson, D.L. and Vecchione, M., 2005. "Lophenteropneust" hypothesis refuted by collection and photos of new deep-sea hemichordates. Nature 434, 374-376.

Howe, J., Wilson, C.R., Shimmield, T. Diaz, R. and Carpenter, L., 2007. Recent deep-water sedimentation, trace metal and radioisotope geochemistry across the Southern Ocean and Northern Weddell Sea, Antarctica. Deep-Sea Research II, 54, 1652-1681

IIED, 2002. Mining for the Future: Appendix A: Large volume waste working paper. Mining, Minerals and Sustainable Development Project Report. International Institute for Environment and Development, 55 pp.

Ivanov, L.I., Backhaus, J.O., Ozsoy, E. and Wehde, H., 2001). Convection in the Black Sea during cold winters. Journal of Marine Systems 31, 65-76.

Johnson, G.C., Sloyan, B.M., Kessler, W.S., McTaggart, K.E., 2002. Direct measurements of upper ocean currents and water properties across the tropical Pacific during the 1990s. Progress in Oceanography 52, 1), 31-61

Jones, D.O.B, Bett, B.J., Wynn, R.B. and Masson, D.G., 2009. The use of towed camera platforms in deep-water science. International Journal of the Society for Underwater Technology, 28, 41-50.

Jones, S.G. and Ellis, D.V., 1995. Deep-water STD at the Misima gold and silver mine, Papua New Guinea. Marine Georesources and Geotechnology 13, 183-200.

Josefson, A.B., Hansen, J.L.S., Asmund, G. and Johansen, P., 2008. Threshold response of benthic macrofauna to metal contamination in West Greenland. Marine Pollution Bulletin 56, 1265-1274.

Josey, S. A., Kent, E. C. and Taylor, P. K., 2002. Wind stress forcing of the ocean in the SOC climatology: comparisons with the NCEP-NCAR, ECMWF, UWM/COADS, and Hellerman and Rosenstein datasets. Journal of Physical Oceanography, 32, (7), 1993-2019. doi:10.1175/1520-0485(2002)032<1993:WSFOTO>2.0.CO;2

Kamenov, G. D., 2004. Magmatism and ore deposit formation in SW Pacific Island Arcs. Unpublished thesis, University of Florida.

Kamenov, G.D., Perfit, M.R., Jonasson, I.R., and Mueller, P.A., 2005. High-precision Pb isotope measurements reveal magma recharge as a mechanism for ore deposit formation: examples from Lihir Island and Conical Seamount, Papua New Guinea. Chemical Geology, 219, 131-148.

Kessler, T.A. 1986. Mixing - Primary Production Coupling in Holberg Inlet, a Tidally Energetic Fjord. PhD. Thesis. University of BC.

Ketcham, V.J., O'Reilly, J.F., and Vardill, W.D, 1993. The Lihir Gold Project; Process Plant Design. Minerals Engineering 6, 1037-1065

Kline, E.R. and Stekoll, M.S., 2001. Colonization of mine tailings by marine invertebrates. Marine Environmental Research 51: 301-325.

Lancellotti, D.A. and Stotz, W.B., 2004. Effects of shoreline discharge of iron mine tailings on a marine soft-bottom community in northern Chile. Marine Pollution Bulletin 48, 303-312.

Lee, M.R. and Correa, J.A., 2004. Copper mine tailings disposal: consequences for the interstitial polychaete *Saccocirrus sonomacus* (Canalipalpata, Protodrilida). Journal of the Marine Biological Association of the United Kingdom 88: 603-606.

Lee, M.R. and Correa, J.A., 2005. Effects of copper mine tailings disposal on littoral meiofaunal assemblages in the Atacama region of northern Chile. Marine Environmental Research 59, 1-18.

Lee, M.R. and Correa, J.A., 2007. An assessment of the impact of copper mine tailings disposal on meiofaunal assemblages using microcosm bioassays. Marine Environmental Research 64: 1-20.

Lee, M.R., Correa, J.A. and Seed, R., 2006. A sediment quality triad assessment of the impact of copper mine tailings on the littoral sedimentary environment in the Atacama region of northern Chile. Marine Pollution Bulletin 52: 1389-1395.

Lewis, R.W. and Wilson, G.I., 1990. Misima gold deposit. In: Hughes, F.E., Geology of the mineral deposits of Australia and Papua New Guinea, vol., 2, 1741-1746.

Lihir Gold Limited, 2005. Preliminary Environmental assessment for the floatation circuit bankable feasibility study (BFS). Volume 1 – Report.

Lihir Gold Limited, 2006. Environment Annual Report 2006.

Longhurst, A., Sathyendranath, S., Platt, T. and Caverhill, C., 1995. An estimate of global primary production in the ocean from satellite radiometer data. Journal of Plankton Research 17: 1245-1271.

MacDonald, R.W. and O'Brien, M.C., 1996. Sediment trap evaluation of mine tailings transport. Marine Georesources and Geotechnology 14, 97 – 109.

Maurer, D., 2000. The Dark Side of Taxonomic Sufficiency (TS). Marine Pollution Bulletin 40, 98-101.

Martin, T.E.and Davies, M.P.,2000. Trends in the stewardship of tailings dams AGRA Earth & Environmental Limited, Burnaby, B.C. Canada. http://www.infomine.com/publications/docs/Martin2000.pdf

Milliman, J.D., 1995. Sediment discharge to the ocean from small mountainous rivers: the New Guinea example. Geo-Marine Letters 15, 127-133.

Milliman, J.D., Farnsworth, K.L. and Albertin, C.S., 1999. Flux and fate of fluvial sediments leaving large islands in the East Indies. Journal of Sea Research 41, 97-107.

Misima Mines Limited, 2000. Environmental Monitoring Report. No. 26.

Misima Mines Limited, 2001. Misima Mines Sustainability Report 2001.

Misima Mines Limited, 2003. Environmental Monitoring Review. Main Report. No. 32.

Moyle, A.J., Doyle, B.J., Hoogvliet, H. and Ware, A.R., 1990. Ladolam gold deposit, Lihir Island. In: Hughes, F.E. (Ed) Geology of the Mineral Deposits of Australia and Papua New Guinea., vol. 2, 1793-1805.

Müller, D., Kaminski, K., Uhlig, S., Graupner, T., Herzig, P.M., and Hunt, S., 2002. The transition from porphyry- to epithermal-style gold mineralization at Ladolam, Lihir Island, Papua New Guinea: a reconnaissance study. Mineralium Deposita 37, 61-74

Murray, S., E. Lindstrom, J. Kindle and E. Weeks, 1995): Transport through the Vitiaz Strait. WOCE Notes, 7(1), 21-23.

Naryanaswamy, B.E., Nickell, T.D. and Gage, J.D., 2003. Appropriate levels of taxonomic discrimination in deep-sea studies: species vs. family. Marine Ecology Progress Series 257, 59-68.

Newmont, 1994. Pre-mine environmental impact assessment Minahasa Raya.

Newell, G.E. and Newell, R.C., 1967. Marine plankton. a practical guide. London: Hutchinson Educational Ltd, 221 pp.

Newmont, 2002. Now and Beyond 2002. www.newmont.com

NSR, 1996). Review of the Effects on the Marine Environment, Misima Mine, Papua New Guinea.

NSR, 1999. Ramu Nickell Project Environmental Plan. CR/161/9/v4. NSR Environmental Consultants Pty Ltd.

NSR, 2001. NSR Lihir Gold Project. Seafloor Sediment Sampling Study. Report to Lihir Management Company Pty Ltd.

NSR, 2001. Seafloor sediment sampling: Lihir Gold Project.

NSR, 1996. Review of the Effects on the Marine Environment, Misima Mine, Papua New Guinea. Report prepared by NSR Environmental Consultants Pty Ltd., CR 206/19/v5, 45 pp.

NSR, 1997. Review of submarine tailing disposal, Misima Mine, Papua New Guinea. Report prepared by NSR Environmental Consultants Pty Ltd., CR 206/21/v4, 41 pp.

NSR, 1997. Review of submarine tailings disposal, Misima Mine, Papua New Guinea.

Odhiambo, B.K., MacDonald, R.W., O'Brien, M.C., Harper, J.R. and Yunker, M.B., 1996. Transport and fate of mine tailings in a coastal fjord of British Columbia as inferred from the sediment record. Science of the Total Environment 191, 77-94.

Olsgard, F. and Hasle, J.R., 1993. Impact of waste from titanium mining on benthic fauna. Journal of Experimental Marine Biology and Ecology 172: 185-213.

Plimer, I.R., Andrew, A.S., Jenkins, R. And Lottermoser, B.G., 1988. The geology and geochemistry of the Lihir gold deposit, Papua New Guinea. In: Bicentennial Gold, 88, Geological Society of Australia, Abstracts, 22, 139-143.

Plumlee, G.S., Morton, R.A., Boyle, T.P., Medlin, J.H. and Centeno, J.A. , 2000. An Overview of Mining-Related Environmental and Human Health Issues, Marinduque Island, Philippines: Observations from a Joint U.S. Geological Survey – Armed Forces Institute of Pathology Reconnaissance Field Evaluation, May 12-19, 2000. U.S. Geological Survey Open-File Report 00-397.

Powell., J.H and Powell, R.E., 2001). Trace elements in fish overlying subaqueous tailings in the tropical west Pacific. Water, air and soil pollution. 125:81-104

Rex, M.A., Etter, R.J., Morris, J.M., Crouse, J., McClain, C.R., Johnson, N.A., Stuart, C.T., Deming, J.W., Thies, R. and Avery, R., 2006. Global bathymetric patterns of standing stock and body size in the deep-sea benthos. Marine Ecology Progress Series 317: 1-8.

Ritcey, G.M., 2005. Tailings management in gold plants. Hydrometallurgy 78, 3-20

Rose, M., 1933. Faune de France, 26, Copepodes Pelagiques. Paris: Paul Lechevalier, 374 pp.

Rysgaard, S., Glud, R.N., Risgaard-Petersen, N. and Dalsgaard, T., 2004. Denitrification and anammox activity in Arctic marine sediments. Limnology and Oceanography 49: 1493-1502.

Salazar, R.C. and Dira, D.C., 1977. The tailings disposal system of Atlas consolidated Mining and Development Corporation. 5th Symposium Mining Research Development and 24th Annual Mining Safety Conference, Philippines.

Shirayama, Y., 1984a. The abundance of deep sea meiobenthos in the Western Pacific in relation to environmental factors. Oceanologia Acta 7: 113-121.

Shirayama, Y., 1984b. Vertical distribution of meiobenthos in the sediment profile in bathyal, abyssal and hadal deep sea systems of the Western Pacific. Oceanologia Acta 7: 123-129.

Smith, D.L. and Johnson, K.B., 1996. A guide to Marine Coastal Plankton and Marine Invertebrate Larvae. Dubuque, Iowa: Kendall/Hunt, 221 pp.

Smith, K.L. Jr., Holland, N.D. and Ruhl, H.A., 2005. Enteropneust production of spiral fecal trails on the deep-sea floor observed with time-lapse photography. Deep-Sea Research I, 52, 1228-1240.

Southward, E.C., Schulze, A. and Tunnicliffe, V., 2002. Vestimentiferans (Pogonophora) in the Pacific and Indian Oceans: a new genus from Lihir Island (Papua New Guinea) and the Java Trench, with the first report of *Arcovestia ivanovi* from the North Fiji Basin. Journal of Natural History 36: 1179-1197.

Stecher, J., Tunnicliffe, V. and Türkay, M., 2003. Population characteristics of abundant bivalves (Mollusca, Vesicomyidae) at a sulphide-rich seafloor site near Lihir Island, Papua New Guinea. Canadian Journal of Zoology 81: 1815-1824.

Stoker, M.S., 1997. Mid- to late Cenozoic sedimentation on the continental margin off NW Britain. Journal of the Geological Society, London, 154, 509-515.

Stow, D.A.V., 1986. Deep clastic seas. In: Sedimentary Environments and Facies, Reading H.G. (Ed) Blackwell Scientific.

Stow, D.A.V. and Piper, D.J.W. 1984. Deep-water fine-grained sediments: facies models. In: Stow, D.A.V. and Piper, D.J.W. (Eds) Fine-grained sediments: deep-water processes and facies. Geological Society of London Special publication 15, 611-646

Taylor, B., Goodliffe, A., Martinez, F., Hey, R., 1995. Continental rifting and initial sea floor spreading in the Woodlark basin. Nature, 374, 534-537.

Taylor, B., Goodliffe, A.M. and Martinez, F., 1999. How continents break up: insights from Papua New Guinea. Journal of Geophysical Research 104, 7497-7512.

Terlizzi, A., Bevilacqua, S., Fraschetti, S. and Boero, F., 2003. Taxonomic sufficiency and the increasing insufficiency of taxonomic expertise. Marine Pollution Bulletin 46, 556-561.

Thamdrup, B., Dlasgaard, T., Jensen, M.M., Ulloa, O., Farías, L. and Escribano, R., 2006. Anaerobic ammonium oxidation in the oxygen-deficient waters off northern Chile. Limnology and Oceanography 51, 2145-2156.

Thomas, S., Ridd, P.V. and Day, G., 2003. Turbidity over fringing coral reefs near a mining site at Lihir Island, Papua New Guinea. Marine Pollution Bulletin, 46, 1006-1014.

Todd, C.D., Laverack, M.S. and Boxshall, G.A., 2000. Coastal marine zooplankton: a practical manual for students. Cambridge: Cambridge University Press, 106 pp.

Tsuchiya, M., Lukas, R., Fine, R.A., Firing, E., Lindstrom, E., 1989. Source waters of the Pacific Equatorial Undercurrent. Progress in Oceanography 23, 101-147

Tunnicliffe, V. and Southward, A.J., 2004. Growth and breeding of a primitive stalked barnacle *Leucolepas longa* (Cirripedia: Scalpellomorpha: Eolepadidae: Neolepadinae) inhabiting a volcanic seamount off Papua New Guinea. Journal of the Marine Biological Association of the United Kingdom 84: 121-132.

Vetter, E.W. and Dayton, P.K., 1998. Macrofaunal communities within and adjacent to a detritus-rich submarine canyon system. Deep-Sea Research II 45, 25-54.

Vetter, E.W. and Dayton, P.K., 1999. Organic enrichment by macrophyte detritus, and abundance patterns of megafaunal populations in submarine canyons. Marine Ecology Progress Series 186, 137-148.

Waldichuk, M., 1978. Disposal of mine wastes in the sea. Marine Pollution Bulletin 9, 141-143.

Welsh, T.C. and McCulla, M.S., 1987. A review of the Porgera, Ladolam (Lihir Island) and Misima gold deposits and the Wild Dog and Lakekamu gold prospects, Papua New Guinea:deposit types and geological settings. Geological Survey of Papua New Guinea, Report 87/30, 21pp.

White, N.C., Leake, M.J., McCaughey, S.N., and Parris, B.W.(1995. Epithermal gold deposits of the southwest Pacific. Journal of Geochemical Exploration 54, 87-136.

Woodd-Walker, R.S., Ward, P. and Clarke, A., 2002. Large-scale patterns in diversity and community structure of surface water copepods from the Atlantic Ocean. Mar. Ecol. Prog. Ser. 236: 189-203.

Zenk, W., Siedler, G., Ishida, A., Holfort, J., Kashino, Y., Kuroda, Y., Miyama, T., Müller, T.J., 2005. Pathways and variability of the Antarctic Intermediate Water in the western equatorial Pacific Ocean. Progress in Oceanography 67, 1-2), 245-281

8. List of Appendices

1: Bathymetry and Seabed sediments (Figures)

- Core Logs Basamuk

- Core Logs Lihir and Misima

2A: Physical Oceanography (Figures)

2B: SAMS CTD data Processing Protocol

2C: Salinity Calibration Procedures

2D: Fluorescence calibration and figures

3A: Water Column Geochemistry (Figures)

- Nutrients

- Suspended Particulate Matter

3B: Water Column Geochemistry (Tables)

- Nutrients

- Suspended Particulate Matter

4A: Sediment Geochemistry (Figures)

- Pore-water Nutrients

- Pore-water Metals

- Solid Phase Carbon and Nitrogen

- Solid Phase Metals

- Aluminium ratios

- Solid Phase ^{210}Pb

4B: Sediment Geochemistry (Tables)

- Pore-water Nutrients

- Pore-water Metals

- Solid Phase Carbon and Nitrogen

- Solid Phase Metals

- Aluminium ratios

- LOD and reference materials

- Solid Phase ^{210}Pb

- Lihir Statistics and Inventory Tables

5: Benthos (Tables)

- Benthos I

- Benthos II

6: Microzooplankton (Tables)

- Microzooplankton Basamuk

- Microzooplankton Lihir and Misima

7: Cruise Report Lihir and Misima

8: Cruise Report Basamuk

9: Deep-Sea Tailing Placement: A Review

10: Draft Guidelines for Deep-Sea Tailing Placement